LOW FREQUENCY RADIO EMISSIONS FROM THE GALAXY

P. A. Hamilton

Abstract:

The thesis presents the results of three radio surveys of the southern sky together with an analysis of these and other surveys of the same region. A model of the emission and absorption of radio waves in the Galaxy is derived in which the free electron content of the interstellar medium is consistent with the observations of related phenomena.

The low resolution measurements of the radio spectra in the direction of the galactic poles are reviewed to obtain a reference spectrum for calibrating high resolution surveys. It is apparent that there are considerable differences between the emissions in the two galactic hemispheres, and it is concluded that the electron distributions responsible for the emission in each region have different energy spectra.

The three surveys of the southern sky are described, at 4.7 MHz (beamwidth $4^{\circ} \times 10^{\circ}$), 10 MHz (beamwidth $4^{\circ} \times 5^{\circ}$) and 153 MHz (beamwidth 2.2° circular); lists of discrete sources measured are presented together with contour maps of equivalent aerial temperature. The results of three other surveys of the

same region are summarised, and the six surveys are analysed in terms of a model in which the line of sight intensity is the combined effects of a local region (called for convenience the "disk" region) and a region remote from the sun (the "extra-disk" region). The processes of synchrotron emission and thermal absorption are assumed to occur in the disk region, while there is emission and no absorption in the extra-disk region. The parameters of the model are the emissivity of the disk region, the optical depth at each line of sight in the disk region, and the total intensity at each line of sight from the extra-disk region.

The extra-disk emission is found to be strongly anisotropic and the distribution is consistent with the existence of a galactic halo that is ellipsoidal in shape with axes of 18 Kpc and 20 Kpc. The assumption that the halo is dynamically stable implies that the mean magnetic field strength is 2×10^{-6} Gauss and the differential spectrum of the radiating electrons is

$$n_e(E) \simeq 8\times10^{-2}\, E^{-2.3} \quad el\ cm^{-2}\ sec^{-1}\ ster^{-1}\ GeV^{-1}.$$

These electrons would interact with the 3 degK black body radiation field via the inverse Compton effect to produce x-ray photons in the 3 - 20 KeV range with intensities close to those observed.

The properties derived for the emission from the disk region suggest a mean field strength of a few microgauss and an electron flux slightly higher than that estimated for the solar

neighbourhood from measurements near the earth.

The distribution of thermal absorption in the disk region suggests a uniform electron gas throughout the galactic plane, with a somewhat greater mean density towards the galactic centre. For the line of sight at the south galactic pole we obtain

$$\int n_e^2/T_e^{3/2}\, d\ell \simeq 9\times10^{-6}\ cm^{-6}\ degK^{-3/2}\ pc,$$

where n_e is the electron number density and T_e is the electron kinetic temperature. It is concluded that a model of the interstellar medium in which the intercloud region has a density of 0.5 cm^{-3}, a temperature of 1000 degK and an ionization of 6% will explain the observations of hydrogen-line emission, Faraday rotation, pulsar dispersion and low frequency absorption.

LOW FREQUENCY RADIO EMISSIONS FROM THE GALAXY

by

P. A. HAMILTON, B.Sc.(Hons.)

submitted in fulfilment of the requirements for the degree of Doctor of Philosophy

UNIVERSITY OF TASMANIA

HOBART

AUGUST 1969

This thesis contains no material which has been submitted or accepted for the award of any other degree or diploma in any university.

To the best of my knowledge and belief, the thesis contains no copy or paraphrase of material previously published or written by another person, except where due acknowledgement is made in the text.

CONTENTS

CHAPTER 1

INTRODUCTION

Summary

This thesis presents the results of three radio surveys of the southern sky, together with an analysis of these and other surveys of the same region. A model of the emission and absorption of radio waves in the Galaxy is derived in which the free electron content of the interstellar medium is consistent with observations of related phenomena.

The low resolution measurements of the radio spectra in the direction of the galactic poles are reviewed with the aim of obtaining a spectrum for calibrating high resolution surveys. It is apparent that there are considerable differences between the emissions in the two galactic hemispheres, and it is concluded that the differences must be in the electron distributions responsible for the emission rather than in the magnetic field.

Three surveys of the southern sky are described, at 4.7 MHz (beamwidth $4^{o} \times 10^{o}$), 10 MHz (beamwidth $4^{o} \times 5^{o}$) and 153 MHz (beamwidth 2.2^{o} circular). The results of these surveys are presented in contour maps of equivalent aerial temperature together with lists of discrete sources measured.

The results of three other surveys of the same region, at 2.1 MHz, 30 MHz and 85 MHz are summarised, and the six surveys are analysed in terms of a model in which the line of sight intensity is the combined effects of a local region (called for convenience the "disk" region) and a region remote from the sun (the "extra-disk" region). Both synchrotron emission and thermal absorption are assumed to occur in the disk region, while there is emission and no absorption in the extra-disk region. The analysis is performed in two independent ways. In the first case a single scan at declination -37^{o} yields values for the parameters by virtue of the differences in *shape* of the scan at different frequencies; the data are normalized for one direction and no absolute measurements are required. In the second analysis, which extends over the whole of the region covered by all six surveys, the intensities are adjusted for agreement with the low resolution spectrum

of the same region and the *spectrum* in each line of sight is used to solve the model.

The parameters of the model are the emissivity of the disk region, the optical depth at each line of sight in the disk region, and the total intensity at each line of sight from the extra-disk region. Values are also obtained for the line of sight averages of (emissivity / absorption per unit volume) and $(n_e^2/T_e^{3/2})$ for the disk region, where n_e and T_e are the free electron number density and kinetic temperature respectively, although the evaluation of the last-mentioned requires the assumption of a distance scale for the model (i.e. the effective width of the disk region). The two methods of analysis give virtually identical results.

The extra-disk emission is strongly anisotropic, and the distribution is consistent with the existence of a galactic halo or corona that is ellipsoidal in shape, extending about 29 Kpc in the galactic plane and 26 Kpc normal to the plane. The dimensions of the halo are somewhat less than those usually assumed, and slightly larger than the model proposed by Mills at the 1958 Paris Symposium on Radio Astronomy. A stable halo with the

properties deduced would have a mean field strength of about 10^{-6} Gauss and a differential electron energy spectrum of the form

$$n_e(E) \simeq 4\times10^{-2}\ E^{-2.3}\ el\ cm^{-2}\ sec^{-1}\ ster^{-1}\ GeV^{-1}.$$

These electrons would interact with the 3 degK black body radiation field via the inverse Compton effect to produce x-ray photons in the 3 - 20 KeV range with intensities close to those that have been observed.

The properties of the emission from the disk region are consistent with a field strength of a few microgauss and an electron flux slightly higher than that estimated for the solar neighbourhood from measurements in the vicinity of the earth. The current uncertainty in estimating the solar modulation effects makes it difficult to pursue this point very far. The spatial distribution of the disk component displays the steps in emission that have been explained by others as indications of the spiral structure of the galaxy.

The distribution of thermal absorption in the disk region suggests a uniform electron gas throughout the galactic plane, with a somewhat greater mean density towards the galactic centre. For the line of sight at the south galactic pole we obtain

$$\int n_e^2/T_e^{3/2}\, d\ell \simeq 9\times10^{-6}\ cm^{-6}\ degK^{-3/2}\ pc,$$

and this integral is approximately proportional to cosec$b$ over most of the range of galactic latitudes. A brief review of current ideas on the interstellar medium is given, with emphasis on observations relating to the free electron content. It is concluded that a model in which the intercloud medium has a free electron density of 0.03 cm^{-3} at a temperature of 1000 degK will explain the observations of Faraday rotation, pulsar dispersion and low frequency absorption. This is consistent with the model of Radhakrishnan and Murray and implies 6% ionization, which could be sustained by the passage of cosmic ray particles.

Notation and Units:

In astronomical discussions it is frequently necessary to refer to two distinct quantities with the same name. In this thesis problems arise in references to degrees (temperature) and degrees (of arc), as well as minutes (of time) and minutes (of arc). The notation adopted is such that 10^{o} refers to an angle while 10 degK refers to the absolute temperature, and $10'$ refers to an angle while 10^{m} refers to time.

A departure has been made from the standard way of representing a large number as the product of a smaller one with the appropriate power of ten: e.g. 2.998×10^{8}. The main reason for this change is that the multiplication sign '×' can sometimes be mistaken for the letter 'x' in an expression. An elegant solution to this problem has been adopted in the international algorithm language ALGOL, in which the power of ten is indicated by a subscript: $2.998_{10}8$. This notation has been adopted throughout this thesis.

Frequent references have been made to the system of galactic coordinates. The italic letters l and b have been used to indicate galactic longitude and latitude respectively. The so-called new galactic coordinates are

used exclusively, defined by (Epoch 1950.0)

pole: $12^h\ 42^m\ 24^s$ right ascension,

$+27^\circ\ 36'$ declination;

origin: $17^h\ 42^m\ 24^s$ right ascension,

$-28^\circ\ 55'$ declination.

A mixture of units has been used, with an attempt made to specify quantities in the units most commonly used in the literature; at times this has meant a rather arbitrary choice. Frequent reference is made to the *flux unit* (abbreviated f.u.):

$$1 \text{ flux unit} = 10^{-26} \textit{ Watt metre}^{-2} \textit{ Hertz}^{-1} \textit{ sterad}^{-1}.$$

In reference to particle energy the abbreviation GeV has been used in preference to BeV. $1 \text{ GeV} = 10^9 \text{ eV}$.

Acknowledgements:

It is impossible to give adequate acknowledgement to the advice and assistance received over the period of several years during which the work leading to this thesis was done. However the acknowledgement must be attempted, and I apologise to all concerned for the omissions which result from the necessary brevity.

Financial support was received during the early part of the work in the form of a Commonwealth Postgraduate Scholarship. The remainder was carried out on a part-time basis during the tenure of a lectureship in Physics, and thanks are due to the University and the Head of the Physics Department, Professor G.R.A.Ellis, for permission to continue the project in this way.

Technical assistance was obtained from a large number of people at different times, although the ready help of Mr.G.G.Harman and Mr.G.Gowland requires explicit mention. I have had the benefit of discussions with most of the staff of the Physics Department, as well as Dr.G.Reber and Dr.V.Radhakrishnan, and their help is appreciated. Mention must be made of Mr.P.M.McCulloch, Mr.R.F.Haynes and Mr.R.J.Francey with whom I have worked in various aspects of the project.

The sections of the analysis which required extensive use of the computer could not have been completed without the continued advice and assistance of Mr.J.Boothroyd, Officer-in-Charge of the Hydro-University Computer Centre.

This project was initiated by Professor G.R.A.Ellis and sustained by his guidance and enthusiasm.

Finally I acknowledge the moral support and indulgence of my wife and family without which this stage could not have been reached.

CHAPTER 2

EMISSION AND ABSORPTION PROCESSES AT LOW RADIO FREQUENCIES

INTRODUCTION

Cosmic radio emissions can be divided into two classes, line emission and continuum emission. Line emission is monochromatic and is the result of transitions between energy levels in atoms or molecules of the source. Continuum emission extends over virtually the whole spectrum with varying intensity and is the result of a non-resonant process. Two such processes are known, the synchrotron mechanism and thermal (black body) emission.

Line emissions have proved unimportant at frequencies below a few hundred megahertz. This is because the synchrotron process normally leads to a spectrum which increases with wavelength while the spontaneous transition probability for the line emission is proportional to the cube of the frequency. No discussion will therefore be given of line emission.

Of the two continuum processes the synchrotron process dominates at frequencies of interest in this thesis. However the radiation received is the combined result of synchrotron emission and thermal absorption and hence a discussion of the thermal process is necessary.

SYNCHROTRON EMISSION

Synchrotron emission is the result of the inward acceleration of a relativistic charged particle spiralling in a magnetic field. It was originally observed as optical radiation from an electron synchrotron (Elder *et al*, 1948) but in most astrophysical situations the low magnetic field strengths (1 - 10 μgauss) lead to emission in the radio range.

The theory of the process has been developed in some detail (Schwinger, 1949; Westfold, 1959) and is mathematically rather involved, but the basic principles are simple. An electron in a region of uniform magnetic field will move in a circular orbit of radius

$$R = \frac{mv}{eB_\perp} \quad \textit{metres}$$

where m = electron mass, *kg*

v = electron velocity, $m\ sec^{-1}$

e = electronic charge, *coulomb*

$B_\perp$ = component of magnetic flux density normal to the electron velocity, $weber\ m^{-2}$ ($1\ weber\ m^{-2} = 10^4\ gauss$).

For low electron energies ($v \ll c$; c = speed of light) the radiation field in the plane of the orbit at a large distance from the electron will vary at the orbital (gyro) frequency

$$\nu = \frac{eB_\perp}{2\pi m} \quad Hz.$$

As the energy of the electron is increased ($v \to c$) the radiation is effectively concentrated in a cone of angle θ centred on the direction of instantaneous velocity. The angle θ is given by

$$\theta = 2\left[1 - \left(\frac{v}{c}\right)^2\right]^{1/2} \qquad (1).$$

Thus an observer in the plane of the orbit will receive pulses of duration

$$\Delta t \simeq \frac{R\theta}{c}\left[1 - \left(\frac{v}{c}\right)^2\right]$$

$$= \frac{2\,m_o}{e\,B_\perp}\left[1 - \left(\frac{v}{c}\right)^2\right] \quad seconds$$

where m_o is the electron rest mass. The duration of the pulse is very short in comparison with the repetition period, and the frequency spectrum can be regarded as continuous. The maximum radiation from the electron (power per unit bandwidth) occurs at

$$\nu_{max} \simeq \frac{1}{2\pi\Delta t}$$

$$\simeq \frac{e\, B_\perp}{4\pi m_o} \left[1 - \left(\frac{v}{c}\right)^2\right]^{-1} \quad Hz,$$

where e = electronic charge, *coulomb*

$B_\perp$ = flux density, *weber* m^{-2}

m_o = electron rest mass, *kg*

v = electron velocity, *m* sec^{-1}

c = speed of light, *m* sec^{-1}.

In a more complete treatment (e.g. Westfold, 1959) it is convenient to introduce a *characteristic frequency* ν_c

where $\nu_c \simeq 16.1\ B_\perp\ E^2$ *MHz*

for $B_\perp$ in microgauss and the electron energy E in GeV (1 GeV = 10^9 eV). The spectral distribution of power radiated by a single electron is shown to be

$$P(\nu) \simeq 2.34_{10}\text{-}29\ B_{\perp}\ F\left(\frac{\nu}{\nu_c}\right) \quad \textit{Watts MHz}^{-1} \quad (2)$$

where F is the function

$$F(x) = x \int_{x}^{\infty} K_{5/3}(t)\, dt$$

and $K_{5/3}$ is the modified Bessel function of order (5/3). The integral for F cannot in general be evaluated analytically, and the function F(x) is given in tabulated and graphical form by Westfold (1959). The function has been approximated for various ranges of the argument by suitable series and a general method for evaluation is given in the Appendix in the form of an ALGOL procedure. The radiation spectrum (2) of a relativistic electron is shown in figure 1 for several values of the characteristic frequency ν_c.

The foregoing discussion is appropriate for an observer in the plane of the electron orbit where the radiation is concentrated by the small cone angle θ (equation 1). The radiation will be plane polarised with the electric vector normal to the magnetic field. It is generally assumed that the emission from interstellar space within the galaxy is from regions with randomly oriented

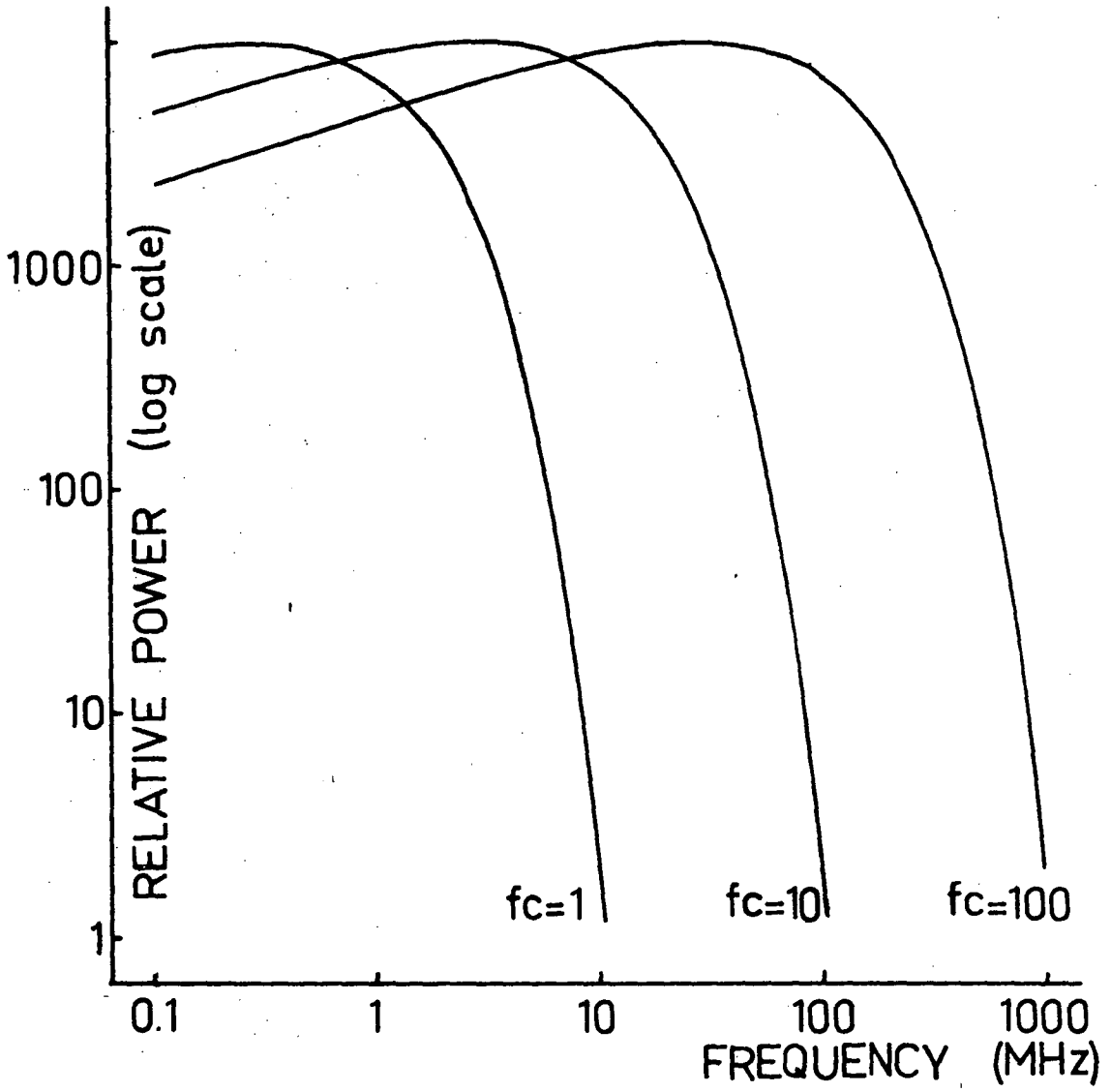

FIGURE 1

SYNCHROTRON EMISSION SPECTRUM FOR A SINGLE ELECTRON

magnetic fields, and this assumption is borne out by the absence of a significant degree of polarization. The emissivity of such a region will be isotropic, and this isotropy will be assumed henceforth.

The spectrum of the radiation from an assembly of relativistic electrons will be a function of the energy spectrum of the electrons. If $n_e(E)dE$ is the number of electrons with energy in the range E to E+dE, the emissivity $\varepsilon(\nu)$ will be given by

$$\varepsilon(\nu) \propto B_\perp \int n_e(E)\, F\left(\frac{\nu}{\nu_c}\right) dE \ .$$

We obtain

$$\varepsilon(\nu) \simeq 2.34_{10}{}^{-35}\, B_\perp \int n_e(E)\, F\left(\frac{\nu}{16.1\, B_\perp E^2}\right) dE$$

$$W\, m^{-3}\, Hz^{-1} \qquad (3),$$

where ν = wave frequency, *MHz*

$B_\perp$ = magnetic field strength, *microgauss*

E = electron energy, *GeV*

n_e = electron spectrum, *el* m^{-3} GeV^{-1}

and the integration is over all electron energies.

Kiepenheuer (1950) was the first to propose that the electrons responsible for the galactic radio emission are in fact cosmic ray electrons. For energies above about

0.5 GeV the differential energy spectrum of cosmic ray electrons is of the form

$$n_e(E) \propto E^{-\gamma} , \quad \text{where} \quad \gamma \simeq 2.2 .$$

At lower energies the spectrum is uncertain. If all the radiation is assumed to take place at the characteristic frequency ν_c it can be shown (Mills, 1964) that

$$\varepsilon(\nu) \propto B_\perp^{\frac{1+\gamma}{2}} \nu^{-\left(\frac{\gamma-1}{2}\right)}$$

i.e. $$\varepsilon(\nu) \propto \nu^{-\alpha}$$

where $$\alpha = \frac{\gamma-1}{2} = 0.6 \quad \text{for } \gamma = 2.2 .$$

In the frequency range 20 - 200 MHz the agreement with the observed galactic spectrum is good. However at frequencies below 20 MHz there is a change in the observed spectral index α, and in this case the so-called δ-function approximation used by Mills for the radiation spectrum of a single electron is inadequate, because of the long low-frequency tail of the function F(x) (see figure 1). The radiation spectrum for a given electron distribution must therefore be obtained by the actual integration of (3). The most rapid cut-off possible in a synchrotron emission spectrum is illustrated in figure 2. Curve (a) gives the

spectrum from an electron distribution

$$n_e(E) \propto E^{-2.2} .$$

Curves (b) and (c) result from

$$n_e(E) \propto E^{-2.2} \qquad E \geq E_c ,$$

$$n_e(E) = 0 \qquad E < E_c ,$$

where the cut-off energy is specified in terms of the synchrotron characteristic frequency, ν_c:
curve (b): ν_c = 7 MHz, corresponding to E_c = 0.3 GeV
curve (c): ν_c = 12 MHz, corresponding to E_c = 0.4 GeV;
the magnetic field strength in each case is $B_\perp$ = 5 μgauss.

THERMAL ABSORPTION

An ionized gas will emit radiation at high frequencies and absorb it at low frequencies. The mechanism is that of free-free transitions of the detached electrons in the coulomb fields of the ions. The theory of the process is well understood (Scheuer, 1960; Shklovsky, 1960; Ginzburg, 1961). Under conditions applicable to the interstellar medium at redio frequencies,

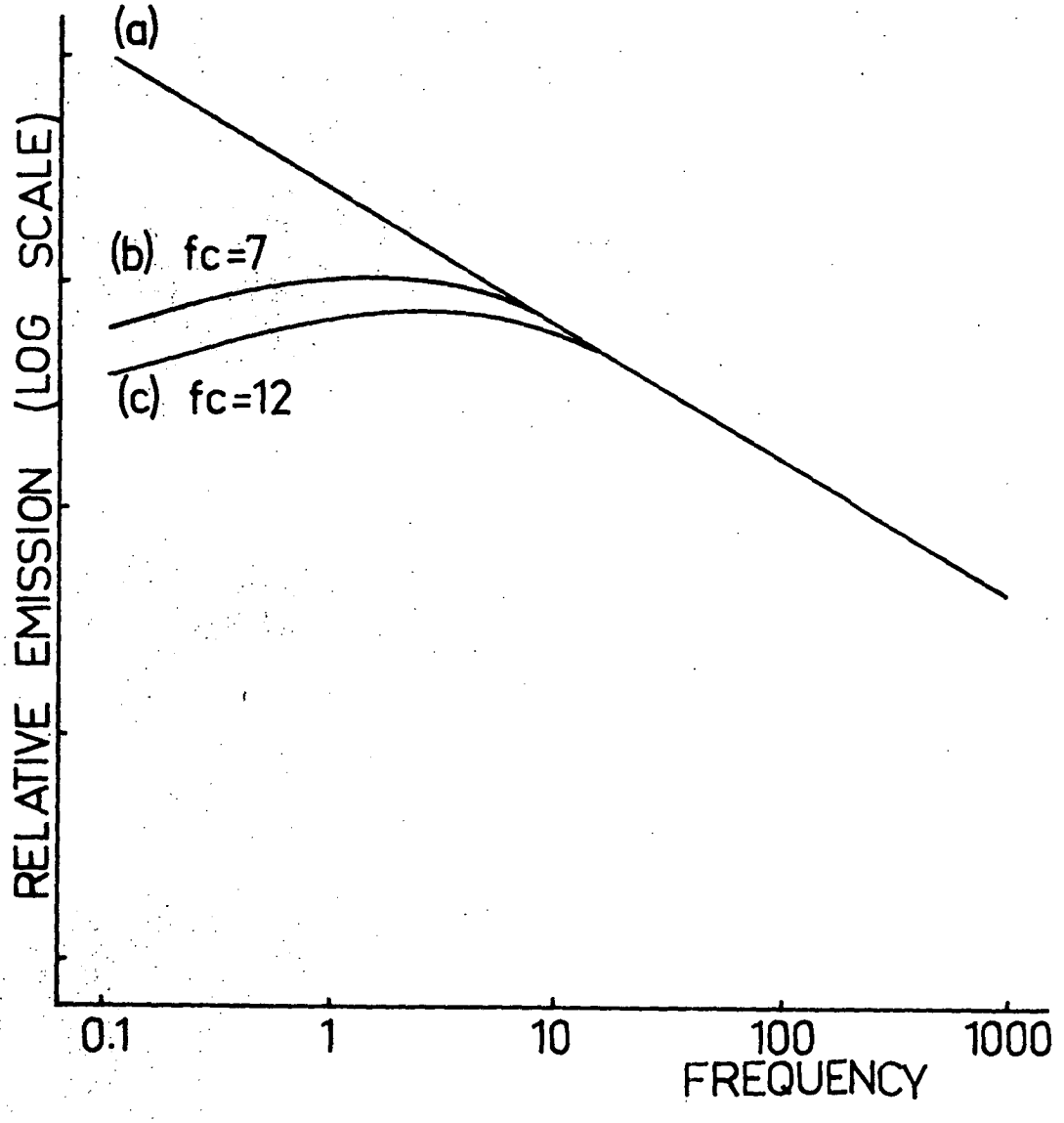

FIGURE 2
SYNCHROTRON SPECTRA PRODUCED BY CUT-OFF IN ELECTRON DISTRIBUTION

that is a) $h\nu << kT$,

b) $\lambda >>$ (electron number density)$^{-1/3}$,

c) $\omega^2 >>$ collision frequency,

d) electrically neutral ionized hydrogen,

the absorption coefficient is

$$K \simeq \frac{10^{-2} n_e^{\,2}}{T_e^{\,3/2} \nu^2} \left[17.7 + \ln\left(\frac{T_e^{\,3/2}}{\nu}\right)\right] \quad neper\ cm^{-1}$$

(Ginzburg, page 725),

where n_e = free electron number density, $el\ cm^{-3}$

T_e = electron *kinetic* temperature, $degK$

ν = wave frequency, Hz.

It is customary to write

$$K = \frac{\zeta\, n_e^{\,2}}{T_e^{\,3/2}\, \nu^2}$$

where $$\zeta \simeq 10^{-2} \left[17.7 + \ln\left(\frac{T_e^{\,3/2}}{\nu}\right)\right]$$

is regarded as constant, and not a function of frequency. It is clear from Table I that this simplification is reasonable.

TABLE I

Values of $\zeta = {}_{10}{}^{-2}\left[17.7 + \ln\left(\frac{T_e^{3/2}}{\nu}\right)\right]$

T_e *degK*	ν *MHz*						
	1	3	5	10	20	50	100
500	.132	.125	.115	.109	.102	.093	.086
1000	.143	.146	.126	.119	.113	.103	.096
2000	.153	.150	.137	.130	.123	.114	.107
5000	.167	.160	.151	.144	.137	.128	.131
10000	.177	.170	.161	.154	.147	.138	.131

The optical depth in ionized hydrogen of dimension L is then

$$\tau = \int_0^L K \, dr \quad \textit{neper}$$

$$\simeq \frac{\zeta}{\nu^2} \int_0^L \frac{n_e^2}{T_e^{3/2}} \, dr \quad \textit{neper}$$

and radiation travelling through this region will be reduced in intensity by a factor of $e^{-\tau}$ by absorption.

COMBINED EMISSION AND ABSORPTION

The observed spectrum from a region of the sky is generally the result of synchrotron emission and thermal absorption, and the shape of the spectrum depends on the relative positions of the emission and absorption regions. In preparation for later discussions it is instructive to consider a number of cases.

(a) Emission only:

Suppose a configuration as shown in figure 3, with an emission region remote from the observer. Let the volume

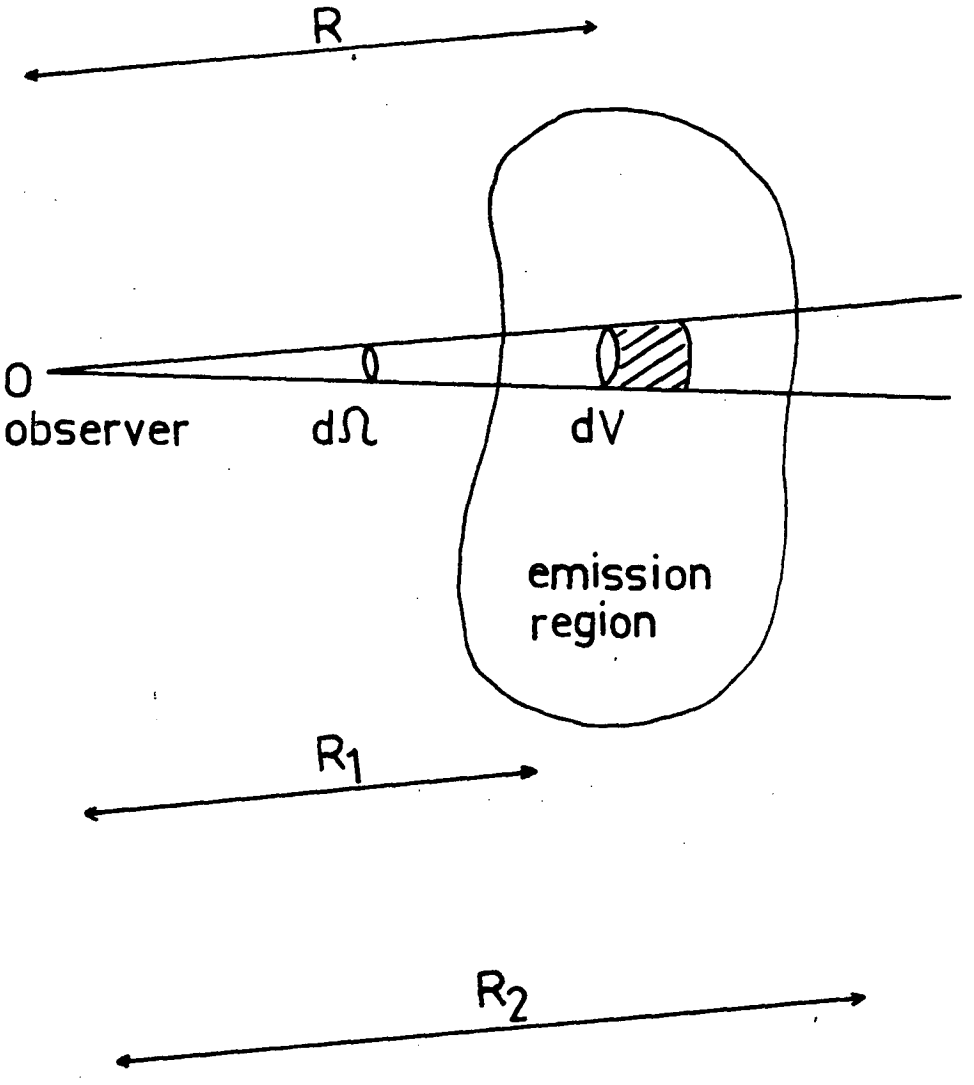

FIGURE 3

emissivity in this region be $\varepsilon(\nu)$ $W\,m^{-3}\,Hz^{-1}$. Then the spectral power from volume dV is

$$dW(\nu) = \varepsilon(\nu)\, dV \qquad W\,Hz^{-1}.$$

The flux density dS due to emission from dV at a distance r from dV is

$$dS(\nu) = \frac{dW(\nu)}{4\pi r^2}$$

$$= \frac{\varepsilon(\nu)\, dV}{4\pi r^2} \qquad W\,m^{-2}\,Hz^{-1},$$

and the brightness

$$dB(\nu) = \frac{dS(\nu)}{d\Omega}$$

$$= \frac{\varepsilon(\nu)\, dV}{4\pi r^2\, d\Omega}$$

$$= \frac{1}{4\pi}\,\varepsilon(\nu)\, dr \qquad W\,m^{-2}\,Hz^{-1}\,ster^{-1},$$

since $dV = r^2\, dr\, d\Omega$.

The brightness of the whole region is therefore

$$B(\nu) = \frac{1}{4\pi} \int_{R_1}^{R_2} \varepsilon(\nu)\, dr \qquad W\,m^{-2}\,Hz^{-1}\,ster^{-1}.$$

For a region with differential electron energy spectrum

$$n_e(E) \propto E^{-\gamma}$$

we will have

$$\varepsilon(\nu) \propto \nu^{-\alpha} \quad \text{where } \alpha = \frac{\gamma-1}{2}$$

$$= 4\pi A \nu^{-\alpha} \quad \text{for some constant A.}$$

We obtain

$$B(\nu) = \int_{R_1}^{R_2} A(r)\, dr \;\; \nu^{-\alpha}$$

$$= A(R_2 - R_1)\, \nu^{-\alpha}$$

if A is constant throughout the region.

(b) A thermal absorption region in front of an emission region:

Suppose a configuration as shown in figure 4, and let the absorption coefficient of the absorber be K *neper* m^{-1}. Then the optical depth of the path from R_3 to R_4 is

$$\tau = \int_{R_3}^{R_4} K(r)\, dr \,,$$

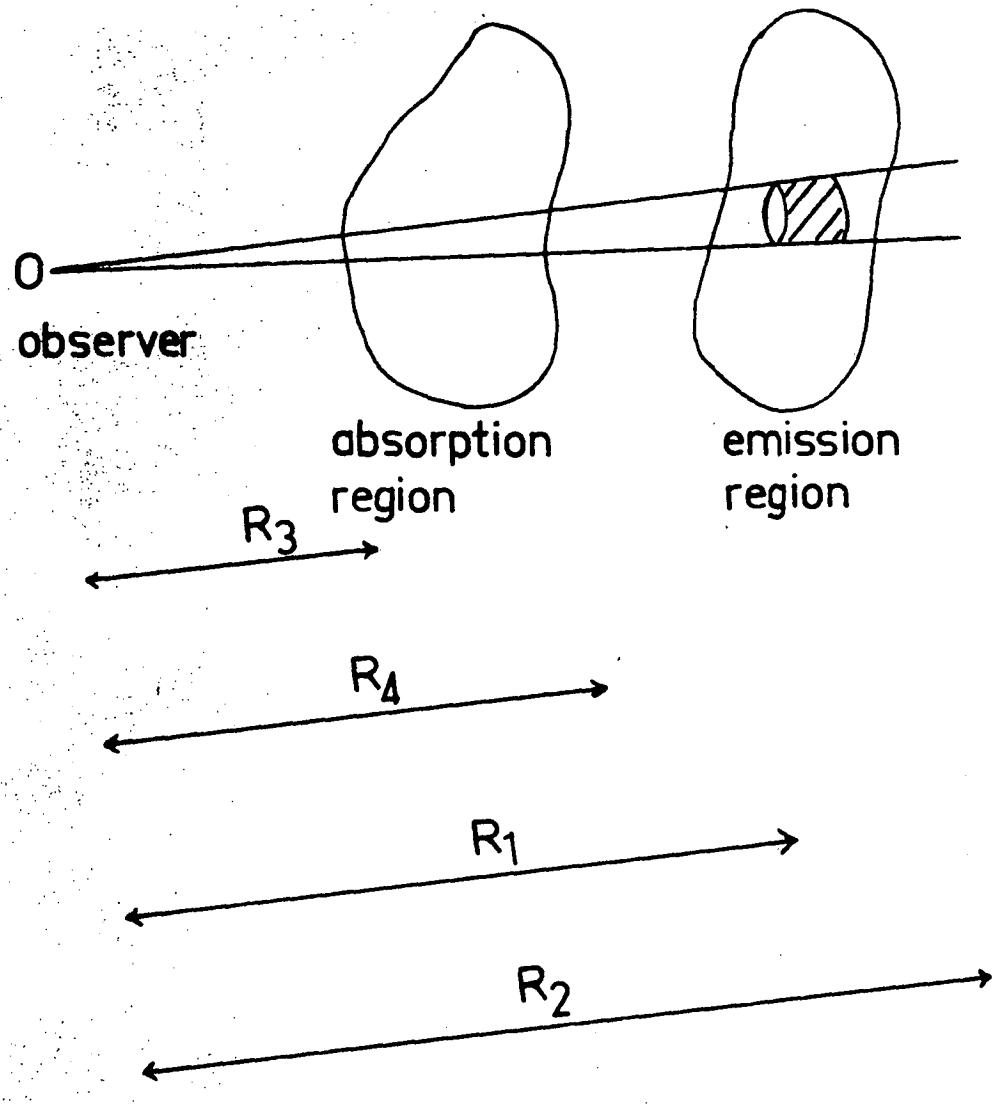

FIGURE 4

and the observed brightness after absorption is

$$B(\nu) = \int_{R_1}^{R_2} A(r)\, dr\, \nu^{-\alpha} \cdot e^{-\int_{R_3}^{R_4} K(r)\, dr}$$

$$= A(R_2 - R_1)\, \nu^{-\alpha}\ e^{-K(R_4 - R_3)}$$

if A and K are constant throughout the respective regions. For free-free transitions we have seen that

$$K = \frac{k}{\nu^2} \qquad (4)$$

and $B(\nu)$ has the form

$$B(\nu) = a\, \nu^{-\alpha}\ e^{-(c/\nu^2)} \qquad (5).$$

The shape of this function is illustrated in figure 5 for $c = 16$ and $\alpha = 0.6$.

(c) Emission and absorption together:

Suppose the region in figure 6 has emissivity $\varepsilon(\nu)$ per unit volume and absorption coefficient K per unit length. Then the contribution to the total brightness seen at O due to volume dV is

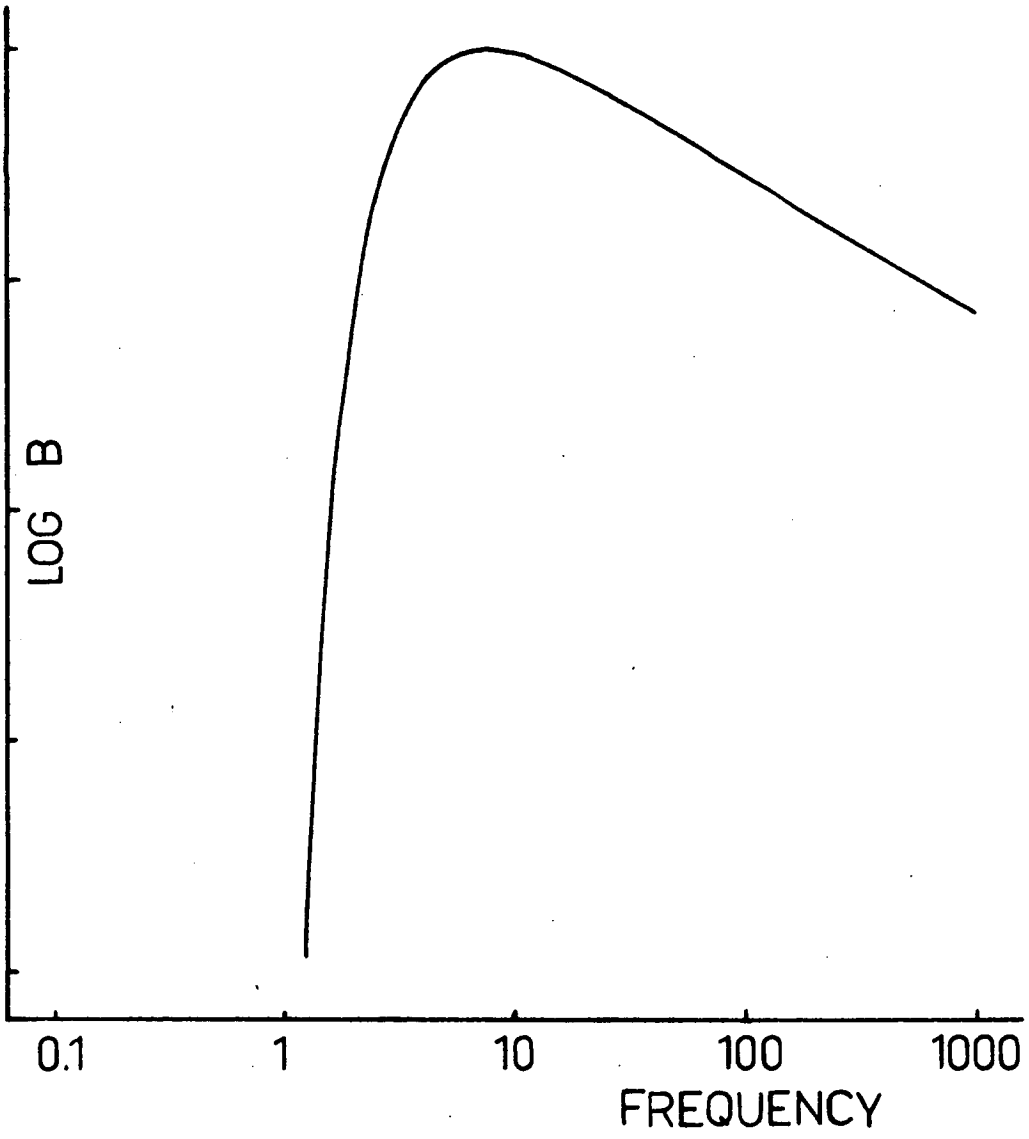

FIGURE 5

THE FUNCTION $B(f) = af^{-0.6}e^{-16/f^2}$

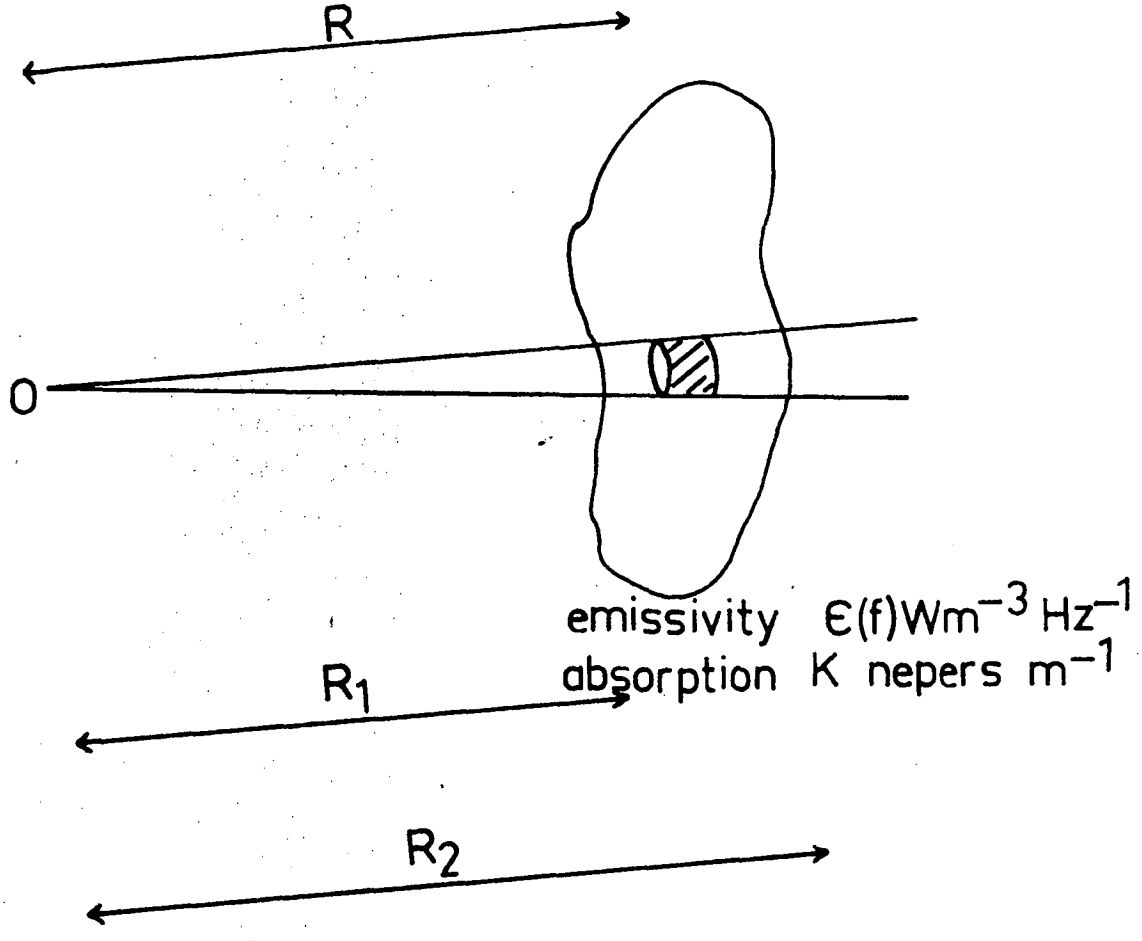

FIGURE 6

$$dB(\nu) = \frac{1}{4\pi}\,\varepsilon(\nu)\,dr\; e^{-\int_{R_1}^{r} K(s)\,ds}$$

and the total brightness is therefore

$$B(\nu) = \int_{R_1}^{R_2} \frac{1}{4\pi}\,\varepsilon(\nu)\; e^{-\int_{R}^{r} K(s)\,ds}\; dr\ .$$

If $\varepsilon(\nu)$ is constant throughout the region, and we can write

$$\varepsilon(\nu) = 4\pi A\nu^{-\alpha} \quad \text{and} \quad K = \frac{k}{\nu^2}$$

where k is constant (I.e. there is uniform thermal absorption), we obtain

$$B(\nu) = A\nu^{-\alpha} \int_{R_1}^{R_2} e^{-k(r-R_1)/\nu^2}\; dr$$

$$= \frac{A}{k}\,\nu^{2-\alpha}\,[1 - e^{-k(R_2-R_1)/\nu^2}]$$

which is in the form

$$B(\nu) = a\,\nu^{2-\alpha}\,[1 - e^{-(c/\nu^2)}]$$

This function is illustrated in figure 7 for c = 16 and α = 0.6.

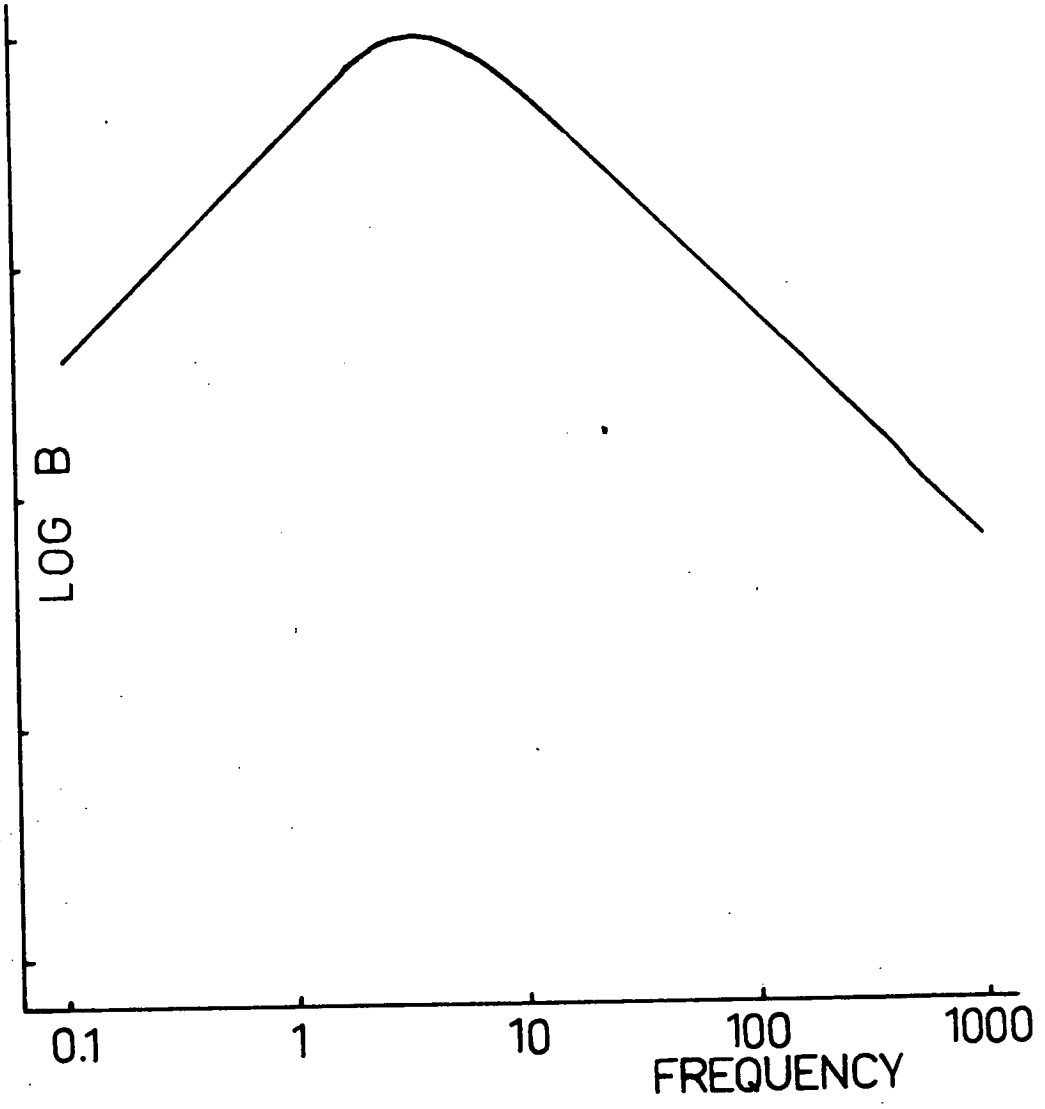

FIGURE 7

THE FUNCTION $B(f) = af^{1.4}(1 - e^{-16/f^2})$

(d) A region of emission and absorption in front of an emission region:

This configuration is illustrated in figure 8. Under conditions of uniform emissivity and uniform absorption, and where the spectral indices of the two emissivities are the same, we obtain an expression for the brightness of the form

$$B(\nu) = a\,\nu^{-\alpha}\,e^{-(c/\nu^2)} + b\,\nu^{2-\alpha}\,[1-e^{-(c/\nu^2)}].$$

This function is shown in figure 9 and figure 10 for $\alpha = 0.6$ and $c = 16$, with $(b/a) = 0.01$ (figure 9) and $(b/a) = 0.03$ (figure 10).

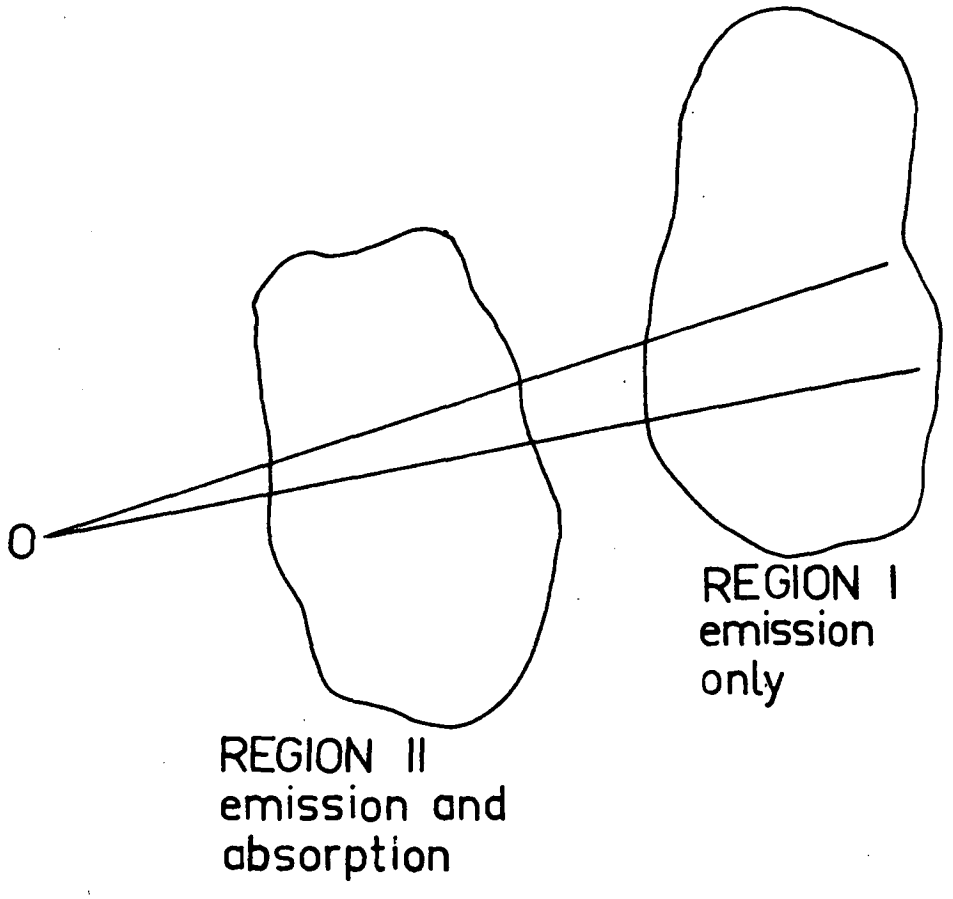

FIGURE 8

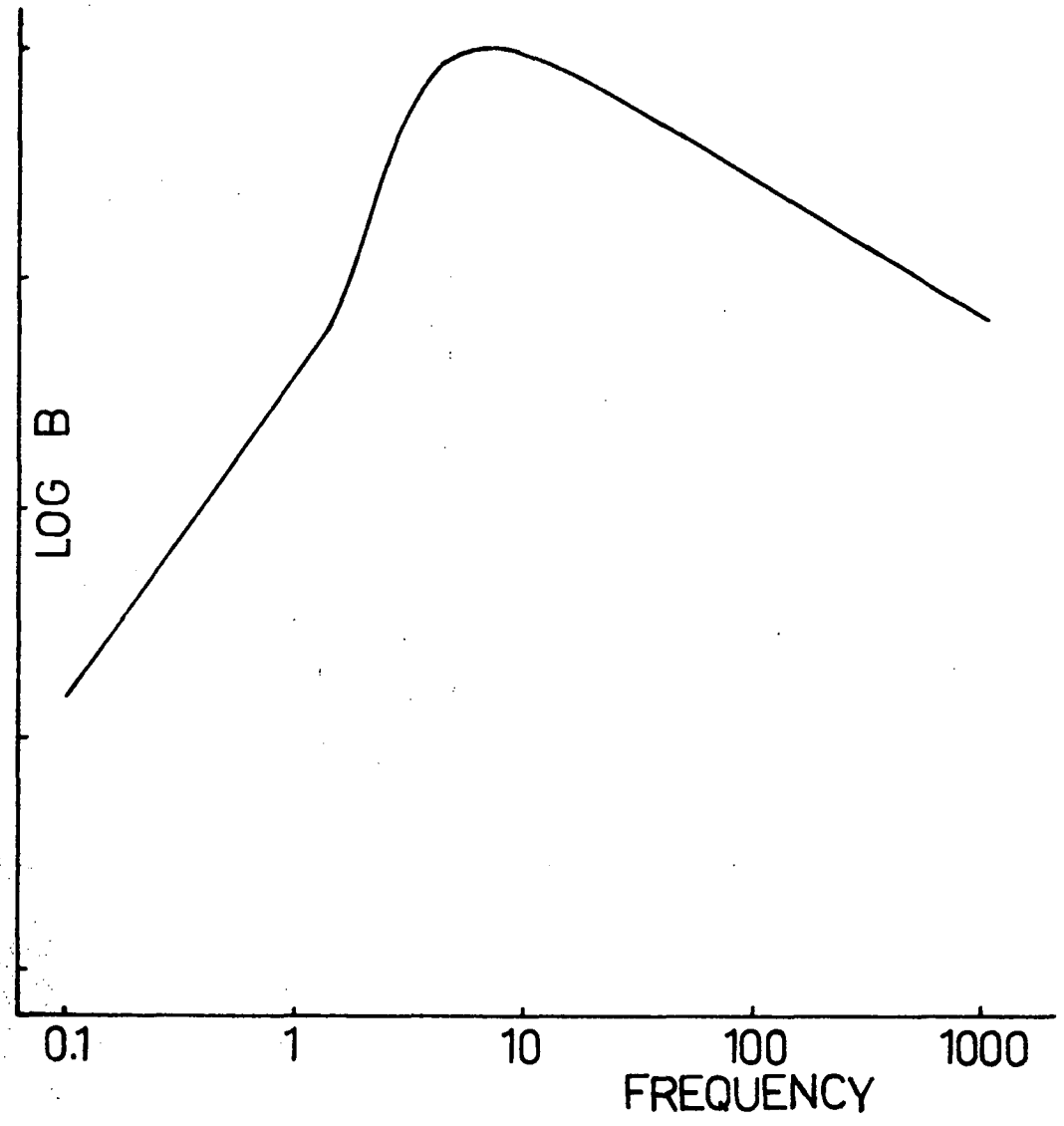

FIGURE 9

THE FUNCTION $B(f) = f^{-0.6} e^{-16/f^2} + 0.01 f^{1.4}(1 - e^{-16/f^2})$

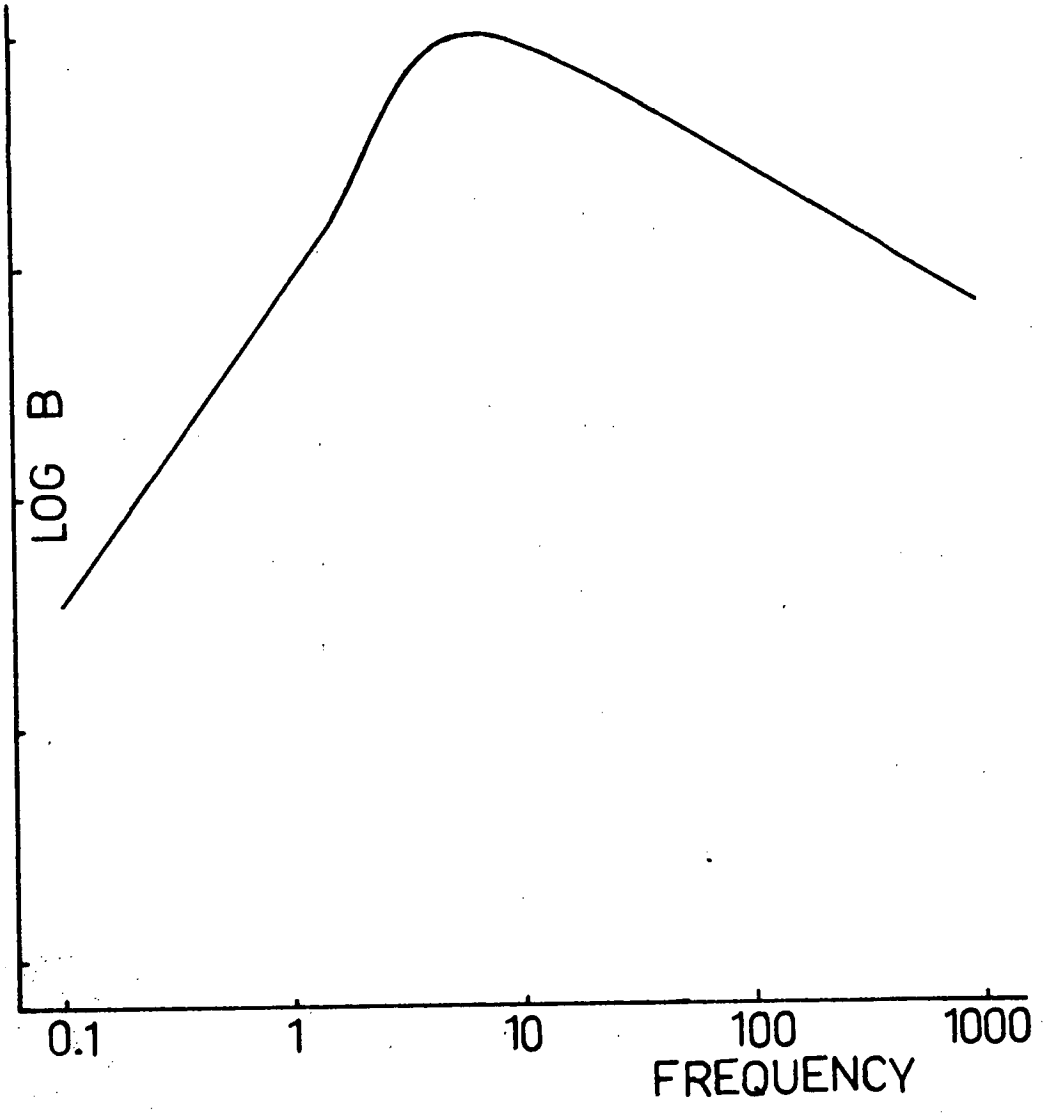

FIGURE 10

THE FUNCTION
$B(f)=f^{-0.6}e^{-16/f^2}+0.03f^{1.4}(1-e^{-16/f^2})$

REFERENCES FOR CHAPTER 2

Elder,F.R., Langmuir,R.V. and Pollack,H.C. 1948 *Phys. Rev. 74* 52.

Ginzburg,V.L.. 1961 *The propagation of Electromagnetic Waves in Plasmas* (North Holland).

Kiepenheuer,K.O. 1950 *Phys. Rev. 79* 738.

Mills,B.Y. 1964 *Annual Reviews of Astronomy and Astrophysics 1964* 185.

Scheuer,P.A.G. 1960 *Mon. Not. Roy. Astr. Soc. 120* 231.

Schwinger,J. 1949 *Phys. Rev. 11* 1912.

Shklovsky,I.S. 1960 *Cosmic Radio Waves* (Harvard).

Westfold,K.C. 1959 *Astrophys. J. 130* 241.

CHAPTER 3

DIFFICULTIES IN LOW FREQUENCY MEASUREMENTS

INTRODUCTION

The considerable advances that have been made in radio and related fields as a result of needs in radio astronomy indicate that few radio astronomy measurements are easy. As well as general problems, such as the achievement of large effective aerial apertures, each region of the spectrum has its own peculiar difficulties. In Chapter 4 intensity measurements of cosmic noise in the range 1 - 400 MHz are reviewed, and it is appropriate to preface this review with some comments on factors which influence the accuracy of these measurements.

CALIBRATION

Radio astronomy measurements are expressed in terms of *Equivalent Aerial Temperature*. This is the temperature of a black-body enclosure such that the power available from the aerial when placed in the enclosure is the same as when it is directed at the source. The calibration of a radio telescope consists of determining the function relating the output of the receiver to the equivalent aerial temperature.

The usual method is to replace the aerial with a calibrated noise source of the same impedance, and it is desirable that the range of noise temperatures available from the calibrator be similar to the range of aerial

temperatures obtained in the measurements. At frequencies above 100 MHz the aerial temperatures corresponding to all but the brightest regions of the sky are within the range of thermal loads. It is then possible to calibrate the system by replacing the aerial with a resistor of the same impedance whose temperature can be varied until a similar output is obtained. Difficulties arise in obtaining a thermal load with the same impedance characteristics as the aerial over the pass band of the receiver, and in estimating the losses in the aerial feeder cables.

At lower frequencies the equivalent aerial temperature is much higher ($T \propto \nu^{-2.6}$ approximately) and thermal loads are not suitable. The accepted standard in this frequency range is the temperature-saturated noise diode with a load equal to the aerial impedance. The action of the noise diode has been described by Van der Ziel (1955) and equivalent temperatures of up to 10000 degK can be obtained. However the noise diode is only a secondary standard and must itself be calibrated against a thermal source. Purton (1966) discusses the problems associated with this calibration, and figure 1 of his paper shows that although different diodes agree with one another, the agreement with thermal standards is not good.

Finally, at frequencies below 20 MHz the problem of a suitable standard becomes acute as the equivalent aerial temperatures corresponding to galactic observations are in the range 10^5 - 10^6 degK. The most satisfactory method appears to be that of Ellis (1965); he used a noise diode and a calibrated broad-band amplifier to achieve a noise signal approximately equal to the cosmic noise. However it must be accepted that the calibration error in low frequency measurements are much more serious than at higher frequencies.

GROUND-BASED MEASUREMENTS

Ionospheric effects:

Ground-based measurements below 20 MHz are liable to show ionospheric effects. These can be minimised by the choice of a suitable observatory site and the selection of favourable observing periods. Those influences remaining can be estimated with good accuracy and the intensities corrected accordingly.

For galactic radio noise to be observed from the ground the ionospheric critical penetration frequency f_oF_2 must be less than the observing frequency. World contours of f_oF_2 show that it is lowest during winter nights in

years of low solar activity, and that it is minimal for geomagnetic latitudes between 40^{o} and 60^{o}. Figure 1 (after Ellis and Hamilton, 1966) shows the variation of f_oF_2 with geographic latitude observed by the *Alouette* satellite. Figure 2 (after Ellis, 1965) gives the number of hours per night that f_oF_2 was less than 4 MHz for the years 1961 - 63 at Hobart. It is clear that for suitably located observatories the observing time at these frequencies can be considerable. In fact in 1955 f_oF_2 was less than 2 MHz for 60 nights out of 90 during the months of June, July and August (Reber and Ellis, 1956).

When the critical frequency is sufficiently low for the reception of cosmic noise there is still the possibility that the observed intensity is depressed below the actual intensity by ionospheric absorption and screening due to ionospheric refraction. These effects can be estimated and the subject is discussed fully by Ellis (1965); his conclusions are summarised in figures 3 - 5 and in Table 1 which details the corrections applied to his low frequency observations.

The reliability of observing conditions at 4.7 MHz at Hobart is illustrated in figures 6 and 7 from Ellis and Hamilton (1966). Figure 7 illustrates the reproducibility

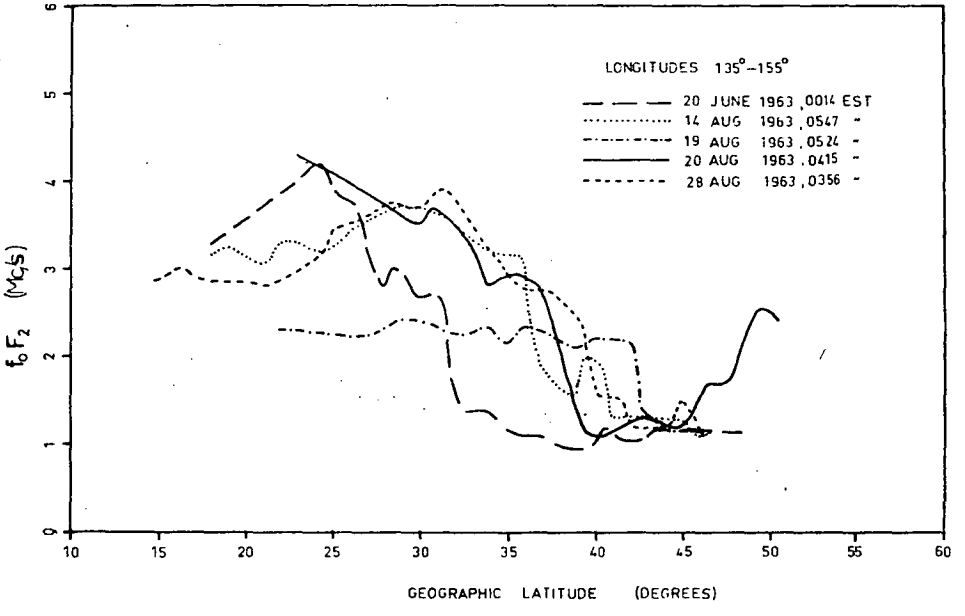

Sample curves showing the variation of ionospheric critical frequency f_0F_2 with geographic latitude observed by Alouette satellite.

FIGURE 1

after Ellis and Hamilton (1966)

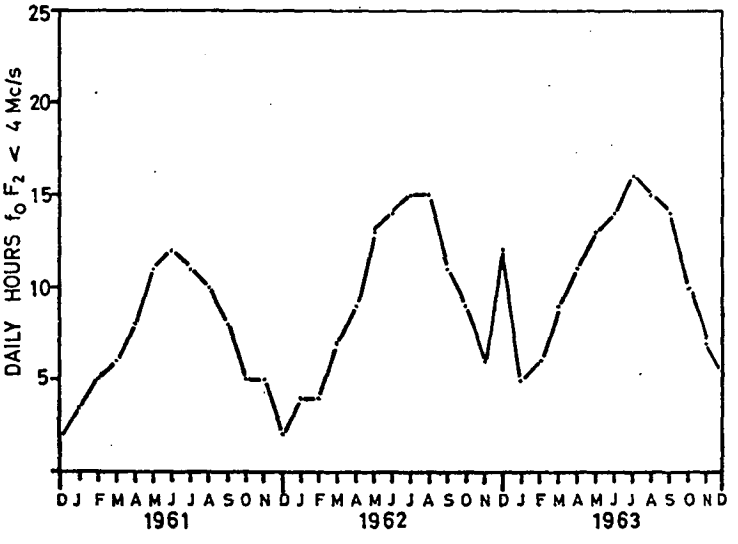

Year by year variation of the number of hours per night for which $f_0F_2 < 4$ Mc/s at Hobart.

FIGURE 2

after Ellis (1965)

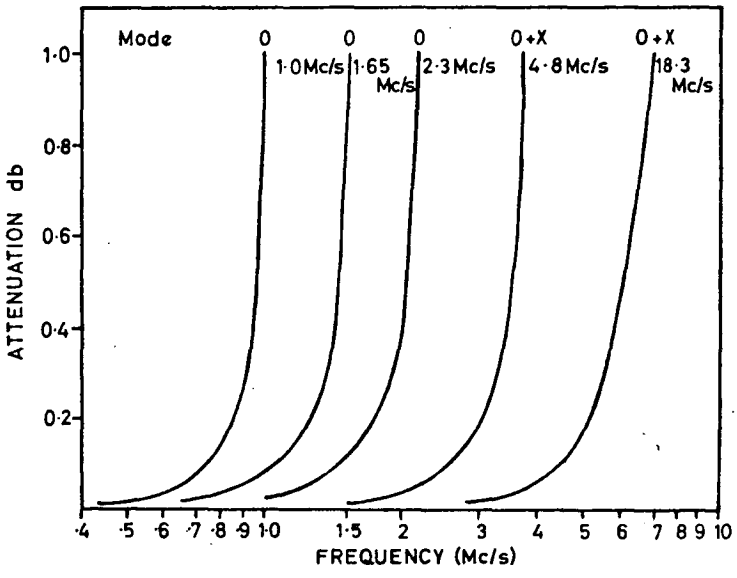

Variation of F region attenuation with f_0F_2

FIGURE 3

after Ellis (1965)

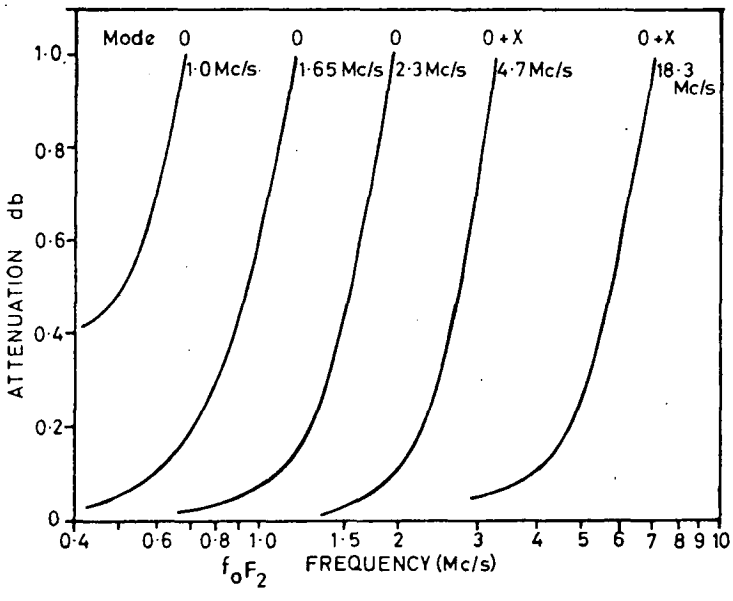

Attenuation due to screening of antenna beam by F region.

FIGURE 4

after Ellis (1965)

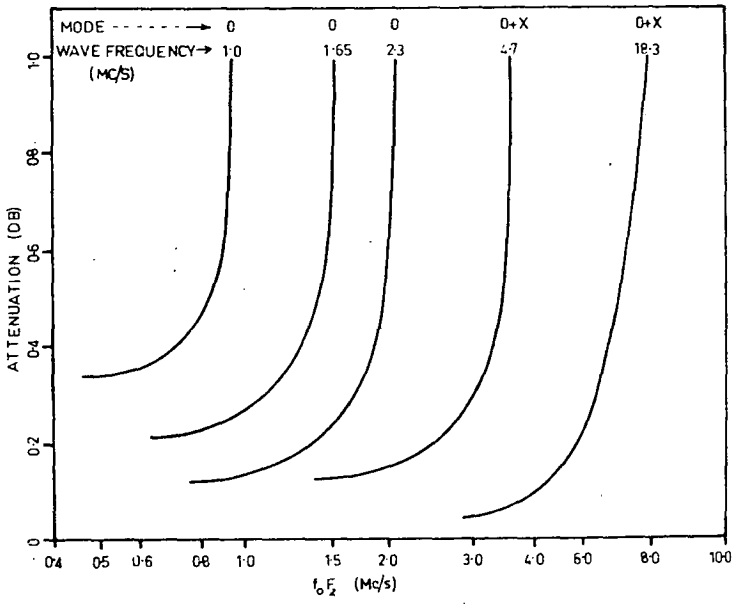

Ionospheric attenuation as a function of f_0F_2 for different observing frequencies (after Ellis 1965).

FIGURE 5

TABLE I

ATTENUATION (dB) DUE TO IONOSPHERIC EFFECTS

after Ellis (1965)

Frequency (MHz)	1.65	2.3	4.8	9.6
	O-mode	only		
D region	0.25	0.14	0.13	0.05
F region absorption	0.1	0.05	0.05	-
F region screening	0.6	0.25	0.05	-

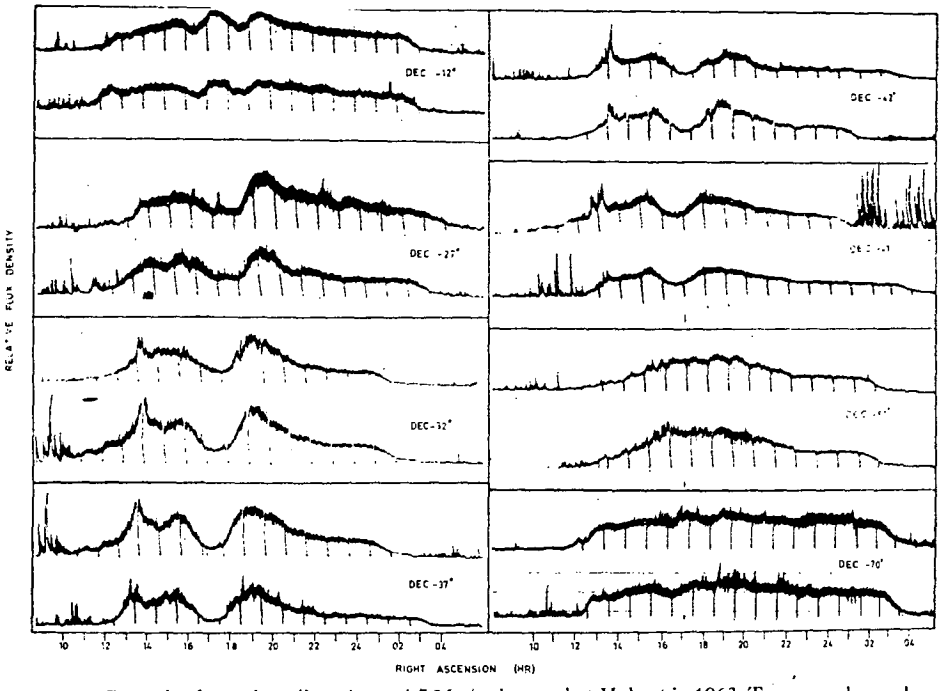

Records of cosmic radio noise at 4.7 Mc/s observed at Hobart in 1963. Two records are shown for each declination.

FIGURE 6

after Ellis and Hamilton (1966)

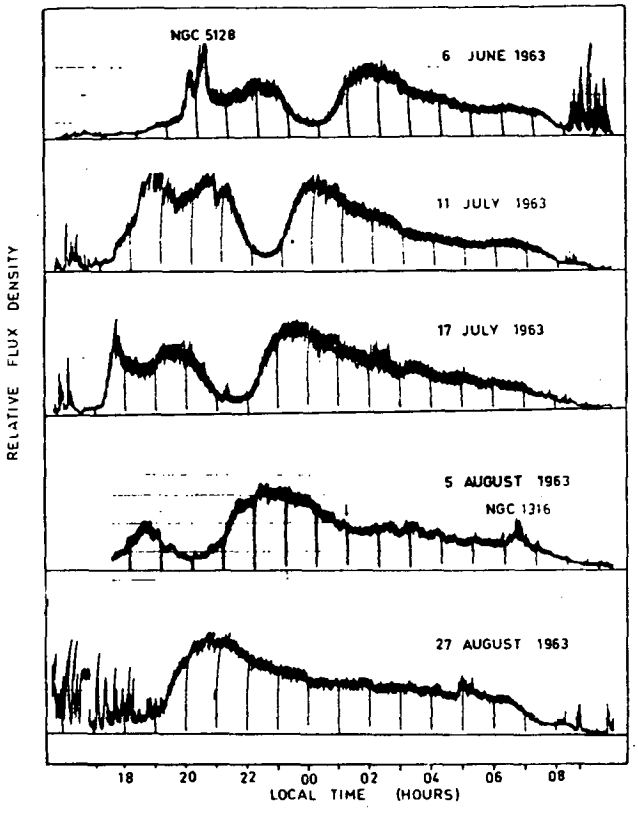

Records of cosmic radio noise for declination −37° obtained at different times showing sidereal variation.

FIGURE 7

after Ellis and Hamilton (1966)

of records throughout a 14 week period.

Man-made interference:

Interference from transmitting stations can place more restrictionc on observing time than ionospheric effects. High level interference is easily recognised by aural monitoring, but low level interference is difficult to detect and the only safeguard is the duplication of records of each region of the sky at different times of the year.

SATELLITE AND ROCKET MEASUREMENTS

In spite of the availability of ionospheric data to the contrary it has been a common belief that observations at frequencies less than 10 MHz must be made from above the ionosphere. However those measurements that have been made by rocket and satellite have given widely varying results. While the problems of ionospheric absorption and refraction are certainly reduced, the difficulties associated with calibration and man-made interference are increased by the remoteness of the receiver in the case of satellites and the brevity of the observing period in the case of rockets (typically 25 minutes). In addition to the problem of determining where the aerial is pointing two new sources of

error are encountered, varying aerial impedance and exospheric emissions.

Aerial impedance:

The effects of the residual ionospheric plasma at the receiver altitude can be to produce marked variations in aerial impedance as a function of frequency or height (Haddock, Schulte and Walsh, 1963). This has made absolute calibration of the measurements impossible in most cases, and rendered relative measurements unreliable in others.

Exospheric emissions:

Ellis (1964) has considered the possibility that cyclotron radiation is generated by electrons in the exosphere and radiated in the direction away from the earth. He concluded that the total radiated power may be from 1 to 1000 Watts in the frequency range 200 KHz to 1 MHz. The measurements of Huguenin (1963) at 900 KHz are completely inconsistent with other measurements of the galactic spectrum, being an order of magnitude too high, and they may provide experimental verification of the theory.

CONCLUSIONS

The assessment of any experiment requires a knowledge of the difficulties that must be overcome in making the measurements. In the case of low frequency radio astronomy attention must therefore be given to the calibration procedure, especially at frequencies below 20 MHz where no suitable primary standard exists, as well as to the elimination of problems that arise from the choice of observatory. Ground-based measurements may be subject to ionospheric effects and transmitting station interference. Satellite and rocket experiments may be affected by variations in aerial impedance and pointing accuracy, as well as interference from transmitting stations and the exosphere.

REFERENCES FOR CHAPTER 3

Ellis,G.R.A. 1964 *Aust. J. Phys.* *17* 63.

Ellis,G.R.A. 1965 *Mon. Not. Roy. Astr. Soc.* *130* 429.

Ellis,G.R.A. and Hamilton,P.A. 1966 *Astrophys. J.* *143* 227.

Haddock,F.T., Schulte,H.F. and Walsh,D. 1963 *Astron. J.* *68* 75.

Huguenin,G.R. 1963 *Ph.D. Thesis* (Harvard University).

Purton,C.R. 1966 *Mon. Not. Roy. Astr. Soc.* *133* 463.

Reber,G. and Ellis,G.R.A. 1956 *J. Geophys. Res.* *61* 1.

Van der Ziel,A. 1955 *Noise* (Chapman & Hall) p. 90.

CHAPTER 4

THE LOW RESOLUTION GALACTIC SPECTRUM

INTRODUCTION

In this chapter the low resolution (i.e. beamwidth > 25^{o}) measurements of cosmic noise are reviewed with the aim of obtaining spectra of the galactic emission for the directions of the galactic poles. The extraction of this information has not been assisted by the variety of equipments and methods that have been used, nor by the manner in which many of the results have been presented. It is necessary therefore to commence with a discussion of problems associated with the comparison of different measurements, followed by the system used in selecting the observations. Each experiment is then briefly summarised, the measurements are assessed and the implications discussed.

COMPARISON OF DIFFERENT MEASUREMENTS

There are now available results from a large number of low resolution measurements of cosmic noise, made with a variety of aerial systems and receivers. For example ground-based systems have included single dipoles over a ground screen, blocks of dipoles over an earth ground and corner reflectors, while satellite and rocket measurements have used aerials with widely varying directional characteristics. Different measurements could be expected to give similar results only if the radio sky shows no small scale structure.

Unfortunately the high resolution surveys show that there are no regions of the sky 30° in diameter that are free from small scale structure. The best that can be done is to select regions where the fine structure appears at the lowest contrast, that is in the directions of the galactic poles. It is likely that much of the discrepancy between observations is due to differences in aerial space factor. Comparable results are only possible if the aerial systems are identical when scaled with wavelength.

Observers have quoted measurements for a variety of directions. It was common at one time to quote maximum and

minimum values over the daily cycle and to compare these results for different frequencies, the implied assumption being that maximum and minimum occur at the same positions for all frequencies. A comparison of the 2.1 MHz survey by Reber (1968) with any survey above 20 MHz shows how misleading it can be to quote extreme values.

A further problem in comparing different results is that of the calibration method adopted. The difficulty of calibration has already been discussed; a re-calibration of noise standards used by Turtle *et al* (1962) led to a revision of their results at 38 MHz by 13% (Purton, 1966) and this indicates the magnitude of *systematic* errors that are possible in ground-based measurements. Calibration problems are even more serious when measurements are made from satellites (Hartz, 1964).

Finally, the problem of extracting a spectrum has been difficult because of the methods of displaying results that have been used in the literature. Many observers have presented their measurements in graphical form only, and on log-log graphs where 3 cycles by 2 cycles are given less than 4 square inches on the journal page. It seems possible that this has contributed to the unfortunate tendency for results to be misquoted in subsequent papers.

It is suggested that in future the results of these important measurements should be presented numerically in terms of equivalent aerial temperature, since this is the unit of actual measurement and there is no ambiguity of interpretation. The confusion between flux density and brightness (flux density per solid angle) which is apparent in some papers, and which has led to the inclusion or exclusion of factors of 4π, would then be of little consequence.

THE OBSERVATIONS

The various measurements are summarised below. The experiments are described first, in alphabetical order of first author with the observations in the two hemispheres presented separately. The results are then given in two tables, in equivalent aerial temperature (degK) and brightness (Watts metre^{-2} Hertz^{-1} steradian^{-1}). The conversion from temperature to brightness is the usual one based on the Rayleigh-Jeans law (Krauss, 1966):

$$\text{brightness } B = \frac{2kT}{\lambda^2} \qquad W\,m^{-2}\,Hz^{-1}\,ster^{-1}$$

where k = Boltzmann's constant, 1.3805_{10}-23 *joule deg*$^{-1}$

T = temperature, *degK*

λ = wavelength, *metres*.

Where results for a range of observing directions were given in the original paper the values for the position closest to the north or south galactic pole are quoted. Apart from this selection of observing direction and possible conversion of units the results are as originally presented. No attempt has been made to allow for differences in telescope resolution.

NORTHERN HEMISPHERE OBSERVATIONS

Adgie and Smith, 1956:

Observations were made at 38 MHz, 81.5 MHz and 175 MHz using aerials scaled with wavelength, with fan beams of $25^{o} \times 70^{o}$. Calibrations were against thermal standards. Profiles for 24 hours are presented and the results were taken from these for 13^{h} RA. The results are quoted in units of Watts metre^{-2} Hz^{-1} but are apparently in Watts metre^{-2} Hz^{-1} sterad^{-1}.

Alexander and Stone, 1965:

Observations were made by rocket using a "short

dipole antenna, four TRF receivers, a reference noise source and an antenna impedance probe". The results quoted were obtained in the 5 minutes the rocket was above the 1000 Km level, and refer to "the hemisphere centred at about $l = 100^{o}$, $b = 80^{o}$".

Andrew, 1966:

Single dipoles were used at each frequency above a wire ground screen. Calibration was against a noise diode source which had itself been calibrated against thermal sources by Purton (1966). Only observations made when the ionosphere critical frequency was less than one-fifth the observing frequency were used. A table of aerial temperatures against sidereal time for declination $+52^{o}$ is given and the values selected here are for 13^{h} RA.

Benediktov *et al*, 1965:

These observations were made from the satellites *Electron-2* and *Electron-4* at a height of about 70 000 Km above the earth. Measurements were made with single dipoles in each case and calibration was against a noise generator every hour. Sporadic radio emissions, apparently from the ionosphere, were detected from time to time and "sometimes a general rise of radiation level was observed".

These emissions fell off with increasing distance from the earth, and their directional properties correspond with those predicted by Ellis (1964).

Costain, 1960:

Identical corner reflectors scaled with wavelength were used, with beamwidths of $15^{\circ} \times 40^{\circ}$. Thermal and noise diode calibrations were used. Profiles at several declinations are given and the results are quoted in equivalent aerial temperature.

Cottony and Johler, 1952:

Single half-wave dipoles were used at each frequency and calibration was against a noise diode. Results in this classic paper were quoted for daily maxima and minima in a wide variety of units to suit everyone. The diurnal variations are shown in their figure 4, and this has been used to correct the numerically quoted temperatures to those in the direction of $b \simeq 90^{\circ}$.

Hartz, 1964:

Measurements were made from the *Alouette* satellite using a swept-frequency receiver designed primarily as an ionosonde receiver. The AGC line of the receiver was monitored to measure cosmic noise.

" .... the spectrum of the galactic radio emission between 1.5 and 5 MHz has been determined fairly reliably, but it has not been possible .... to extend this up to 10 MHz with any accuracy. Although there is no provision for absolute gain calibration of the receiver in flight, the data are so consistent as to give confidence to the pre-flight calibration. .... galactic noise measurements have been made under a variety of local electron densities .... these values have then been extrapolated to zero electron density and the free space values obtained .... are taken as a measure of the galactic emission".

Hugill and Smith, 1965:

A 40 metre dipole on the *Ariel II* satellite was used for cosmic noise measurements between 0.7 and 3.5 MHz. In-flight calibration was against a 1 MHz oscillator calibrated before the flight, and the receiver was designed to have a high input impedance so that it acted as a voltmeter, effectively measuring the open-circuit voltage at the aerial terminals. In this way the effects of changing aerial impedance were minimised. The results were quoted as brightness for the region 12^h - 16^h RA and 40° - 50° declination, which is close to the north galactic pole.

Korobkov, 1964:

These measurements refer to the region $l = 98.5^{\circ}$ $b = -5.3^{\circ}$ and are therefore not included in the final spectra. They are quoted because others have included them in reviews of the spectrum. The observations were made with scaled dipole arrays with identical parameters, and the beamwidths were $35^{\circ} \times 25^{\circ}$. Calibration was against a diode noise generator. The results were presented as a graph of aerial temperature against frequency.

Papagiannis, 1964:

Measurements at 7 MHz were made by satellite. A signal generator was used for calibration. Measurements at 0.7 and 2.2 MHz were made from a rocket flight, and again a signal generator was used for calibration. It is apparent that the observations at 0.7 MHz in particular do not represent a measure of cosmic noise in view of the disagreement with all other measurements; it is probable that the records were strongly influenced by outward emissions from the exosphere (Ellis, 1964).

Parthasarathy and Lerfald, 1965:

Observations were made with aerials of identical beamwidth (30°). Particular attention was given to the

elimination of ionospheric effects using a dual polarization method of recording. Calibration was with a diode noise source and an auxiliary amplifier for the lower frequencies. Profiles of aerial temperature in sidereal time are given for declination $+65^{\circ}$, and the results quoted here are for 13^{h} RA scaled from these profiles.

Purton, 1966:

Purton went to some lengths to calibrate a number of diode noise generators against thermal standards, and the scatter in his calibration graphs (figure 1 of his paper) indicates the magnitude of the low frequency calibration problem. He summarises his own work and that of Bridle (1967), and presents a re-assessment of the measurements of Turtle *et al* (1962) following the new calibrations. In all cases the aerials used were corner reflectors with $15^{\circ} \times 50^{\circ}$ beams. A table of aerial temperatures against frequency for the "halo" region is given.

Walsh *et al*, 1963:

These results are not directly applicable since they apply to a hemisphere centred at $l = 114^{\circ}$, $b = -19^{\circ}$. Measurements were made by rocket during the few minutes that

it was at a suitable height. Some difficulty was experienced in allowing for (a) ionospheric emissions and (b) variations in aerial impedance apparently produced by plasma sheath which formed about the antenna.

SOUTHERN HEMISPHERE OBSERVATIONS

Chapman and Molozzi, 1961:

Observations at 3.8 MHz were made by satellite. Calibration was by some signal of unspecified nature coupled to the antenna with a calibrated loop. Difficulties were initially encountered in explaining the variations in signal strength with satellite position; these were subsequently explained as (a) variations of aerial impedance due to the ionosphere, (b) restrictions in antenna aperture due to ionospheric refraction, and (c) variations in sky brightness. The exact process of determining the sky brightness temperature is not clear and the result is apparently rather high. The results are quoted for 0530^h RA and -30^o declination.

Ellis, 1957:

Measurements at 3.8 MHz were made with a dipole array with a $50^o \times 26^o$ beam, and at the other frequencies with single half-wave dipoles. Calibration was with diode

noise generators. The results are presented on graphs of aerial temperature and "total intensity" against frequency, points being plotted for daily maxima and minima. Temperatures for the galactic pole were obtained by interpolation between the maxima and minima.

Ellis, 1965:

Scaled aerials of $32^{o} \times 40^{o}$ at each frequency were used, above an earth ground. The measurements were corrected for ground losses following a series of experiments on ground conductivity. Diode noise generators were used with calibrated amplifiers to achieve calibration signals of the same magnitude as the cosmic noise signals. This paper is notable for the discussion on the effects of the ionosphere. Results are given graphically as flux density per steradian for the direction of the south galactic pole.

Hamilton and Haynes, 1969:

This is not a low resolution measurement, but is quoted in the absence of any low resolution measurements above 85 MHz for the southern sky. The measurement was made using the 210 foot telescope at Parkes at 153 MHz (beamwidth 2.2^{o}) during the high resolution survey reported later in this thesis. The aerial was replaced with a thermal standard to give a

temperature at the south *celestial* pole. The temperature corresponding to a low resolution measurement at the south galactic pole was obtained from the survey.

Higgins and Shain, 1954:

Observations were made with a dipole array with beamwidth = 29^{o}. Calibration was against a diode noise generator. A profile of equivalent aerial temperature against sidereal time for declination -32^{o} is given, from which the value at 0030^{h} RA is taken.

Reber and Ellis, 1956:

These measurements were made in a similar manner to those of Ellis (1957), and the results were taken from the graph in that paper, where the presentation was more suitable.

Shain and Higgins, 1954:

A profile of aerial temperature against sidereal time was obtained for declination -32^{o}, with an aerial beam of 17^{o}. Calibration of this survey was against a diode noise generator.

Yates and Wielebinski, 1966:

Measurements were made with a single folded half-wave

dipole at each frequency, with ground screens of 2 inch wire mesh. Calibration was against diode noise generators, with the aerial signal attenuated to the level of the noise generator. Profiles of aerial temperature are given and the aerial temperatures at 0040^h RA and -34^o declination are also given numerically. The latter results are nearest to the south galactic pole and are quoted here.

SUMMARY

The observations in the two hemispheres are summarised in Table I and Table II, which are keyed to the list of observers given in Table III. Figures 1 - 4 present this information graphically as plots of aerial temperature and brightness against frequency.

The agreement between the measurements in each hemisphere is good, and the elimination of the less satisfactory points (e.g. *North:* Hartz [2.3 MHz], Papagiannis [0.7 MHz, 7 MHz]; *South:* Hartz [2.3 MHz], Chapman and Molozzi [3.8 MHz]) emphasizes the agreement within those remaining.

The great variety of methods and equipments that have led to these results can only increase one's confidence in accepting figure 2 and figure 4 as reliable measures of the galactic polar spectra.

TABLE I

SPECTRAL MEASUREMENTS OF NORTH GALACTIC POLE

Frequency (MHz)	Equivalent Aerial Temperature (degK)	Sky Brightness ($W\,m^{-2}\,Hz^{-1}\,ster^{-1}$)	Observer
0.7	$4.0_{10}8$	$6.0_{10}-20$	9
0.72	$3.3_{10}7$	$5.2_{10}-21$	4
1.1	$2.2_{10}7$	$8.0_{10}-21$	4
1.25	$2.3_{10}7$	$1.1_{10}-20$	8
1.5	$2.2_{10}7$	$1.5_{10}-20$	8
1.6	$1.1_{10}7$	$8.7_{10}-21$	4
1.75	$1.6_{10}7$	$1.5_{10}-20$	8
1.91	$2.0_{10}7$	$2.2_{10}-20$	2
2.0	$1.1_{10}7$	$1.3_{10}-20$	8
2.2	$9.4_{10}6$	$1.4_{10}-20$	9
2.3	$1.1_{10}7$	$1.8_{10}-20$	7
2.5	$7.3_{10}6$	$1.4_{10}-20$	8
2.85	$1.1_{10}7$	$2.7_{10}-20$	2
3.0	$5.1_{10}6$	$1.4_{10}-20$	8
3.4	$4.9_{10}6$	$1.8_{10}-20$	8
3.6	$4.3_{10}6$	$1.7_{10}-20$	2
4.7	$3.2_{10}6$	$2.2_{10}-20$	2
5.0	$1.1_{10}6$	$8.1_{10}-21$	10

TABLE I continued

Frequency (MHz)	Equivalent Aerial Temperature (degK)	Sky Brightness ($W\ m^{-2}\ Hz^{-1}\ ster^{-1}$)	Observer
7.0	$1.5_{10}6$	$2.3_{10}-20$	9
10.0	$2.3_{10}5$	$6.9_{10}-21$	3
10.0	$2.9_{10}5$	$8.9_{10}-21$	10
13.1	$1.0_{10}5$	$5.4_{10}-21$	3
13.15	$9.0_{10}4$	$4.8_{10}-21$	11
17.5	$5.4_{10}4$	$5.0_{10}-21$	3
17.5	$4.8_{10}4$	$4.5_{10}-21$	11
20.0	$4.3_{10}4$	$5.2_{10}-21$	10
25.0	$2.6_{10}4$	$5.0_{10}-21$	6
26.3	$1.8_{10}4$	$3.7_{10}-21$	11
26.5	$2.0_{10}4$	$4.2_{10}-21$	3
30.0	$1.7_{10}4$	$4.7_{10}-21$	10
35.0	$1.1_{10}4$	$4.1_{10}-21$	6
38.0	$9.7_{10}3$	$4.3_{10}-21$	1
38.0	$8.0_{10}3$	$3.5_{10}-21$	3
38.0	$7.0_{10}3$	$3.1_{10}-21$	5
38.0	$7.8_{10}3$	$3.5_{10}-21$	11
50.0	$5.0_{10}3$	$3.8_{10}-21$	6
50.0	$4.3_{10}3$	$3.3_{10}-21$	10

TABLE I continued

Frequency (MHz)	Equivalent Aerial Temperature (degK)	Sky Brightness ($W\ m^{-2}\ Hz^{-1}\ ster^{-1}$)	Observer
75.0	$1.8_{10}3$	$3.1_{10}-21$	6
81.5	$1.5_{10}3$	$3.0_{10}-21$	1
81.5	$1.1_{10}3$	$2.3_{10}-21$	11
81.5	$1.2_{10}3$	$2.4_{10}-21$	5
110.0	700	$2.6_{10}-21$	6
175.0	266	$2.5_{10}-21$	1
178.0	169	$1.6_{10}-21$	11
178.0	185	$1.8_{10}-21$	5
404.0	17.9	$9.0_{10}-22$	11

TABLE II

SPECTRAL MEASUREMENTS OF SOUTH GALACTIC POLE

Frequency (MHz)	Equivalent Aerial Temperature (degK)	Sky Brightness ($W\ m^{-2}\ Hz^{-1}\ ster^{-1}$)	Observer
0.9	$1.8_{10}7$	$4.5_{10}-21$	17
1.43	$1.1_{10}7$	$6.6_{10}-21$	17
1.65	$1.0_{10}7$	$8.6_{10}-21$	14
2.13	$8.0_{10}6$	$1.1_{10}-20$	17
2.3	$8.0_{10}6$	$1.3_{10}-20$	14
2.3	$1.8_{10}7$	$2.9_{10}-20$	7
3.8	$8.1_{10}6$	$3.6_{10}-20$	12
3.8	$4.0_{10}6$	$1.8_{10}-20$	13
4.4	$2.9_{10}6$	$1.7_{10}-20$	13
4.8	$3.0_{10}6$	$2.1_{10}-20$	14
5.65	$1.8_{10}6$	$1.8_{10}-20$	13
9.15	$6.0_{10}5$	$1.5_{10}-20$	16
9.6	$7.2_{10}5$	$2.0_{10}-20$	14
10.05	$3.8_{10}5$	$1.2_{10}-20$	13
14.1	$1.3_{10}5$	$7.7_{10}-21$	19
18.3	$7.5_{10}4$	$7.7_{10}-21$	18

TABLE II continued

Frequency (MHz)	Equivalent Aerial Temperature (degK)	Sky Brightness ($W\ m^{-2}\ Hz^{-1}\ ster^{-1}$)	Observer
20.0	$5.5_{10}4$	$6.7_{10}-21$	19
30.0	$1.7_{10}4$	$4.8_{10}-21$	19
48.5	$5.1_{10}3$	$3.7_{10}-21$	19
85.0	$1.2_{10}3$	$2.7_{10}-21$	19
153.0	240	$1.7_{10}-21$	15

TABLE III

LIST OF OBSERVERS

1	Adgie and Smith (1956)
2	Alexander and Stone (1965)
3	Andrew (1966)
4	Benediktov *et al* (1965)
5	Costain (1960)
6	Cottony and Johler (1952)
7	Hartz (1964)
8	Hugill and Smith (1965)
9	Papagiannis (1964)
10	Parthasarathy and Lerfald (1965)
11	Purton (1966)
12	Chapman and Molozzi (1961)
13	Ellis (1957)
14	Ellis (1965)
15	Hamilton and Haynes (1969)
16	Higgins and Shain (1954)
17	Reber and Ellis (1956)
18	Shain and Higgins (1954)
19	Yates and Wielebinski (1966)

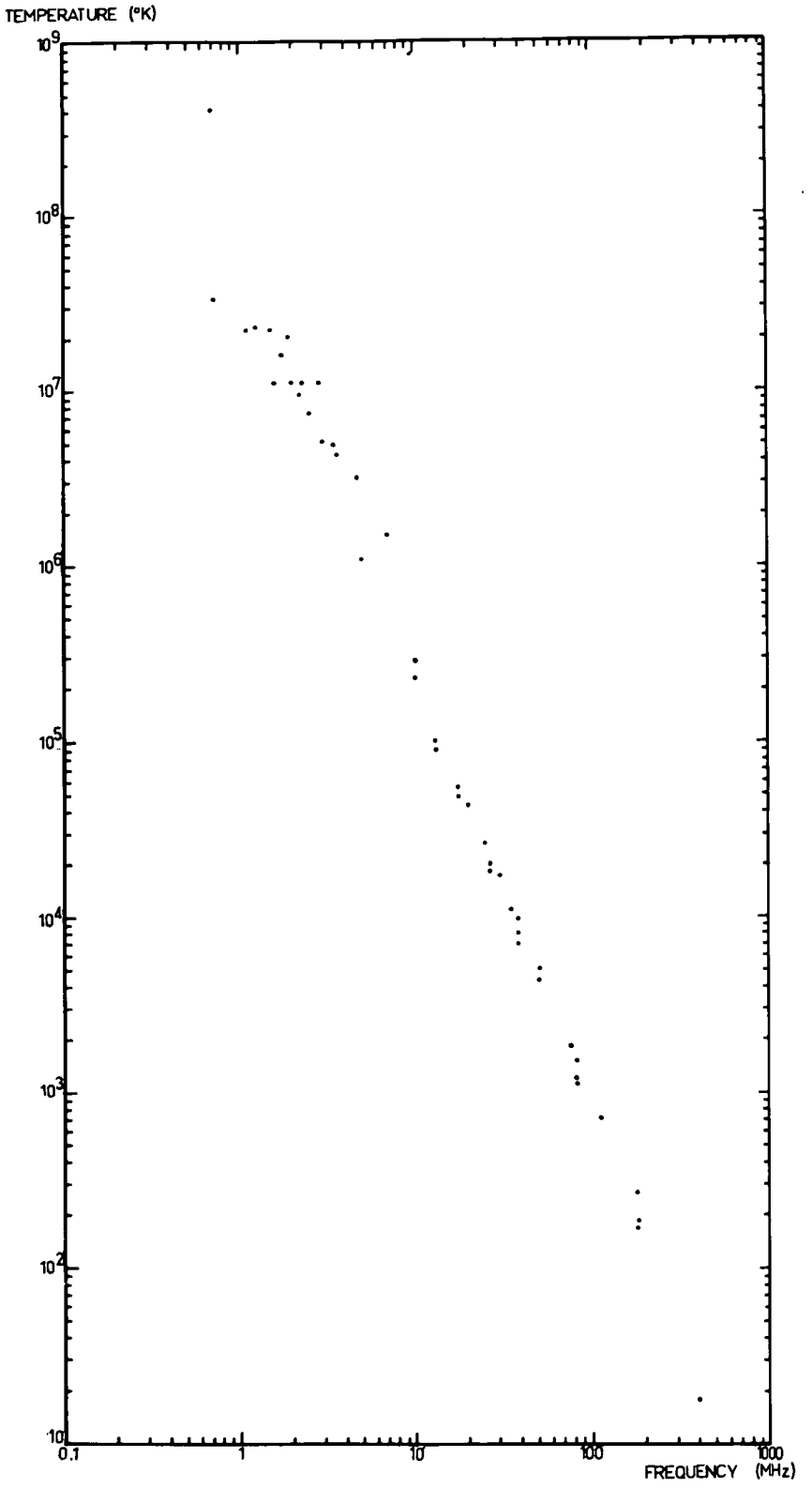

SPECTRUM OF NORTH GALACTIC POLAR REGION

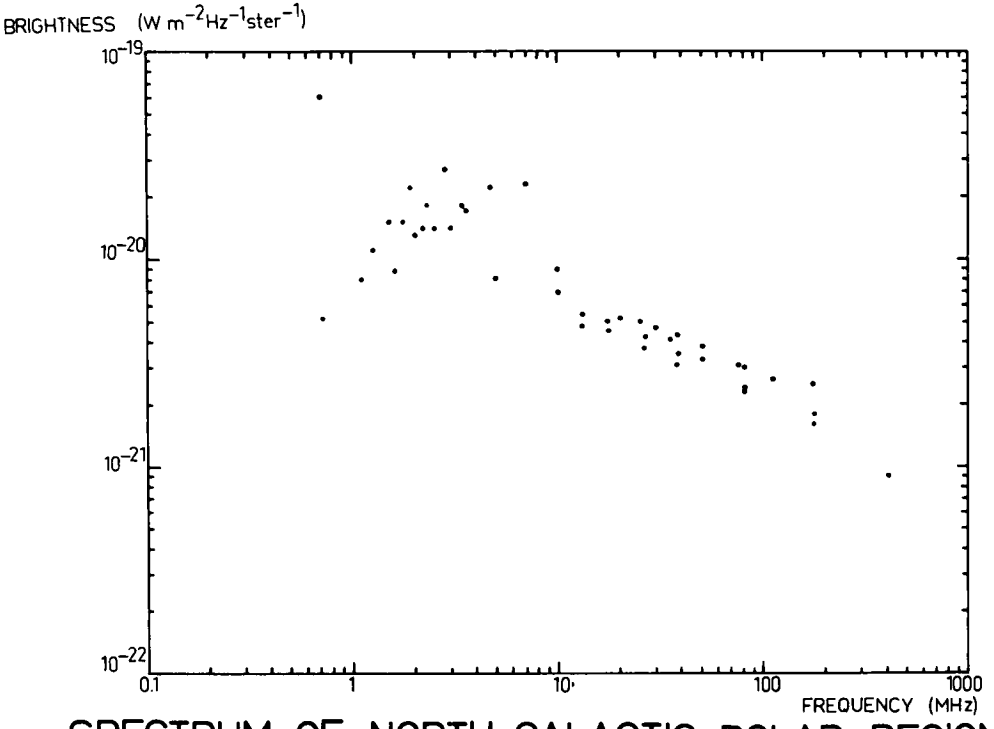

SPECTRUM OF NORTH GALACTIC POLAR REGION

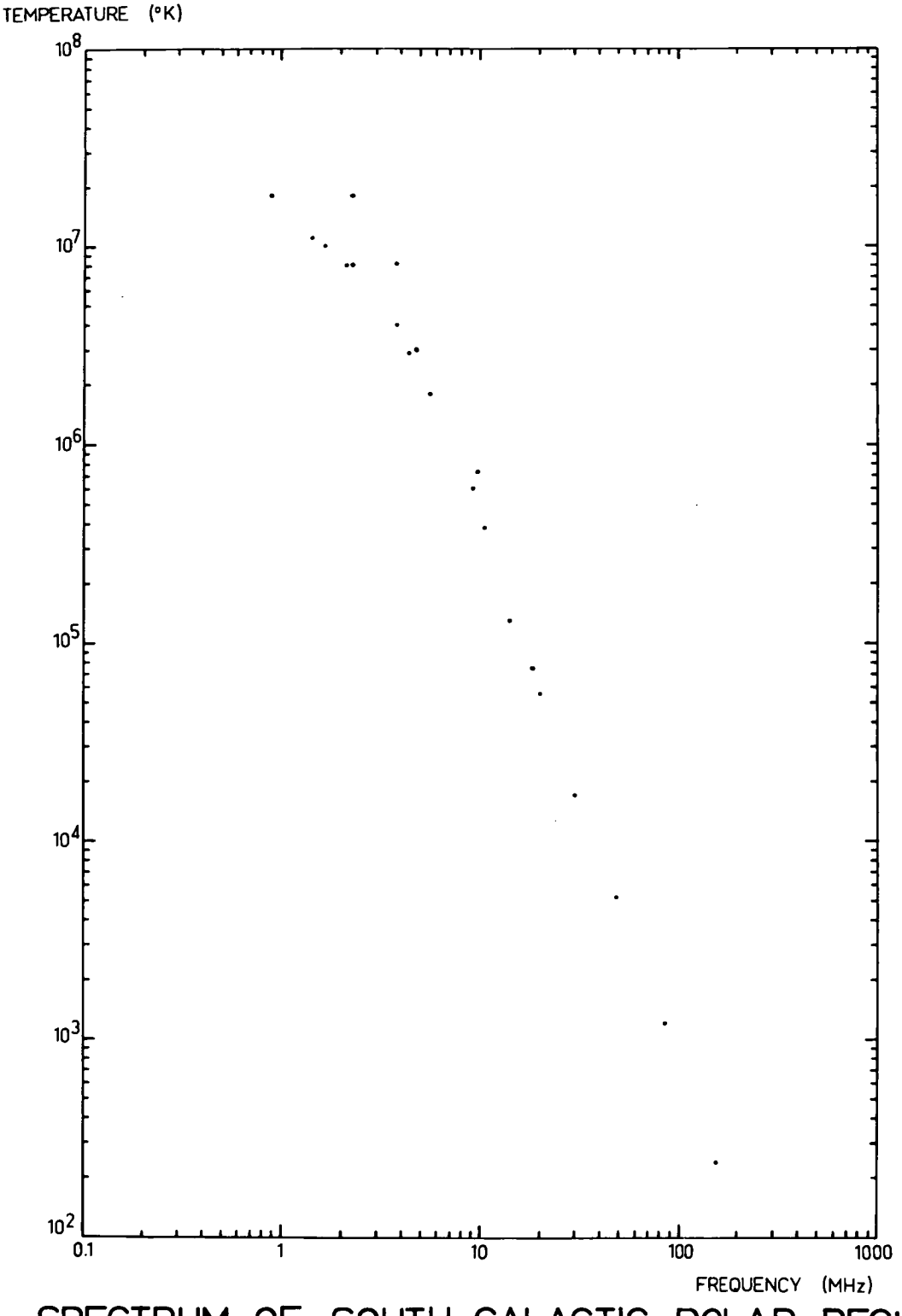

SPECTRUM OF SOUTH GALACTIC POLAR REGION

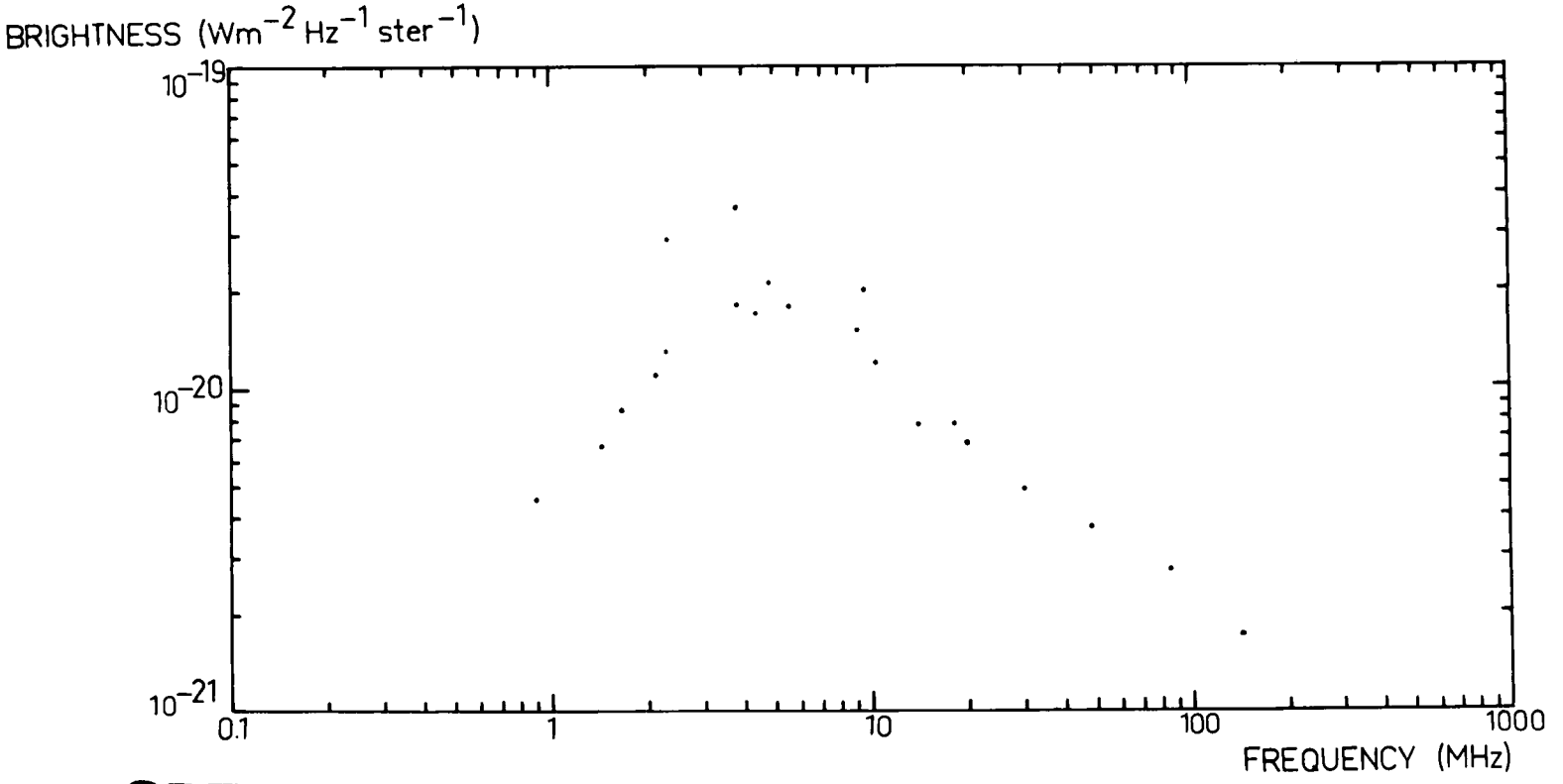

SPECTRUM OF SOUTH GALACTIC POLAR REGION

DISCUSSION

It has been the custom in discussions of the low resolution spectra to present the data from both hemispheres together, and to regard them as measurements of the same phenomenon. Indeed, if the points from figures 2 and 4 are plotted on the one graph this view is apparently justified as they are more or less uniformly distributed about a smooth curve. However in figure 5 the results are presented in a different way; the hemispheres are identified and the two sets of points are plotted with displaced vertical scales. This presentation suggests that there are real differences between the two spectra.

It is convenient to divide the spectrum into three regions for discussion.

The spectrum above 10 MHz:

The difference in slopes in the region from 10 - 100 MHz is striking. The variation of brightness S with frequency ν is well described by

$$S \propto \nu^{-\alpha} \qquad (1)$$

where the spectral index α has the values

$\alpha \simeq 0.4$ (north galactic pole),

and $\alpha \simeq 0.6$ (south galactic pole).

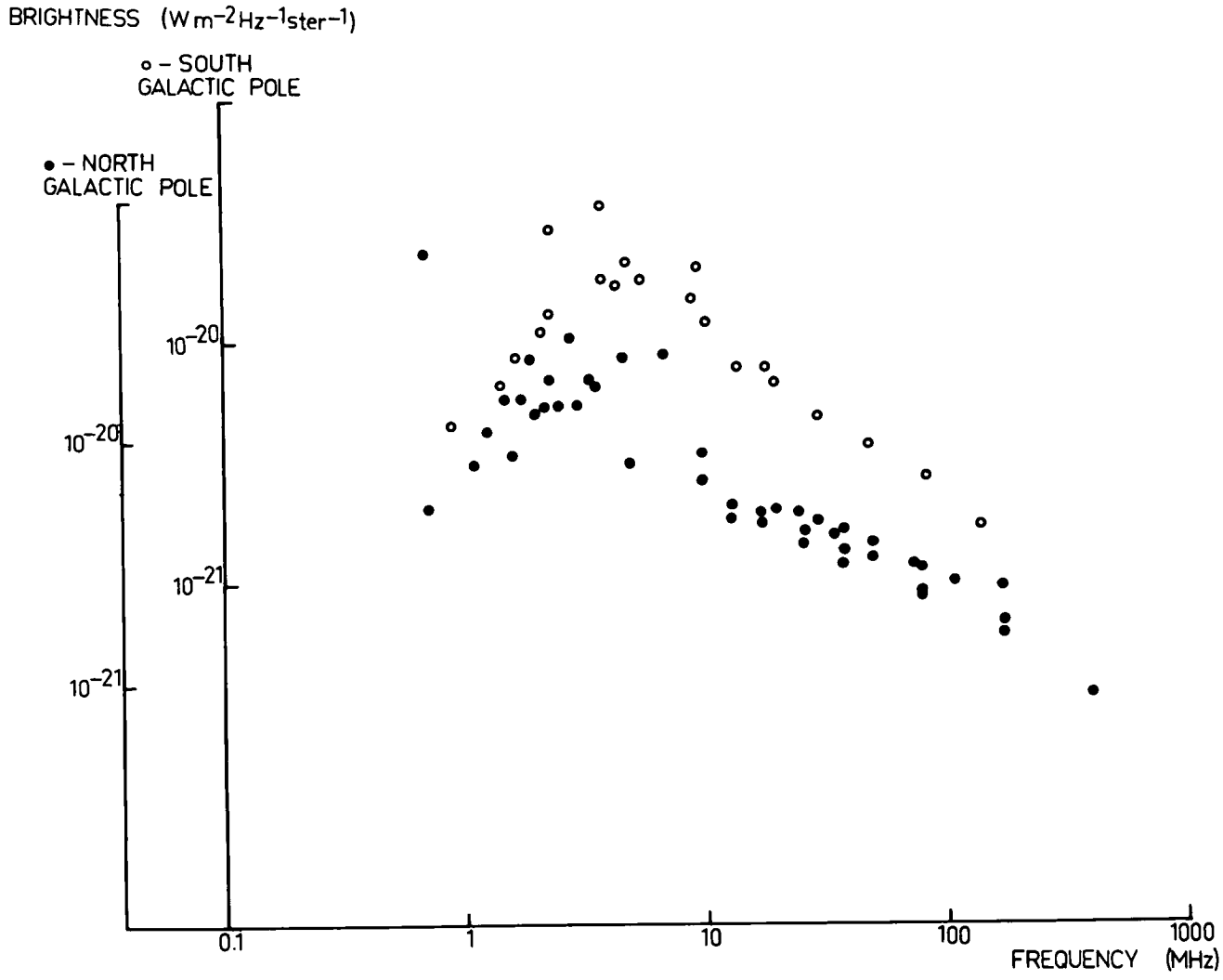

THE GALACTIC POLAR SPECTRA

(NOTE DISPLACED VERTICAL SCALES)

The galactic radio spectrum in this range is usually explained as synchrotron emission from cosmic ray electrons in the galactic magnetic field. In Chapter 2 it is recalled that a differential electron energy spectrum of the form

$$n_e(E) \propto E^{-\gamma} \qquad (2),$$

where $n_e(E)dE$ is the number of electrons with energy in the range E to E+dE, will give rise to a radio spectrum as in (1) with

$$\alpha = \frac{\gamma - 1}{2} \quad ;$$

and the radiation from an electron with energy E will be emitted near the synchrotron characteristic frequency ν_c:

$$\nu_c(MHz) \simeq 16\ B_{\perp}(\mu G)\ E^2(GeV) \qquad (3).$$

Assuming a galactic magnetic field of $\sim$2 μG, we find that the electrons responsible for the observed spectra have energies in the range 0.5 - 2 GeV.

Measurements of the cosmic ray electron flux in the solar neighbourhood have been summarised by Webber (1968) and his summary is reproduced in figure 6. The differential spectrum in the vicinity of 1 GeV is of the form given in (2) with $\gamma \simeq 1.55$. Unfortunately the interstellar electron

spectrum cannot be obtained directly from figure 6, as the measurements were made in the vicinity of the earth and allowance must be made for solar modulation effects. The generally accepted form of this modulation, relating the electron density at the earth n_o to that at infinity n_∞, is given by

$$n_o = n_\infty e^{-(\eta/R\beta)} \qquad (4),$$

where R is the electron rigidity, *GV*

β is the electron velocity, *units of c*

and η is the residual modulation parameter, *GV*.

It has not yet been possible to determine η by experiment. Various values have been proposed as being consistent with other measurements, such as

η = 0.4 GV, by Ramaty and Lingenfelter (1968)

and η = 0.9 GV, by Gloeckler and Jokipii (1967).

Webber (1968) deduces a value of 0.75 GV from the radio spectrum but the radio spectrum he uses is not self-consistent as it includes measurements made in a variety of directions. We cannot therefore regard the value of γ in the cosmic ray electron distribution as being known at the present time, at least for the energy range of relevance to this discussion. The information currently available only provides the limits

$$1.55 \lesssim \gamma \lesssim 2.5 .$$

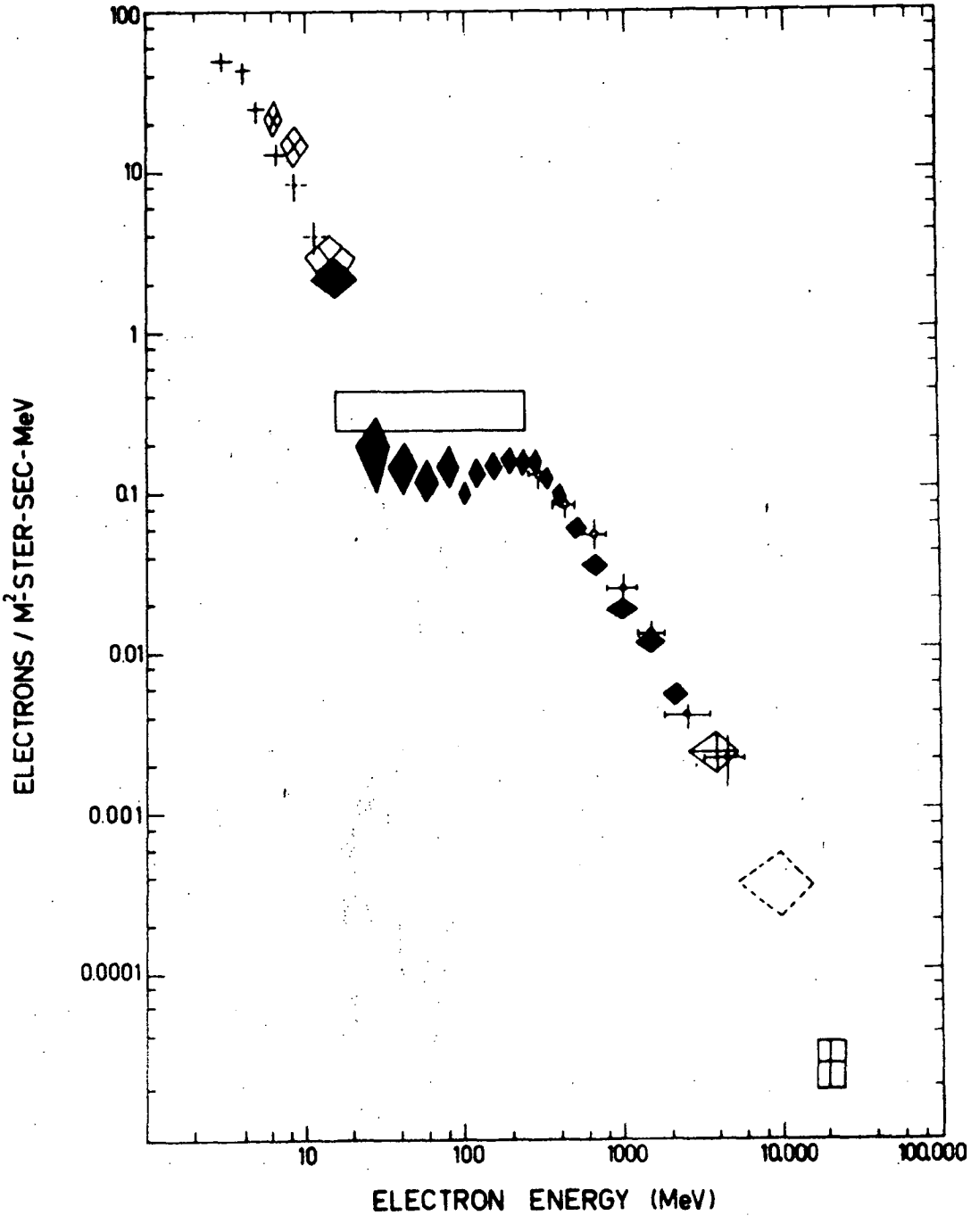

FIGURE 6

Electron spectrum in the solar neighbourhood

after Webber (1968)

The radio spectra imply electron distributions with $\gamma \simeq 1.8$ (north galactic pole) and $\gamma \simeq 2.2$ (south galactic pole). We can interpret this difference in one of two ways. If the electron spectrum of figure 6 is taken as representative of the galactic electron flux, then the differences in slope of the radio spectra must imply substantially different magnetic field strengths in the two galactic hemispheres, so that the electrons responsible for the emission in the north lie in the flatter region of figure 6. Although the uncertainty in estimating the solar modulation effects makes it impossible to determine precisely the energy region where this change in slope occurs, we can assert that the implied field strength is $\gtrsim 10$ μG in the north, a value which seems rather high in the light of recent evidence (Radhakrishnan, 1969). The alternative explanation is that there are real differences in the electron distributions in the two regions and that figure 6 represents some sort of local mean.

The discrimination between these models requires observations of a phenomenon which is a function of the electron distribution without involving the magnetic field. Such a phenomenon is the generation of x-rays and gamma rays by the inverse Compton effect, that is the production of a

high energy photon by the collision of a fast electron with a low energy photon. The full discussion of this mechanism and its relation with synchrotron emission is postponed to Chapter 7, but it is worth anticipating a little of the results here. The inverse Compton process between photons with a black body distribution and electrons described by (2) will yield an x-ray intensity of the form

$$I \propto \varepsilon^{-\alpha}, \qquad \alpha = \frac{\gamma - 1}{2} \tag{5}$$

where ε is the energy of the x-ray photon produced. The mean energy $\langle\varepsilon\rangle$ is related to the electron energy E and the temperature of the black body field T by

$$\langle\varepsilon\rangle(eV) \simeq 1.2_{10}3\, E^2(GeV)\, T(degK) \tag{6}.$$

Thus in a 2 μG magnetic field and a 3 degK black body radiation field, 1 GeV electrons will produce synchrotron emission at ∿30 MHz and x-ray photons at ∿3.6 KeV, and the spectra of both these emissions will show the same dependence on the electron energy spectrum.

The measurements of the diffuse x-ray background have been reviewed by Hamilton and Francey (1969) and a summary is given in Chapter 7. Unfortunately there have only been three satisfactory measurements in the directions of the galactic poles in the energy range 1 - 10 KeV, although the agreement between the radio and x-ray spectral

indices obtained in these experiments is remarkable. In the north the x-ray data yield $\alpha \sim 0.35 - 0.4$, while in the south the only measurement made gives $\alpha \sim 0.7$. However there are a number of other processes that may contribute to the x-ray flux, and in any case the number of times these difficult measurements have been made is too small for definite conclusions to be drawn.

We return to the original argument, and conclude that while a mean field strength of 10 μG is regarded as too high for the regions generating the synchrotron emission in the range 10 - 100 MHz the observed spectra must be taken as evidence of different electron distributions in the two galactic hemispheres.

The frequency range 6 - 10 MHz:

Both spectra show a sharp increase in brightness in the range 6 - 10 MHz, although this is less marked in the southern spectrum. We will attempt to explain this as the result of a change in the energy distribution of the radiating electrons.

The determination of the electron energy spectrum from the observed synchrotron spectrum requires the inversion of an integral equation of the form

$$B(\nu) = a \int_0^{E_{max}} n_e(E)\, F\left(\frac{\nu}{bE^2}\right) dE \qquad (7)$$

where $B(\nu)$ is the observed radio spectrum,

$n_e(E)$ is the required electron energy spectrum,

E_{max} is the highest electron energy,

a and b are constants

and F is the function given by Westfold (see Chapter 2). Wallis (1959) has obtained a solution to this equation in terms of Laplace transforms, but it is desirable to use Fourier transforms since they are more suitable for automatic computation. In the development which follows equation (7) is expressed in the form of a convolution integral by a suitable change of variable, and the solution is obtained by inversion of the convolution.

First of all we introduce into (7) the characteristic frequency ν_c, related to the electron energy by (3). We write then

$$N_e(\nu_c) = n_e\left(E(\nu_c)\right)$$

and obtain from (7)

$$B(\nu) = c \int_0^{\nu_{max}} N_e(\nu_c)\, F\left(\frac{\nu}{\nu_c}\right) d\nu_c \qquad (8)$$

where the various constants arising from the change of integration variable are absorbed in c, and ν_{max} is the characteristic frequency corresponding to energy E_{max}. We can extend the definition of $N_e(\nu_c)$ by defining

$$N_e(\nu_c) \equiv 0 \qquad \text{for} \quad \nu_c > \nu_{max},$$

and this allows the upper limit of integration to go to infinity:

$$B(\nu) = c \int_0^\infty N_e(\nu_c) \; F\left(\frac{\nu}{\nu_c}\right) \; d\nu_c \qquad (9).$$

Equation (9) is in the form of the Mellin transform, and the appropriate expression for the inverse could be used at this stage. We proceed to the standard convolution form by introducing new variables ζ and ζ_c, defined by

$$\zeta = ln(\nu) \quad \text{and} \quad \zeta_c = ln(\nu_c).$$

We can then introduce new functions

$$B(\zeta) = B(e^{\zeta}) = B(\nu),$$

$$N_e(\zeta_c) = N_e(e^{\zeta c}) = N_e(\nu_c),$$

$$F(x) = F(e^{x}),$$

and rewrite (9) as

$$B(\zeta) = d \int_{-\infty}^{\infty} N_e(\zeta_c)\ F(\zeta-\zeta_c)\ d\zeta_c \qquad (10),$$

where as before the constants are absorbed in d. Note that this change of integration variable causes the lower limit of integration to become $(-\infty)$.

Equation (10) is the standard form of the convolution or *faltung* integral. If the functions B, N_e, and F have Fourier transforms $B^\dagger$, $N_e^\dagger$ and $F^\dagger$, taking the transforms of each side of (10) gives

$$B^\dagger(s) = d\ N_e^\dagger(s)\ F^\dagger(s) \qquad (11).$$

We obtain

$$N_e^\dagger(s) = d\ [F^\dagger(s) / B^\dagger(s)] \qquad (12),$$

and taking the inverse transform of each side of (12) yields the function $N_e(\zeta)$ from which the required electron distribution $n_e(E)$ can be obtained. The necessary transformations can be performed with great speed and accuracy using the "Fast Fourier Transform" algorithm of Cooley and Tukey (1965), and a suitable ALGOL implementation has been published by Boothroyd (1968).

There is, of course, no unique solution for $n_e(E)$ in equation (7) as the convolution process in general involves the loss of information; on this matter the remarks of Bracewell and Roberts (1954) are relevant although they were discussing aerial smoothing of brightness distributions. However we may expect to gain some idea of the electron distribution causing the emission.

The method was applied to the northern polar spectrum for the range 8 - 100 MHz. The measurements at lower frequencies could not be included since, as discussed below, the shape of the spectrum in the lower region cannot be produced by synchrotron emission alone. A possible electron spectrum is shown in figure 7, and the radio spectrum obtained by direct integration of equation (7) with this distribution is shown in figure 8. It is interesting to note that this is the frequency range in which emission from secondary electrons produced by spallation of the primaries might become significant. The expected fluxes and spectra of these secondaries have been discussed by Ramaty and Lingenfelter (1966), and once again we are faced with an unknown parameter — in this case the total amount of matter traversed by the primaries. It seems that the generally accepted upper limit of $6\ g\ cm^{-2}$ would result in the required

flux of secondaries, although the slope of the secondary spectrum predicted by Ramaty and Lingenfelter is not as steep as is required by figure 7.

We must consider the possibility that the sharp increase in the brightness in this frequency range is instrumental in origin. The problems of calibration were outlined in Chapter 3 and it should be noted that it is in this frequency range that the absence of a suitable primary standard is the most serious. The original interpretation is, however, supported to some extent by the measurements of extragalactic sources by Braude *et al* (1968) in the range 12.6 - 25 MHz. They find that a considerable number of sources show an increase in spectral index in this frequency range; the variety of spectral shapes represented in their results supports the view that this class of radio spectrum is genuine, and not the result of a discontinuity in calibration. They remark that the spectral characteristics of these sources cannot be explained by "synchrotron radiation, negative reabsorption, or other known mechanisms". The actual explanation, when found, may prove suitable for the spectrum of our galaxy as well.

facing page 90.

FIGURE 7 (facing page)

The theoretical electron energy spectrum derived from the radio spectrum above 8 MHz.

FIGURE 8 (overleaf)

The radio emission spectrum computed for the electron distribution of figure 7.

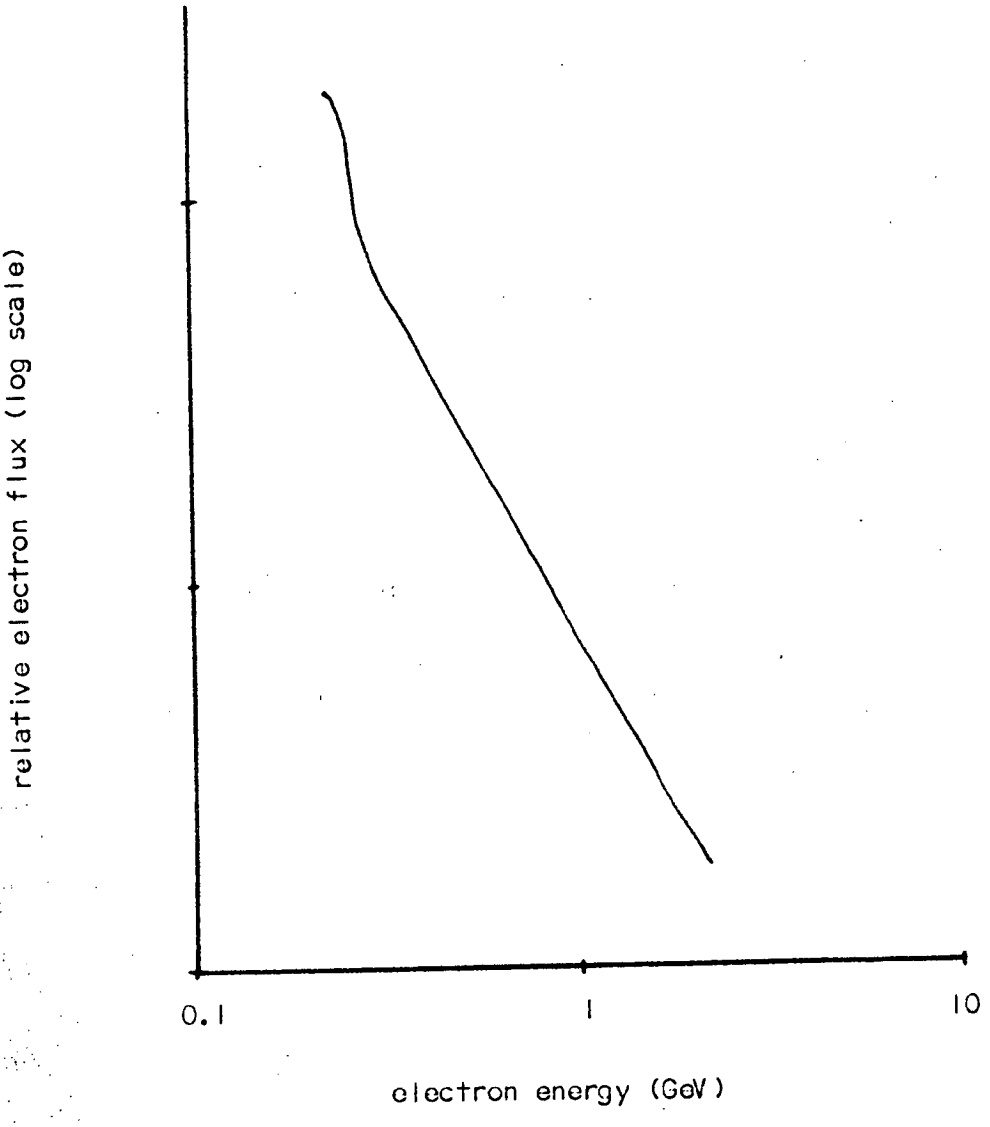
relative electron flux (log scale)
0.1
1
10
electron energy (GeV)

FIGURE 7

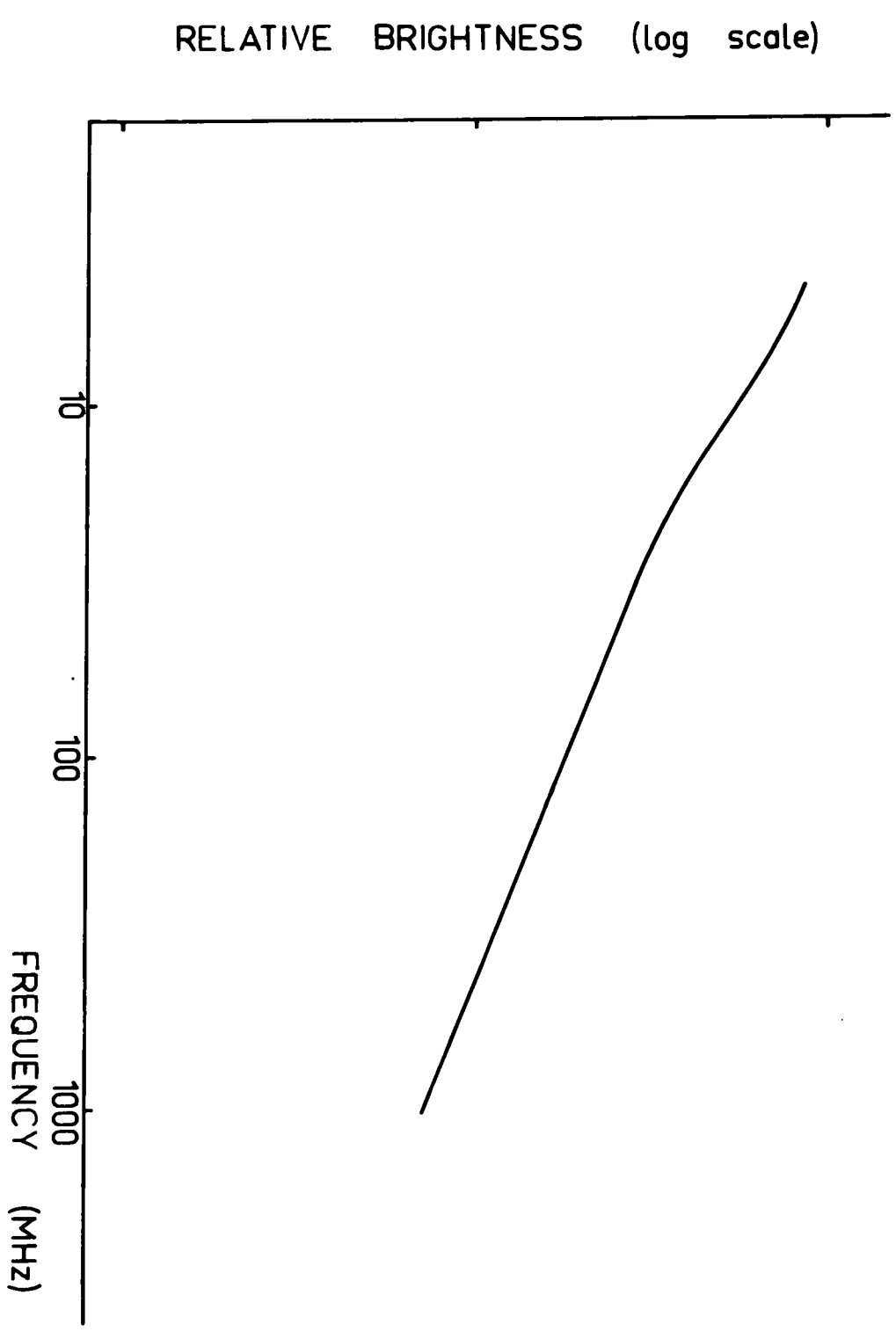
RELATIVE BRIGHTNESS (log scale)
10
100
1000
FREQUENCY (MHz)

The spectrum below 6 MHz:

In the directions of both galactic poles the spectral index goes to zero somewhere between 2 and 5 MHz, and at lower frequencies the brightness falls with increasing wavelength. This rapid turn-over cannot be produced by a cutoff in the emission spectrum and must therefore be the result of absorption.

The spectrum for the southern polar region above 10 MHz is approximately represented by (1) with a spectral index of 0.6. The theoretical curve (c) in figure 2 of Chapter 2 was obtained for an electron spectrum of the form

$$n_e(E) \propto E^{-2.2} \qquad E > 0.4 \text{ GeV}$$
$$\equiv 0 \qquad E \lesssim 0.4 \text{ GeV}$$

in a field strength of 5 μG. This therefore indicates the sharpest possible cutoff in emission consistent with a maximum at about 5 MHz and a spectral index of 0.6 at higher frequencies. The brightness at 1 MHz predicted by this extreme case is higher by a factor of about 5 than the observed spectrum, and it is clear that the emission is seen through an absorbing region with an optical depth of at least 2 at 1 MHz.

The characteristics of thermal absorption have been summarised in Chapter 2, and the spectral shapes that result from various combinations of non-thermal emission and thermal

absorption were illustrated in figures 5, 9 and 10 of that chapter. It seems that the observed spectrum cannot be the result of combined emission and absorption in a single region (case c of Chapter 2) because of the steep slope below 3 MHz, but the parameters of the other absorption cases can be chosen to fit the observations. However the simple model of emission behind an absorbing region will yield the observed spectral shape only if the emission spectrum exhibits the sharp cutoff discussed above. The remaining case considered in Chapter 2 is that of emission behind a region of combined emission and absorption. Such a model can fit the data well, although it is not unique in this respect. In particular a model in which distant emission passes through a region of discrete absorbing clouds will satisfy the data provided that there are small regions of the sky where the line of sight does not pass through a cloud.

The magnitude of the sky brightness:

The general agreement between the observed cosmic ray energy spectrum and the radio brightness spectrum has encouraged the view that the one is responsible for the other. Any discrepancy between the two has always remained within the rather large uncertainties in the measurements (especially

of the interstellar electron spectrum), and no satisfactory alternative model has been proposed.

However, very real problems still exist in relating the magnitude of the particle flux to that of the radio brightness. The number of electrons seems too small. Webber (1968) has examined this problem in detail and although a more consistent selection of radio data requires a minor revision of his numerical results the general conclusions remain unaltered. He finds that the observed radio spectrum can be produced by the observed electron spectrum if he takes $\eta = 0.75$ GV and $B_\perp = 6$ μG. When the corrected spectrum is used we find that if the same value of the residual modulation parameter η is used we need $B_\perp \simeq 8$ μG, and hence a total mean field strength near 10 μG within the galactic disk. Lower values of the field strength require a higher value for η, but Gloeckler and Jokipii (1967) have advanced strong reasons for requiring $\eta \lesssim 1.2$ GV. On the other hand a mean field strength of 1 - 3 μG seems more reasonable than 10 μG, and the recent measurements of Faraday rotation of pulsar radiation, where both $\int n_e dr$ and $\int n_e B_\parallel dr$ are available for the path length, suggest that mean line of sight field strengths of less than 1 μG are appropriate (Smith, 1968).

It appears that although the cosmic ray electrons have an energy spectrum in agreement with the shape of the radio spectrum, the constraints on the particle fluxes and the magnetic field strengths imposed by other measurements leave us with an expected radio brightness that is too small by nearly an order of magnitude. Further experimental work is required to settle the matter, and it is likely that the next year or so will at least see the question of solar modulation of cosmic rays cleared up by satellite observations.

REFERENCES FOR CHAPTER 4

Adgie,R. and Smith,F.G. 1956 *Observatory 76* 181.

Alexander,J.K. and Stone,R.G. 1965 *Astrophys. J. 142* 1327.

Andrew,B.H. 1966 *Mon. Not. Roy. Astr. Soc. 132* 79.

Bracewell,R.N. and Roberts,J.A. 1954 *Aust. J. Phys. 7* 615.

Braude,S.Ya., Zhuk,I.N., Lebedeva,S.M., Men',A.V. and Ryabov,B.P. 1968 *Doklady 180* 1323 English Translation: *Soviet Physics - Doklady 13* 512 (1968).

Benediktov,E.A., Getmanser,G.G., Mitjakov,N.A., Rapoport,V.O., Sazonov,J.A., and Tarasov,A.F. 1965 *Space Research VI* 110.

Boothroyd,J. 1968 *The Computer Journal 10* 414.

Chapman,J.H. and Molozzi,A.R. 1961 *Nature 191* 480.

Cooley,J.W. and Tukey,J.W. 1965 *Mathematics of Computation 19* 297.

Costain,C.H. 1960 *Mon. Not. Roy. Astr. Soc. 120* 248.

Cottony,H.V. and Johler,J.R. 1952 *Proc. Instn. Radio Engrs. 40* 1053.

Ellis,G.R.A. 1957 *J. Geophys. Res. 62* 229.

Ellis,G.R.A. 1964 *Aust. J. Phys.* *17* 63.

Ellis,G.R.A. 1965 *Mon. Not. Roy. Astr. Soc.* *130* 429.

Gloeckler,G. and Jokipii,J.R. 1967 *Astrophys. J.* *148* 141.

Hamilton,P.A. and Francey,R.J. 1969 *Nature: in press.*

Hamilton,P.A. and Haynes,R.F. 1969 *Aust. J. Phys.: in press.*

Hartz,T.R. 1964 *Ann. d'Astrophys.* *27* 823.

Higgins,C.S. and Shain,C.A. 1954 *Aust. J. Phys.* *7* 460.

Hugill,J. and Smith,F.G. 1965 *Mon. Not. Roy. Astr. Soc.* *131* 137.

Kiepenheuer,K.O. 1950 *Phys. Rev.* *79* 738.

Korobkov,Yu.S. 1964 *Isz. Vyssh. Ucheb. Zaved . Radiofiz.* *7* 983.

Kraus,J.D. 1966 *"Radio Astronomy"* (McGraw-Hill) p.85.

Papagiannis,M.D. 1964 *Ph.D. Thesis* (Harvard).

Parthasarathy,R. and Lerfald,G.M. 1965 *Mon. Not. Roy. Astr. Soc.* *129* 395.

Purton,C.R. 1966 *Mon. Not. Roy. Astr. Soc.* *133* 463.

Ramaty,R. and Lingenfelter,R.E. 1966 *J. Geophys. Res.* *71* 3687.

Ramaty,R. and Lingenfelter,R.E. 1968 *Phys. Rev. Letters* *20* 120.

Reber,G. 1968 *J. Franklin Inst.* *285* 1.

Reber,G. and Ellis,G.R.A. 1956 *J. Geophys. Res.* *61* 1.

Shain,C.A. and Higgins,C.S. 1954 *Aust. J. Phys.* *7* 130.

Smith,F.G. 1968 *Nature* *218* 325.

Turtle,A.J., Pugh,J.F., Kenderdine,S. and Pauliny-Toth,I.I.K. 1962 *Mon. Not. Roy. Astr. Soc.* *124* 297.

Wallis,G. 1959 in *Paris Symposium on Radio Astronomy* ed. R.N.Bracewell (Stanford: Stanford Univ. Press) p. 595.

Webber,W.R. 1968 *Aust. J. Phys.* *21* 845.

Yates,K.W. and Wielebinski,R. 1966 *Aust. J. Phys.* *19* 389.

CHAPTER 5

HIGH RESOLUTION SURVEYS OF THE SOUTHERN SKY

INTRODUCTION

In this chapter the high resolution surveys of the southern sky at frequencies below 200 MHz are reviewed. Six whole-sky surveys have been completed, with resolutions from 2° to 8°. The surveys at 2.1 MHz (Reber, 1968), 30 MHz (Mathewson *et al*, 1965) and 85 MHz (Yates *et al*, 1967) are discussed first. Surveys at 4.7 MHz, 10 MHz and 153 MHz, which are the work of the author and which form the experimental part of this thesis, are then presented in detail.

Two other surveys have been made in the frequency range of interest, at 19.7 MHz (Shain *et al*, 1961) and 85 MHz (Mills, 1959). The survey by Shain covers only the portion of the galactic plane visible from the southern hemisphere, and is with a beamwidth of 1.4°. This resolution is too fine to permit direct comparison with the lower frequency maps, and the extent of the surveyed region is too limited for smoothing to a lower resolution to be

feasible. No detailed use has therefore been made of this survey in the analysis and hence a summary has been omitted. The 85 MHz survey by Mills was made with a resolution of 0.8^{o} while the map by Yates at the same frequency was obtained with a beam of 4^{o} using an instrument more suited to large-scale surveys. This latter resolution was more suitable for comparison with the other maps.

THE 2.1 MHZ SURVEY

The 2.1 MHz survey was made by Reber (1968) and is presented in great detail in his paper. The instrument was a completely filled dipole array of circular outline with an aperture of about three quarters of a mile, situated in the central highlands of Tasmania. The site is a flat valley some three miles in diameter ringed by low hills. The receiver was battery operated and the nearest power line is several miles from the telescope. The site is thus almost completely free from man-made electrical noise, and is favourably located for such low frequency measurements since the ionosphere critical penetration frequency f_oF_2 falls to low values over Tasmania.

The array was constructed to the usual high engineering standard one associates with Grote Reber, and all

possible sources of error were investigated and either eliminated or calibrated.

The telescope was operated as a single beam instrument (beamwidth 8° between half-power points when directed to the zenith), and the beam could be moved in declination by mechanical adjustment of the transmission line lengths. Reber made no attempt to calibrate his survey against an absolute standard; all calibrations were referred to a signal generator and a map of relative sky brightness temperature was produced. This map is reproduced in figure 1.

THE 30 MHZ SURVEY

Mathewson, Broten and Cole (1965) made the 30 MHz survey with the 210 foot telescope at Parkes, N.S.W. The reflector was illuminated with a helical feed giving a circular beam approximately 11° between half-power points. The Parkes telescope has an alt-azimuth mount and is normally driven in equatorial coordinates by causing it to follow an equatorial optical telescope mounted coaxially. However on this occasion the zenith angle of the instrument was set to 57° and the azimuth scanned from 70° through 180° to 290°. The south celestial pole passed through the middle of each

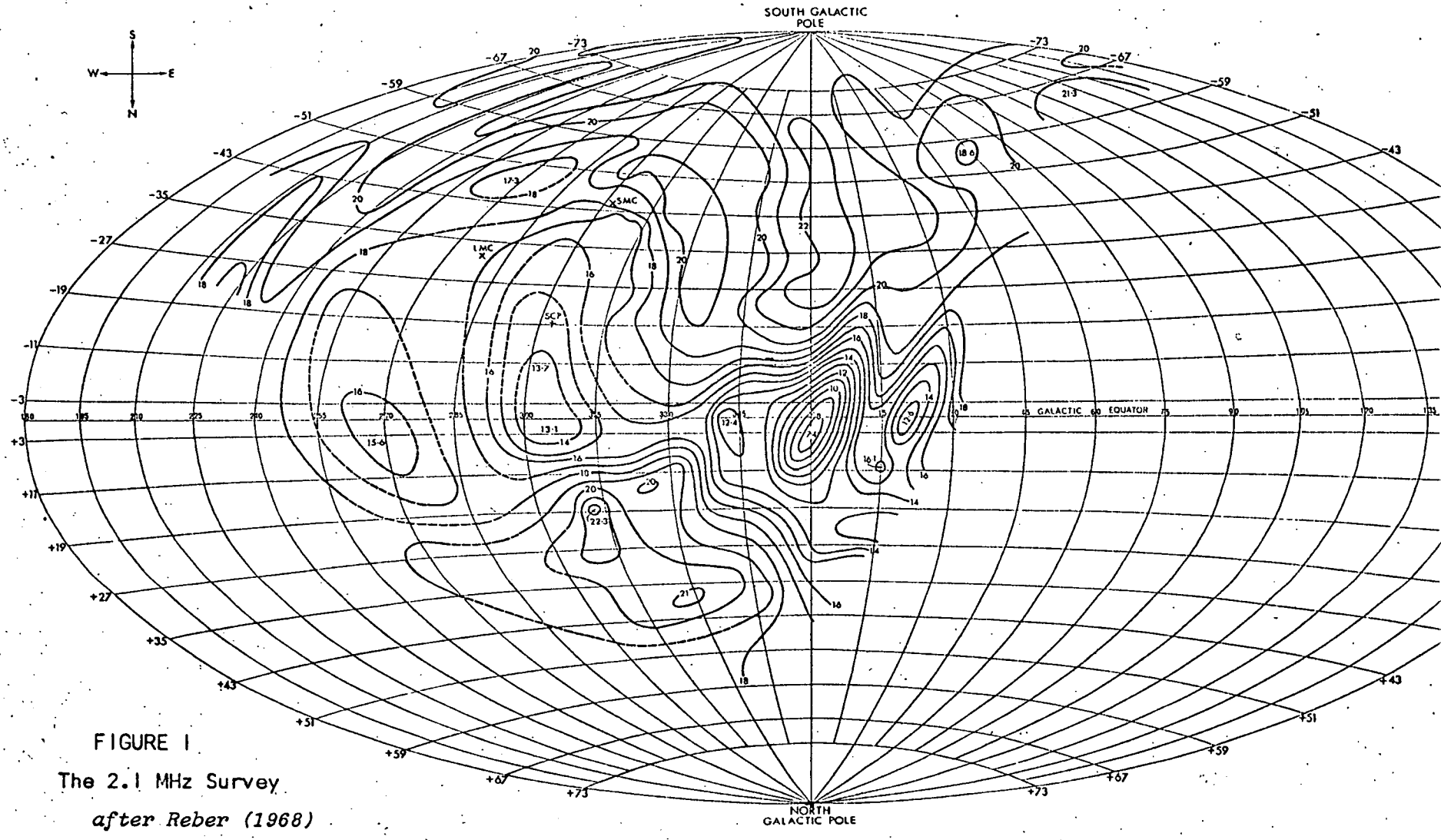

FIGURE 1

The 2.1 MHz Survey

after Reber (1968)

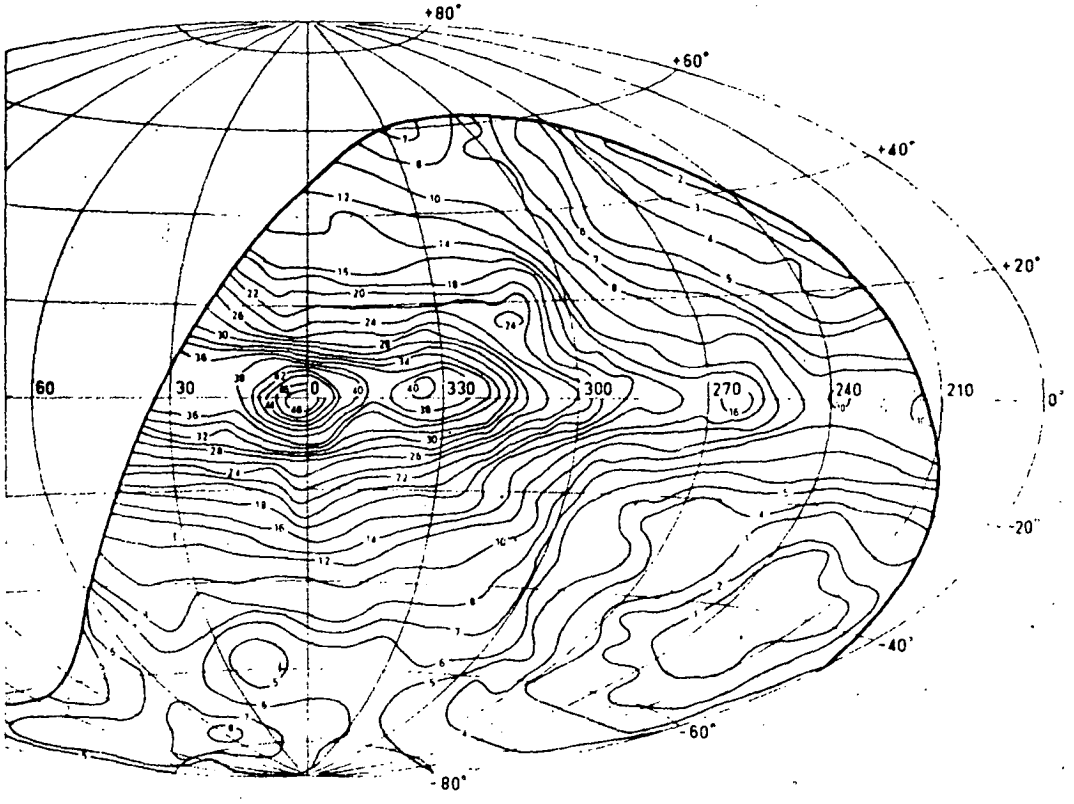

The 30 Mc/s isophotes plotted on an Aitoff projection in new galactic coordinates. The brightness temperature contour unit is 1800 degK. The thick line marks the limit of the survey.

FIGURE 2

after Mathewson et al (1965)

scan, and this point was used as the reference for the survey. Calibration was against the strong source *Fornax A*, and the results were given in the form of a contour map of known contour interval above an arbitrary level at the south celestial pole.

The final 30 MHz map, in galactic coordinates, is reproduced in figure 2.

THE 85 MHZ SURVEY

The 85 MHz survey by Yates, Wielebinski and Landecker (1967) was also made with the 210 foot reflector at Parkes. In this case the dish was illuminated with a single half-wave dipole giving a slightly elliptical beam of $3.5^{o} \times 3.8^{o}$. Considerable attention was paid to the calibration of the survey, and an overall accuracy of ±7% is claimed.

The final map, in galactic coordinates, is given in figure 3, " .... showing modified temperatures with strong discrete sources removed".

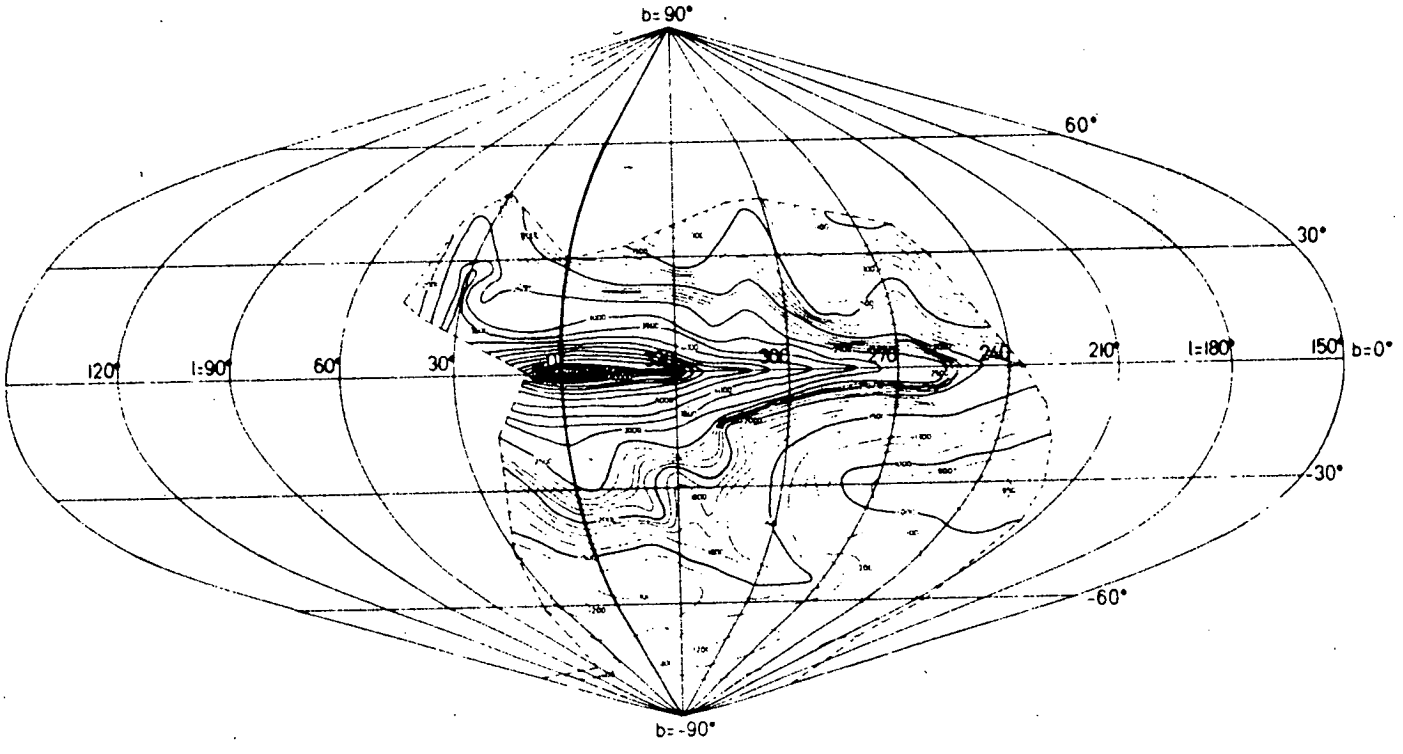

Galactic map showing modified beam temperatures with strong discrete sources removed

FIGURE 3 *after Yates et al (1967)*

THE 4.7 MHZ SURVEY

The 4.7 MHz survey was made at Penna, near Hobart, at latitude 42.9° S, longitude 147.0°E, and most of the observations were obtained between May and December 1963. A filled rectangular dipole array was used with a beamwidth of 3° × 10°. This survey has been reported by Ellis, Green and Hamilton (1963) and more fully by Ellis and Hamilton (1966).

(a) Equipment:

The antenna consisted of an array of 272 half-wave dipoles 0.1 wavelengths above ground, and disposed as shown in figure 4. The dipoles each had an impedance of 20Ω at this height, and the quarter-wave transmission lines shown in the figure increased this to about 20,000Ω. At this point the lines were connected to a 500Ω line running the full east-west extent of the array and terminated in the characteristic impedance at each end. The severe mismatch meant that only a small fraction of the incident power was actually input to the receiver, but the negligible loading of the main 500Ω lines at the connecting points made the phasing of the array a simple matter. At the centre of each 500Ω line the signal was fed to 70Ω coaxial cable using

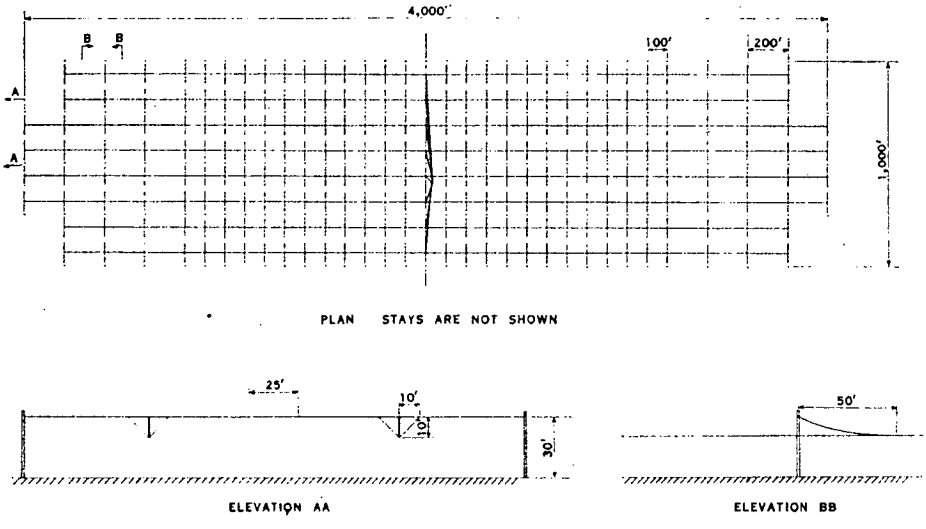

Layout of 4·7 Mc/s antenna.

FIGURE 4

after Ellis, Green and Hamilton (1963)

a lattice network as shown in figure 5, which performed the 250Ω → 70Ω impedance transformation and also the balance-to-unbalance conversion. Thus each of the 8 east-west lines of aerials was connected independently to the receiver.

A block diagram of the receiving equipment is shown in figure 6. Each of the 8 input signals passed through separate preamplifiers and mixers, the latter all fed from a single oscillator. These circuits were adjusted so that the original phase relationships were preserved at the outputs from the mixers. Each of the 8 signals then passed through a distribution network dividing the signal among 6 outputs. The signals from the six sets of outputs were combined in 6 different phase relations to give simultaneous beams in the meridian directed at different declinations. The phase shifts were introduced in the IF amplifiers by slight de-tuning; the actual setting up of the phase shifts was achieved by balancing out the phase delay introduced by a known length of delay cable.

After inserting the phase shifts the signals were summed and passed through a final stage of IF amplification with a bandwidth (-6 dB) of 2.1 KHz determined by a mechanical filter. A stage tuned to twice the IF frequency (i.e. to 910 KHz) followed whose output was thus proportional to the

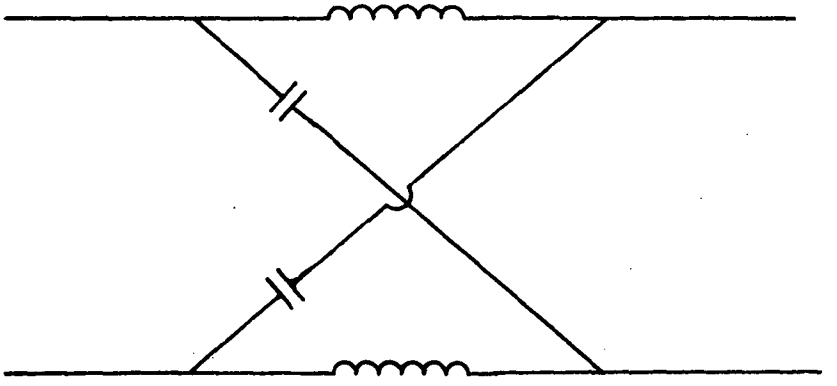

FIGURE 5

Lattice network for
impedance transformation

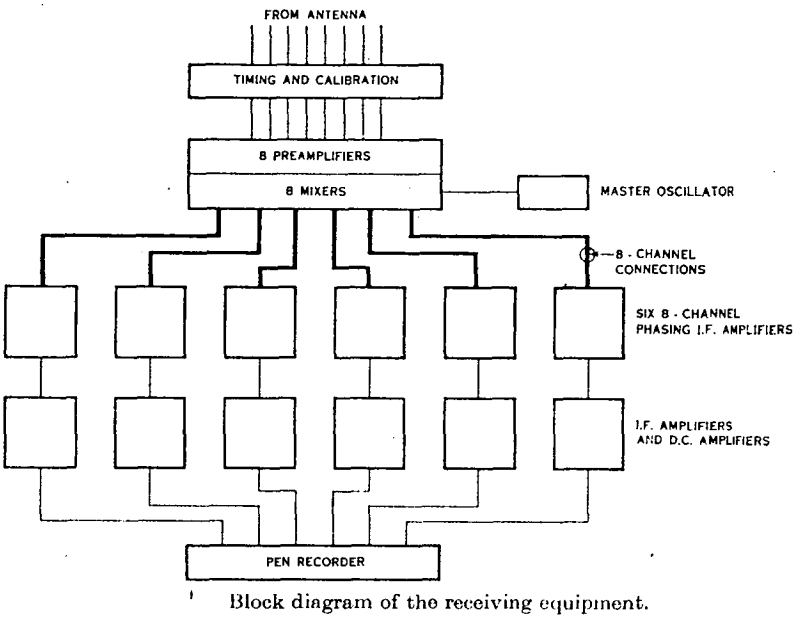

Block diagram of the receiving equipment.

FIGURE 6

after Ellis, Green and Hamilton (1963)

square of the input. A linear diode detector followed and the resulting d.c. signal was proportional to the power received. Finally a minimum-reading d.c. amplifier led to the pen recorder.

(b) Observing procedure:

The main difficulty in making the observations proved to be not the ionosphere but interference from transmitting stations. This led to the use of the very narrow bandwidth and the minimum-reading d.c. amplifier (Ellis, 1960), whose actual circuit and equivalent circuit are shown in figure 7.

The receiver centre-frequency was swept over a frequency range of 10 KHz, that is five times the passband. A transmitting station within this range then appeared as a periodic impulse at the second detector. This impulse was ignored by the minimum-reading circuit and the background signal of cosmic noise was recorded. Provided that the transmitting stations were separated by more than the 2.1 KHz receiver bandwidth good records were obtained. Once every hour the aerials were disconnected and replaced by dummy loads at room temperature. This gave time marks on the record and also gave indications of the zero level. Once every 24 hours a noise calibration signal was injected to check for drifts

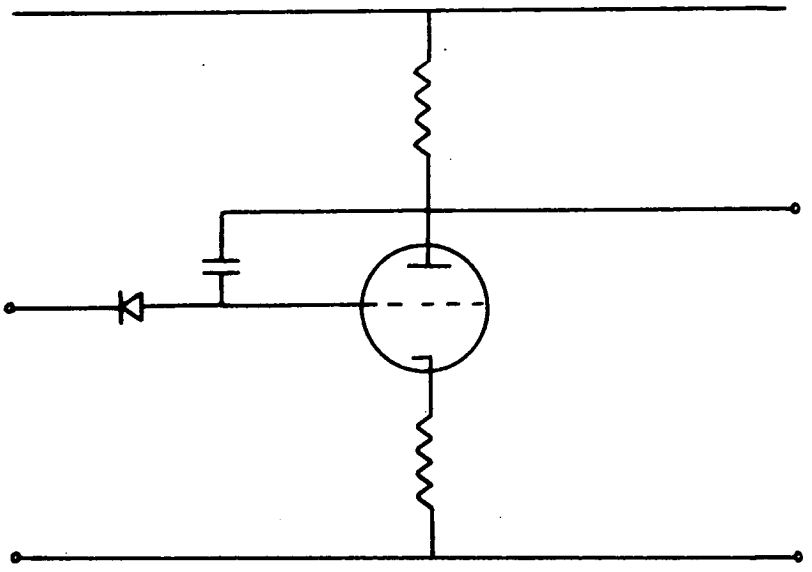

FIGURE 7a

Circuit of minimum-reading amplifier

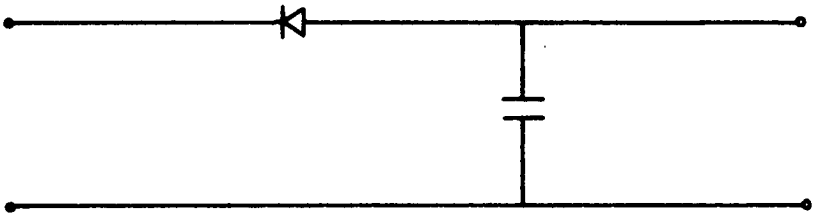

FIGURE 7b

Equivalent circuit of minimum reader

in gain, and this was found to hold to within 5%. Since the settings of the aerial beams were determined by phase shifts in the receiver the whole system was re-aligned every week, although the tests made on these occasions indicated that this was unnecessarily often.

(c) Observations:

The telescope was operated continuously for about 18 months, with occasional interruptions for maintenance of the array.

Figure 8 shows pairs of records for various declinations, illustrating the reproducibility of the results. The high fluctuation level resulting from the narrow bandwidth is evident. The pronounced trough for right ascensions near the galactic plane is noteworthy; this is not an ionospheric effect as its position in sidereal time is constant, as shown in figure 9.

(d) Reduction of data:

For each declination the best records were selected for smoothness of trace, reproducibility and the absence of transmitting station interference. The recorded intensity was plotted at 5-minute intervals and the highest values (at least 10) were averaged. This was done to eliminate

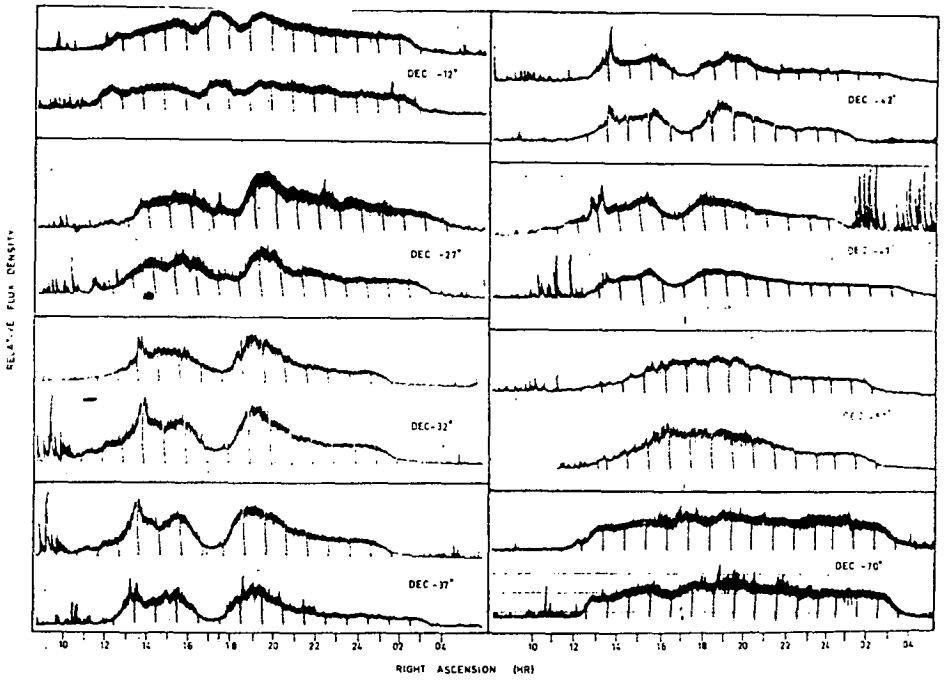

Records of cosmic radio noise at 4.7 Mc/s observed at Hobart in 1963. Two records are shown for each declination.

FIGURE 8

after Ellis and Hamilton (1966)

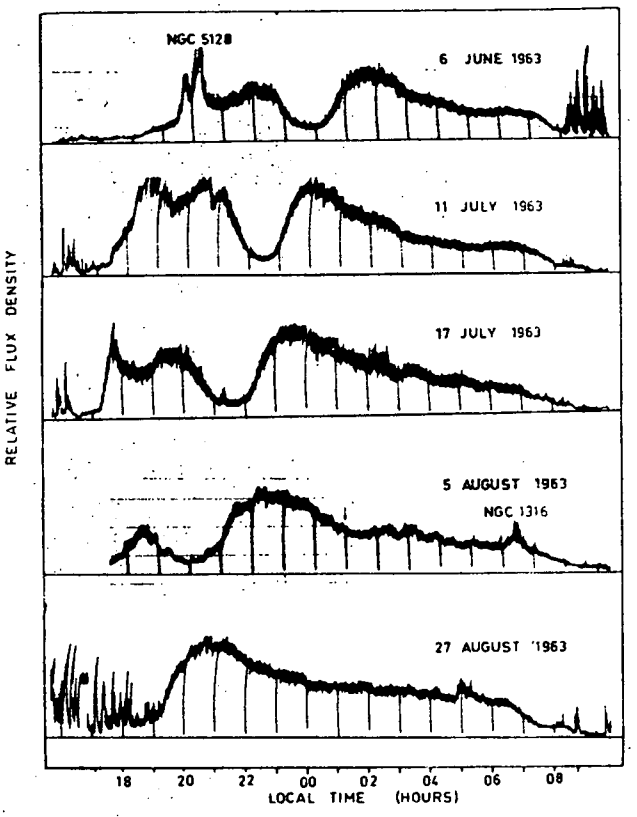

Records of cosmic radio noise for declination −37° obtained at different times showing sidereal variation.

FIGURE 9

after Ellis and Hamilton (1966)

ionospheric absorption effects, which would be expected to reduce the intensity if present. This procedure was not adopted for the trough between 18^h and 19^h RA. It was observed that disturbed ionospheric conditions sometimes led to higher intensities in this region than at other times, possibly because of scattered radiation from adjacent bright areas of the sky. Records of this region were therefore selected for the greatest brightness contrast, that is for greatest relative depth of the trough.

No other corrections for ionospheric attenuation were made as the errors discussed in Chapter 3 would in total be less than errors in reading the chart records.

(e) Results:

Background radiation:

The final map from the survey is shown in figure 10; equivalent aerial temperature contours are given and the map is in galactic coordinates. The most noticeable feature is the region of low brightness near the galactic centre, in contrast with surveys at higher frequencies where this area appears bright.

Discrete sources:

The sensitivity of this telescope for the detection of discrete sources was poor. The high fluctuation level in

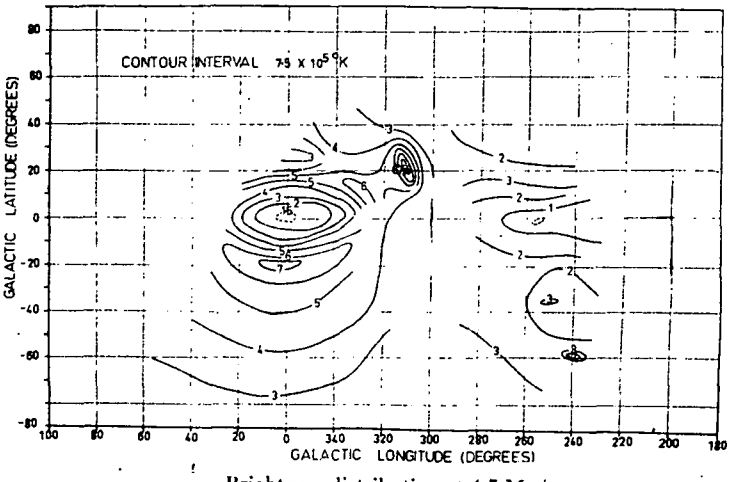

Brightness distribution at 4.7 Mc/s

FIGURE 10

after Ellis and Hamilton (1966)

the records resulting from the use of narrow bandwidth, short second-detector time constant and the high brightness temperature of the sky ($\sim 10^6$ degK), set the lowest observable source flux density at about 1000 flux units. In addition some reduction in observability was caused by ionospheric scintillations; rapidly scintillating sources were rejected by the minimum-reading d.c. amplifier.

Sources which were observed reliably are listed in Table I, and spectra of four of them are shown in figure II.

TABLE I

DISCRETE SOURCES OBSERVED AT 4.7 MHZ

R.A.	declination	flux density *(f.u.)*	notes
0320	-37	13500	Fornax A
0518	-46	10000	Pictor A
0821 0834	-43 -46	3600	Puppis A (not separated)
0916	-12	4700	Hydra A
1322	-43	51000	Centaurus A
1512 1549	-59 -56	2000	(not resolved)
1610	-61	4000	IAU 16S6A
1636	-46	1500	
1711	-38	1500	
1744	-29	3000	IAU 17S2A
1757 1802	-23 -21	2000	(not resolved)
2356	-61	1000	

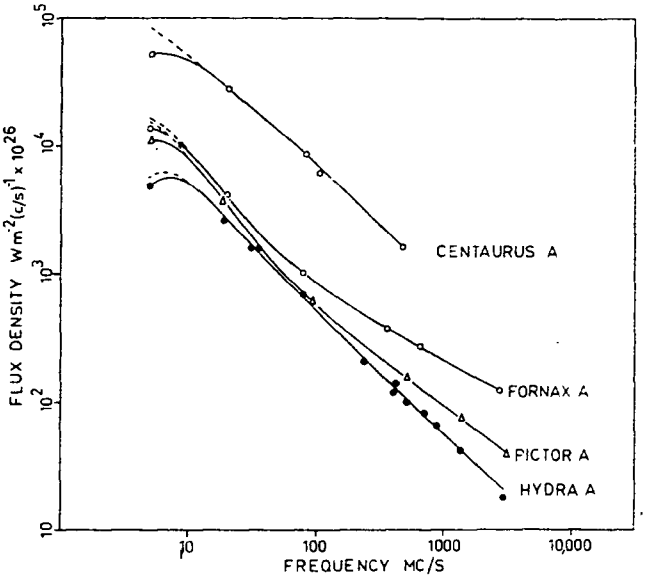

Spectra of the four sources Centaurus A, Fornax A, Pictor A, and Hydra A. Dotted lines show the spectra after correction for galactic absorption. Observations at 2650, 1410, and 408 Mc/s from Bolton, Gardner, and Mackey (1964); at 600 Mc/s from Piddington and Trent (1956); at 400 Mc/s from McGee, Slee, and Stanley (1955); at 100 Mc/s from Bolton, Westfold, Stanley, and Slee (1954); at 85 Mc/s from Mills, Slee, and Hill (1960); at 19.7 Mc/s from Shain (1958); and at 18.3 Mc/s from Shain and Higgins (1954).

FIGURE 11

after Ellis and Hamilton (1966)

THE 10 MHZ SURVEY

The 10 MHz survey was made at Penna, at the same site used for the 4.7 MHz work. A filled rectangular array with a beamwidth of $4^{\circ} \times 5^{\circ}$ was used. This survey has been reported by Hamilton and Haynes (1968); the receiver has been described separately by Hamilton (1968).

(a) Equipment:

The antenna consisted of an array of 24 × 15 half-wave dipoles at a height of a quarter-wave above ground. A plan of the array is shown in figure 12. The feed system resembled that used in the 4.7 MHz array. Each dipole was coupled with a quarter-wave line to a transmission line running the full east-west extent of the array, and the signal from each of these lines was connected independently to the receiver via baluns and coaxial cables.

A block diagram of the receiver is shown in figure 13. The signals from the 15 east-west lines of aerials were passed through individual amplifiers and broad-band mixers. The RF amplifiers were adjusted for similar phase shifts across the passband of the system. The broad-band mixers were all fed from Oscillator 1. Thus at the line AA in the figure the 15 signals were available at any carrier frequency in the range 2.5 - 5 MHz (the upper sideband is also present

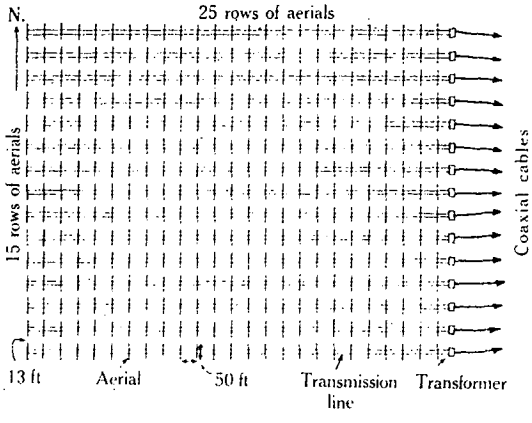

FIGURE 12

Plan of 10 MHz array

after Hamilton and Haynes (1968)

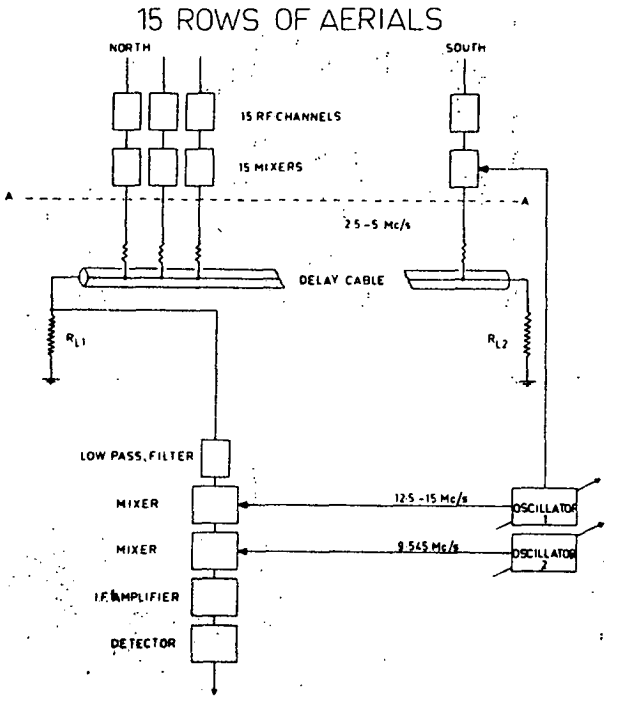

Block diagram of single beam receiver. The signals from the 15 aerial lines are added in the delay line and the output from the resulting beam appears across R_{L1}.

FIGURE 13

after Hamilton (1968)

at this stage but is removed later by a low-pass filter).

A phasing delay line was set up using delay cable and terminated at each end by a resistor equal to the characteristic impedance of the cable. The 15 signals were lightly coupled to the delay line from high impedance outputs (represented by resistors in the diagram) so that the line was not loaded by the signal sources. The coupling points were spaced uniformly along the line. The signals were therefore combined in a phase relationship determined by the electrical length in wavelengths between the coupling points. The phase difference ϕ inserted between adjacent aerial rows was

$$\phi = \frac{2\pi\nu\ell}{cv} \qquad radians,$$

where ν is the IF frequency, ℓ is the distance between coupling points on the delay line, c is the speed of light and v is the velocity factor of the cable. Thus the phase difference between adjacent channels was proportional to the intermediate frequency.

The final signal appeared across R_{L_1}. The upper sideband, in the range 12.5 - 15 MHz, was removed at this stage by a low-pass filter. A second mixer, also fed from Oscillator 1, restored the signal to the original carrier

frequency, so that at the point B in figure 13 a signal was available at the original frequency corresponding to an aerial beam directed at some angle θ to the zenith. The value of θ will have been determined by the inserted phase difference ϕ which in turn was set by Oscillator 1. The remainder of the system was a conventional receiver tuned to the original frequency. In operation, Oscillator 1 determined the beam position and Oscillator 2 determined the signal frequency.

In figure 13 the signal available across R_{L_1} is from a beam directed at an angle θ south of the zenith. At the same time there is a signal across R_{L_2} corresponding to a beam directed at an angle θ north of the zenith, and this can also be amplified and detected to give a second beam.

A block diagram of the whole equipment is given in figure 14. Three phasing lines of different electrical length were used, giving six simultaneous beams. A seventh beam directed always at the zenith was obtained with a resistive summing network in place of the delay line, and this beam provided a check on the operation of the system at different intermediate frequencies.

The d.c. amplifiers incorporated minimum-reading stages, and the technique for minimising station interference

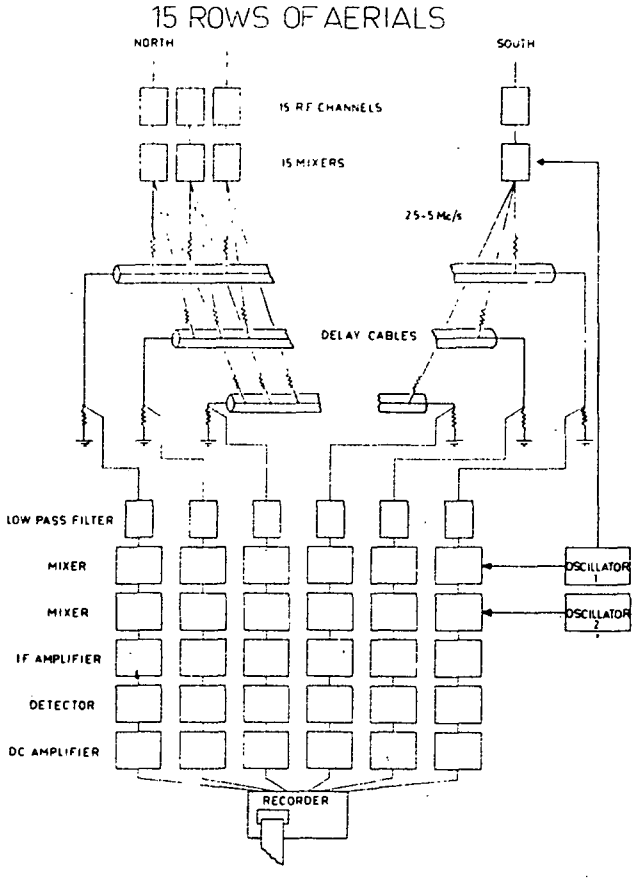

The complete six-beam receiver.

FIGURE 14

after Hamilton (1968)

described for the 4.7 MHz equipment was again used here. The receiver centre-frequency was scanned through 10 KHz five times a second by sweeping Oscillator 2, and mechanical filters restricted the bandwidth (-6 dB) to 2.1 KHz.

(b) Operation of the equipment:

The receiving system was re-aligned weekly to keep a check on gain and phase stability. The zero level was recorded every hour by replacing the aerials with resistive terminations at room temperature.

The telescope was operated in 1965 and 1966; observations were terminated prematurely in February 1967 when the array was destroyed in a bush fire.

(c) Results:

Sample records are given in figure 15 for eight declinations. Final records were chosen from night-time observations only, and the data reduction was similar to that adopted for the 4.7 MHz survey.

Background radiation:

The distribution of sky brightness is given in figure 16 in galactic coordinates. The contour interval was chosen to bring the temperature of the featureless region in the vicinity of the south galactic pole into agreement with

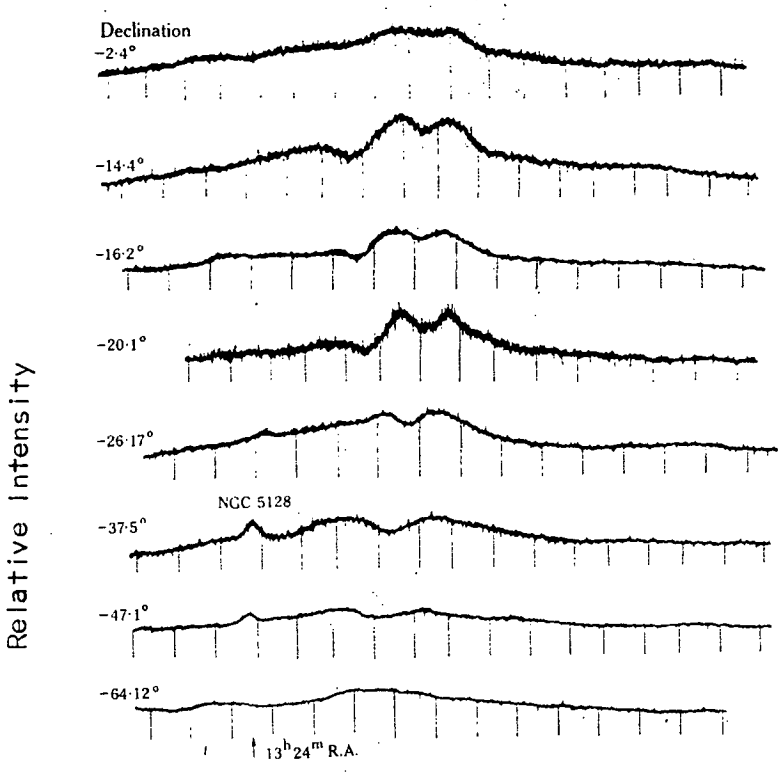

Sample records at eight declinations.

FIGURE 15

after Hamilton and Haynes (1968)

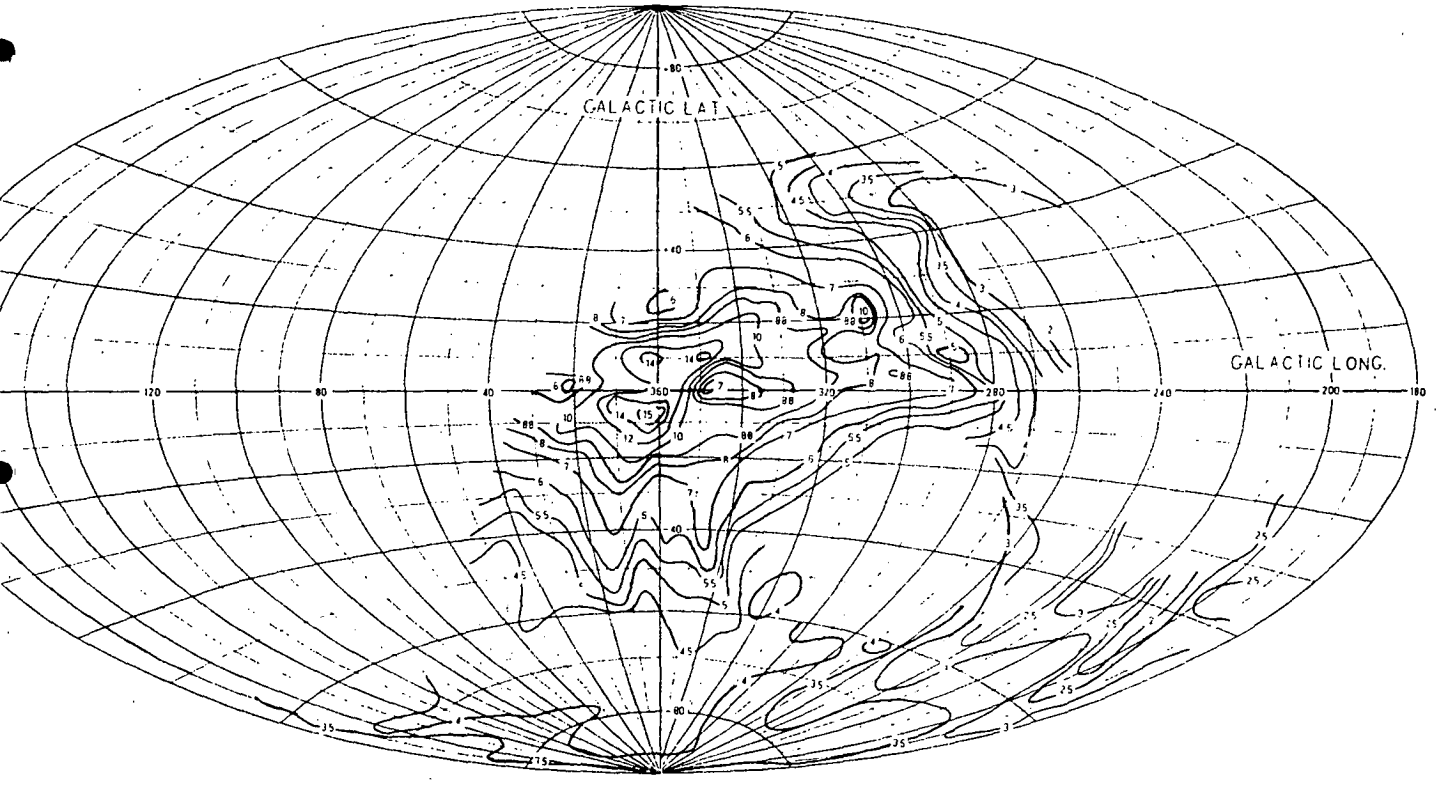

Background survey at 10·02 MHz (contour intervals of 2×10^5 degK).

FIGURE 16

after Hamilton and Haynes (1968)

the low resolution observations of the same area. The temperature of this region has been taken to be $6.3_{10}5$ degK in agreement with the spectrum obtained in Chapter 4. This makes the contour interval $2.0_{10}5$ degK.

The galactic plane is seen in absorption, as in the maps at 2.1 MHz and 4.7 MHz, although the contrast in the 10 MHz map is not as great.

Discrete sources:

Problems of transmitting station interference led to the combination of narrow bandwidth and short second-detector time constant. The resulting fluctuation in record level was rather high, making the measurements of discrete sources difficult. The smallest observable flux density was calculated to be in the range 800 - 1400 flux units, depending on the brightness of the background.

The flux densities of those sources whose records reproduced accurately a sufficient number of times are given in Table II. Spectra are shown in figure 17.

TABLE II

DISCRETE SOURCES OBSERVED AT 10 MHZ

Parkes Catalogue Number	R.A.	declination	flux density *(f.u.)*	notes
0821-43 0834-46			2800	Puppis A (not resolved)
1322-42	1322	-43	43000	Centaurus A
1343-60	1343	-60	1500	IAU 13S6A
1549-56	1549	-56	1400	
1648+05	1648	+05	7800	Hercules A
1711-38	1711	-38	1600	

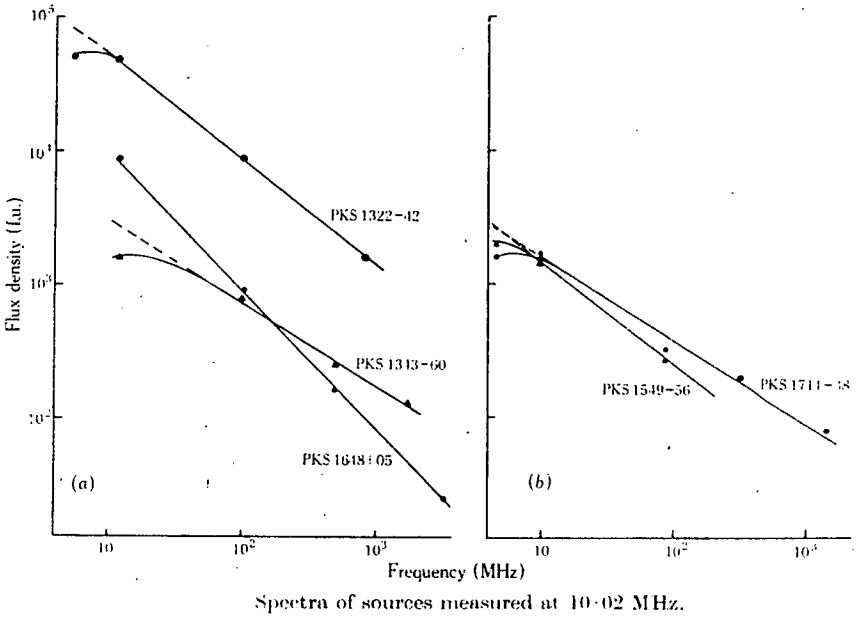

Spectra of sources measured at 10·02 MHz.

FIGURE 17

after Hamilton and Haynes (1968)

THE 153 MHZ SURVEY

The 153 MHz survey was made with the 210 foot reflector at Parkes, N.S.W. The continuum survey has been reported by Hamilton and Haynes (1969) and the discrete source observations by Hamilton and Haynes (1967).

(a) Equipment:

The receiver was a solid-state total power receiver with a nominal centre-frequency of 153 MHz and a bandwidth of 3.8 MHz. The peak-to-peak fluctuations at the output were about 1.5 degK when the second detector time constant was 1 second.

The feed consisted of a pair of half-wave dipoles with a reflector. The aerial response pattern was determined from a number of scans through strong, isolated sources and found to be close to circular with a beamwidth of 2.18° and a Gaussian profile.

No attempt was made to keep the feed angle constant during the survey.

(b) Observing procedure:

The survey was made with scans in declination. The telescope was driven through 30° at a drive rate of $2.5\ ^{\circ}$/minute with the right ascension constant. A grid of

these scans was built up at a spacing of 12^m in RA. Regions showing fine detail were then examined again with a scan separation of 6^m.

A number of reference scans were made in right ascension to tie together the main declination scans. The telescope was driven at 2.5^o/minute for a range of 3^h and then pointed to the south celestial pole. In this way the declination scans were related to one another, and the whole survey was referred to the south celestial pole.

The relative accuracy of the survey was established by making a number of scans across the same region of the sky at different times; the relative accuracy is believed to be ±5%.

(c) Calibration:

Thermal loads were used to calibrate a temperature-saturated noise diode which was used as a secondary standard throughout the survey. An additional check was made by comparing the noise diode calibrations with scans through the standard sources *Hydra A* and *Hercules A*. The results obtained were in close agreement with the flux densities of 340 f.u. and 420 f.u. respectively, given by Conway, Kellermann and Long (1963).

Noise diode calibrations were made at the beginning and end of each scan, and the appropriate small adjustments made to the records.

The survey reference point was the south celestial pole, and the absolute calibration required the determination of the equivalent aerial temperature of this region. This was done by replacing the feed with a thermal load and adjusting the temperature of the load to give the same output from the receiver. The value obtained in this way was 280±15 degK.

(d) Results:

Discrete sources:

The survey was undertaken primarily for the information on the background emission. A consequence of the scanning grid was that very few scans passed directly through a source, and corrections to the observations were accordingly required. The method adopted was as follows. The charts for each scan were examined for sources and the position of each one was determined within the limits of the scanning grid. The *Parkes Catalogue of Radio Sources* was then searched for a source within 0.6° of this position. Provided that no other sources were catalogued within 0.6° and, further, that no strong sources were listed within a

beamwidth of the telescope position a tentative identification was made. Measurements of the aerial response pattern showed it to be close to Gaussian in profile, and the source flux densities were corrected on this basis using the source position given in the *Parkes Catalogue*.

Of the 1300 possible source records only 312 were retained as completely reliable profiles free from confusion with neighbouring sources. The flux measurements of 64 of these (given in parentheses in the Table) may include the effects of a weak source catalogued within a beamwidth of the source position.

Table III contains details of the 248 sources whose measurements are considered reliable, together with the 64 sources whose measurements should be regarded as upper limits. Spectra of some of the more interesting sources are shown in figure 18.

TABLE III

DISCRETE SOURCES OBSERVED AT 153 MHZ

after Hamilton and Haynes (1967)

The following table contains details of the 248 sources selected as reliable records from the 153 MHz survey scans. A further 64 measurements have been given in parentheses where the measurement may have included the effects of a nearby weak source. Details of the columns are:

Column 1: Source catalogue number in the *Parkes Catalogue.*

Columns 2 and 3: Position for Epoch 1950.0 from the *Parkes Catalogue.*

Columns 4 - 9: Flux densities at a number of frequencies. Observations at 85.5 MHz are from Mills, Slee and Hill (1958); at 159 and 178 MHz from the 3C catalogue (Edge *et al*, 1959); at 408, 1410 and 2650 MHz from the *Parkes Catalogue.*

Column 10: Spectral index as determined at 400 MHz (C indicates curved spectrum).

Columns 11 and 12: Catalogue numbers as given in 3C and MSH catalogues.

FLUX DENSITIES OF OBSERVED SOURCES

Flux density values shown in parentheses are uncertain

(1)	(2)			(3)		(4)	(5)	(6)	(7)	(8)	(9)	(10)	(11)	(12)
Parkes Cat. No.	Position (1950·0) R.A. h	m	s	Dec. °	′	Flux Densities at (MHz): 85·5	153	159	408	1410	2650	Spectral Index α_{400}	Other Cat. Nos. 3C	MSH
0000+00														
2357+00	23	57	22	+00	26·3		18·03		2·3	<0·5	0·3	1·1±0·2		
0003+00														
0000−17	00	00	48	−17	43·9		14·69		5·5	2·2	1·4	0·7±0·2		
0003−42	00	03	28	−42	52·3	17	14·35		4·6	1·7	0·9	0·8		00−42
0004−83	00	04	09	−83	22·5		24·70		7·9	2·5	1·3			
0007−44	00	07	58	−44	40·0	31	26·82		6·5	1·7	0·9	1·0		00−43
0008−42	00	08	22	−42	10·2		9·31		6·4	5·4	2·6			
0010+00	00	10	34	+00	35·2	20	11·4		5·1	1·6	0·9	0·9±0·1	5	00+02
0012−38	00	12	52	−38	21·1	19	12·86		4·9	1·6	0·7	0·9		00−35
0013−63	00	13	35	−63	27·6	27	13·84		7·4	1·9	0·7	0·8		00−61
0020−25	00	20	38	−25	19·3	21	11·00		4·8	2·4	1·4	0·9		00−27
0021−29	00	21	58	−29	45·7	33	19·95		8·2	3·3	1·6	0·9		00−29
0022−60	00	22	53	−60	46·6		10·94		3·5	1·4	0·7			
0023−13	00	23	32	−13	04·7		(37·10)		5·0	1·3	0·6	1·1±0·2		
0031+01	00	31	49	+01	05·3	20	(18·3)		(3·0)	0·5	0·3	1·2±0·1		00+06
0032−20	00	32	39	−20	20·7	19	7·12		5·9	2·4	1·0	0·7		00−216
0036−62	00	36	30	−62	48·2		8·49		3·1	1·4	0·8			
0036+03	00	36	45	+03	03·5	14	(22·3)		4·1	1·6	1·1	0·7±0·1		00+010
0037+04	00	37	18	+04	39·0		36·69		3·8	0·8	0·5	1·1±0·2		
0047−02	00	47	12	−02	59·8	18	14·63		4·2	1·3	0·8	0·9±0·1		00−014
0048−44	00	48	25	−44	45·1	16	15·68		4·2	1·6	0·7	0·9		
0053−01	00	53	39	−01	34·5		42·23		10·3	2·0	(0·9)	1·2±0·1		00−413
0055−01	00	55	01	−01	39·6	(72)	46·16	17·0	12·1	4·7	3·6	0·6±0·1	29	00−017
0056−17	00	56	38	−17	16·8	29	12·60		5·5	1·7	0·9	1·0±0·1		00−126
0057−18	00	57	42	−18	04·6		(18·57)		3·9	1·2	0·7	0·9±0·2		
0101−12	01	01	53	−12	51·6	18	16·61		4·4	1·8	1·3	0·7±0·1		01−11
0103−45	01	03	06	−45	22·0	41	17·29		7·5	2·8	1·5	1·1		01−41

(1)	(2)			(3)		(4)	(5)	(6)	(7)	(8)	(9)	(10)	(11)	(12)
Parkes Cat. No.	Position (1950·0) R.A. h	m	s	Dec. °	′	Flux Densities at (MHz): 85·5	153	159	408	1410	2650	Spectral Index α_{400}	Other Cat. Nos. 3C	MSH
0105−16	01	05	48	−16	20·4	53	30·17	20·0	12·3	3·8	2·2	0·9 ± 0·0	32	01−12
0109+02	01	09	32	+02	40·7		8·60		1·9	0·6	0·3	1·0 ± 0·3		
0110−69	01	10	01	−69	17·2		(24·23)		5·5	2·0	1·0			
0114−21	01	14	26	−21	07·7	18	(25·30)		11·6	4·1	1·9	0·3		01−26
0115+02	01	15	49	+02	42·9		13·01		(4·5)	1·5	1·0	0·6 ± 0·3	(37)	
0116−19	01	16	07	−19	05·3	14	(16·78)		2·6	1·2	0·7	0·8 ± 0·1		01−18
0118−03	01	18	29	+03	28·3	(16)	(8·12)		(5·0)	1·2	0·6	1·1 ± 0·3	(39)	(01−03)
0122−25	01	22	26	−25	33·6	9	8·70		4·2	1·3	0·7	0·5		01−29
0123−01	01	23	28	−01	38·5	88	25·14	26·0	16·4	4·5	(1·9)	1·0 ± 0·1	40	01−05
0125−14	01	25	03	−14	18·7	30	23·3		8·9	2·4	1·5	0·8 ± 0·1		01−111
0126−53	01	26	29	−53	10·4	11	16·4		3·8	0·9	0·6	0·7		01−54
0124−40	01	24	12	−40	59·1		12·26			1·4	2·6			
0128+03	01	28	40	+03	58·6	18	(9·15)		5·3	2·2	1·0	0·8 ± 0·1		01+06
0128−26	01	28	07	−26	25·5	18	10·7		5·7	1·2	0·6	0·7		01−211
0129−07	01	29	35	−07	10·8	19	9·31		(4·7)	1·2	0·7	0·9 ± 0·1		01−06
0129−51	01	29	11	−51	18·5	8	(18·33)		3·1	1·0	0·5	0·6		01−55
0131−36	01	31	42	−36	44·6	56	31·79		16	7·1	3·4	0·8		01−311
0132+07	01	32	39	+07	56·2	15	10·75		6·8	2·4	1·3	0·8 ± 0·1		01+08
0137−10	01	37	44	−10	12·3		4·4		(2·0)	1·2	0·6	0·9 ± 0·4		
0139−14	01	39	17	−14	59·6		13·3		2·2	0·4	0·3	1·0 ± 0·3		
0146+00	01	46	16	+00	07·2		19·0		2·6	(0·5)	(0·5)			
0146+06	01	46	08	+06	06·3	19	11·7		3·4	0·8	0·4	1·1 ± 0·1		01+011
0148−29	01	48	20	−29	46·5		11·8		2·8	1·8				01−217
0150+00	01	50	15	+00	07·3		(20·6)		1·9	0·5	0·3	1·0 ± 0·3		
0152−76	01	52	14	−76	29·8		9·3		3·9	0·8				
0157+01	01	57	38	+01	10·3	16	10·1		4·5	0·6	0·4	1·1 ± 0·1		01+014
0157−31	01	57	57	−31	08·2	26	13·4		9·3	3·7	2·4	0·7		01−315
0202−76	02	02	00	−76	34·1	18	11·2		8·0	2·6	1·3	0·6		01−71?
0213−13	02	13	12	−13	13·4	(42)	(30·6)	(13)	11·9	5·0	2·7	0·7 ± 0·1	(62)	02−15
0214−48	02	14	53	−48	03·4	31	18·5		9·5	2·4	1·3	0·8		02−43
0215+02	02	15	50	+02	44·1		24·7		3·5	0·7	0·3	1·3 ± 0·2		
0216−25	02	16	29	−25	03·1	15	(19·3)		4·7	1·3	0·7	0·7		02−25
0218−02	02	18	21	−02	10·5	74	(73·8)	26	12·4	3·9	1·7	1·0 ± 0·0	63	02−07
0220−42	02	20	21	−43	13·9	17	11·5		4·2	0·9	1·6	0·9		02−45
0222−23	02	22	49	−23	26·3	19	16·5		6·2	1·9	1·1	0·7		02−27
0235+09	02	35	46	+09	59·3		14·5		2·6	1·3	(0·4)	0·6 ± 0·3		
0237+09	02	37	43	+09	44·6				(1·1)	<0·5	0·3			

(1)	(2)			(3)		(4)	(5)	(6)	(7)	(8)	(9)	(10)	(11)	(12)
Parkes Cat. No.	Position (1950·0) R.A. h	m	s	Dec. °	′	Flux Densities at (MHz): 85·5	153	159	408	1410	2650	Spectral Index α_{400}	Other Cat. Nos. 3C	MSH
0241−51	02	41	52	−51	22·7	37	22·8		11·8	2·9	0·8	0·7		02−*53*
0245−55	02	45	27	−55	54·2	48	35·9		12·2	2·4	1·2	0·9		02−*54*
0246−13	02	46	15	−13	35·3	15	13·7		2·1	0·8	0·6	0·9 ± 0·1		02−*114*
0255+05	02	55	04	+05	50·7	51	37·3	25*	16·2	5·9	3·3	0·8 ± 0·0	75	02+*010*
0257−05	02	57	32	−05	44·3		12·0		2·9	0·4	0·3	1·2 ± 0·3		
0304−12	03	04	34	−12	17·6		36·3		5·5	1·5	0·8	1·0 ± 0·2		
0312−03	03	12	54	−03	27·3	20	15·3		4·0	1·2	0·8	0·9 ± 0·1		03−*01*
0319−45	03	19	39	−45	21·8	19	12·3		9·5	3·4	1·7	0·5		03−*43*
0320−37	03	20	42	−37	25·0	950	474·2		249		89			03−*31*
0332−05	03	32	09	−05	44·8		(18·2)		3·3	1·6	1·0	0·6 ± 0·2		
0331−01	03	31	42	−01	21·2	64	43·8	19·5	11·9	2·5	1·5	1·1 ± 0·6	89	03−*03*
0332−39	03	32	17	−39	10·5	10	(18·7)		4·5	1·7	0·9	0·5		03−*32*
0336−01	03	36	59	−01	56·2		19·5		3·5	1·5	2·2	C		
0344−34	03	44	40	−34	31·5	33	18·9		9·3	3·0	1·7	0·8		03−*36*
0347+05	03	47	08	+05	43·0	15	(27·9)		9·0	3·3	2·0	0·7 ± 0·3		03+*010*
0349−14	03	49	10	−14	38·3	44	16·6	(8·5)	11·6	2·9	(1·4)	0·9 ± 0·4	(95)	03−*19*
0356+10	03	56	15	+10	17·7		44·2	44*	27·5	10·8	(5·8)	0·7 ± 0·1	98	
0410−75	04	10	11	−75	15·3	87	55·30		40	13·5	7·5	0·5		04−*71*
0418−05	04	18	22	−05	44·6		(46·5)		3·8	0·8	0·6	0·9 ± 0·2		
0424−26	04	24	41	−26	49·9		18·2		3·7	1·2	0·6			
0427−36	04	27	52	−36	37·5	35	15·2		7·2	2·1	1·1	1·0		04−*36*
0427−53	04	27	51	−53	56·1	50	39·5		14·6	5·6	2·7	0·8		04−*54*
0431−13	04	31	49	−13	29·0	(38)	17·9				0·4			}
	04	31	55	−13	17·0				(7·7)	1·4	0·8	1·1 ± 0·1		} 04−*112*
0442−28	04	42	38	−28	14·8	82	66·0		22	7·1	3·9	0·9		04−*218*
0446−20	04	46	25	−20	36·0	19	18·6		4·2	0·9	0·4	1·0		04−*219*
0448−04	04	48	30	−04	36·4	(23)	6·9		(5·0)	(0·7)	0·5	1·1 ± 0·1		04−*117*
0452+10	04	52	20	+10	04·4		13·7		2·8	0·6	0·3	1·2 ± 0·3		
0453−20	04	53	13	−20	40·5	18	(18·1)		9·3	4·7	3·1	0·4		04−*222*
0455−40	04	55	49	−40	29·9	13	9·5		3·7	1·0	0·6	0·8		04−*410*

(1)	(2)			(3)		(4)	(5)	(6)	(7)	(8)	(9)	(10)	(11)	(12)
Parkes Cat. No.	Position (1950·0) R.A. h	m	s	Dec. °	′	Flux Densities at (MHz): 85·5	153	159	408	1410	2650	Spectral Index α_{400}	Other Cat. Nos. 3C	MSH
0456−30	04	56	33	−30	10·8		28·2			2·7	1·6			
0458−01	04	58	08	−01	26·5	15	11·3		3·4	0·8	0·6	0·9 : 0·1		04 − 114
0502−10	05	02	30	−10	19·5	20	7·0		4·8	1·4	0·8	0·9 : 0·1		05 − 11
0503−28	05	03	42	−28	59·7	30	26·7		5·5	1·1	0·6	1·1		05 − 22
0508−07	05	08	37	−07	38·1		(21·4)		3·1	1·1	0·6	0·8 : 0·2		
0510−04	05	10	18	−04	0·18		25·5		3·1	0·6	0·5	0·9 : 0·3		
0511−30	05	11	44	−30	31·7	29	10·13		8·9	2·7	1·2	0·8		05−33
0511−48	05	11	35	−48	28·0	41	(43·8)		13·2	3·5	2·1	0·7		05 − 42
0514+10	05	14	05	+10	53·3		(21·3)		3·3	1·1	0·7	0·8 : 0·2		
0517−56	05	17	36	−56	16·3		30·7		4·6	1·2	0·8			
0518−45	05	18	24	−45	49·8	570	343·0		166	66	30	0·8		05 −43
0521−36	05	21	14	−36	30·0	66	54·5		37	18·6	11·4	0·4		05 − 36
0532−05	05	32	51	−05	25·0	(69)	41·6	45	(213)	(289)	(49·0)	HII region	145	05 011
0604−20	06	04	29	−20	22·2	23	20·0		8·9	3·3	2·0	0·6		06 − 22
0611−74	06	11	36	−74	30·0		5·4		2·6	1·1				
0612−47	06	12	16	−47	26·1	27	12·2		5·8	1·2	0·7	1·0		06 43
0625−53	06	25	18	−53	39·3	113	73·3		26	6·7	3·5	1·0		06 − 55
0637−75	06	37	20	−75	14·4	20	13·0		9·7	6·7	4·9	0·4		06 − 71
0646−39	06	46	33	−39	53·1	26	23·6		7·0	2·6	1·5	0·8		06 − 372
0651−56	06	51	53	−56	38·3	18	8·6		4·9	1·1	0·7	0·8		06 − 57
0656−24	06	56	54	−24	12·5	59	50·3		13·0	3·1	1·3	1·0		06−216
0709−20	07	09	39	−20	37·3	33	26·8		8·7	2·0	1·1	0·8		07 − 23
0710+11	07	10	12	+11	52·1		21·8	17·2*	8·6	2·7	1·3	1·0 ± 0·1	175	
0727−36	07	27	20	−36	34·3		8·3		4·9	2·0	1·3			
0748−44	07	48	08	−44	04·7	27	14·6		8·0	2·3	1·1	0·8		07 − 413
0800−09	08	00	15	−09	49·8		8·09		6·1	1·7	(1·1)	1·0 ± 0·2		
0806−10	08	06	31	−10	19·1	40	25·44	21·0	13·7	3·4	2·3	0·8 ± 0·0	195	08 − 14
0809−05·2	08	09	33	−05	10·9		}			0·6				
0809−05·7	08	09	35	−05	40·8	22	} 25·17		4·8	1·3	0·8	0·9 ± 0·1		08 − 04
0812−02	08	12	56	−02	59·3	35	19·54		(9·4)	1·6	0·9	1·0 ± 0·1	196·1	08 − 05
0812·02	08	12	51	+02	04·8	22	26·66		6·0	2·0	1·0	0·9 ± 0·1		08 + 02
0818−74	08	18	57	−74	44·6		(47·2)			0·6				
0819+06	08	19	53	+06	06·9	60	(62·76)	17·8*	6·6	2·3	(0·8)	1·1 ± 0·1	198	08 + 03
0825−20	08	25	07	−20	16·3	26	20·63		11·7	3·7	2·1	0·5		08 − 24
0832−07	08	32	36	−07	36·0	13	11·13		3·5	0·4		1·1 ± 0·2		08 − 010

* Flux values measured at 178 MHz.

(1)	(2)			(3)		(4)	(5)	(6)	(7)	(8)	(9)	(10)	(11)	(12)
Parkes Cat. No.	Position (1950·0) R.A. h	m	s	Dec. °	′	Flux Densities at (MHz): 85·5	153	159	408	1410	2650	Spectral Index α_{400}	Other Cat. Nos. 3C	MSH
0837−12	08	37	27	−12	04·1		27·91		5·7	1·8	1·0	0·9±0·2		
0842−75	08	42	12	−75	29·5	58	51·6		10·5	4·3	2·4	1·1		08−71
0843−33	08	43	10	−33	38·3	17	(26·61)		4·6	2·0	1·3	0·8		08−38
0850−20	08	50	47	−20	36·0	19	(11·99)		6·2	2·2	1·3	0·7		08−216
0850−03	08	50	56	−03	29·3		13·84		4·3	1·2	0·8	0·8±0·2		
0851−14	08	51	28	−14	16·7	24	(48·01)		6·1	1·6	0·9	0·9±0·1	209	
0853+03	08	53	00	+03	24·4		(84·58)		2·6	0·7	0·4	1·0±0·3		
0855−19	08	55	48	−19	39·3	17	(15·49)		3·4	1·3	1·0	0·8±0·1		08−119
0859−05	08	59	58	−05	04·4	18	13·93		5·0	1·0	0·6	1·0±0·1		08−015
0859−14	08	59	55	−14	04·0	12	8·68		5·4	3·1	2·6	0·4±0·1		09−11
0859−25	08	59	37	−25	44·2	54	51·03		16·4	5·8	3·3	0·8		08−219
0905+04	09	05	17	+04	26·8		12·27		2·9	0·6	0·3	1·2±0·3		
0905−68	09	05	59	−68	16·9		18·09		6·1	1·7	0·9			
0906+01	09	06	27	+01	33·7		(66·78)		2·6	1·3	1·2	0·3±0·2		
0909+08	09	09	30	+08	23·8	13	7·25		2·3	0·8	0·4	1·0±0·1		09+01
0912−16	09	12	53	−16	18·9		13·44		2·7	0·8	0·4	1·0±0·3		
0933+04	09	33	51	+04	36·9	24	(24·32)	9·7*	5·1	0·9	0·3	1·2±0·1	222	09+03
0941+10	09	41	34	+10	00·0	32	17·77	14·6*	8·7	2·3	1·0	1·0±0·0	226	09+05
0943−76	09	43	25	−76	06·7		48·1		6·6	2·1	1·2			
0944−13	09	44	58	−13	32·5		12·2		3·2	0·6		1·2±0·3		
0945+07	09	45	06	+07	39·9	89	41·0	30·0*	22·1	7·8	4·3	0·8±0·0	227	09+07
0949+00	09	49	26	+00	11·8	(36)	33·6	23·0*	(12·0)	(3·2)	1·5	1·0±0·1	230	} (09+08)
0950+00	09	50	13	+00	14·4	(36)	37·0		(12·0)	(3·2)	0·5			
0955−28	09	55	50	−28	50·2	18	(27·3)		6·0	1·4	0·7	0·7		09−212
0955+03	09	55	33	+03	39·7	18	7·8		4·4	0·9	0·4	1·1±0·1		09+010
0957+00	09	57	42	+00	19·5		10·7		3·1	1·0	0·6	0·9±0·2		
1002−21	10	02	52	−21	33·3	48	33·1		7·7	1·8	0·7	1·2		10−21
1005+07	10	05	20	+07	46·1	30	22·3	26*	16·4	6·2	3·5	C	237	10+01
1008+06	10	08	19	+06	40·0	39	24·0	14·0*	12·3	3·1	1·3	C	238	10+02
1011+31	10	11	33	+31	37·6	10	9·1		3·7	1·4	0·9	0·6		10−33

(1)	(2)			(3)		(4)	(5)	(6)	(7)	(8)	(9)	(10)	(11)	(12)
Parkes Cat. No.	Position (1950·0) R.A. h	m	s	Dec. °	′	Flux Densities at (MHz): 85·5	153	159	408	1410	2650	Spectral Index α_{2400}	Other Cat. Nos. 3C	MSH
1015−31	10	15	55	−31	28·5	14	14·1		5·5	3·5	3·0	0·6		10−35
1023+06	10	23	54	+06	44·4	35	13·0		5·2	0·9	0·4	1·3±0·1	243	10+06
1027+00	10	27	35	+00	51·9		11·2		2·1	1·0	0·9	0·4±0·3		
1030−34	10	30	58	−34	03·4	20	13·7		6·2	1·4	0·8	0·8		10−38
1031−40	10	31	13	−40	48·2		14·0		4·2	1·2	0·4			10−410
1031+11	10	31	23	+11	30·0		(49·5)*		5·1	1·3	(0·5)	1·1±0·2		
1056+09	10	56	59			19	17·6		3·2	0·5	0·3	1·2±0·1		10+011
1108+03	11	08	48	+03	25·5	15	12·8		4·7	1·2	0·5	1·0±0·1		11+02
1110−01	11	10	59	−01	56·8	18	10·2	8·0	4·6	1·4	0·9	0·8±0·1	253	11−05
1116−02	11	16	51	−02	46·7	31	19·5	15·0	10·2	1·6	0·6	C	255	11−08
1116−46	11	16	05	−46	17·9		21·4		7·3	2·4	1·6			
1122−37	11	22	56	−37	06·0	7	9·1		4·9	1·3	0·7	0·2		11−32
1123−35	11	23	28	−35	06·7	17	17·7		7·2	2·6	1·6	0·5		11−33
1131−17	11	31	51	−17	12·1	(19)	11·3		4·7	1·5	0·9	0·8±0·1		(11−17)
1131−19	11	31	08	−19	37·9	32	18·0		4·6	1·2	0·5	1·1±0·1		11−16
1134+01	11	34	53	+01	34·1		15·51		3·6	1·1	0·6	1·0±0·2	(262)	
1136−13	11	36	38	−13	34·1	44	42·6		12·8	4·1	2·8	0·8±0·0		11−18
1136−32	11	36	48	−32	05·8	28	23·8		5·8	2·5	1·2	1·0		11−38
1138+01	11	38	37	+01	30·1	15	(17·99)		7·2	2·1	1·6	0·7±0·1	(262)	11+08
1138−26	11	38	02	−26	12·9	28	8·9		4·1	0·9	0·4	1·2		11−27
1143−48	11	43	04	−48	19·3	28	30·1		9·3	3·3	1·8	0·7		11−46
1146+05	11	46	17	+05	12·4	11	7·68		(3·0)	0·6	0·3	1·0±0·1		11+012
1146−11	11	46	36	−11	48·1	17	13·8		4·2	1·4	0·7	0·9±0·1		11−113
1148−00	11	48	10	−00	07·2		7·80		3·5	2·9	2·6	0·1±0·2		
1152+04	11	52	23	+04	40·4	12	(13·74)		4·0	0·8	0·3	1·1±0·1		11+013
1211−41	12	11	39	−41	43·2	18	(21·2)		5·1	1·6	1·0	0·8		12−41
1215−45	12	15	28	−45	45·2	19	11·3		10	5·4	3·2	0·4		12−43
1226+02	12	26	34	+02	19·1	167	(150·1)	72*	55·1	41·2	37·3	C	273	12+08
1232−41	12	32	59	−41	36·5	11	7·3		7·1	2·2	1·0	0·3		12−44
1245−19	12	45	45	−19	43·0		19·1		7·9	5·1	3·5	0·4±0·1		
1245−41	12	45	54	−41	01·7	45	34·6		10·3	4·1	2·4	1·0		12 45
1246+09	12	46	17	+09	33·1	14	8·7		4·2	0·8	0·4	1·1±0·1		12+010
1247−19	12	47	41	−19	29·7		14·3		4·3	1·2	0·7	0·9±0·2		
1249+09	12	49	11	+09	12·2		7·2		5·1	1·8	1·0	0·9±0·1		
1252−12	12	52	00	−12	17·1	53	37·9	42·0	17·6	6·8	4·5	0·7±0·0	278	12−118
1259−44	12	59	38	−44	30·4		8·2		4·2	1·7	0·9			

* Flux values measured at 178 MHz.

(1)	(2)			(3)		(4)	(5)	(6)	(7)	(8)	(9)	(10)	(11)	(12)
Parkes Cat. No.	Position (1950·0) R.A. h	m	s	Dec. °	′	Flux Densities at (MHz): 85·5	153	159	408	1410	2650	Spectral Index α_{400}	Other Cat. Nos. 3C	MSH
1508−05	15	08	13	−05	31·8	8	(17·2)		8·9	3·9	2·5	C		15−05
1510−08	15	10	09	−08	54·9		(9·7)		3·0	3·0	3·0	−0·0±0·2		
1514+00	15	14	14	+00	26·1	16	(17·7)		4·4	2·5	1·8	0·6±0·1		15+06
1514+07	15	14	18	+07	12·6	140	43·0	46*	26·4	5·6	2·2	1·2±0·0	3·7	15+05
1523+03	15	23	23	+03	19·2		14·8		5·0	2·2	1·2	0·8±0·1		
1539−09	15	39	26	−09	18·3		7·3		2·4	1·2	1·0	0·4±0·3		
1547−79	15	47	45	−79	32·6		33·0			4·0	2·8			
1549−79	15	49	36	−79	06·3		(20·1)			6·2	4·9			
1603+00	16	03	42	+00	08·6	35	30·5		(7·9)	2·2	1·4	0·9±0·1		16+03
1609−14	16	09	17	−14	12·0		(33·6)		2·3	1·2	(0·4)			
1621−11	16	21	13	−11	34·0	20	21·3		8·6	2·2	1·3	0·8±0·1		16−18
1635−14	16	35	55	−14	10·0		9·2		(4·3)	1·2	1·0	0·6±0·3		
1640−15	16	40	59	−15	20·2	30	(27·7)		5·7	1·2	0·5	1·1±0·1		16−17
1648+05	16	48	42	+05	04·5	890	424	350*	161	46·0	24·6	1·0±0·0	348	16+010
1644−10	16	44	43	−10	39·0		(42·9)		6·9	2·2	1·4	0·8±0·1		
1701+05	17	01	08	+05	06·1		5·5		3·1	0·6	0·3	1·2±0·2		
1712−03	17	12	25	−03	17·7	21	(53·0)		8·3	1·5	0·5	C		17−04
1712−12	17	12	51	−12	03·0		(10·0)		3·1	1·0	0·6	0·8±0·2		
1717+00	17	17	56	−00	55·9	475	324·7	180*	138	50·2	27·5	0·8±0·2	353	17−06
1754−59	17	54	35	−59	46·3	25	44·4		15	3·9	1·5	0·4		17−51
1802+11	18	02	44	+11	01·3		(169·9)	15*	4·3	1·1	0·7	1·1±0·1	368	
1914−45	19	14	04	−45	36·5	13	28·1		3·5	0·8	0·4	0·8		19−42
1928−34	19	28	25	−34	01·7		13·1		3·1	1·2	0·4			
1932−46	19	32	20	−46	28·2	141	(157·2)		39	13·4	6·9	0·8		19−46
1933−58	19	33	18	−58	45·9	17	25·4		6·8	3·5	1·8	0·6		19−56
1951−50	19	51	25	−50	09·9	14	(23·2)		4·0	1·5	0·9	0·8		19−42
1954−55	19	54	21	−55	17·8	54	21·6		14·8	7·0	4·0	0·8		19−57
1955−35	19	55	43	−35	43·3	45	17·5		9·6	2·4	1·2	1·0		19−35
2006−56	20	06	31	−56	37·8	81	(87·3)		12·2	1·9	0·4	1·2		20−52
2019+09	20	19	43	+09	52·0	27	15·8	15*	9·4	3·4	1·4	0·9±0·0	411	$20+09_{81}$
2030−23	20	30	18	−23	02·8	22	13·1		8·2	3·0	1·6	0·6		20−28
2032−35	20	32	35	−35	05·1	41	19·9		12·8	6·4	3·7	0·7		20−37
2044−02	20	44	34	−02	47·5		9·6	9·5	7·2	2·3	1·5	0·7±0·1	422	
2045+06	20	45	40	+06	50·1	22	41·6	13·4*	(9·8)	2·6	1·1	0·9±0·1	424	20+010
2049−36	20	49	08	−36	51·8	19	11·4		4·3	1·4	0·6	1·0		20−38
2058−13	20	58	57	−13	30·6	14	9·1		3·7	1·3	0·6	0·9±0·1		20−119

* Flux values measured at 178 MHz.

(1)	(2)			(3)			(4)	(5)	(6)	(7)	(8)	(9)	(10)	(11)	(12)
Parkes Cat. No.	Position (1950·0) R.A. h	m	s	Dec. °	′		Flux Densities at (MHz): 85·5	153	159	408	1410	2650	Spectral Index α_{400}	Other Cat. Nos. 3C	MSH
2059−09	20	59	38	−09	33·3			15·1			0·4	0·3	0·6±0·7		
2101−49	21	01	41	−49	01·5			7·3			1·1	0·7			
2104−25	21	04	23	−25	39·0		100	54·1		31	12	7·3	0·8		21−21
2105−48	21	05	24	−48	59·1			8·4		3·1	1·2	1·0			
2107−34	21	07	44	−34	03·6		14	15·2		3·8	1·3	0·7	0·8		21−32
2119−16	21	19	18	−16	54·6		(30)	(17·2)			0·6	0·3			21−19
2120−16	21	20	14	−16	40·8		(30)	(14·5)		(9·0)	1·3	0·6	0·8±0·4		
2123+00	21	23	14	+00	42·4			17·8		1·9	0·7	0·4	0·8±0·3		
2126+07	21	26	34	+07	19·8		27	19·9	10·3*	6·6	2·4	1·1	0·9±0·0	435	21+04
2141−81	21	41	14	−81	46·6			14·2		10	3·1	1·7			
2146−13	21	46	46	−13	18·6		(13)	12·3		5·6	1·5	0·9	0·9±0·1		21+119
2149−20	21	49	04	−20	00·4		18	10·7		6·5	2·1	1·4	0·7±0·1		21−121
2149−28	21	49	12	−28	43·0		12	8·3		5·4	3·2	1·9	0·5		21−214
2150−52	21	50	51	−52	04·6		28	14·6		10	4·2	2·1	0·7		21+58
2152−69	21	52	58	−69	55·8		253	113·7		80	32	17·5	0·8		21−64
2154−11	21	54	03	−11	41·2		28	20·1		6·5	1·1	0·5	1·1±0·1		21−114
2154−18	21	54	12	−18	28·3		25	22·2		8·8	3·6	0·9	C		21+123
2201−55	22	01	44	−55	32·8			8·4		4·9	2·1	1·0			
2203−18	22	03	26	−18	50·3		16	(18·7)		7·8	6·2	4·9	0·3±0·1		22−11
2207−43	22	07	57	−43	48·4		13	(14·6)		4·0	1·1	0·7	0·8		22−42
2207−45	22	07	15	−45	57·7			17·0		5·9	1·6	0·9			
2210−25	22	10	12	−25	43·3			5·4		3·2	1·3	0·9			
2211+08	22	11	12	+08	59·6		31	(29·0)		2·5	0·8	0·5	1·2±0·1		22+03
2213−45	22	13	49	−45	36·4			13·6		5·6	2·3	1·3			
2216−03	22	16	16	−03	50·6		(18)	8·5		2·8	0·9	1·0	C		22−06
2216−28	22	16	56	−28	12·1			16·1		6·8	2·6	1·9			
2218−50	22	18	05	−50	33·8			7·2			2·0	0·8			
2219−15	22	19	49	−15	01·5			(20·2)			0·4	0·3	0·6±0·7		
2220−15	22	20	00	−15	26·2			(40·1)		(3·3)	0·6	0·3	1·2±0·4		
2220−50	22	20	26	−50	32·6			7·7			1·2	0·7			

(1)	(2)			(3)		(4)	(5)	(6)	(7)	(8)	(9)	(10)	(11)	(12)
Parkes Cat. No.	Position (1950·0) R.A. h	m	s	Dec. °	′	Flux Densities at (MHz): 85·5	153	159	408	1410	2650	Spectral Index α_{2400}	Other Cat. Nos: 3C	MSH
2221−02	22	21	16	−02	21·9	60	19·6	(20·5)	17·5	5·3	(2·3)	0·8 ± 0·1	445	22 −09
2226+08	22	26	36	+08	58·8	19	17·2		5·0	0·6	0·5	1·1 ± 0·1		22 +06
2226−38	22	26	52	−38	39·7		13·1		8·4	2·6	0·9			
2226−41	22	26	25	−41	07·3	28	13·1		8·9	3·2	1·6	0·7		22−43
2250+03	22	50	07	+03	29·1	11	16·1		1·7	0·5	0·3	1·0 ± 0·1		22+077
2252−53	22	52	48	−53	01·4	22	23·5		7	3·5	1·7	0·7		22 · 54
2253−52	22	53	48	−52	14·9	28	27·2		7·8	3·1	1·3	0·8		22 - 55
2258+08	22	58	59	+08	22·5		4·9		2·3	0·6	0·4	0·9 ± 0·3		
2304+00	23	04	13	+00	38·7		(40·1)		1·6	<0·5	0·3	0·9 ± 0·3		
2305−41	23	05	06	−41	49·3		11·4		4·4	1·9	0·9			
2307+10	23	07	59	+10	39·7		12·8		3·1	0·7	0·7	0·7 ± 0·2		
2309+09	23	09	55	+09	03·5	29	23·4	14*	8·8	2·6	1·5	0·9 ± 0·0	456	23 +03
2310−41	23	10	07	−41	43·0		11·4		4·4	1·8	0·9			
2313+03	23	13	59	+03	48·3	57	26·9	24*	14·8	4·6	2·3	0·9 ± 0·0	459	23 +05
2313−18	23	13	09	−18	17·1		20·18		4·7	1·3	0·9	0·8 ± 0·2		
2317−27	23	17	19	−27	44·5	23	22·7		9·2	3·3	1·8	0·7		23−24
2319−55	23	19	14	−55	02·5		12·3		4·5	2·2	1·0			
2322−05	23	22	44	−05	14·2		27·4		4·3	1·5	0·8	0·9 ± 0·2		
2323−40	23	23	51	−40	44·3	15	8		8·0	3·9	2·2	0·5		23 −43
2325−15	23	25	55	−15	11·2	14	12·7		6·1	2·0	1·3	0·7 ± 0·1		23−173
2331−41	23	31	45	−41	42·8	50	24·9		15·6	5·7	2·9	0·9		23−44
2331−09	23	31	11	−09	20·9		22·9		6·0	1·2	0·5	1·3 ± 0·2		
2332−66	23	32	15	−66	54·4	26	11·0		7·8	2·5	1·3	0·8		23−63
2334−35	23	34	14	−35	01·8	24	13·6		4·5	1·3	0·6	1·1		23 −34
2335+03	23	35	30	+03	11·6		4·7		3·4	1·4	1·1	0·6 ± 0·2		
2337−06	23	37	13	−06	21·0		11·2		3·4	1·3	0·8	0·7 ± 0·2		
2338+04	23	38	27	+04	14·0		7·4		5·4	1·6	1·0	0·9 ± 0·1		
2338−03	23	38	55	−03	02·2		6·8		3·8	1·0	0·4	1·2 ± 0·2		
2338−16	23	38	37	−16	37·8		17·2		4·2	1·4	0·8	0·8 ± 0·2		
2338−58	23	38	31	−58	32·4	25	11·6		7·4	3·3	1·8	0·6		23−52
2354−35	23	54	27	−35	02·4	39	23·5		5·9	1·3	0·5	1·2		23−37

* Flux values measured at 178 MHz.

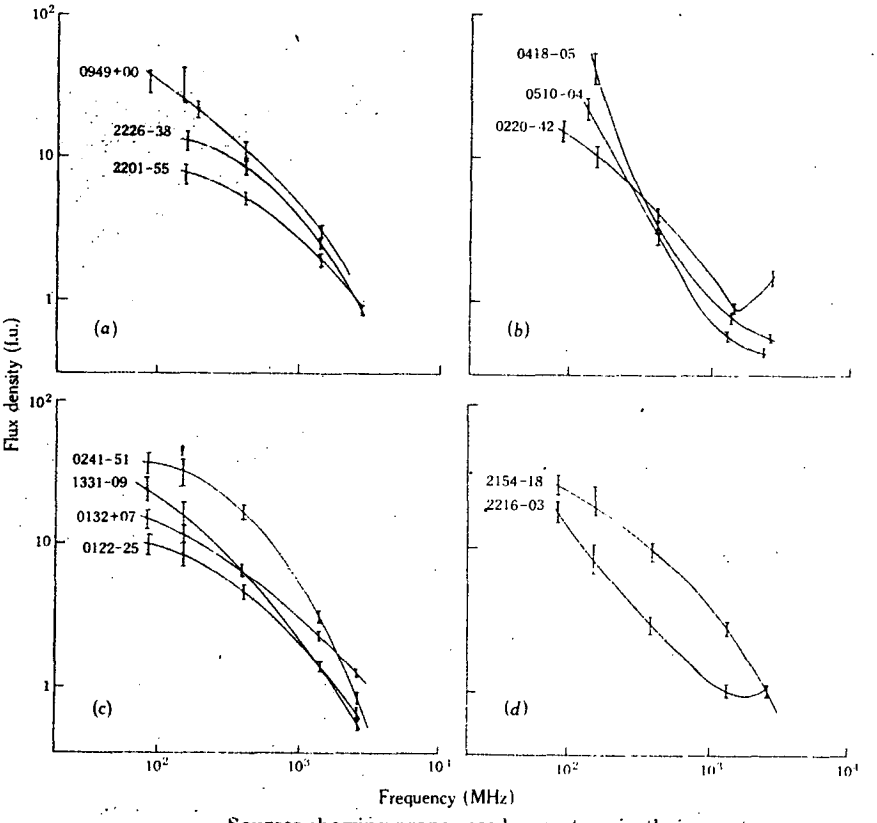

Sources showing pronounced curvature in their spectra.

FIGURE 18

after Hamilton and Haynes (1967)

Background radiation:

The results of the background survey are presented in figure 25 as smoothed contours of effective aerial temperature. The coordinates of the map are galactic coordinates. The dashed line in the figure indicates the limits of the observations. The effects of small sources have been removed from the map, but no attempt was made to remove the larger extended sources such as the region $l = 310^{\circ}$, $b = 20^{\circ}$ due to Centaurus A, because of the difficulty in assessing the relative contributions of the source and the background.

The most notable feature of the map is the spur at $l = 300^{\circ}$, $b = -50^{\circ}$ extending from the direction of the galactic centre into the large cold region centred on $l = 240^{\circ}$, $b = -40^{\circ}$. The position of the cold region corresponds to that of the similar region seen in northern maps, but they do not show any feature corresponding to this spur. The part of the well-kown northern spur near $l = 40^{\circ}$ that extends into the southern galactic hemisphere is prominent, and the feature near $l = 280^{\circ}$, $b = 70^{\circ}$ could well be the continuation of this spur, as proposed by Quigley and Haslam (1965).

Along the plane a number of steps in emission are apparent. These agree with the corresponding effects noted by Mills (1959), who suggested that in these directions the line of sight is tangential to a spiral arm. The present survey agrees well with the survey of the galactic plane by Wielebinski *et al* (1968), who discuss the emission steps in more detail. Agreement is also good with the northern survey at 178 MHz by Turtle and Baldwin (1962) in the region common to the two maps.

COMPARISON OF THE SURVEYS

The comparison of the high-resolution surveys is facilitated by their presentation on the same projection grid. The original maps have therefore been redrawn by hand on the Hammer Equal Area Projection, and the original contours are presented in this form in figures 20 - 25. The 85 MHz map was obtained from the composite whole-sky map given by Yates (1968). He combined the survey already discussed (Yates *et al*, 1967) with those from the northern hemisphere by Baldwin (1955) at 85 MHz, Turtle and Baldwin (1962) at 178 MHz, and Pauliny-Toth and Shakeshaft (1962) at 408 MHz. Yates states that " .... maximum relative error between directions in opposite hemispheres

is estimated to be 10 %." The original composite map is shown in figure 19.

A brief examination of the six survey maps shows clearly the value of low frequency radio astronomy. The three maps at frequencies above 20 MHz show essentially the same features — in particular the spurs and the extensive cold region correspond well. Much of the difference between these 3 maps is accounted for by the difference in resolution.

However the agreement between any of these surveys and the maps below 20 MHz is poor, and the agreement between the low frequency maps themselves is confined to the broad features. The low frequency maps are strongly affected by absorption in interstellar ionized hydrogen, which has an absorption coefficient

$$k \propto \nu^{-2}$$

where ν is the wave frequency (see Chapter 2). This rapid variation in absorption coefficient with frequency is the reason for the galactic plane appearing in absorption at 10 MHz and below, in emission at 30 MHz and above, and for the poor agreement in the detail of the three surveys below 20 MHz. Indeed, the analysis described later suggests that a survey at 30 MHz would need a resolution of better than a

degree to show the plane in absorption.

The great changes in appearance of the sky at low frequencies when the receiver frequency is altered by a small amount reflect the information content of the low frequency surveys. In fact the changes are so great as to make the direct comparison of the maps difficult, and further discussion is left to the detailed analysis of the next two chapters.

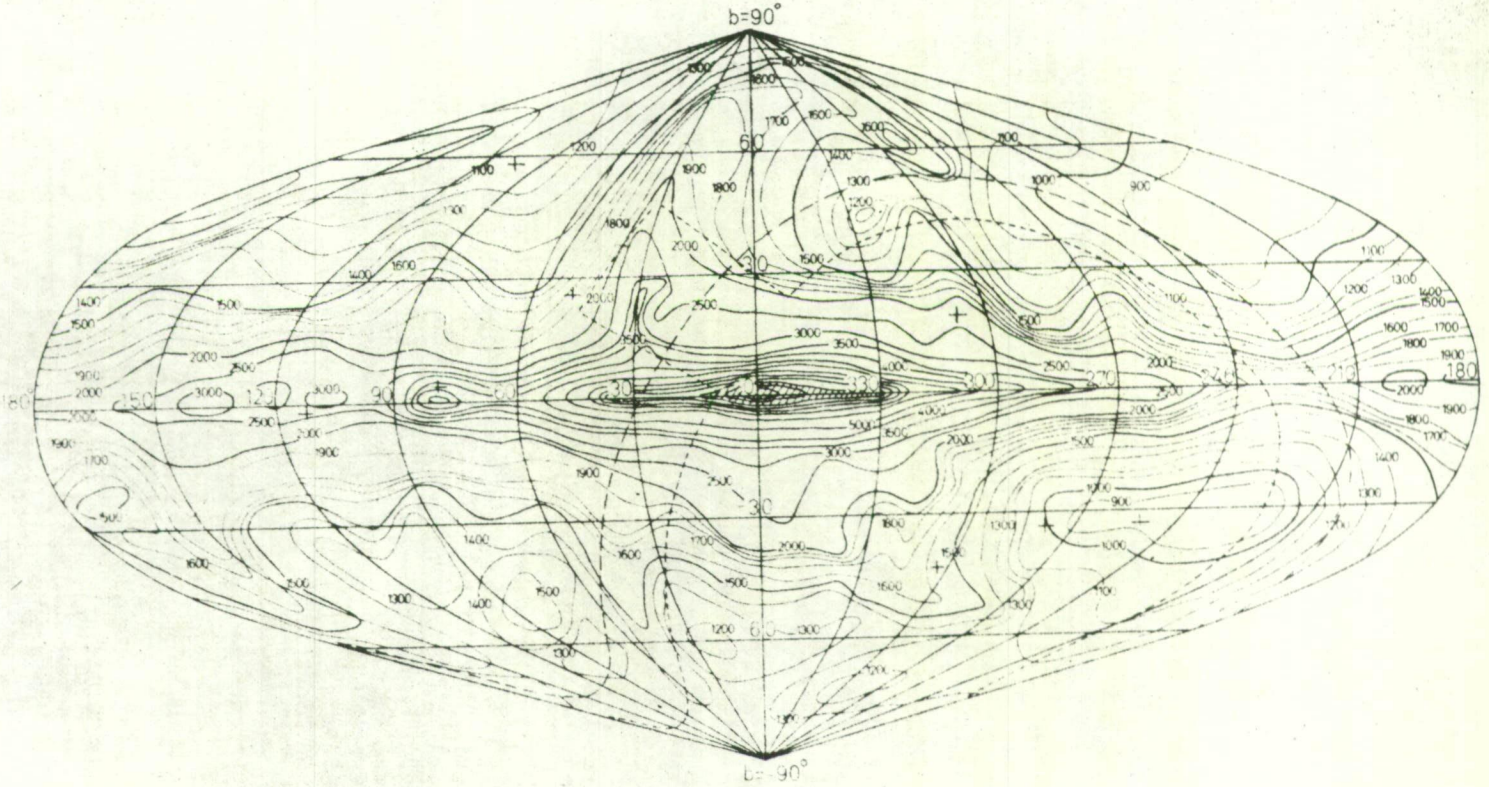

Contours of brightness temperature at 85 MHz obtained from the combination of northern and southern surveys. The zone included by the dashed lines and the directions indicated by the crosses have reduced accuracy. (See Section

FIGURE 19 *after Yates (1968)*

facing page 153.

FIGURES 20 to 25

The six surveys of the southern sky that are reviewed in this chapter are presented as contours of effective aerial temperature in galactic coordinates. Where necessary, the original maps have been re-drawn by hand so that all six are given here on the Hammer equal-area projection.

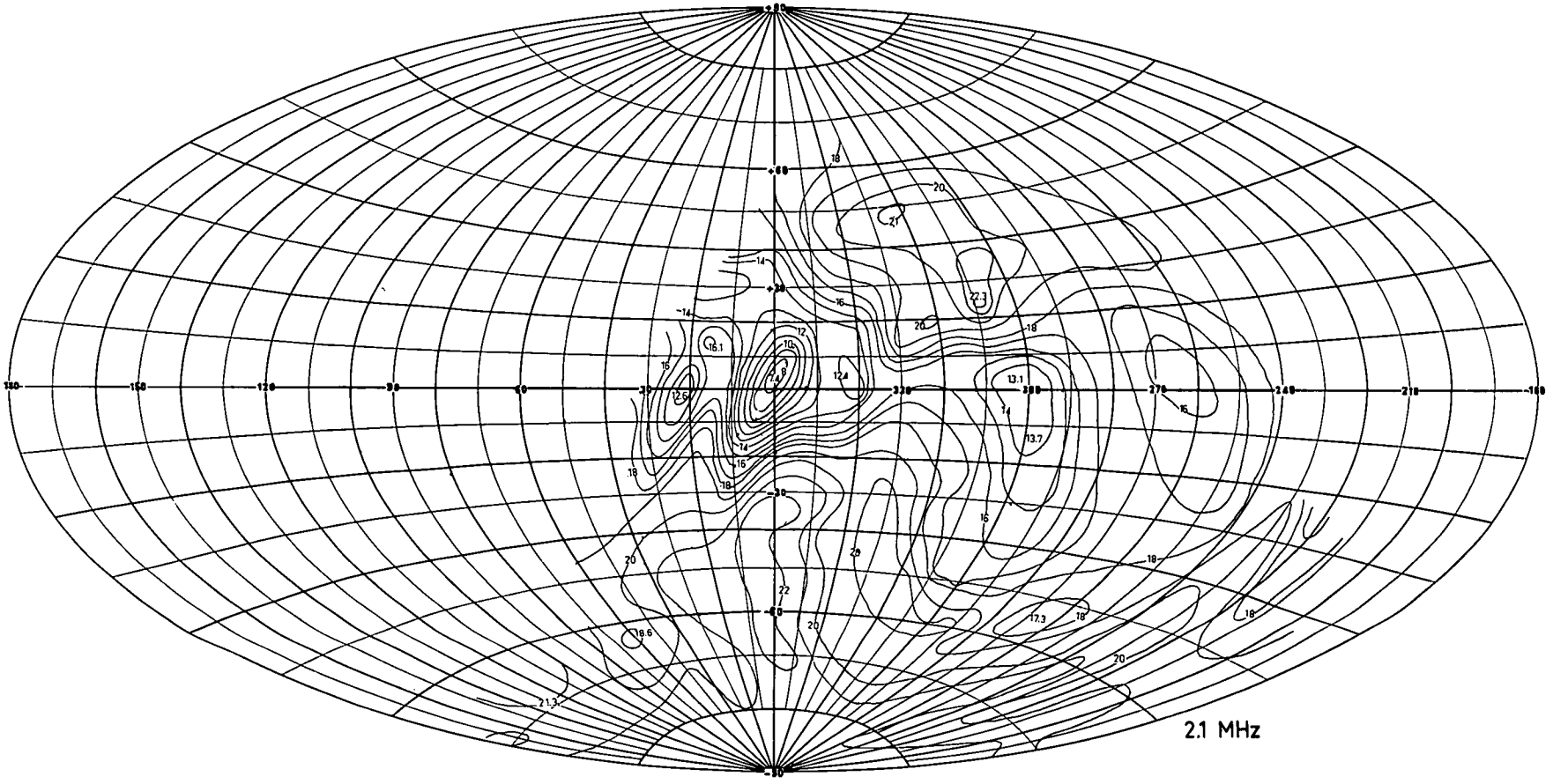
2.1 MHz

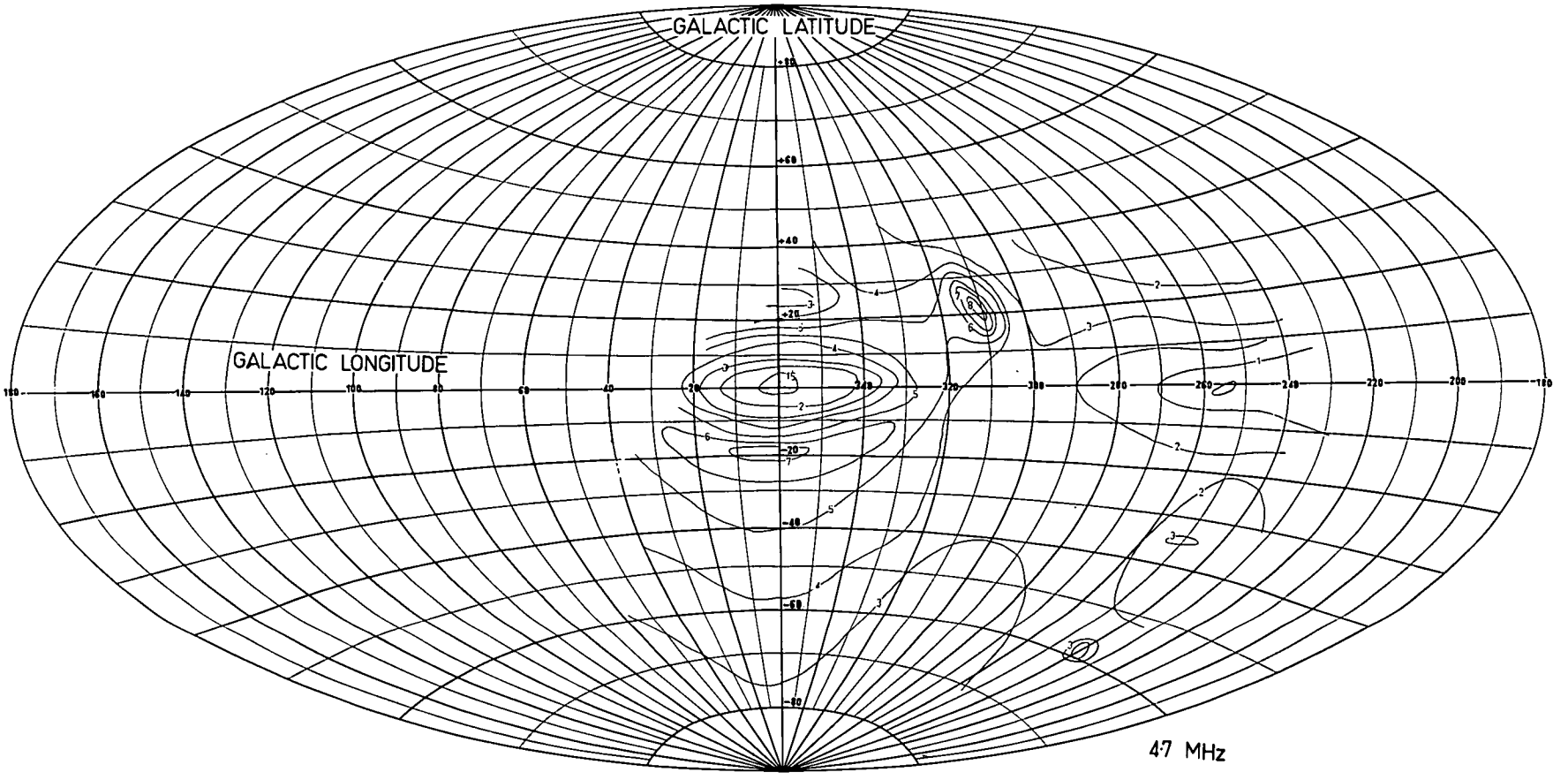
GALACTIC LATITUDE
GALACTIC LONGITUDE
4·7 MHz

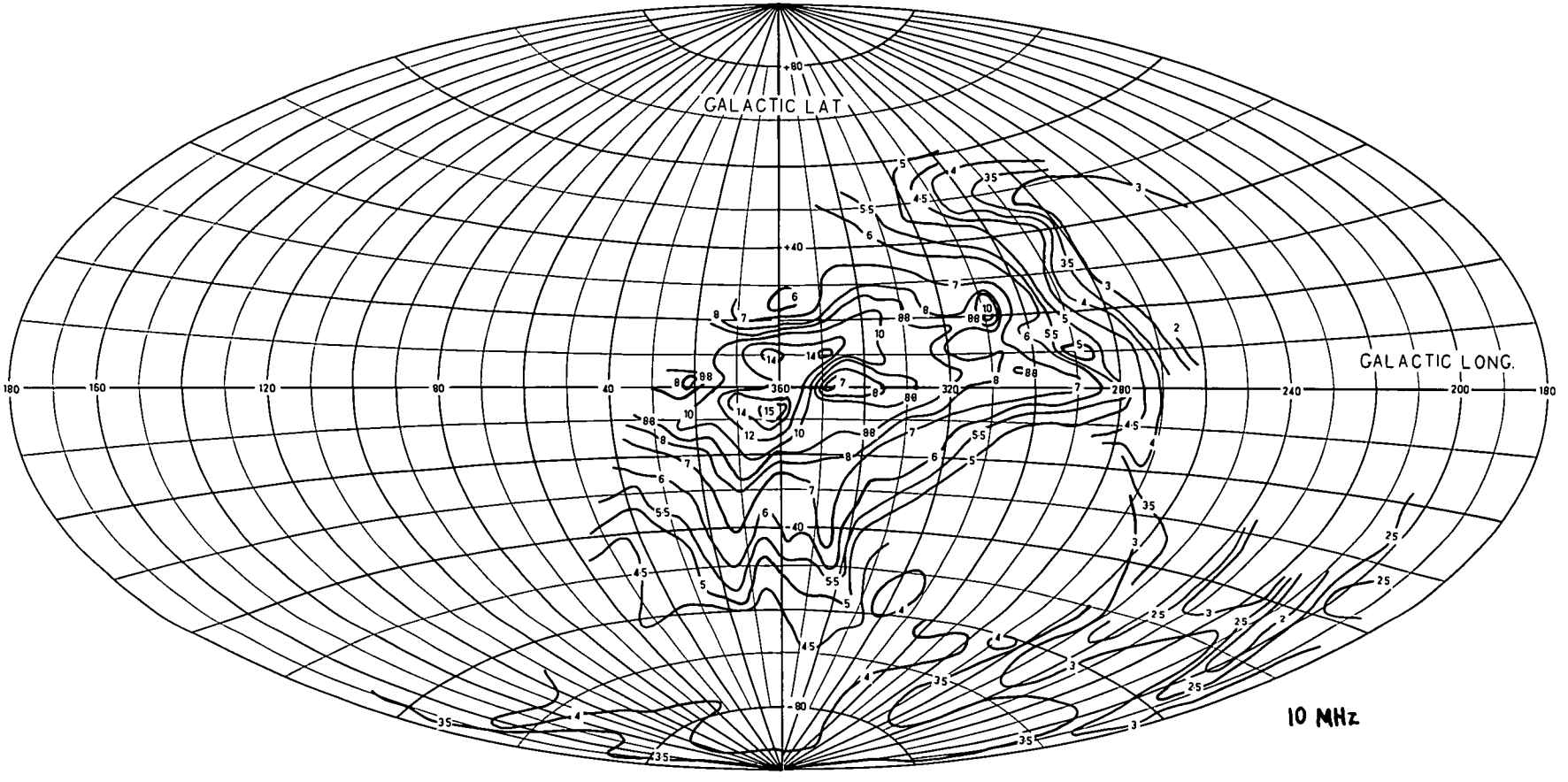
GALACTIC LAT
+80
+40
-80
GALACTIC LONG.
180
160
120
80
40
360
320
280
240
200
180
10 MHz

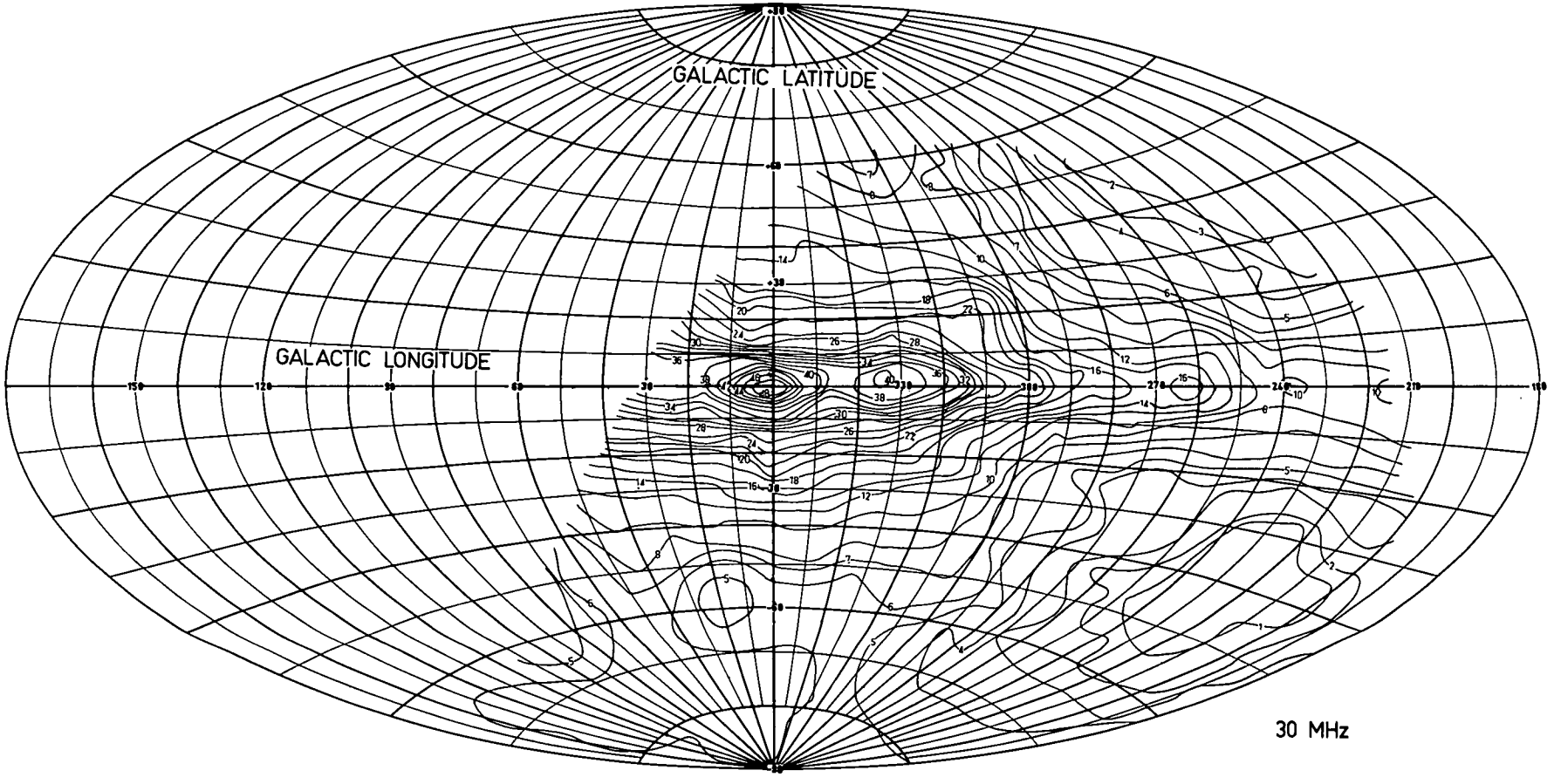
GALACTIC LATITUDE
GALACTIC LONGITUDE
30 MHz

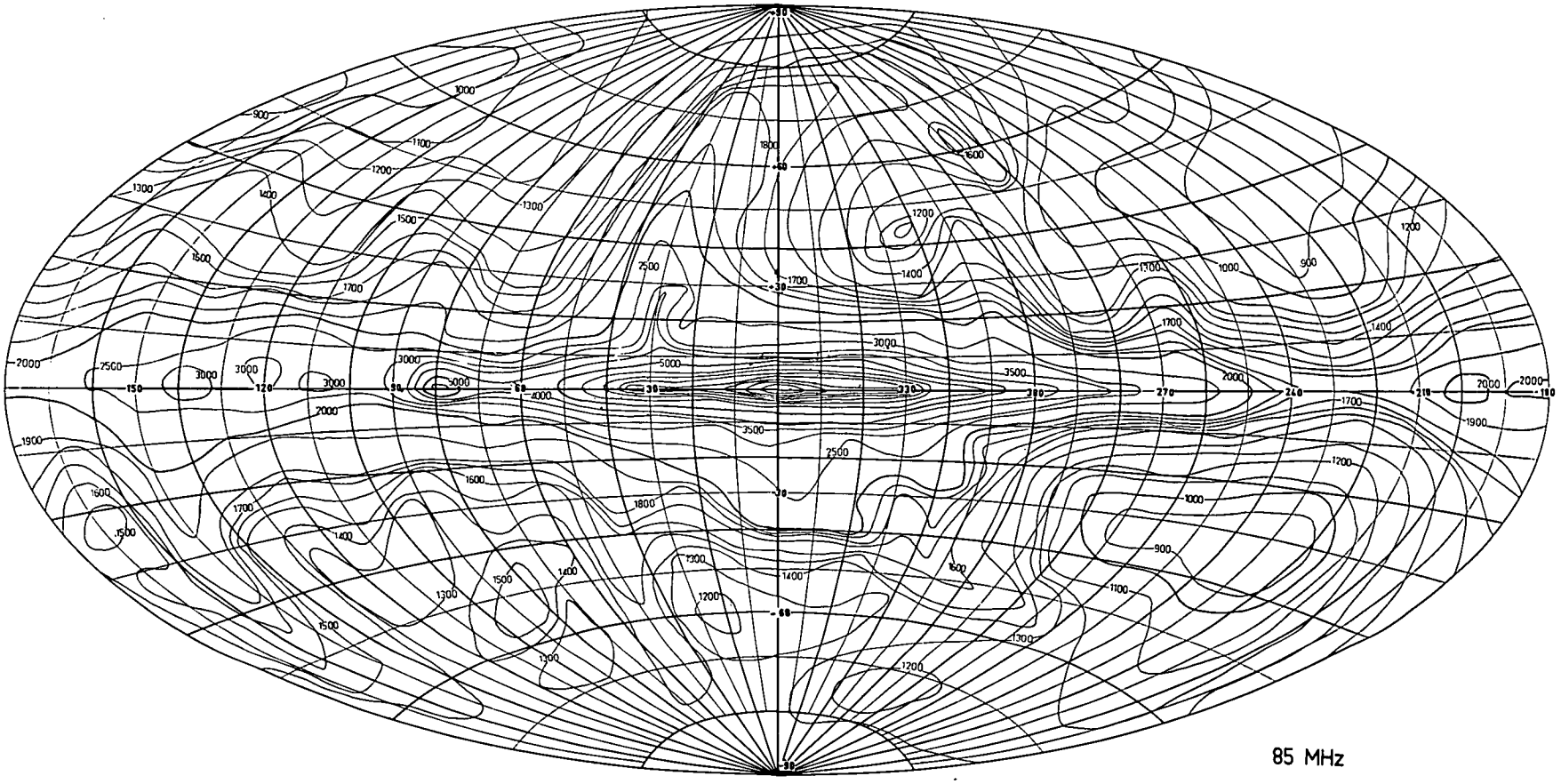
+90
+60
+30
-30
-60
-90
150
120
90
60
30
330
300
270
240
210
180
900
1000
1100
1200
1300
1400
1500
1600
1700
1800
1900
2000
2500
3000
5000
7000

85 MHz

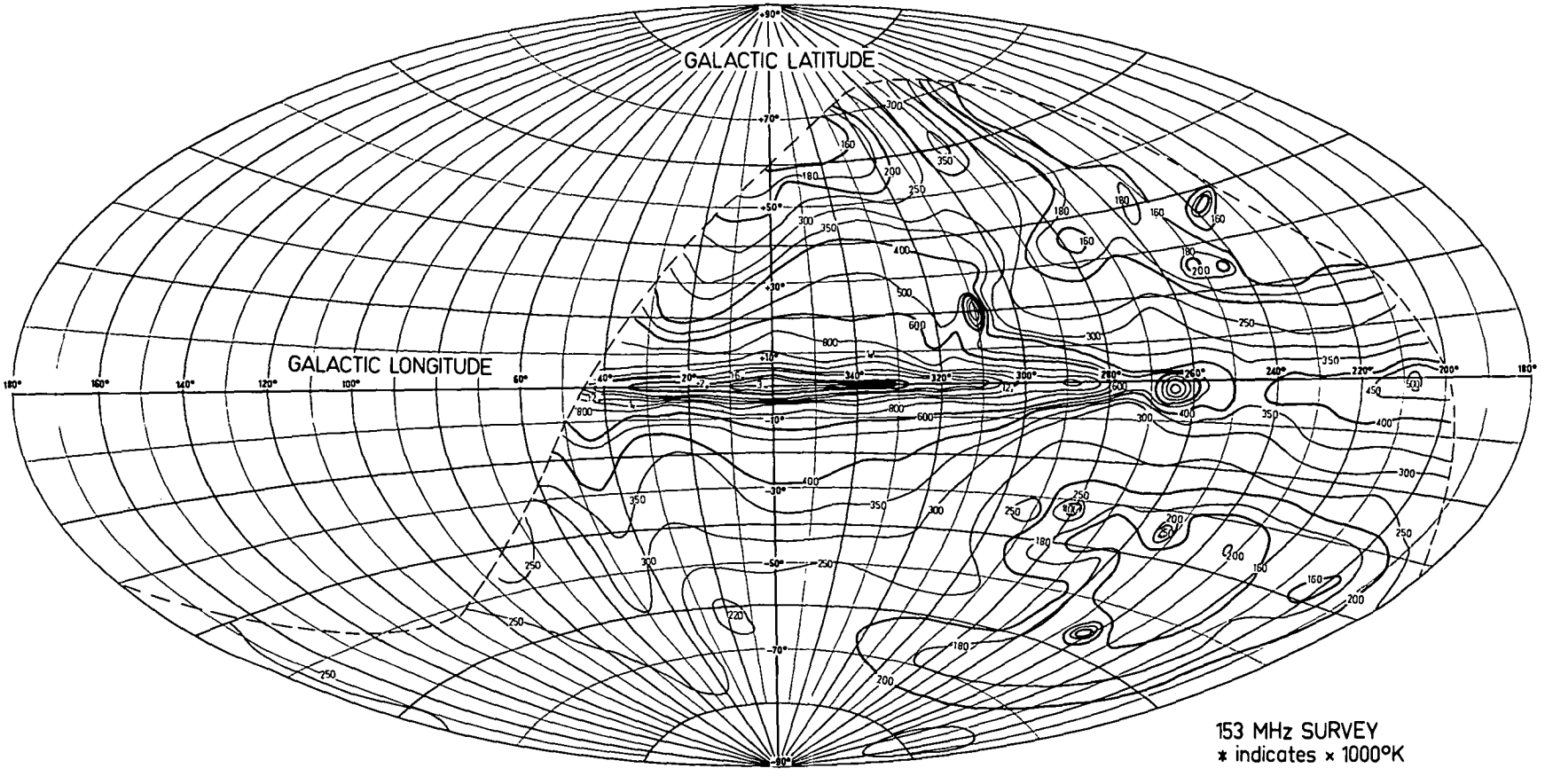
GALACTIC LATITUDE
GALACTIC LONGITUDE
153 MHz SURVEY
* indicates × 1000°K

REFERENCES FOR CHAPTER 5

Baldwin,J.E. 1955 *Mon. Not. Roy. Astr. Soc.* *115* 684.

Conway,R.G., Kellermann,K.I. and Long,R.J. 1963 *Mon. Not. Roy. Astr. Soc.* *125* 261.

Edge,D.O., Shakeshaft,J.R., McAdam,W.B., Baldwin,J.E. and Archer,S. 1959 *Mem. Roy. Astr. Soc.* *68* 37.

Ellis,G.R.A. 1960 *Proc. Instn. Radio Engrs.* *48* 1950.

Ellis,G.R.A., Green,R.J. and Hamilton,P.A. 1963 *Aust. J. Phys.* *16* 545.

Ellis,G.R.A. and Hamilton,P.A. 1966 *Astrophys. J.* *143* 227.

Hamilton,P.A. 1968 *Proc. Instn. Radio Elect. Engrs. Aust.* *29* 56.

Hamilton,P.A. and Haynes,R.F. 1967 *Aust. J. Phys.* *20* 697.

Hamilton,P.A. and Haynes,R.F. 1968 *Aust. J. Phys.* *21* 895.

Hamilton,P.A. and Haynes,R.F. 1969 *Aust J. Phys.: in press.*

Mathewson,D.S., Broten,N.W. and Cole,D.J. 1965 *Aust. J. Phys.* *18* 665.

Mills,B.Y. 1959 *Publs. Astr. Soc. Pacif.* *71* 267.

Mills,B.Y., Slee,O.B. and Hill,E.R. 1960
Aust. J. Phys. *13* 676.

The Parkes Catalogue of Radio Sources:
Bolton,J.G., Gardner,F.F. and Mackey,M.B. 1964
Aust. J. Phys. *17* 340.
Price,R.M. and Milne,D.K. 1965
Aust. J. Phys. *18* 329.
Day,G.A., Shimmins,A.J., Ekers,R.D. and Cole,D.J. 1966
Aust. J. Phys. *19* 35.
Shimmins,A.J., Day,G.A., Ekers,R.D. and Cole,D.J. 1966
Aust. J. Phys. *19* 837.

Pauliny-Toth,I.I.K. and Shakeshaft,J.R. 1962
Mon. Not. Roy. Astr. Soc. *124* 61.

Quigley,M.J.S. and Haslam,C.G.T. 1965 *Nature* *208* 741.

Reber,G. 1968 *J. Franklin Inst.* *285* 1.

Shain,C.A., Komesaroff,M.M. and Higgins,C.S. 1961
Aust. J. Phys. *14* 508.

Turtle,A.J. and Baldwin,J.E. 1962 *Mon. Not. Roy. Astr. Soc.*
124 459.

Wielebinski,R., Smith,D.H. and Garzón Cárdenas,X. 1968
Aust. J. Phys. *21* 185.

Yates,K.W. 1968 *Aust. J. Phys.* *21* 167.

Yates,K.W., Wielebinski,R. and Landecker,T.L. 1967
Aust. J. Phys. *20* 597.

CHAPTER 6

THE LOW FREQUENCY ABSORPTION ANALYSIS - I

INTRODUCTION

This chapter describes the preliminary analysis of the low-frequency absorption, using right ascension scans at declination -37°. The content of this chapter has been published by Ellis and Hamilton (1964, 1966b) and Hamilton (1966).

It is worth noting at this stage that the method of analysis in this chapter is entirely different from that used for the whole-sky surveys in the following chapter, and the results from the two methods are obtained independently of one another. The method here relies on the change of shape of the scan with frequency, and no absolute intensities are required. The results are therefore not dependent on the discussion or conclusions relating to the background spectrum in Chapter 4. Furthermore it is the relative accuracy over the scan at each frequency which is relevant in deciding the uncertainties in the results; the scans are all normalized in one direction and the absolute errors

from scan to scan are of no direct interest.

THE OBSERVATIONS

Smoothed scans of brightness as a function of right ascension for declination -37° are given in figure 1. The relevant parameters of the observations are listed in Table 1.

The scans have been smoothed only to the extent that effects of small sources have been removed; the sources PKS1322-42 (*Centaurus A*), PKS0320-37 (*Fornax A*) and PKS0518-45 (*Pictor A*) are all distinct on the 4.7 MHz scan. All scans have been normalized for the direction closest to the galactic pole, namely 0030^{h}RA ($b \simeq -80^{\circ}$).

METHOD OF ANALYSIS

The analysis is in terms of a model illustrated in figure 2. The sun is taken to be on the central plane of a layer of thickness $2Z_0$ representing the galactic plane. This layer is immersed in a region of radius $R >> Z_0$. The more important terms used are summarised in Table II. The absorption in the extra-disk region is taken to be negligible and the model is kept simple by requiring that the emissivities

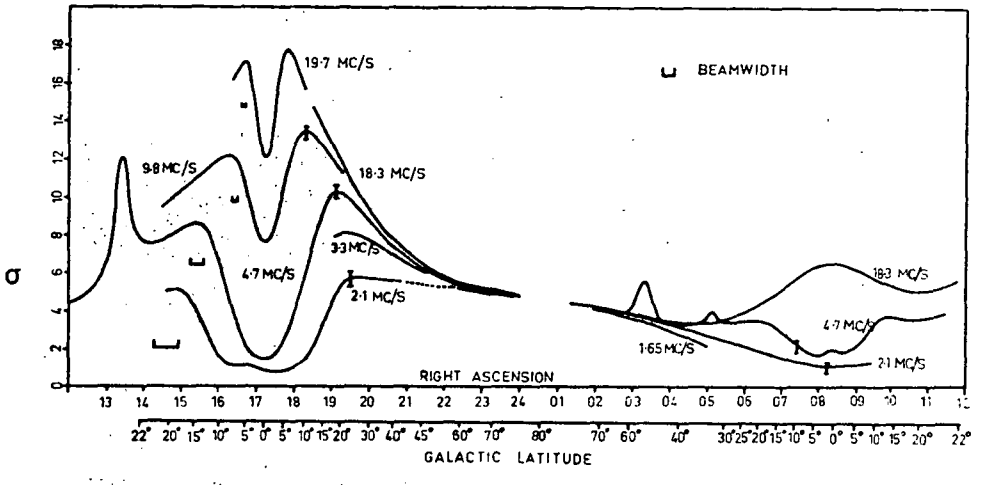

FIGURE 1

The normalized intensities $\sigma(\nu,b)$

after Ellis and Hamilton (1966b)

TABLE I

PARAMETERS OF THE DATA IN FIGURE I

frequency *(MHz)*	resolution	observer
1.65	$32^{\circ} \times 40^{\circ}$	Ellis and Hamilton (1964)
2.1	8°	Reber (1968)
3.35	$32^{\circ} \times 40^{\circ}$	Ellis and Hamilton (1964)
4.7	$4^{\circ} \times 10^{\circ}$	Ellis and Hamilton (1966a)
9.6	$2^{\circ} \times 5^{\circ}$	Ellis and Hamilton (1964)
18.3	17°	Shain and Higgins (1954)
19.7	1.4°	Shain, Komesaroff and Higgins (1961)

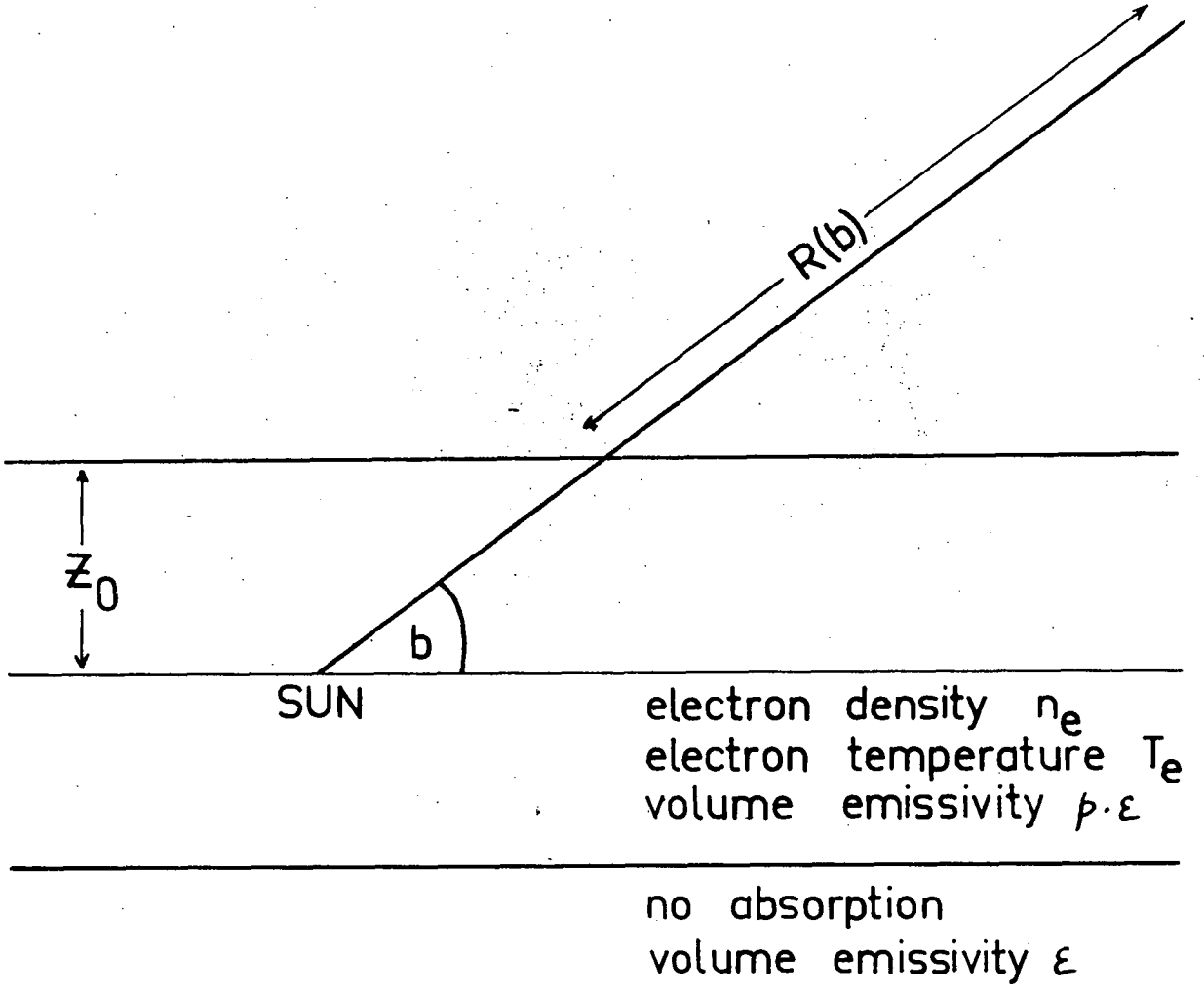

FIGURE 2

The model in the analysis

TABLE II

NOTATION USED IN THE ANALYSIS

symbol	*dimensions*	*significance*
r, b	polar coordinates	r = line of sight distance b = galactic latitude
Z_0	length	half-width of disk
ν	Hz	wave frequency
R	length	characteristic length of extra-disk region
n_e	volume^{-1}	free electron number-density in disk
T_e	degK	free electron temperature in disk
$\varepsilon(\nu)$	volume emissivity	emissivity of extra-disk region at frequency ν
p	dimensionless	ratio of disk/extra-disk emissivities
$L(b)$	length	$L(b) = Z_0 \mathrm{cosec} b$ is total line of sight path in disk for direction b
$S(\nu,b)$	intensity	Observed brightness at ν in line of sight at b
$\sigma(\nu,b)$	dimensionless	normalized intensity $\sigma(\nu,b) = S(\nu,b)/S(\nu,90)$

$\varepsilon(\nu)$ and $p\varepsilon(\nu)$ are constant and isotropic.

We introduce the function

$$\eta(r,b) = \frac{n_e(r,b)^2}{T_e(r,b)^{3/2}} .$$

The thermal absorption coefficient at frequency ν is (Chapter 2)

$$K \simeq \frac{10^{-2}\, n_e^{\,2}}{T_e^{\,3/2}\nu^2}\left[17.7 + \ln\left(\frac{T_e^{\,3/2}}{\nu}\right)\right] \quad neper\ cm^{-1},$$

and the absorption coefficient of the region at (r,b) is then

$$K \simeq \zeta\, \eta(r,b)\, \nu^{-2}$$

where $\zeta \simeq 0.15$ *c.g.s. units* (see Chapter 2).

The analysis yields values of $\eta(r,b)$, or rather the line of sight average

$$\bar{\eta}(b) = \frac{1}{L(b)} \int_0^{L(b)} \eta(r,b)\, dr$$

where $L(b)$ is the length of the line of sight within the disk. The evaluation of either component of $\bar{\eta}$ requires the prior knowledge of the other; values of $\langle n_e^{\,2}\rangle$ are obtained only on the assumption of $\langle T_e^{\,3/2}\rangle$ or its determination by other means.

The intensity of the radiation, $S(\nu,b)$, observed at frequency ν for the line of sight at b is the sum of contributions from the disk and extra-disk regions:

$$S(\nu,b) = \int_0^{L(b)} \frac{p\varepsilon(\nu)}{4\pi} \; e^{-\int_0^{\ell} \zeta\eta(r,b)\,\nu^{-2}\,dr} \; d\ell$$

$$+ \frac{[R-L(b)]\;\varepsilon(\nu)}{4\pi} \; e^{-\int_0^{L(b)} \zeta\eta(r,b)\,\nu^{-2}\,dr} \qquad (1).$$

Writing

$$\kappa(\nu,b) = \int_0^{L(b)} \zeta\eta(r,b)\,\nu^{-2}\,dr$$

$$= \zeta\,\bar{\eta}(b)\,L(b)\,\nu^{-2},$$

and $\xi(\nu,b) = e^{-\kappa(\nu,b)}$,

equation (1) becomes

$$S(\nu,b) = \frac{\varepsilon(\nu)}{4\pi}\left\{pL(b)\,\kappa(\nu,b)^{-1}\,[1-\xi(\nu,b)]\right.$$

$$\left. + \;[R-L(b)]\;\xi(\nu,b)\;\right\} \qquad (2).$$

The ratio of intensities at frequencies ν_1 and ν_2 for a given line of sight b is then

$$\frac{S(\nu_1,b)}{S(\nu_2,b)} =$$

$$\frac{pL(b)\ \kappa(\nu_1,b)^{-1}[1-\xi(\nu_1,b)] + [R-L(b)]\ \xi(\nu_1,b)}{pL(b)\ \kappa(\nu_2,b)^{-1}[1-\xi(\nu_2,b)] + [R-L(b)]\ \xi(\nu_2,b)} \qquad (3).$$

Now the form of the data is not intensity $S(\nu,b)$ but rather normalized intensity $\sigma(\nu,b)$, where

$$\sigma(\nu,90) = 1 \qquad \text{for all } \nu.$$

We therefore introduce a normalizing function $B(\nu_1,\nu_2)$ where

$$\frac{\sigma(\nu_1,b)}{\sigma(\nu_2,b)} = B(\nu_1,\nu_2)\ \frac{S(\nu_1,b)}{S(\nu_2,b)} .$$

$B(\nu_1,\nu_2)$ is thus the ratio of the actual intensities at ν_1 and ν_2 observed in the direction of the galactic pole. In terms of the model

$$B(\nu_1,\nu_2) = \frac{S(\nu_2,90)}{S(\nu_1,90)}$$

$$= \frac{\varepsilon(\nu_2)}{\varepsilon(\nu_1)}\ \frac{pZ_0\ \kappa_0(\nu_2)^{-1}[1-\xi_0(\nu_2)]+[R-Z_0]\ \xi_0(\nu_2)}{pZ_0\ \kappa_0(\nu_1)^{-1}[1-\xi_0(\nu_1)]+[R-Z_0]\ \xi_0(\nu_1)}$$

$$= \frac{\varepsilon(\nu_2)}{\varepsilon(\nu_1)} \cdot A(\nu_1,\nu_2) \qquad (4),$$

where $\kappa_0(\nu) = \zeta\ \bar{\eta}_0\ Z_0\ \nu^{-2}$,

$\bar{\eta}_0 = \bar{\eta}(b=90)$,

and $\xi_0(\nu) = e^{-\kappa_0(\nu)}$.

Then for directions other than $b = 90$ we have

$$\frac{\sigma(\nu_1,b)}{\sigma(\nu_2,b)} =$$

$$\frac{pL(b)\ \kappa(\nu_1,b)^{-1}[1-\xi(\nu_1,b)] + [R-L(b)]\,\xi(\nu_1,b)}{pL(b)\ \kappa(\nu_2,b)^{-1}[1-\xi(\nu_2,b)] + [R-L(b)]\xi(\nu_2,b)} A(\nu_1,\nu_2)$$

(5).

For a model with given dimensions (i.e. Z_0) the unknowns in equation (5) are $\bar{\eta}(b)$, $\bar{\eta}_0$ and the relative disk emissivity p.

If the integrated emission along a line of sight within the disk is negligible compared with the extra-disk emission, we obtain from equation (4)

$$A(\nu_1,\nu_2) = \frac{\xi_0(\nu_2)}{\xi_0(\nu_1)} \qquad (6)$$

and equation (5) becomes

$$\frac{\sigma(\nu_1,b)}{\sigma(\nu_2,b)} = \frac{\xi(\nu_1,b)}{\xi(\nu_2,b)}\frac{\xi_0(\nu_2)}{\xi_0(\nu_1)}$$

$$= e^{[\zeta Z_0(\nu_2^{-2}-\nu_1^{-2})\{\bar{\eta}(b)\ \mathrm{cosec}b - \bar{\eta}_0\}]} \qquad (7).$$

We define a ratio function

$$\rho(\nu_1,\nu_2,b) = \frac{ln[\sigma(\nu_1,b)/\sigma(\nu_2,b)]}{\nu_2^{-2} - \nu_1^{-2}}$$

and from equation (7) we get

$$\rho(\nu_1,\nu_2,b) = \zeta\ Z_0\ [\bar{\eta}(b)\ \mathrm{cosec}b\ - \bar{\eta}_0] \qquad (8).$$

If we make a further simplification and assume that the function

$$\bar{\eta}(b) = \frac{1}{L(b)} \int_0^{L(b)} \frac{n_e(r,b)^2}{T_e(r,b)^{3/2}}\ dr$$

is everywhere constant, that is $\bar{\eta}(b) = \bar{\eta}_0$, then from

equation (8) we obtain

$$\rho(\nu_1,\nu_2,b) = (\zeta Z_0\bar{\eta}_0)(\mathrm{cosec}\,b - 1) \qquad (9).$$

For this simple model the ratio function $\rho(\nu_1,\nu_2,b)$ is independent of the frequencies, and the magnitude of $(\zeta Z_0\bar{\eta}_0)$ can be obtained if observations at any two frequencies are available.

Figure 3 gives values of $\rho(\nu_1,\nu_2,b)$ for pairs of frequencies, obtained from figure 1 and plotted against $\mathrm{cosec}\,b$. It is apparent that ρ is essentially independent of frequency out to $\mathrm{cosec}\,b = 2.2$, and also that the region from $\mathrm{cosec}\,b = 1$ to $\mathrm{cosec}\,b = 1.5$ fits the model of equation (9) well. We can thus obtain a well-defined value for $\bar{\eta}_0$.

For $1.5 < \mathrm{cosec}\,b < 2.2$ the model of equation (8) is appropriate, since ρ is still independent of the choice of frequencies but the varying slope of the graph implies that $\bar{\eta}(b)$ is changing with b. The values of $\bar{\eta}(b)$ can be obtained from equation (8) for this range of latitudes using the value of $\bar{\eta}_0$ given by equation (9) for $\mathrm{cosec}\,b < 1.5$.

The values of $\rho(\nu_1,\nu_2,b)$ from figure 1 for the remaining regions of the scans are shown in figures 4 - 7. It is clear that while the simple model of equation (8) with

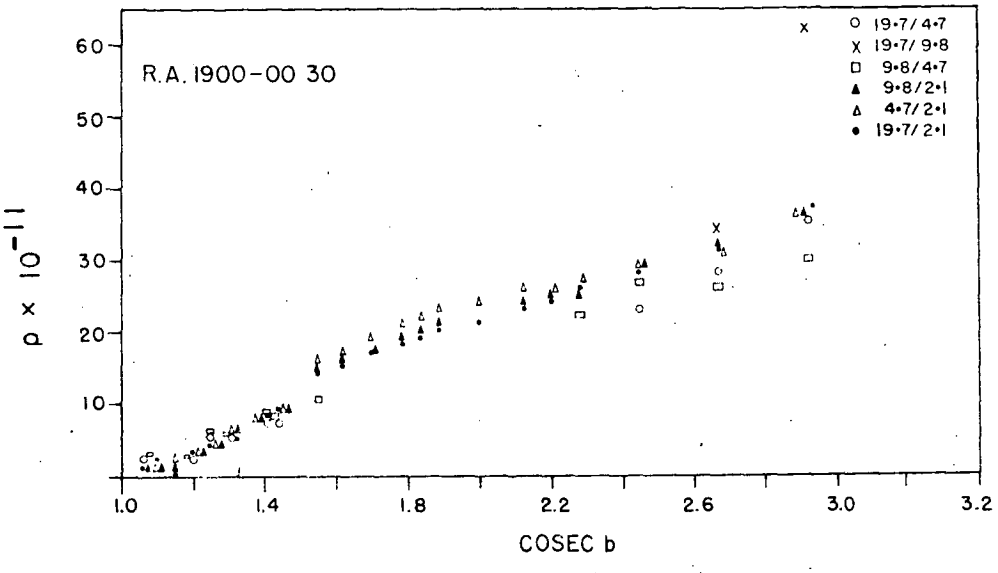

FIGURE 3

after Ellis and Hamilton (1966b)

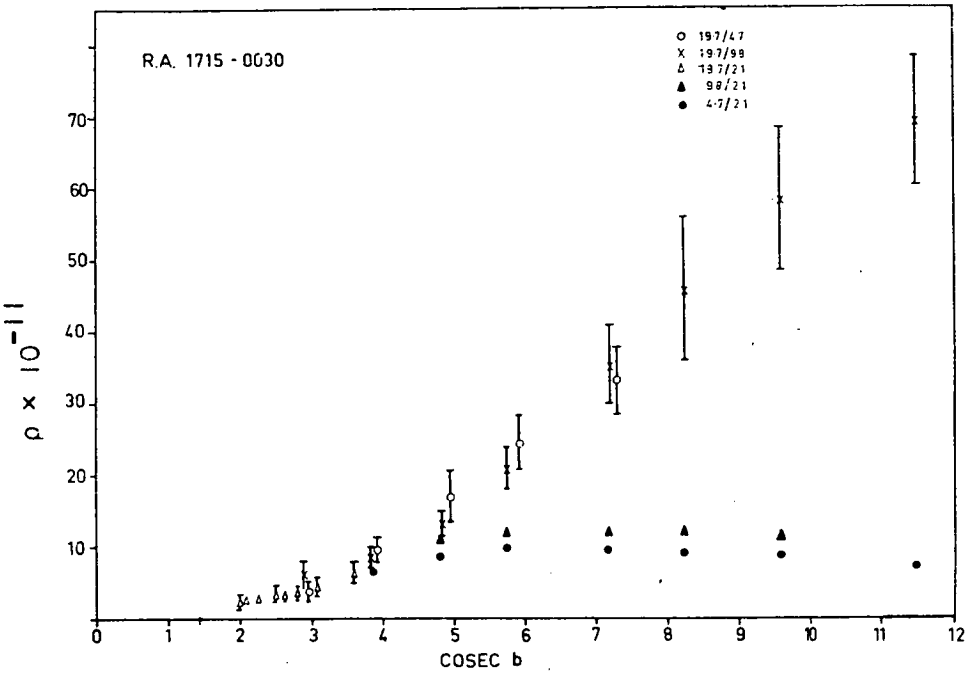

FIGURE 4

after Ellis and Hamilton (1966b)

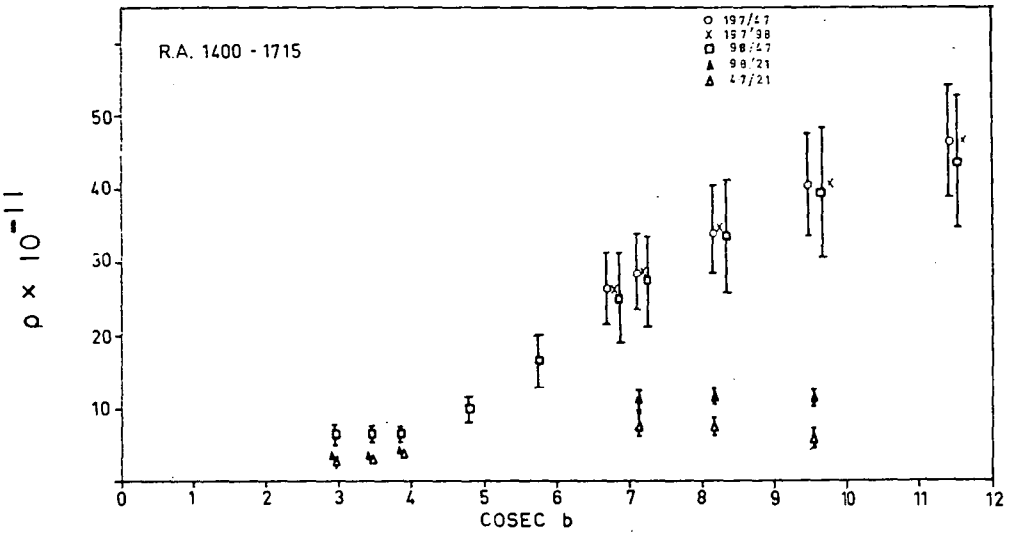

FIGURE 5

after Ellis and Hamilton (1966b)

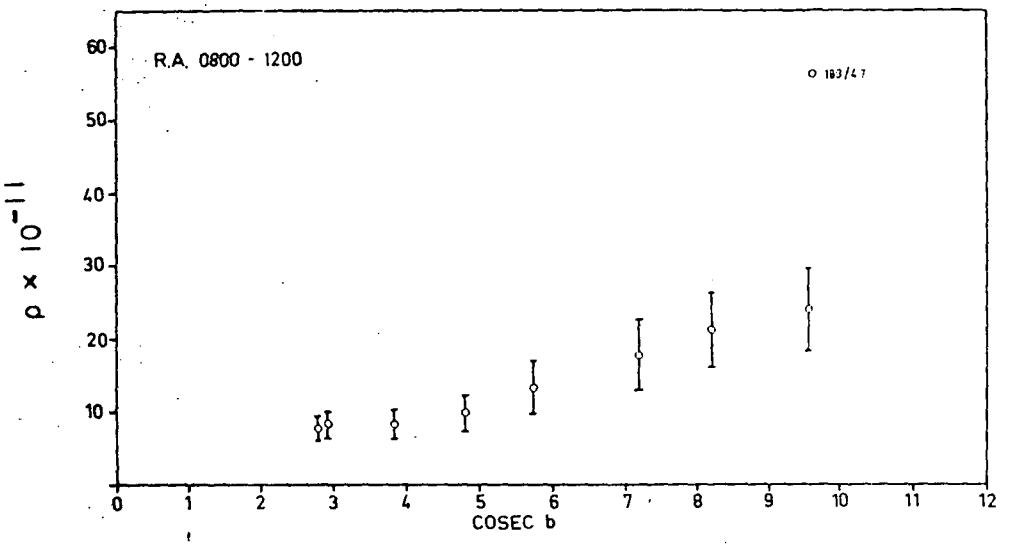

FIGURE 6

after Ellis and Hamilton (1966b)

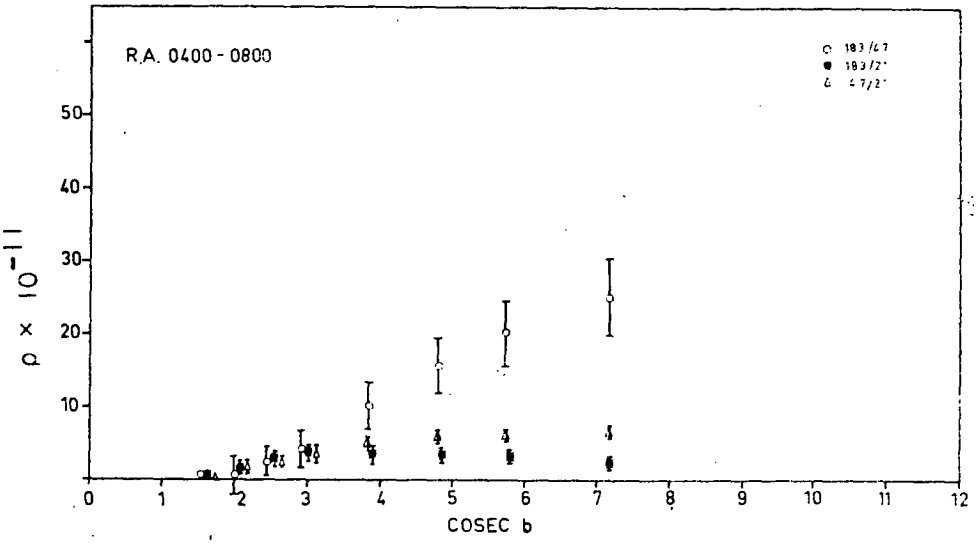

FIGURE 7

after Ellis and Hamilton (1966b)

negligible disk emission is satisfactory for $|b| > 30^{\circ}$, at lower latitudes p depends on the frequencies used, and a more complicated model is needed such as that giving rise to equation (5).

We define a function

$$\Gamma(b) = \frac{R - Z_0 \operatorname{cosec} b}{p\, Z_0 \operatorname{cosec} b}$$

and rewrite equation (5) as

$$\frac{\sigma(\nu_1,b)}{\sigma(\nu_2,b)} =$$

$$\frac{\kappa(\nu_1,b)^{-1}[1-\xi(\nu_1,b)] + \Gamma(b)\,\xi(\nu_1,b)}{\kappa(\nu_2,b)^{-1}[1-\xi(\nu_2,b)] + \Gamma(b)\,\xi(\nu_2,b)}\, A(\nu_1,\nu_2) \qquad (10).$$

The function $\Gamma(b)$ is a measure of the ratio of the integrated emission in direction b from outside the disk to that from within the disk.

The success of the simple model for $|b| > 30^{\circ}$ enables us to write

$$A(\nu_1,\nu_2) = \frac{\xi_0(\nu_1)}{\xi_0(\nu_2)} \qquad (6)$$

$$= e^{-\zeta \bar{n}_0 Z_0 (\nu_2^2 - \nu_1^2)} ,$$

and hence at a given direction b the unknowns in equation (10) are $\bar{\eta}(b)$ and $\Gamma(b)$, and these can be determined by iteration using the data from figure 1.

The integrated emission along a line of sight is the sum of contributions from inside and outside the disk. The relative contributions from each region can be obtained from equation (5) once the other parameters have been determined.

Summary of the method:

1. Compute values of the ratio function

$$\rho(\nu_1,\nu_2,b) = \frac{ln[\sigma(\nu_1,b)/\sigma(\nu_2,b)]}{\nu_2^{-2} - \nu_1^{-2}} .$$

2. Plot $\rho(\nu_1,\nu_2,b)$ against $\mathrm{cosec}b$.
3. Determine $\bar{\eta}_0$ from equation (9) for the region where ρ is proportional to $(\mathrm{cosec}b - 1)$.
4. Determine $\bar{\eta}(b)$ from equation (8) for the region where ρ is independent of the frequencies.
5. Use the values of $\bar{\eta}_0$ and $\bar{\eta}(b)$ thus obtained to solve equation (10) for $\bar{\eta}(b)$ and $\Gamma(b)$ in the remaining regions.
6. Substitute these results back in (5) to obtain the relative contributions of the disk and extra-disk regions.

RESULTS

The analysis yields

$$\zeta\, \bar{\eta}_0\, Z_0 \;=\; 4.2_{10}12 \qquad \textit{c.g.s. units},$$

and, taking $\zeta = 0.15$, we obtain

$$\bar{\eta}_0\, Z_0 \;=\; \int_0^{Z_0} \frac{n_e(r,90)^2}{T_e(r,90)^{3/2}}\, dr$$

$$= 9.1_{10}{-6}\ ,$$

for n_e in electrons/cm^3,

T_e in degK

and Z_0 in parsecs.

The values of $[\bar{\eta}(b)\, Z_0\, \mathrm{cosec} b]$, that is

$$\int_0^{L(b)} \frac{n_e(r,b)^2}{T_e(r,b)^{3/2}}\, dr$$

for other directions, obtained from the analysis, are presented in polar coordinates in figure 8. The results are consistent with a disk-like distribution of free electrons, with a somewhat greater value of $\bar{\eta}(b)$ towards the galactic centre. This could be interpreted as a lower electron temperature or, as is more likely, a greater mean electron density in this direction.

facing page 182.

FIGURE 8

The function

$$\int_0^{L(b)} \frac{n_e(r,b)^2}{T_e(r,b)^{3/2}}\, dr$$

from the analysis is presented in polar coordinates as a function of galactic latitude b. The units of the radial scale are appropriate for

n_e in *electrons* cm^{-3}

T_e in *degK*

$L(b)$ in *parsecs*.

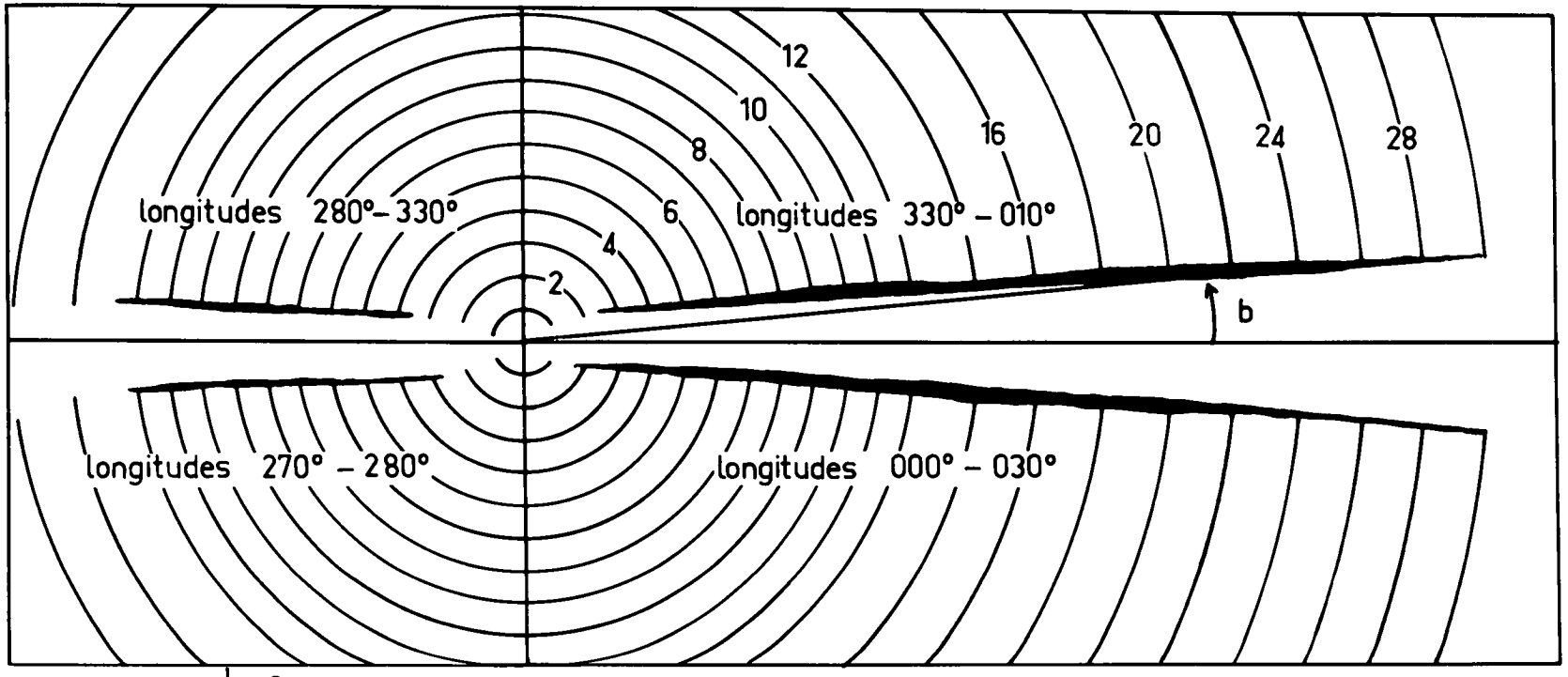

THE FUNCTION $\int_0^L \frac{n_e^2}{T_e^{3/2}}$ FROM THE ANALYSIS.

Values are for n_e in electrons/cm^3
T_e in °K
L in parsecs

The relative contributions to the emission from the disk and extra-disk regions are also presented in polar coordinates, in figure 9. The external component appears to be almost isotropic, at least in the latitude range considered ($|b| < 30^{o}$). Extrapolation back to the direction of the pole suggests that the integrated disk emission is approximately one tenth of the external emission.

Further discussion of these results is postponed to the next chapter.

DISCUSSION OF THE METHOD

The method outlined in this chapter is unusual because no absolute intensities are required. It was necessary to adopt such a method at the time this work was done because of a common impression that even if low frequency radio astronomy observations could be made from the ground, the errors in absolute intensities would be large because of unknown ionospheric effects.

The main limitations of the method lie in the initial solution for $(\zeta\bar{\eta}_0 Z_0)$ since, as figure 1 shows, small errors in the scans near 0030^{h} RA will produce relatively large changes in the ratio function ρ.

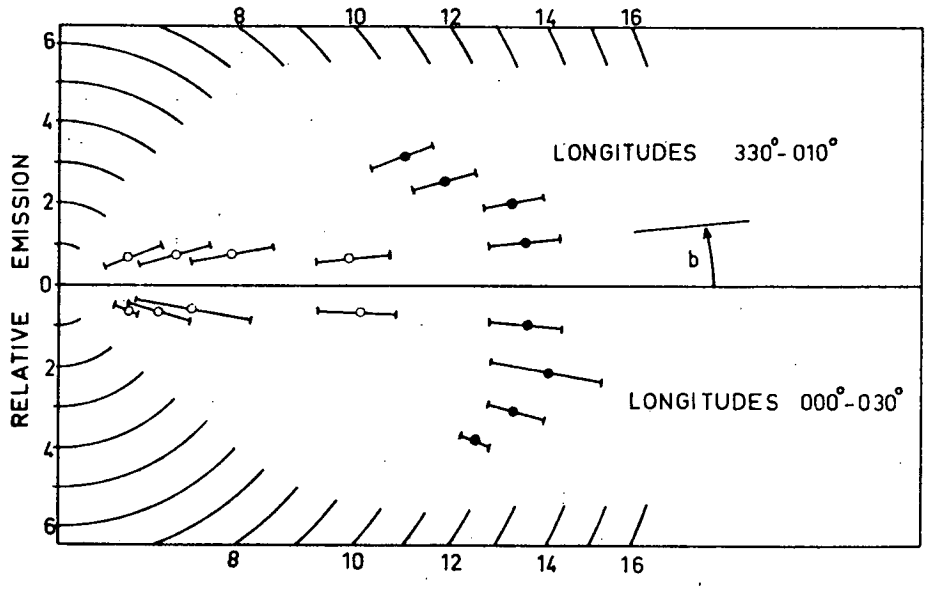

FIGURE 9

The relative contributions to the total Emission from the disk region (open circles) and the extra-disk region (filled circles). This is a polar diagram against galactic latitude *b*. The error bars indicate the uncertainty in the results.

after Ellis and Hamilton (1966b)

REFERENCES FOR CHAPTER 6

Ellis,G.R.A. and Hamilton,P.A. 1964 *Nature* *204* 272.

Ellis,G.R.A. and Hamilton,P.A. 1966a *Astrophys. J.* *143* 227.

Ellis,G.R.A. and Hamilton,P.A. 1966b *Astrophys. J.* *146* 78.

Hamilton,P.A. 1966 In *Radio and Optical Studies of the Galaxy* (Canberra: Mt.Stromlo Obs.) p. 94.

Reber,G. 1968 *J. Franklin Inst.* *285* 1.

Shain,C.A. and Higgins,C.S. 1954 *Aust. J. Phys.* *7* 138.

Shain,C.A., Komesaroff,M.M. and Higgins,C.S. 1961 *Aust. J. Phys.* *14* 508.

CHAPTER 7

THE LOW FREQUENCY ANALYSIS - II

INTRODUCTION

The analysis described in the preceding chapter was initiated at a time when the low frequency end of the galactic spectrum was regarded as uncertain (Mills, 1964). The situation is now much improved; more than one third of the measurements reviewed in Chapter 4 were published during or after 1965. The measurements in each region are self-consistent, and reliable measures of the background emission spectra are now available.

In this chapter the six smoothed surveys discussed in Chapter 5 are standardized using the spectrum of Chapter 4. The spectra for different lines of sight, obtained by sampling the maps at regular intervals in galactic latitude and longitude, are analysed using a curve-fitting technique to yield values of the parameters in a model of the emission and absorption.

Some preliminary results of this analysis were presented at the May 1969 Meeting of the Astronomical

Society of Australia, and the significance of the halo in the interpretation of the diffuse x-ray background has been discussed by Hamilton and Francey (1969). The remainder of the material in the chapter has not been published.

THE DATA

The six standardized surveys are presented in figures 1 - 6. Only the regions common to all the surveys are shown. Each map was normalized so that smoothing to an effective resolution of 30° gave a level of unity for the direction of the south galactic pole. A new scale was chosen so that this low resolution pole temperature agreed with the spectrum in figure 3 of Chapter 4.

The 153 MHz and 85 MHz surveys were found to require no variation from the original scales. The scales of the three low frequency maps had originally been chosen in this manner, and small adjustments were necessary in view of the revised spectrum. The contour interval of the 30 MHz map was originally calibrated against scans of the strong source *Fornax A*, and the zero level of the map was set with reference to the low resolution spectrum. No adjustment of the zero

facing page 188.

FIGURES 1 to 6

The six standardized surveys used in the analysis. The contour intervals have been corrected where necessary so that when these maps are convolved to an effective resolution of 30° the temperatures at $b = -90^{\circ}$ agree with the low resolution spectrum of Chapter 4.

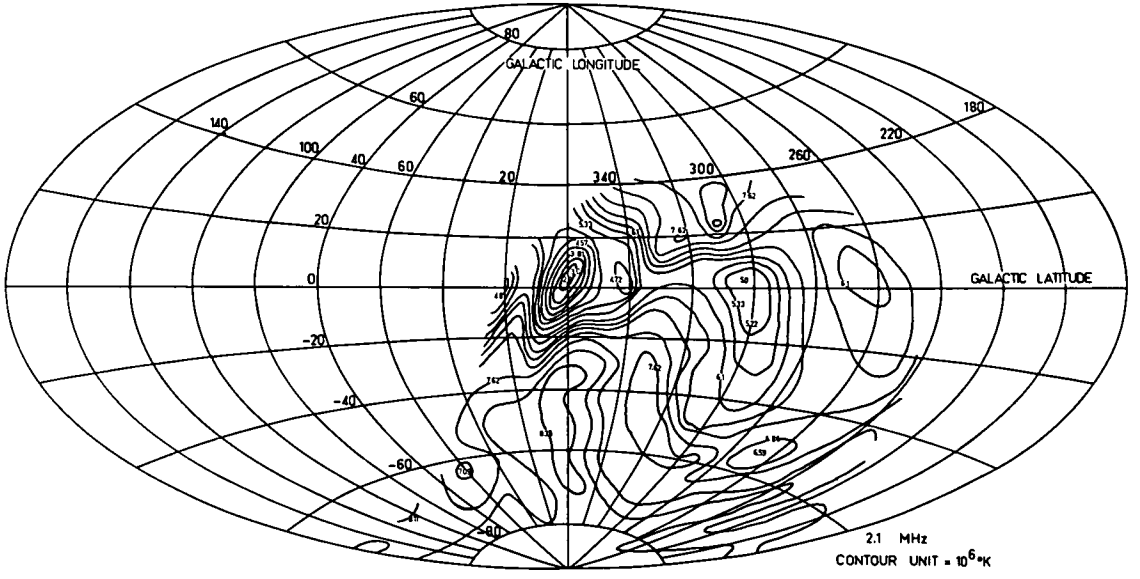
GALACTIC LONGITUDE
GALACTIC LATITUDE
80
60
140
100
40
60
20
340
300
260
220
180
20
0
-20
-40
-60
-80
2.1 MHz
CONTOUR UNIT = 10^6 °K

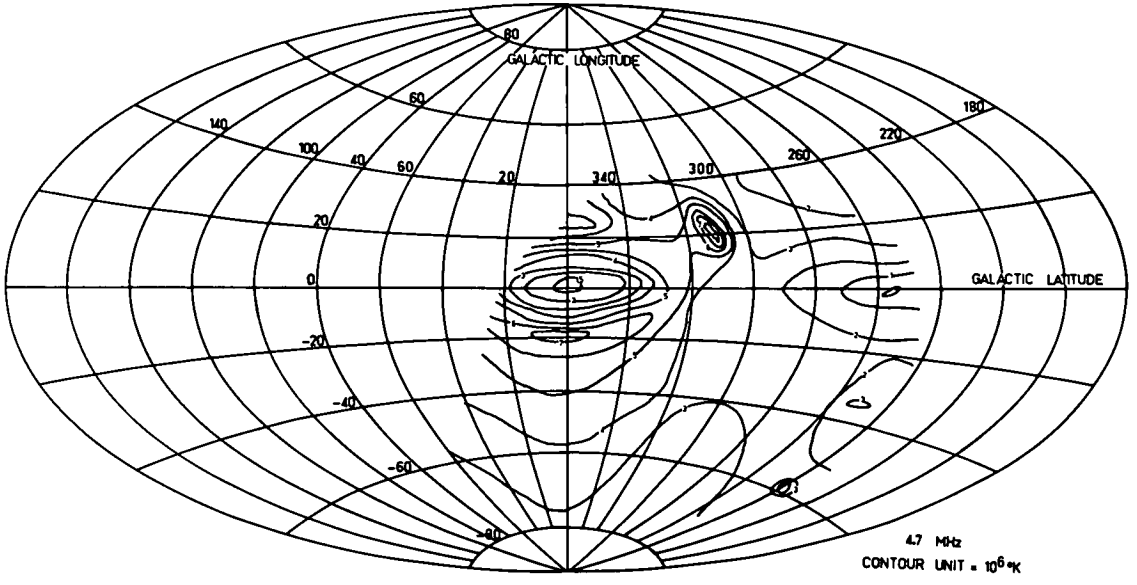
GALACTIC LONGITUDE
80
60
140
100
40
60
20
340
300
260
220
180
20
0
-20
-40
-60
-80
GALACTIC LATITUDE
4.7 MHz
CONTOUR UNIT = 10^6 °K

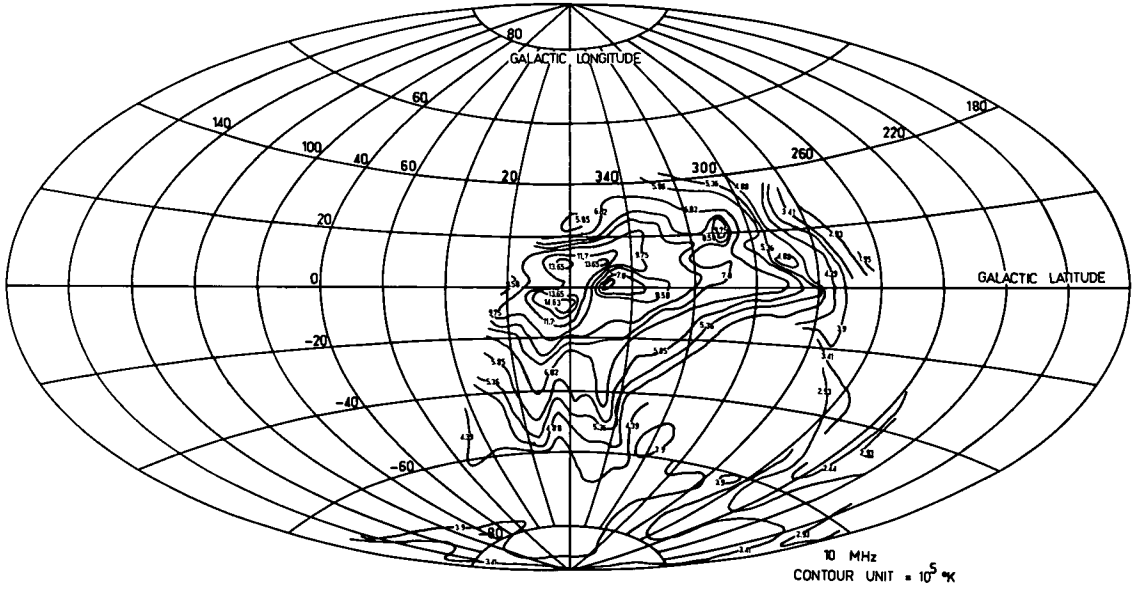
GALACTIC LONGITUDE
GALACTIC LATITUDE
80
60
140
100
40
60
20
340
300
260
220
180
20
0
-20
-40
-60
-80
10 MHz
CONTOUR UNIT = 10^5 °K

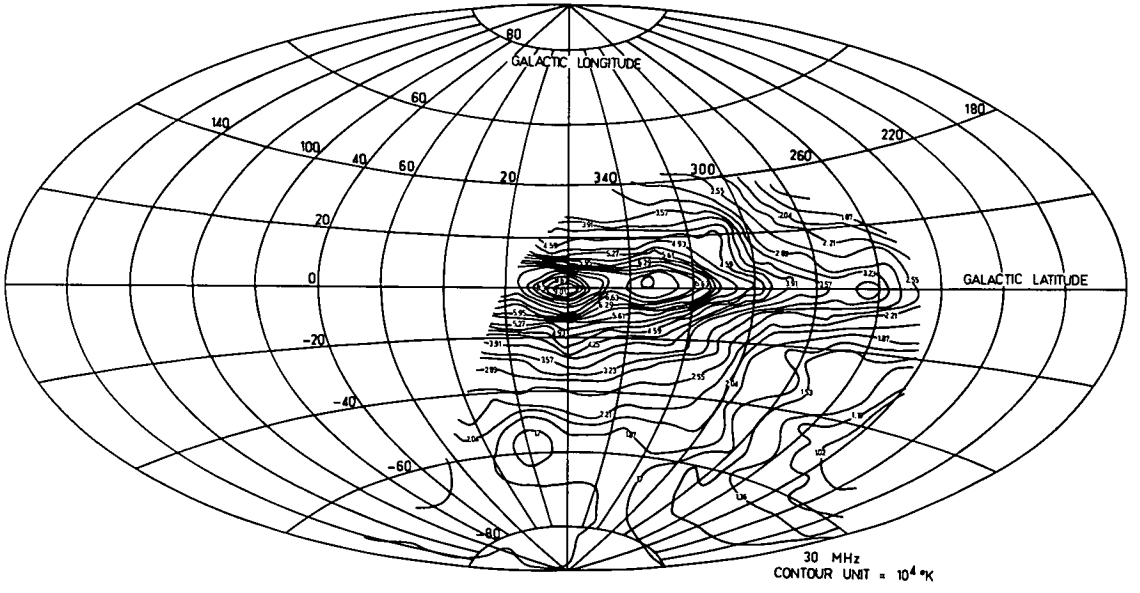
GALACTIC LONGITUDE
GALACTIC LATITUDE
80
60
140
100
40
60
20
340
300
260
220
180
20
0
-20
-40
-60
-80
30 MHz
CONTOUR UNIT = 10^4 °K

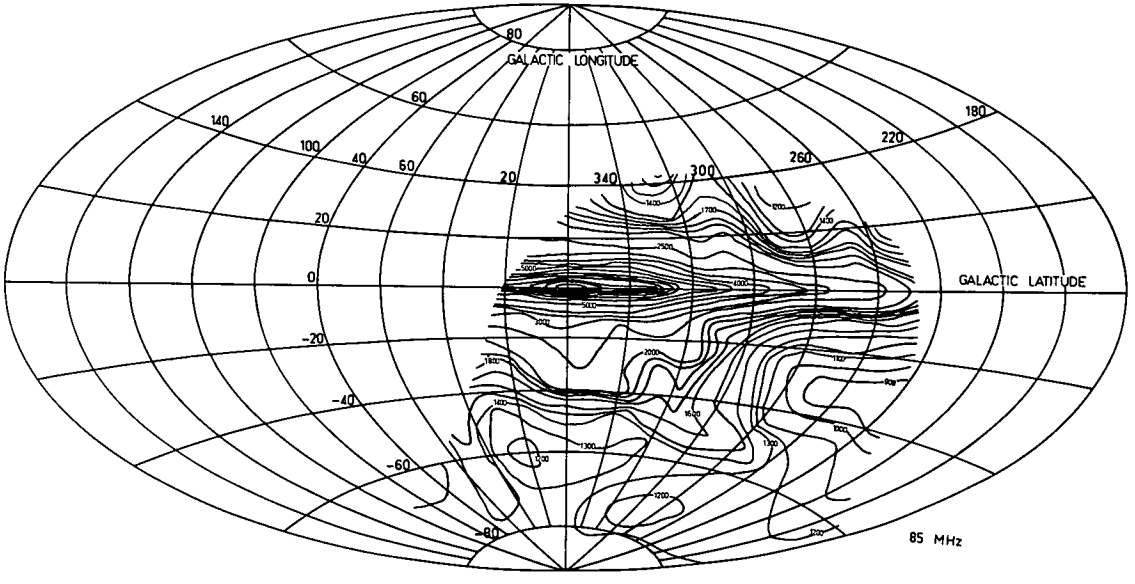
GALACTIC LONGITUDE
GALACTIC LATITUDE
80
60
140
100
40
60
20
340
300
260
220
180
20
0
-20
-40
-60
-80
85 MHz

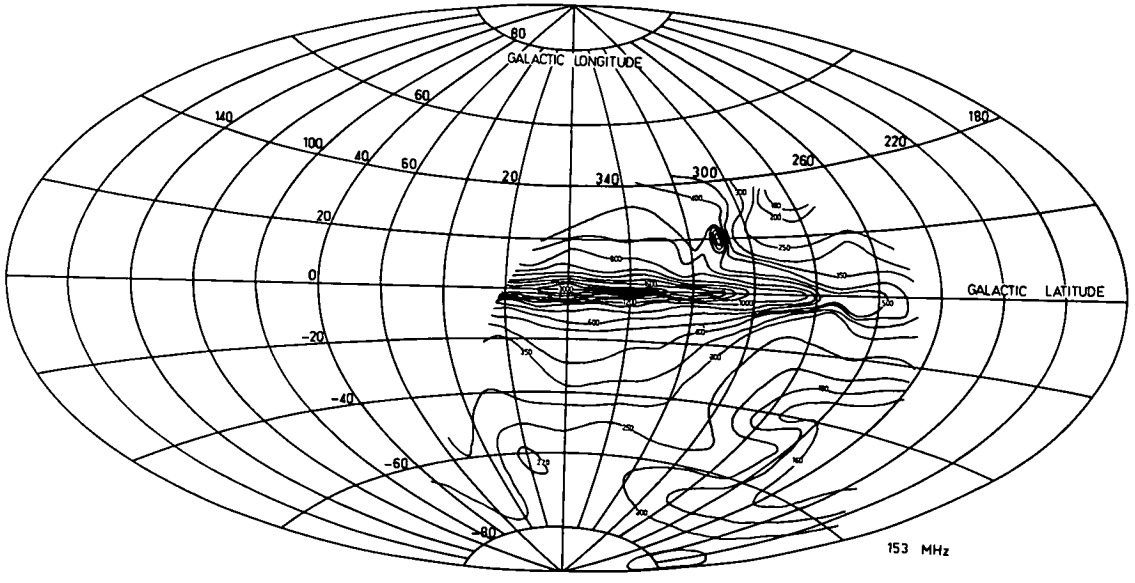
GALACTIC LONGITUDE
80
60
140
100
40
60
20
340
300
260
220
180
20
0
-20
-40
-60
-80
GALACTIC LATITUDE
153 MHz

level was indicated by the above procedure; the contour interval was checked by plotting spectra for different lines of sight from the standardized maps and examining the position of the 30 MHz point in relation to those at 153 MHz, 85 MHz and 10 MHz. A small reduction in the contour level was made to improve the agreement.

The effects of a number of small sources were removed from the 153 MHz map, but no other alterations were made to the original maps.

The effective temperatures were scaled from the standard maps at intervals of 5 degrees in galactic latitude and longitude. The grids of numbers were checked by re-contouring them; the sampling interval was found to be sufficiently small to permit accurate representation of the surveys in all regions except those within a degree or so of the galactic plane. However in this area the differences in the surveys introduced by differing telescope resolutions become serious, and it was clear that the data did not warrant a detailed analysis of this region.

METHOD OF ANALYSIS

The model is an extension of the one used in the preceding chapter. The observed brightness is assumed to be the sum of the effects of two regions, the *extra-disk* region remote from the sun and in which there is emission but no absorption, and the *disk* region in the neighbourhood of the sun and in which there is both emission and absorption. The terms extra-disk and disk are convenient, but do not imply an assumed shape for either region.

We assume the following properties for these regions:

extra-disk region:

The total emission $S_1(l,b)$ at frequency ν falling on the disk region from a line of sight (l,b) is taken to be

$$S_1(l,b) = A(l,b)\ \nu^{-\alpha(l,b)} \quad W\,m^{-2}\,Hz^{-1}\,ster^{-1}.$$

A and α will in general be functions of the particular line of sight.

disk region:

We take an emissivity of the form

$$\varepsilon_2(l,b) = 4\pi\ b(l,b)\ \nu^{-\beta(l,b)} \quad W\,m^{-3}\,Hz^{-1},$$

where $b(l,b)$ is constant for a given line of sight (l,b). The absorption is described by the optical depth τ at frequency ν for each line of sight of length $L(l,b)$ within the region.

$$\tau(l,b) = \zeta \nu^{-2} \int_0^{L(l,b)} \frac{n_e(r,l,b)^2}{T_e(r,l,b)^{3/2}} \, dr$$

where $n_e(r,l,b)$ is the electron number density,

$T_e(r,l,b)$ is the electron kinetic temperature,

$L(l,b)$ is the length of the line of sight

and ζ is a constant $\simeq 0.15$ (see Chapter 2).

We write

$$\eta(l,b) = \frac{1}{L(l,b)} \int_0^{L(l,b)} \frac{n_e(r,l,b)^2}{T_e(r,l,b)^{3/2}} \, dr \ ,$$

hence

$$\tau = \zeta \nu^{-2} \eta L \ .$$

The total intensity at frequency ν from a line of sight (l,b) in the disk region is

$$S_2(\nu) = \frac{1}{4\pi} \int_0^L 4\pi b \nu^{-\beta} \; e^{-\zeta\nu^{-2} \int_0^{\ell} \frac{n_e^2}{T_e^{3/2}} dr} \; d\ell$$

$$= \frac{b\,\nu^{2-\beta}}{\zeta\,\eta} \left[1 - e^{-\zeta\nu^{-2}\eta L}\right] ,$$

since we have assumed that b is constant for each line of sight.

Thus for a line of sight (l,b) the total intensity observed at frequency ν is

$$S(\nu) = A\,\nu^{-\alpha}\, e^{-\zeta\nu^{-2}\eta L} + \frac{b}{\zeta\eta}\,\nu^{2-\beta}\left[1 - e^{-\zeta\nu^{-2}\eta L}\right]$$

where A, α, b, β, η and L are all functions of the particular line of sight chosen. The model actually involves five parameters, rather than the six that are implied, as it is not possible to separate b, η and L in the above expression into three distinct parameters. This becomes

clear when we write

$$B = \frac{b}{\zeta\eta} \qquad \text{and} \qquad K = \zeta\eta L.$$

We obtain for the observed intensity

$$S(\nu) = A\,\nu^{-\alpha}\,e^{-K\nu^{-2}} + B\,\nu^{2-\beta}\,[1 - e^{-K\nu^{-2}}] \qquad (1).$$

The unknowns in (1) are A, α, B, β and K.

The model is solved for a given line of sight by fitting a curve of this form to the experimental data. Radio spectra are usually plotted on log-log graphs, and it is necessary to apply the curve-fitting technique on a log-log scale as well to avoid giving excessive weight to the low frequency measurements. The method therefore consists of minimizing the function

$$F = \sum_i \{ln(S_i) - ln(S(\nu_i))\}^2 \qquad (2),$$

where the S_i are the experimental points at frequencies ν_i, the $S(\nu_i)$ are the values of (1) at frequencies ν_i, and the summation is over all the data points. The values of the parameters at the minimum of F constitute, of course, the least-squares solution to the problem. The resulting curve, when plotted on a log-log scale, presents the most

satisfying fit within the constraints of the model.

Unfortunately the standard methods of achieving a least-squares solution by linearizing the problem are not remotely possible because the expression in equation (1) remains non-linear under all transformations of variables. The process must therefore be an iterative one. A number of methods of locating the local minimum of a function by iteration have been published in recent years, and an extensive programme of reviewing and testing these methods was undertaken. Two methods were selected, based on papers by Nelder and Mead (1965) and Fletcher and Powell (1965); the latter method has gained wide acceptance as the most powerful general technique available at the present time. New algorithms were developed based on these methods, and these are given in the Appendix. Both algorithms have been accepted for publication.

THE SIMPLIFIED MODEL

Equation (1) is capable of a wide variety of shapes, depending on the values of the five parameters. It is therefore essential that the experimental spectrum be well-defined before any attempt is made to solve the full model. In principle observations at six well-spaced frequencies are

sufficient to permit a solution for five parameters, but the observations would have to be virtually error-free for the results to be significant.

The easiest parameters to eliminate are the spectral indices, α and β, since of all the parameters these should vary the slowest from one line of sight to another. The spectral index of synchrotron emission is determined by the energy spectrum of the radiating electrons, and the diffusion time for electrons with these energies is likely to be such that the spectrum changes slowly with position.

The variation of spectral index over the data was examined by fitting the simple power law

$$S(\nu) \propto \nu^{-\alpha}$$

to the three highest frequencies, 153 MHz, 85 MHz and 30 MHz. The results of this fit are given in figure 7, which shows the variation of α with galactic latitude. The plotted points give the mean value of α for each latitude while the bar shows the standard deviation from the mean. The dip at $b = 0$ can be explained as the result of absorption depressing the 30 MHz intensity, and the effects of instrument resolution (all three surveys were made with the Parkes 210 foot reflector). A similar treatment of α against galactic longitude yields

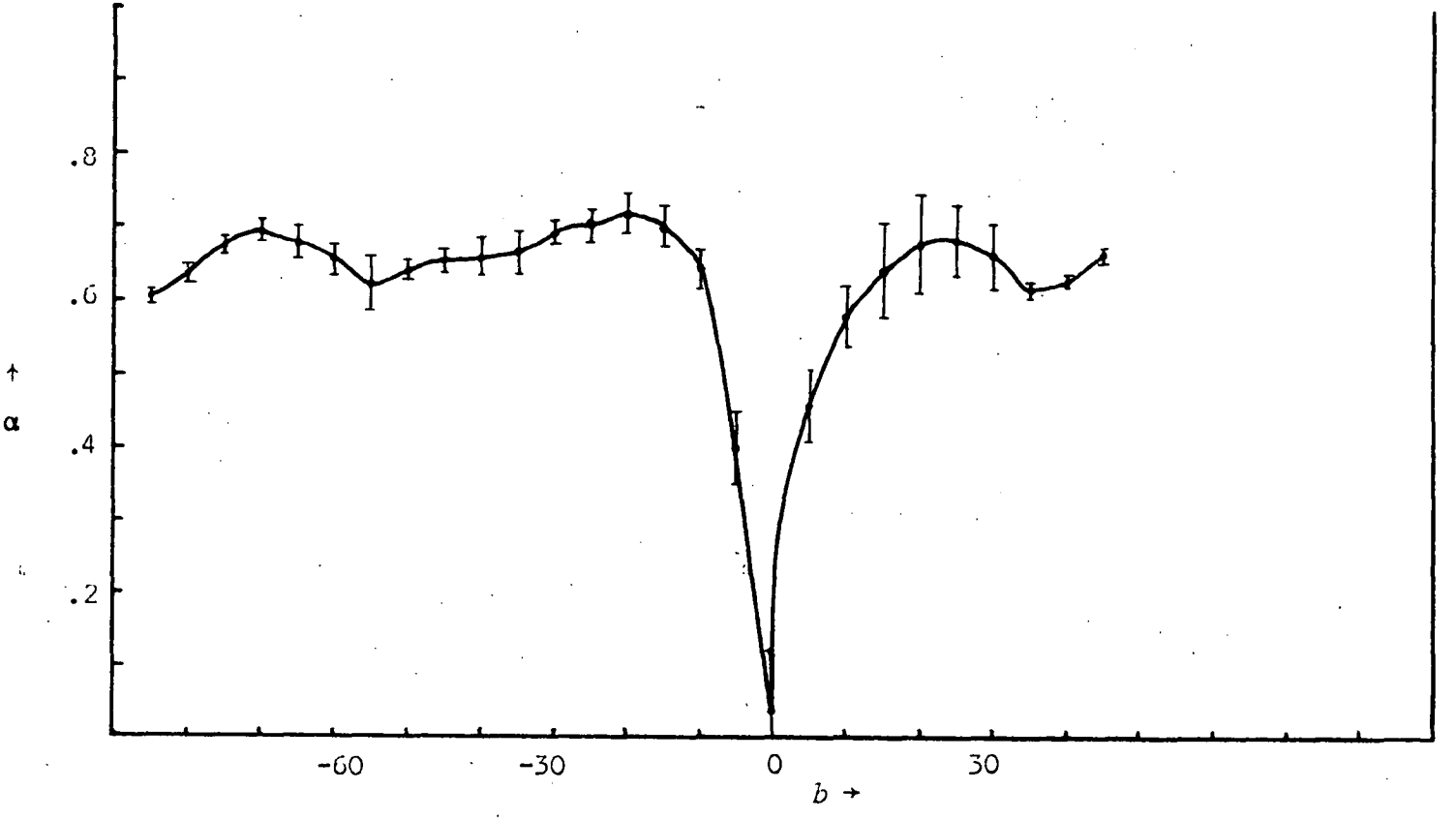

FIGURE 7 Variation of mean spectral index with galactic latitude.

standard deviations that are large, and no significant trend in the mean.

We infer that the spectral index is not a rapid function of l and b, and that it is therefore a suitable candidate for elimination from the model. There may be good reasons for choosing different values for α and β of equation (1). The extra-disk radiation may originate in a region very remote from the disk region, or it may be the integrated emission from extragalactic sources. In either case there is no reason for choosing $\alpha = \beta$. However figure 7 suggests that a single value for the spectral index is adequate for the data, and we therefore choose

$$\alpha = \beta = 0.66.$$

The simplified model for the total intensity at frequency ν becomes

$$S(\nu) = A\,\nu^{-0.66}\,e^{-K\nu^{-2}} + B\,\nu^{1.34}\,[1 - e^{-K\nu^{-2}}] \qquad (3),$$

in which the unknowns are A, B, and K.

RESULTS

The parameters A, B and K were obtained for each line of sight by minimizing the function F given by equation (2) using the $S(\nu_i)$ from equation (3). The results are presented most conveniently in the form of contour maps in galactic coordinates.

Figure 8 gives the variation of A with line of sight. The unit of A in the figure is chosen so that the integrated extra-disk emission at frequency ν is

$$S_1(\nu) = A\,\nu^{-0.66} \qquad W\,m^{-2}\,Hz^{-1}\,ster^{-1},$$

for ν in MHz.

Figure 9 gives a similar map of B. The unit is such that the disk component of the observed brightness is

$$S_2(\nu) = B\,\nu^{1.34}\,[1 - e^{-K\nu^{-2}}] \qquad W\,m^{-2}\,Hz^{-1}\,ster^{-1} \tag{4}$$

for ν in MHz.

The variation of K is given in figure 10. By definition

$$K = 0.15 \int_0^L \frac{n_e^{\,2}(r)}{T_e^{\,3/2}(r)}\,dr$$

where L is the path length in the disk region. Figure 10 actually gives contours of

$$\int_0^L \frac{n_e^2(r)}{T_e^{3/2}(r)}\, dr$$

for n_e in cm^{-3},

T_e in *degK*,

and L in *parsecs*.

To obtain K in units appropriate for equation (4) multiply the contour unit by $4.626_{10}6$.

DISCUSSION

The extra-disk emission:

The contours of the extra-disk emission shown in figure 8 are non-isotropic and suggest immediately that the major part of the emission originates in a near spherical galactic halo. In figure 11 the contours of the regions away from the galactic plane are re-drawn, with the intensities normalized to 100 in the direction of the galactic pole. An attempt was made to reproduce these contours using as a model of the halo an ellipsoid of revolution with uniform emissivity

facing page 205.

FIGURE 8

The halo parameter, A. The intensity of the extra-disk emission, from the analysis, is given by

$$S(\nu) = A\,\nu^{-0.66} \quad W\,m^{-2}\,Hz^{-1}\,ster^{-1}.$$

The units of A in the figure are such that ν in the above expression should be in MHz to obtain the units shown.

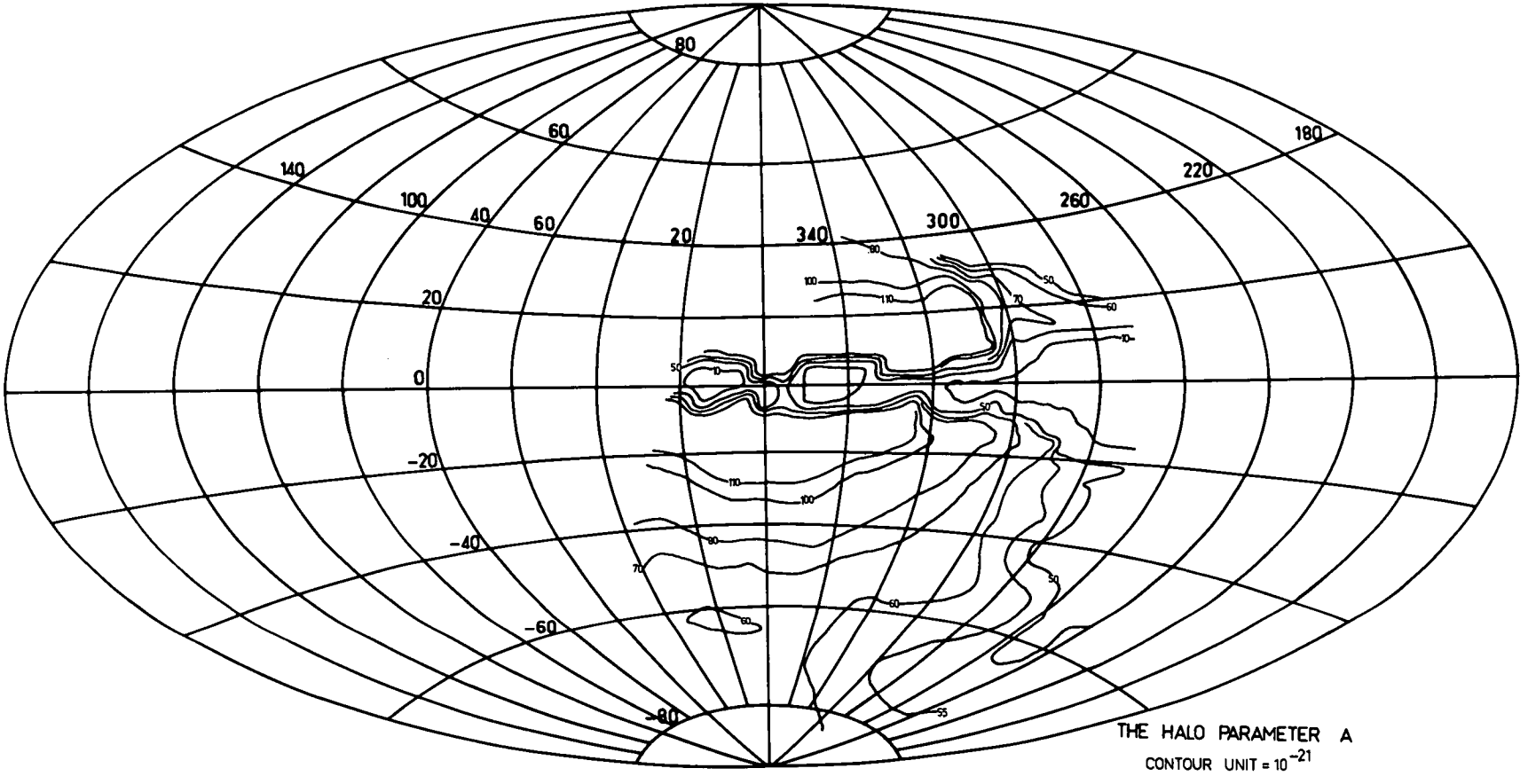
80
60
140
100
40
60
20
340
300
260
220
180
20
0
-20
-40
-60
-80
THE HALO PARAMETER A
CONTOUR UNIT = 10^{-21}

facing page 206.

FIGURE 9

The disk parameter, B. The disk component of the observed brightness, given by the analysis, is

$$S(\nu) = B\,\nu^{1.34}\,(1 - e^{-K\nu^{-2}}) \quad W\,m^{-2}\,Hz^{-1}\,ster^{-1}.$$

For these units to apply with B as given in the figure, ν should be in MHz, and K from figure 10 should be multiplied by $4.626_{10}6$.

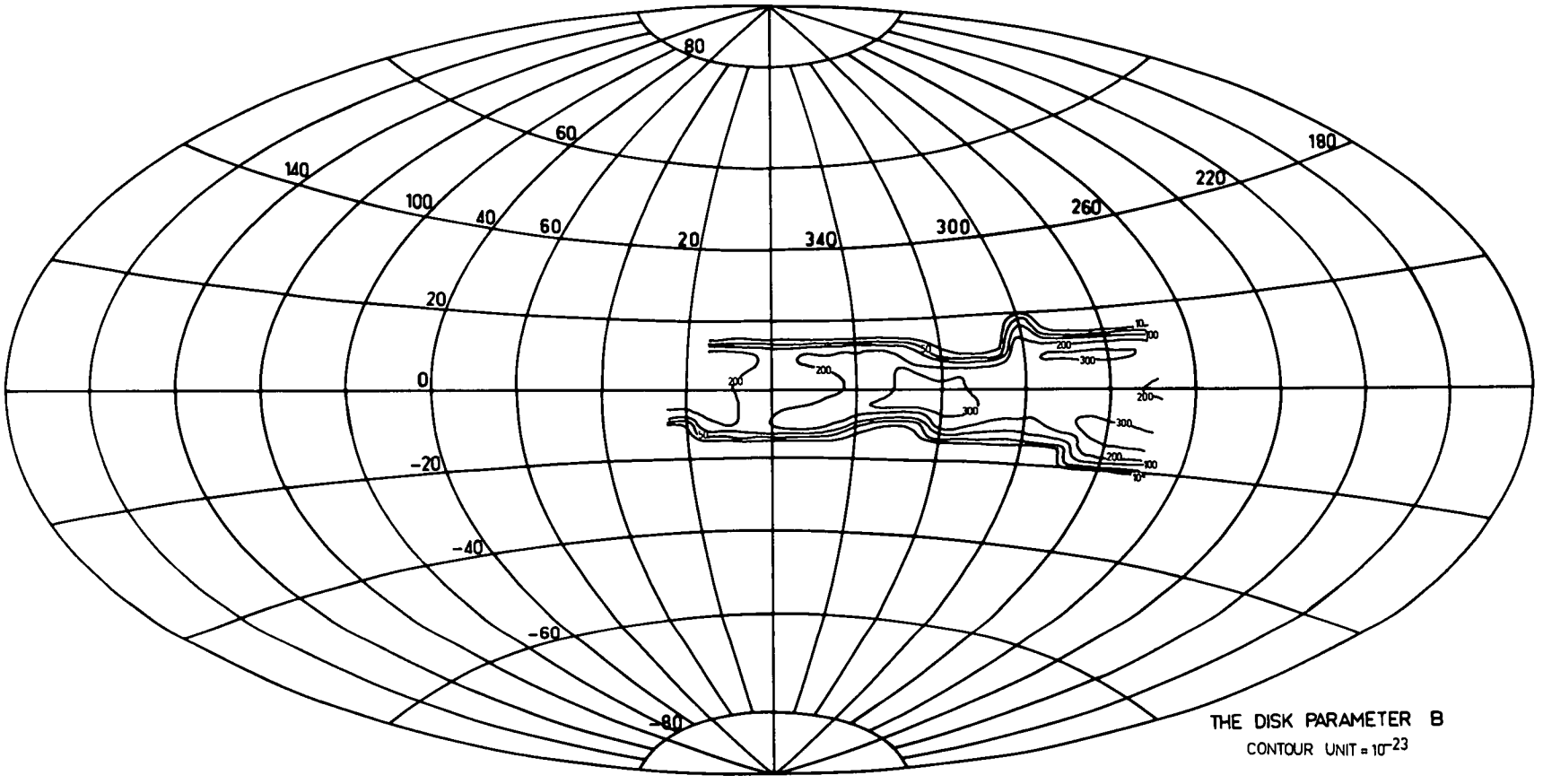
80
60
140
100
40
60
20
340
300
260
220
180
20
0
-20
-40
-60
-80
200
300
THE DISK PARAMETER B
CONTOUR UNIT = 10^{-23}

facing page 207.

FIGURE 10

The absorption parameter, K. By definition

$$K = 0.15 \int_0^L \frac{n_e^2(r)}{T_e^{3/2}(r)}\, dr \,.$$

The figure actually gives contours of the integral, i.e. of (K/0.15), for

n_e in cm^{-3}

T_e in *degK*

L in *parsecs*.

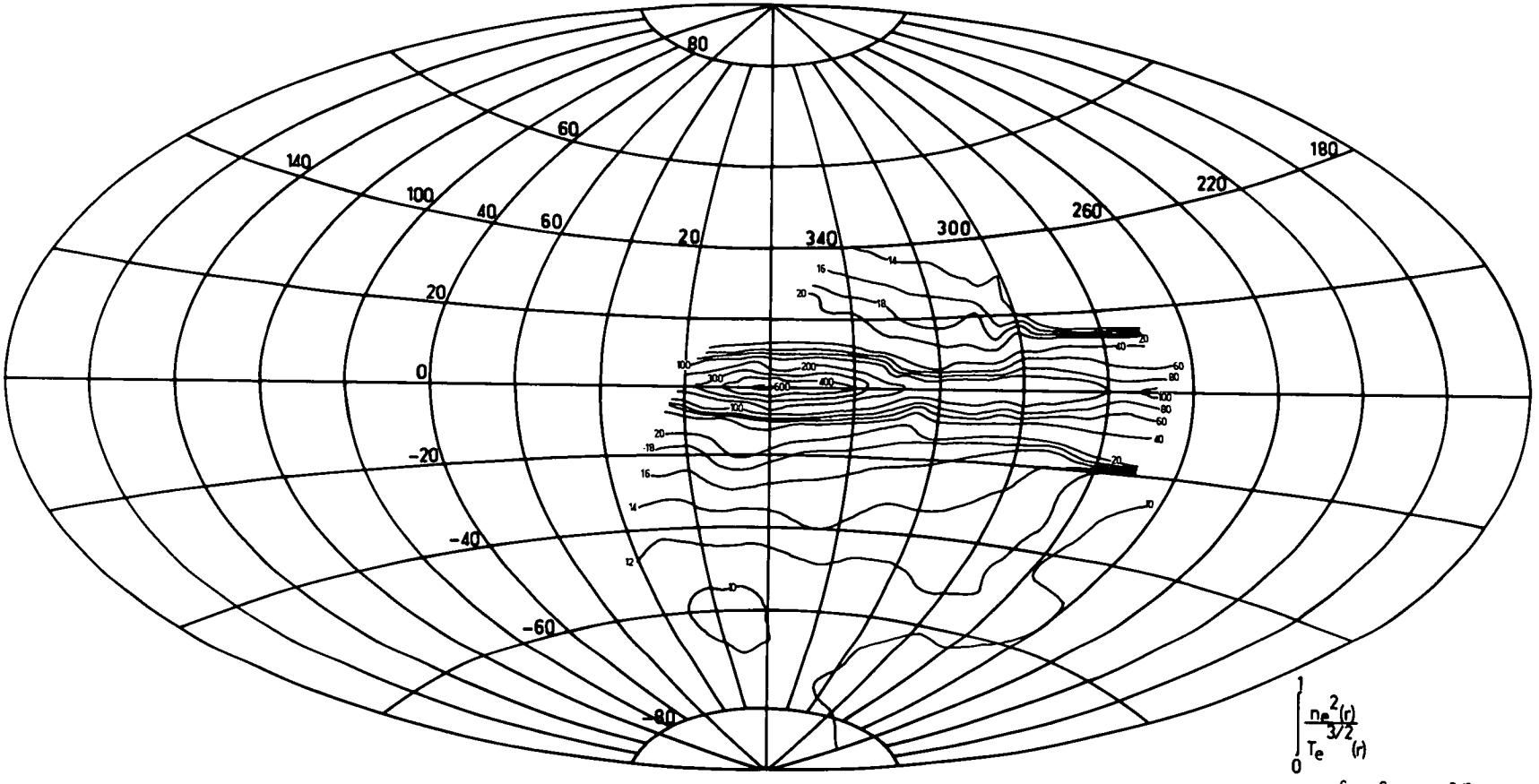
80
60
140
100
40
60
20
340
300
260
220
180
20
0
-20
-40
-60
-80
$\int_0^{\infty} \frac{n_e^2(r)}{T_e^{3/2}(r)}$
CONTOUR UNIT $10^{-6}cm^{-6}pc\ deg^{-3/2}$

facing page 208.

FIGURE 11

The contours of the halo parameter, A, for regions away from the galactic plane, re-drawn from figure 8. The broken lines are contours that would be obtained from an ellipsoidal halo of uniform emissivity, with axes of 29.2 Kpc and 26.6 Kpc (assuming the solar distance is 10 Kpc). The two sets of contours have been normalized to 100 for the direction of the galactic pole.

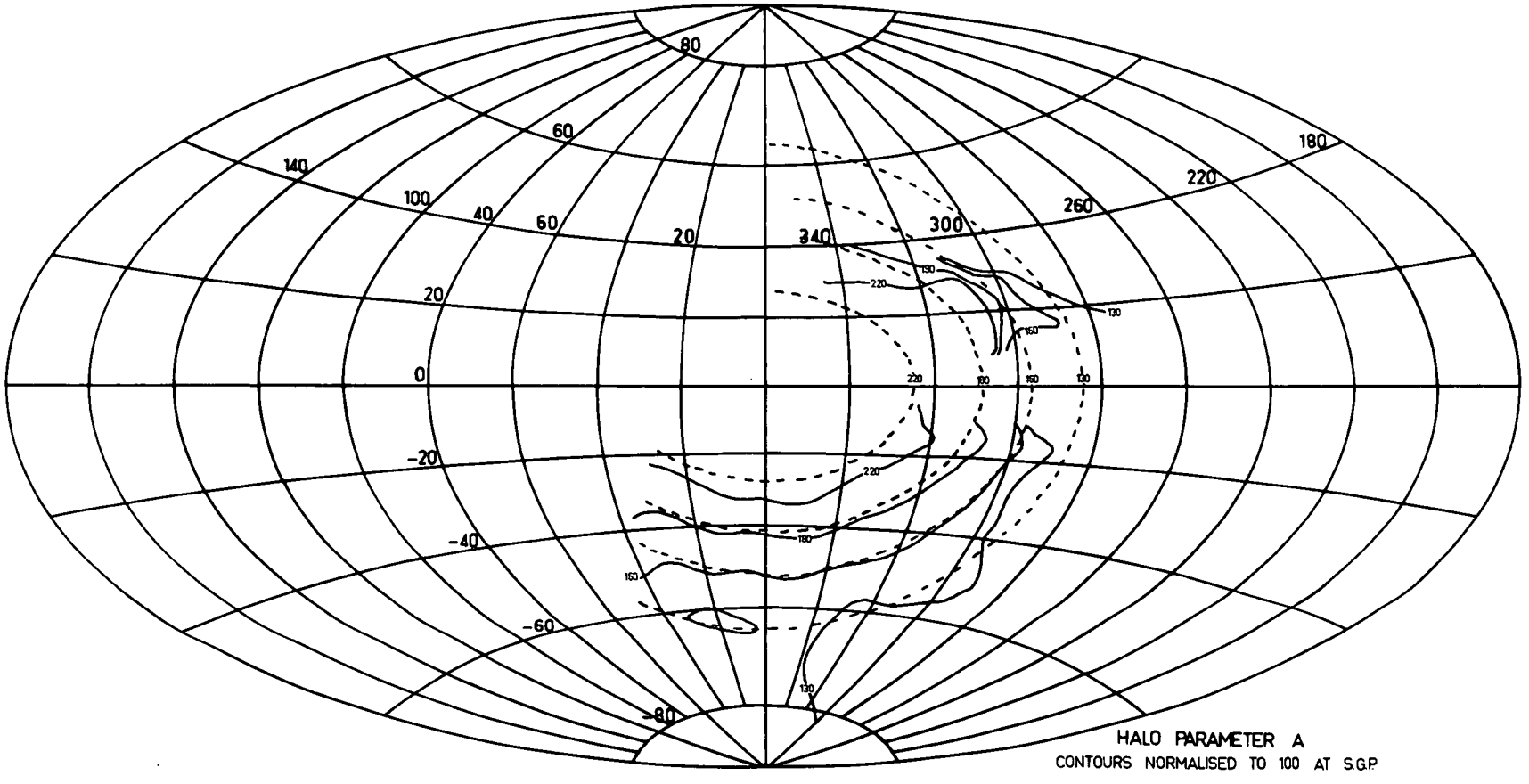

HALO PARAMETER A

CONTOURS NORMALISED TO 100 AT S.G.P

throughout, but it was not possible to match the contours over the whole map. The dotted contours in figure 11 are the predictions of such a model with the dimensions chosen to give a good fit at the high galactic latitudes. It is clear that an ellipsoidal halo with these dimensions and an emissivity that increases somewhat with the approach to the galactic centre will produce contours that agree well with the results of the analysis.

The scale of the model is dependent on the distance from the sun to the galactic centre. If we take this to be 10 Kpc, then the model giving the broken contours of figure 11 is an ellipsoid of revolution with a major axis (lying in the galactic plane) of 29.2 Kpc and a minor axis (normal to the plane) of 26.6 Kpc. The constraints imposed on the relative dimensions by the data are severe; variations of a few percent in the length of either axis lead to predicted contours which are quite different. The absolute scale of the model is however directly proportional to the assumed solar distance. The currently accepted value is 10 Kpc and this will be assumed henceforth.

The dimensions of this model are smaller than those in the initial proposal by Baldwin (1955) who fitted a halo model to his 80 MHz survey of the northern sky and obtained a

characteristic dimension of 30 Kpc and a ratio of minor to major axes of "not less than 0.5". He took the solar distance to be 8 Kpc, and using the current value in place of this he would obtain a characteristic dimension of ∿37 Kpc. He chose finally a more elaborate model consisting of an ellipsoid of revolution with constant emissivity, a rather thick disk component, and a thin disk region close to the galactic plane. The model of figure II in which the emissivity increases towards the centre seems to provide a better fit, at least for the southern galactic hemisphere.

A somewhat smaller halo model was derived by Mills (1959) from his 85 MHz survey. He obtained the best fit by assuming a region with " .... a more or less spherical volume with a radius of approximately 5 kiloparsecs surrounding the galactic nucleus". He also assumed a greater emissivity near the nucleus. The main difference between the model of the present analysis and that of Mills is that in the present model a greater proportion of the total extra-disk emission results from the halo, which is consequently larger than that derived by Mills. This difference in size is exaggerated by the revision of the solar distance; Mills also assumed this to be 8 Kpc.

The integrated extra-disk emission at 10 MHz for the

direction of the galactic pole can be calculated from figure 8. We obtain

$$S(10) = 1.1_{10}{}^{-20} \quad W\,m^{-2}\,Hz^{-1}\,ster^{-1} .$$

If this is the result of a uniform halo with the dimensions quoted above, it is generated over a path length of ∿10 Kpc. The volume emissivity of the halo at 10 MHz is then

$$\varepsilon_1(10) \simeq 4.5_{10}{}^{-40} \quad W\,m^{-3}\,Hz^{-1} .$$

We have taken a constant spectral index of $\alpha = 0.66$ for the model, which implies that the differential energy spectrum of the generating electrons has the form

$$N(E) = \kappa\, E^{-2.32} \qquad (5).$$

The volume emissivity of such a distribution depends on the magnetic field strength, and is given by

$$\varepsilon(\nu) = 2.34_{10}{}^{-35}\, B_\perp \int N(E)\, F\left(\frac{\nu}{16.1\, B_\perp\, E^2}\right) dE$$

$$W\,m^{-3}\,Hz^{-1} ,$$

for $B_\perp$ in μG

E in *GeV*

ν in *MHz*

and N(E) in $el\ m^{-3}\ GeV^{-1}$.

The integration is over all electron energies present in the distribution.

We obtain

$$\varepsilon(\nu) = 2.34_{10}{}^{-35}\, B_{\perp}\, \kappa \int E^{-2.32}\, F\left(\frac{\nu}{16.1\, B_{\perp}\, E^{2}}\right) dE$$

$$= \kappa\, I(B_{\perp})$$

where $I(B_{\perp})$ must be obtained by direct numerical integration. For a frequency of 10 MHz we obtain the values of $I(B_{\perp})$ listed in Table I, and this gives values of κ which depend on the assumed field strength in the halo.

We can calculate the energy density Δ of the radiating electrons from the number density as

$$\Delta(E_0) = \int_{E_0}^{\infty} N(E)\, E\, dE$$

where $\Delta(E_0)$ is the contribution to the total energy density by electrons with energy $\geq E_0$. We obtain

$$\Delta(E_0) = \frac{\kappa}{0.32}\, E_0{}^{-0.32} \qquad (6).$$

Table II gives the results of these calculations for several values of the field strength $B_{\perp}$, using the results in Table I.

TABLE I

THE FUNCTION

$$I(B_\perp) = 2.34_{10}{-35}\, B_\perp \int E^{-2.32}\, F\left(\frac{10}{16.1\, B_\perp\, E^2}\right) dE$$

$B_\perp$	$I(B_\perp)$
microgauss	*MKS units*
0.1	$2.30_{10}{-37}$
1.0	$2.63_{10}{-35}$
10.0	$1.33_{10}{-33}$

TABLE II

Parameters calculated from the halo model

$B_\perp$	κ	$\Delta(E_0=1\ \mathrm{GeV})$
microgauss	*MKS units*	*eV cm*$^{-3}$
0.1	$1.96_{10}{}^{-3}$	6.1
1.0	$1.71_{10}{}^{-5}$	$5.3_{10}{}^{-2}$
10.0	$3.38_{10}{}^{-7}$	$1.05_{10}{}^{-3}$

The actual values of κ and Δ cannot be determined from this model unless an independent measure of the halo field strength is available, or some other assumption is made. A suitable assumption is that the halo is in a state of equilibrium. The condition for equilibrium is that a pressure balance obtains, and this is achieved by equating the cosmic ray pressure to the magnetic field pressure since other pressure terms can be neglected (see Shklovsky, 1960). Assuming that the cosmic ray distribution is isotropic, the pressure P is related to the energy density by

$$P = \Delta/3 .$$

An equivalent equilibrium condition is therefore equality of the cosmic ray energy density and the magnetic energy density. Working in units of $eV\ cm^{-3}$ we obtain

$$\Delta = \frac{B^2}{8\pi \times 1.6} = \frac{B^2}{40}$$

where B is in microgauss.

In figure 12 the energy density of cosmic ray electrons required by the emissivity of this halo model is plotted against assumed field strength, together with the energy density of the magnetic field. There remains one further unknown, namely the ratio of the abundances of cosmic ray protons and electrons. The condition for mechanical

equilibrium is equality of the magnetic energy density with the *total* particle energy density. Two broken lines in figure 12 give energy densities that are 2 times and 100 times the electron energy density. Thus if electrons and protons are present in equal numbers at similar energies, the conditions for a stable halo are a field strength of about 1 μG, a total particle density of about 0.05 $eV\ cm^{-3}$ and an electron energy density of half the total. If the ratio of electron to proton abundances is the same as in the vicinity of the earth (about 1% — Meyer, 1969) we obtain a halo field of 5 μG and a total particle energy density of 0.4 $eV\ cm^{-3}$.

If we compare these electron densities with those observed in the solar neighbourhood (Webber, 1968; figure 6 of Chapter 4 on page 81), we find that the local densities are down by an order of magnitude on the halo density in a field of 1 μG. The problem of reconciling the observed electron densities with the observed radio emissivities was mentioned in Chapter 4 and this general discrepancy of a factor of ten was noted. The discrepancy is removed if we assume field strengths of $\sim$6 μG, and it is interesting to note that the electron densities in the halo and the solar neighbourhood would then be the same. However this higher field strength

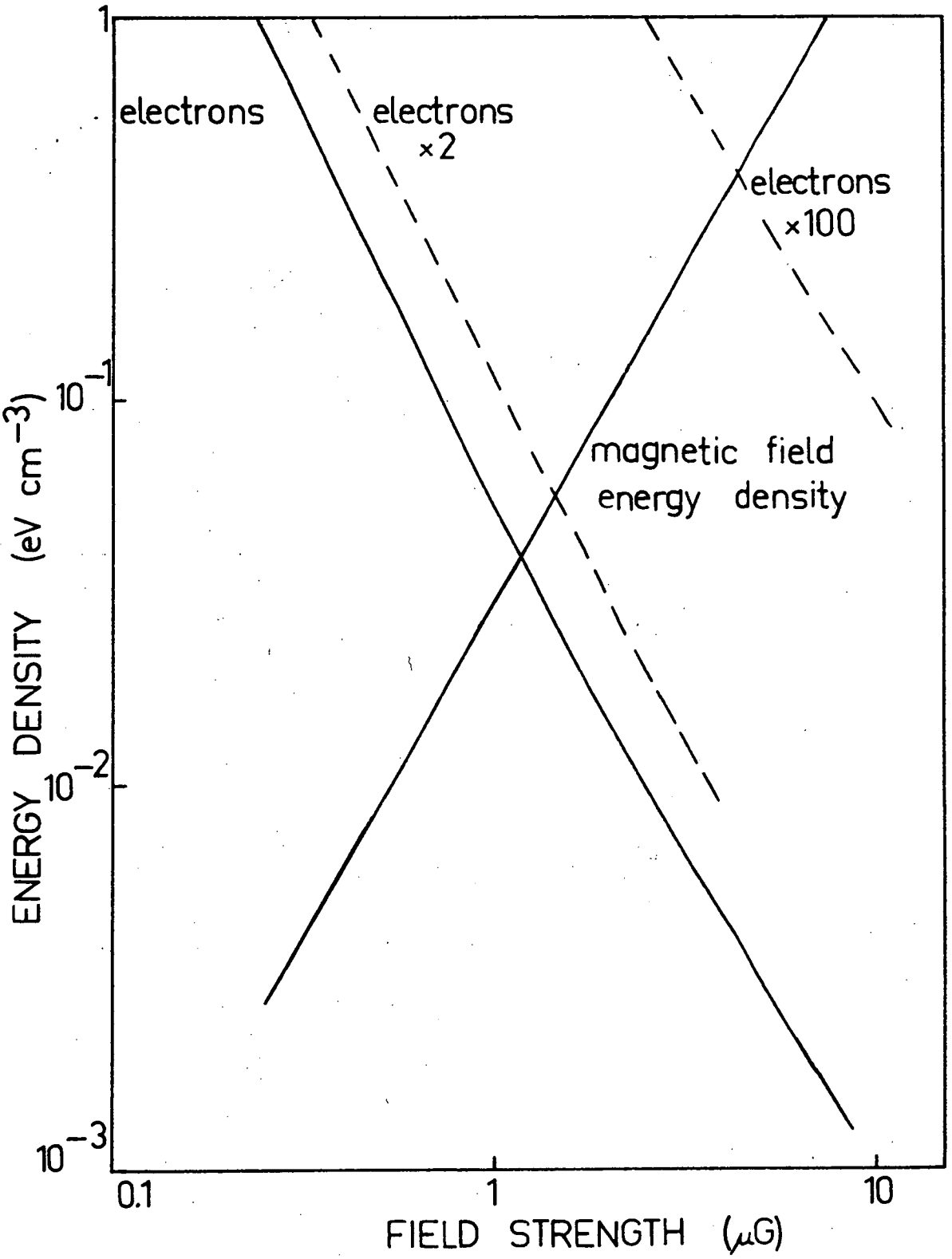
1
10^{-1}
10^{-2}
10^{-3}
ENERGY DENSITY (eV cm^{-3})
electrons
electrons
×2
electrons
×100
magnetic field
energy density
0.1
1
10
FIELD STRENGTH (μG)

FIGURE 12

may imply a greater mean field strength in the halo than in the disk, which would pose further problems on the formation of the halo.

We now return to the question of the diffuse x-ray background mentioned briefly in Chapter 4, and discussed by Hamilton and Francey (1969). Balloon, rocket, satellite and space probe measurements have revealed the existence of a diffuse background of x-rays and γ-rays with energies in the range 1 KeV to 1 GeV. The intensity of this background is sufficiently high to make it a major source of difficulty in the discovery and measurement of discrete x-ray sources. The spectrum of the background is very similar to the radio spectrum above 10 MHz, being approximately of the form

$$(h\nu)^{-\alpha}$$

where $(h\nu)$ is the energy of the x-ray photon. The value of the spectral index α is a topic of much debate, and indeed the current state of the x-ray spectrum is reminiscent of the radio spectrum early in this decade. It is widely believed that the origin of the x-ray background is extragalactic. This is largely due to the apparent lack of a mechanism within the galaxy that can generate intensities as high as those observed. The theory of extragalactic origin is given credence by the indications that " .... there is no real evidence for

anisotropy in this diffuse radiation; variations with direction seem to be, at any rate, not greater than 10 per cent" (Felten and Morrison, 1966). The absence of much of the "evidence for anisotropy" is due simply to a lack of evidence in appropriate directions, as is indicated below.

Possible mechanisms for the generation of the low energy (1 - 10 KeV) radiation include unresolved sources, bremsstrahlung from low energy electrons (Maraschi *et al*, 1968), bremsstrahlung from suprathermal protons and electrons (Boldt and Serlemitsos, 1968) and the inverse Compton effect (Hoyle, 1965). Of all these processes the last-mentioned is by far the most important. The inverse Compton effect is the generation of a high energy photon by the collision of a fast electron with a low energy photon. The theory of the process is discussed in some detail by Felten and Morrison (1966) who use a δ-function approximation for scattering by a single electron to derive brightness formulae for the case of thermal photons and power-law electron distributions. Taking

$$\gamma = \left[1 - \left(\frac{v}{c}\right)^2\right]^{-1/2}$$

where v is the electron speed and c is the speed of light, we can write the electron distribution in terms of γ rather than energy E, and we obtain

$$n(\gamma)d\gamma = n_o \gamma^{-m} d\gamma \qquad (7)$$

where $n(\gamma)d\gamma$ is the number of electrons per unit volume with γ's in the range $d\gamma$ (for 1 GeV electrons, $\gamma \simeq 2000$). For a *black body* distribution of photons, Felten and Morrison show that the average energy of the inverse Compton photons is

$$\langle h\nu \rangle (eV) \simeq 3.1_{10}{}^{-4} \gamma^2 T(degK) \qquad (8)$$

where the electron energy is given by γ and T is the temperature of the black body field. They take electron and photon distributions that are isotropic and homogeneous throughout a region of dimension R, and obtain the specific intensity of the Compton-scattered photons as

$$I(h\nu) \simeq 10^3 (56.9)^{3-m} n_o R \rho T^{(m-3)/2} (h\nu)^{(1-m)/2}$$

$$eV\ (eV\ cm^2\ sec\ ster)^{-1} \qquad (9),$$

where n_o and m describe the electron spectrum, as in (7),

ρ is the energy density of the thermal photons, $eV\ cm^{-3}$

T is the temperature of the radiation field, $degK$

and R is the path length, *light years*.

It is important to note that in this case, namely thermal photons and a power-law electron distribution, the spectral dependence on the electron distribution is the same as for synchrotron emission.

Felten and Morrison attempted to explain the diffuse x-ray background in terms of the inverse Compton effect from electrons and 3 degK black body photons in the galactic halo. They concluded that the x-ray background was in excess of the possible halo emission, although the predicted and observed spectral shapes were compatible. However the model of the halo used in their calculations differs from that derived above, and there is some point in repeating the calculation.

The available evidence (e.g. Penzias and Wilson, 1965) implies the existence in the universe of an equilibrium black body distribution corresponding to T ≃ 3 degK. The radiation density of such a field is given by

$$\rho = \sigma T^4$$

where σ is the Stefan-Boltzmann constant. We obtain

$$\rho \simeq 0.4 \; eV \; cm^{-3} \qquad \text{for} \quad T = 3 \; degK.$$

The average energy of an x-ray photon from the interaction of 1 GeV electrons with this field is given by (7) to be ∿3.6 KeV. In a magnetic field of 1 μG the synchrotron emission from these electrons will be in the range 12 - 20 MHz. If we take m = 2.2 (corresponding to the south halo spectrum of Chapter 4) and T = 3 degK, we obtain from (9)

$$I(3.6 \text{ KeV}) \simeq 54 \; n_o \; R \qquad eV \; (eV \; cm^2 \; sec \; ster)^{-1} \; .$$

The halo model gives

$$n_o = 4_{10}{}^{-7} \quad el\ cm^{-3} \quad per\ unit\ \gamma,$$

and at $b = 30^o$ the path length in the halo is

$$R \simeq 23\ Kpc = 7.5_{10}4\ light\ years.$$

We obtain

$$I(3.6\ KeV) \simeq 1.6 \quad eV\ (eV\ cm^2\ sec\ ster)^{-1},$$

compared with $8_{10}{}^{-2}$ from the model of Felten and Morrison. It should be pointed out that equation (9) is very sensitive to the choice of m; if we take m = 1.8 (corresponding to the north halo spectrum of Chapter 4) we obtain

$$I(3.6\ KeV) = 165\ n_o\ R.$$

The expected intensity in the northern galactic hemisphere cannot be calculated from this because we have no information on n_o and R.

The model of the galactic halo derived here would thus give rise to x-ray spectra with differing spectral indices in the two galactic hemispheres, reflecting the different radio spectra of Chapter 4. The radiation should exhibit a variation with direction within the southern hemisphere that is similar to the radio anisotropy indicated by figure 11. We predict I(3.6 KeV) in the south of $1 - 3\ eV\ (eV\ cm^2\ sec\ ster)^{-1}$ depending on the direction and the assumed halo field strength.

The measurements of the diffuse x-ray background in the range 1 - 10 KeV for which spectral and directional information is available are summarised in Table III. The regions observed are indicated in figure 13. All measurements were made from rocket flights above the atmosphere. It is important to be aware of the problems in comparing data from different experiments. Instrumental uncertainties arise in correcting for detector efficiencies and allowing for the "instrumental background" from the response of the detectors to charged particles as well as the x-ray photons. For this reason the intensities are usually less reliable than the spectral indices. We draw attention to the agreement between the observations in region 1 and the excellent data for region 2, and emphasize that the only satisfactory measurements of spectral index in the direction of the galactic poles are regions 1 and 2 in the north and region 3b in the south. The only available data which might test the anisotropy were obtained on flights by Harries *et al* (1967), but the count rate during the flight was too low to provide a significant measurement. The measurements in region 4 include the minimum contribution from the galaxy, and the count rate was reported to be constant to within 8% over the whole region. This isotropy is in accordance with the halo model, although the

TABLE III

MEASUREMENTS OF THE DIFFUSE X-RAY BACKGROUND AT LOW PHOTON ENERGIES

Region Observed (figure 13)	Energy Range *KeV*	Spectral Index α	Approximate Intensity at 3.5 KeV †	Observer
1	2-20	$.35^{+.07}_{-.1}$	6.6	Boldt *et al*, 1969
2	1.5-8	.4±.1	7.5	Henry *et al*, 1968
3a	4-15	.69±.2	3.9	Seward *et al*, 1967
3b	4-15	.73±.2	4.8	Seward *et al*, 1967
4	1-13	.7±.2	5.1	Gorenstein *et al*, 1969
5	2-10	.68	6.3	Green *et al*, 1968
6	1.5-4	∿.5	8.6	Baxter *et al*, 1969
7	2-10	.3±.1	4.2	Boldt *et al*, 1968

† unit: *eV (eV cm^2 sec ster)$^{-1}$*

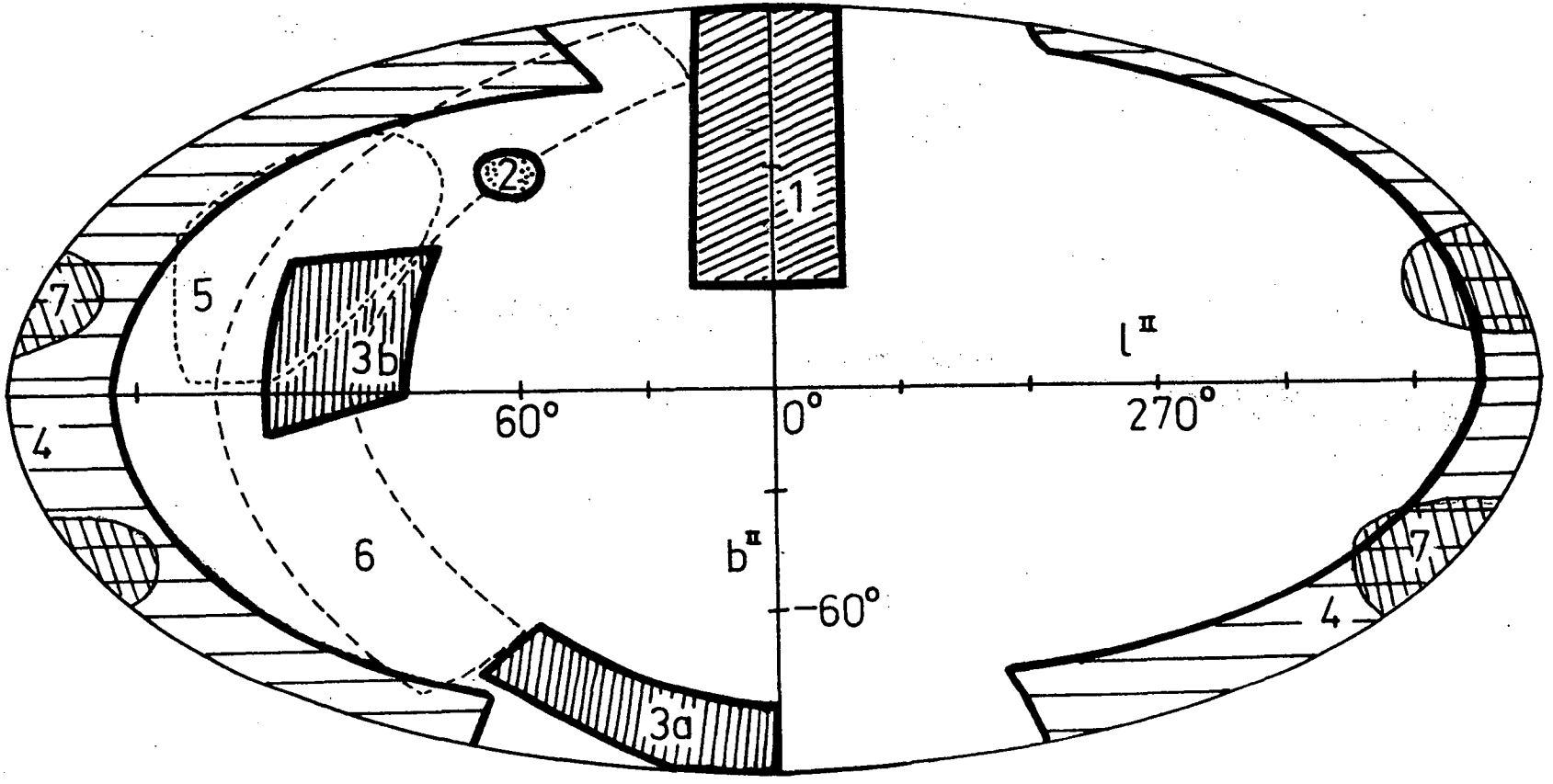

FIGURE 13

Grid of galactic coordinates showing the regions of observations listed in Table III

intensity should be below that seen at similar latitudes in the direction of the galactic centre. The discrepancies between the observations in region 4 and region 7 may well be the result of the instrumental problems encountered in the latter flight.

The correspondence between the spectral indices of the radio and x-ray emissions in the polar directions is remarkable, and in view of the revised intensity calculations the possibility of a substantial x-ray flux generated in the galactic halo can no longer be excluded. The interpretation of the entire x-ray spectrum depends on the origin of the emission, but the acute shortage of suitable data makes it impossible to settle this question at the present time.

We conclude that most of the extra-disk emission can be explained by assuming a halo with the dimensions given above, and that the extragalactic emission is rather small. Shain (1959) has made a direct measurement of this component at 19.7 MHz. He made observations of the HII emission nebula *30 Doradus* in the Large Magellanic Cloud, and compared these with observations in neighbouring directions.

Assuming that the optical depth of the nebula is large at 19.7 MHz it is possible to separate the components of the emission generated before and behind the Cloud. Unfortunately the resolution of the telescope was marginal for the experiment, and the conclusion remains somewhat indefinite: " .... the galactic corona must produce more than two-thirds, perhaps 90 per cent, of the emission." The present analysis suggests that the 90 per cent figure is appropriate. A new low frequency telescope in construction near Hobart (Hamilton, 1968) should enable this measurement to be repeated with a more definite conclusion.

The question of the extragalactic radio background has recently been discussed by Payne (1969) for a number of cosmological models. In an extension of this work (Payne: *private communication*) he has included the effects of evolution of the radio sources themselves, and computed the total intensity of the extragalactic emission observed at 178 MHz. The observational evidence seems to indicate that the cosmology appropriate to our universe is a highly evolutionary one, and for this model Payne obtains an intensity of the extragalactic emission that is about 10 per cent of the total intensity observed, in agreement with the measurement of Shain and the present model of the halo.

The disk emission:

The quantity B from the analysis, contoured in figure 9, was defined in terms of the model as

$$B = \frac{b}{\zeta\eta} \quad .$$

We assumed an emissivity in the disk region of the form

$$\varepsilon_2(\nu) = 4\pi\, b\, \nu^{-\beta} \qquad W\, m^{-3}\, Hz^{-1}$$

where the proportionality factor b was taken to be constant for a given line of sight. The absorption in the disk region was described by the optical depth

$$\tau(\nu) = \zeta\, \nu^{-2}\, \eta\, L \,,$$

where $$\eta = \frac{1}{L} \int_0^L \frac{n_e^{\,2}(r)}{T_e^{\,3/2}(r)}\, dr \,,$$

L is the path length in the disk region, and $\zeta \simeq 0.15$. The quantity B is thus a measure of the ratio

$$\frac{\text{average disk emissivity}}{\text{average absorption coefficient}}$$

where the averages are over the line of sight in the disk region.

The contours in figure 9 show that this ratio increases rapidly as the line of sight approaches the galactic plane. In view of the slower variation of absorption with galactic latitude (figure 10) it seems reasonable to interpret the changes in B as changes in average emissivity. The region at the galactic centre where B falls somewhat is probably the combined result of increased absorption and reduced emissivity. In a high resolution of this central region Drake (1959) noted a reduction in synchrotron emission, and Shklovsky (1960) has attributed this to the high gas density removing the relativistic electrons by collisional processes.

The two regions of high B at contour level 300 near l = 280 invite an interpretation in terms of the spiral structure of the local region of the galaxy. Figure 14, from a paper by McCuskey (1966), is an estimate of the spiral structure within about 3 Kpc of the sun, as outlined by galactic clusters and HII regions. The direction ($l \simeq 280$, $b = 0$) is seen to look along an arm (the so-called Sagittarius arm). Hoyle and Ireland (1961) and Ireland (1961) have proposed a model of the spiral arm magnetic field in which the lines of force are in the form of a helix wound around the arm. Such a model could exhibit an enhanced emissivity in the outer regions of the arm, and the positions of the two regions of high B are appropriate

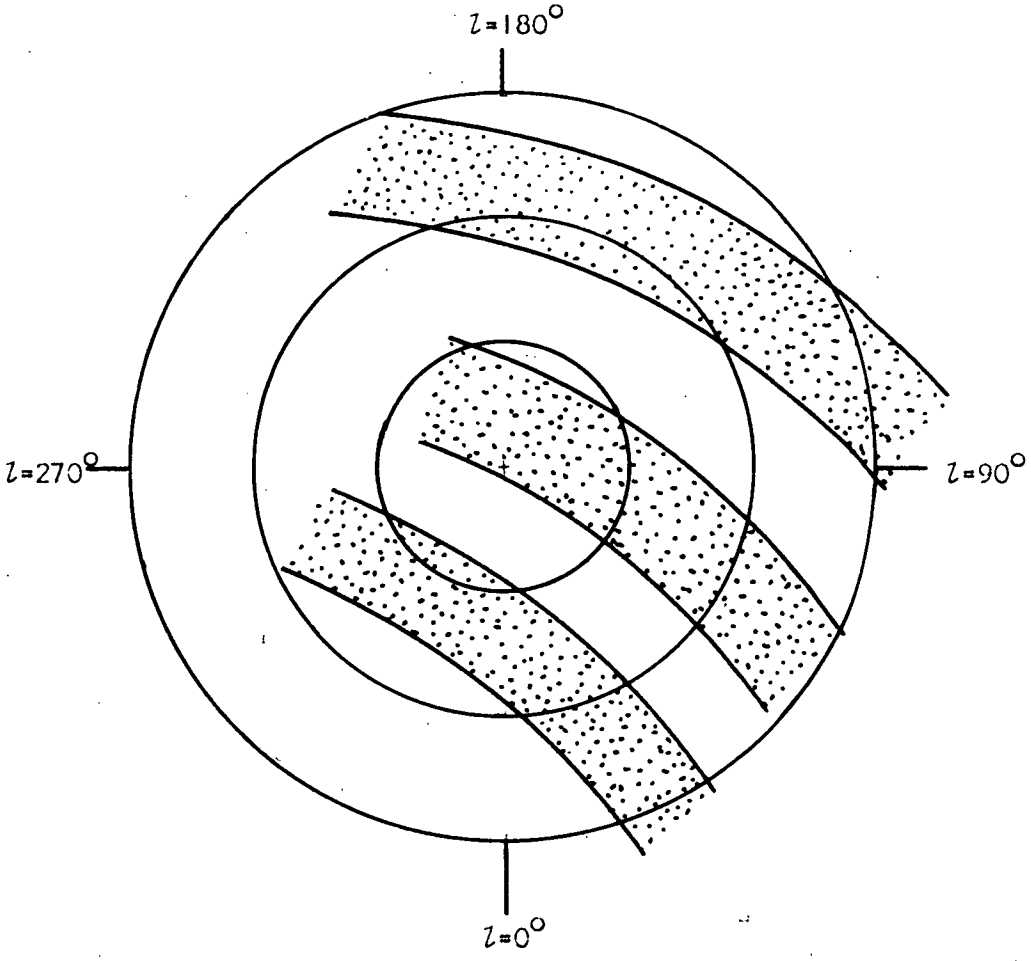

FIGURE 14

Local spiral arm structure

(The circles are 1 Kpc apart)

after McCuskey (1966)

to such a model. The high emissivity of this inner arm should actually appear as an ellipse in figure 9; part of the high region near l = 320 would coincide with this ellipse.

The majority of the high emissivity region near l = 320 is the well-known high emission region that has been interpreted by Westerhout (1958) as a ring of ionized hydrogen encircling the galactic centre with the inner and outer boundaries at distances of 3.5 Kpc and 4.5 Kpc from the nucleus. This interpretation has been supported by Ariskin (1966) on the basis of the deficiency of neutral hydrogen in this direction, but Mills (1959) finds Westerhout's assumption of radial symmetry about the galactic centre unjustified. He offers a model in which this feature is produced by the line of sight becoming tangential to a spiral arm.

Unfortunately the resolutions used in obtaining the data for the present analysis are not sufficiently high to permit an analysis of the disk region in sufficient detail to examine these features further.

The disk emission parameter B was defined as

$$B = \frac{b}{\zeta\eta}$$

where b describes the disk emissivity. The absorption

parameter K was defined as

$$K = \zeta\eta L$$

where L is the total path length in the disk region. We have, then,

$$BK = bL,$$

that is the product (BK) gives a measure of the integrated disk emission along a line of sight that would be observed in the absence of any absorption. Contours of (BK) are given in figure 15.

The structure of these contours in latitude is of some interest, as the very sharp edge to the central region is characteristic of a disk structure seen by an observer in the plane of the disk but *beyond* the edge of it. This interpretation agrees with the model of figure 14 if we assume that the sun is very close to the edge of the local arm, and the emissivity of the inter-arm region is low. The sharp increase in emission is then due to the Sagittarius arm which therefore subtends an angle of about 20° at the sun. If the width of the arm normal to the plane is 500 pc, the distance from the sun to the centre of the arm is about 1400 pc. The edge of the arm is well defined by the emission, which would support a model of the arm with a substantial magnetic field at

facing page 232.

FIGURE 15

Contours of the product (BK) from the analysis. As explained on page 231, this product gives a measure of the integrated emission along a line of sight generated in the disk region. In the absence of any extra-disk emission, and in the absence of any absorption in the disk, this is the intensity that would be observed.

The unit in the figure is such that the integrated disk emission at frequency ν is

$$(BK)\ \nu^{-0.66} \quad W\ m^{-2}\ Hz^{-1}\ ster^{-1}$$

for ν in MHz.

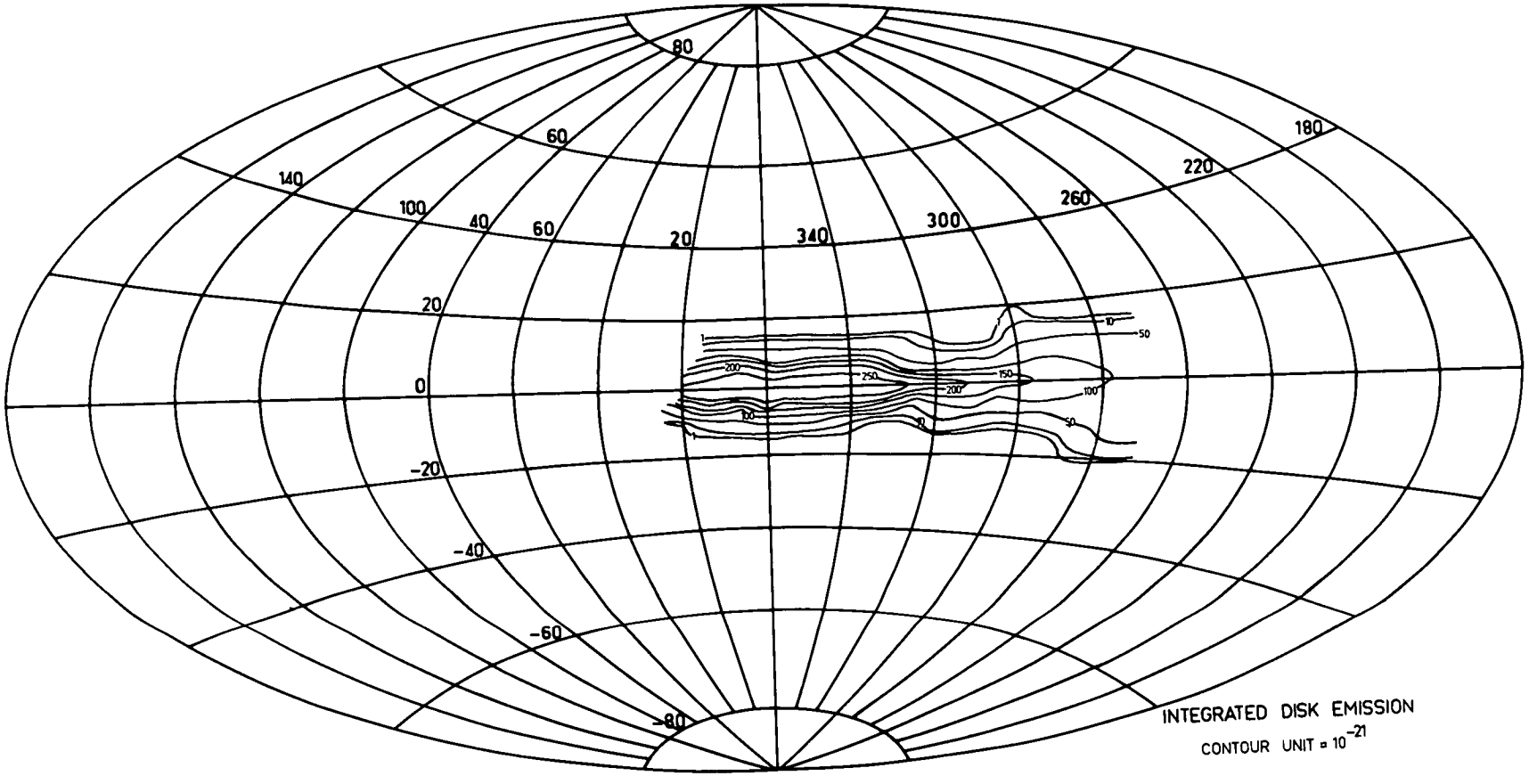
80
60
140
100
40
60
20
340
300
260
220
180
20
0
-20
-40
-60
-80
1
200
250
150
100
50
10
INTEGRATED DISK EMISSION
CONTOUR UNIT = 10^-21

the edge, such as the model of Hoyle and Ireland.

The general lowering of contrast in figure 15 as $l \to 260$ is explained by this model as the line of sight moving round into the local (Orion) arm. We would expect the contours near $l = 180$ to suggest a disk structure as seen from within.

The contours of figure 15 exhibit a structure in longitude that agrees well with the spiral arm model of Mills (1959). In particular the directions proposed by Mills as being tangential to arms, namely longitudes 281, 310, 328 and 24 are all associated with changes in the disk emission, although there are no features at 345 and 14.5 corresponding to the innermost arm segments of his model. These could well show up in an analysis based on data from higher resolution measurements.

From figure 15 the integrated disk emission at 10 MHz for directions with $b \simeq 5$ is approximately

$$S(10) \simeq 5_{10}\text{-}20 \qquad W\,m^{-2}\,Hz^{-1}\,ster^{-1}.$$

If we assume that the thickness of the disk region is 500 pc as before, the total path length over which this radiation is generated is

$$L = 250\ \mathrm{cosec}(5)\ pc = 7.7_{10}19\ m\ .$$

If we ignore the spiral arm model and assume that the emissivity

is uniform along this path, the emissivity of the disk region is

$$\varepsilon_2(10) = 9_{10}{}^{-39} \qquad W\,m^{-3}\,Hz^{-1}.$$

This is about five times the emissivity of the halo region obtained above. Adoption of the spiral arm model means that the generating path is much shorter than this figure and a higher emissivity is required.

The absorption:

The general distribution of the absorption parameter K implies a disk-like model in which the absorption is distributed more or less uniformly, and the total absorption is proportional to the path length L which will have the form

$$L = Z_0 \operatorname{cosec}(|b|) .$$

It is clear from the way the absorption extends out to the galactic pole that the observer is immersed in the absorbing region, in contrast to the distribution of the disk emission. In figure 16 the distribution of absorption in latitude is given in polar form for $l = 0$. This diagram shows that the absorber is not in fact in a uniform disk but rather the spiral

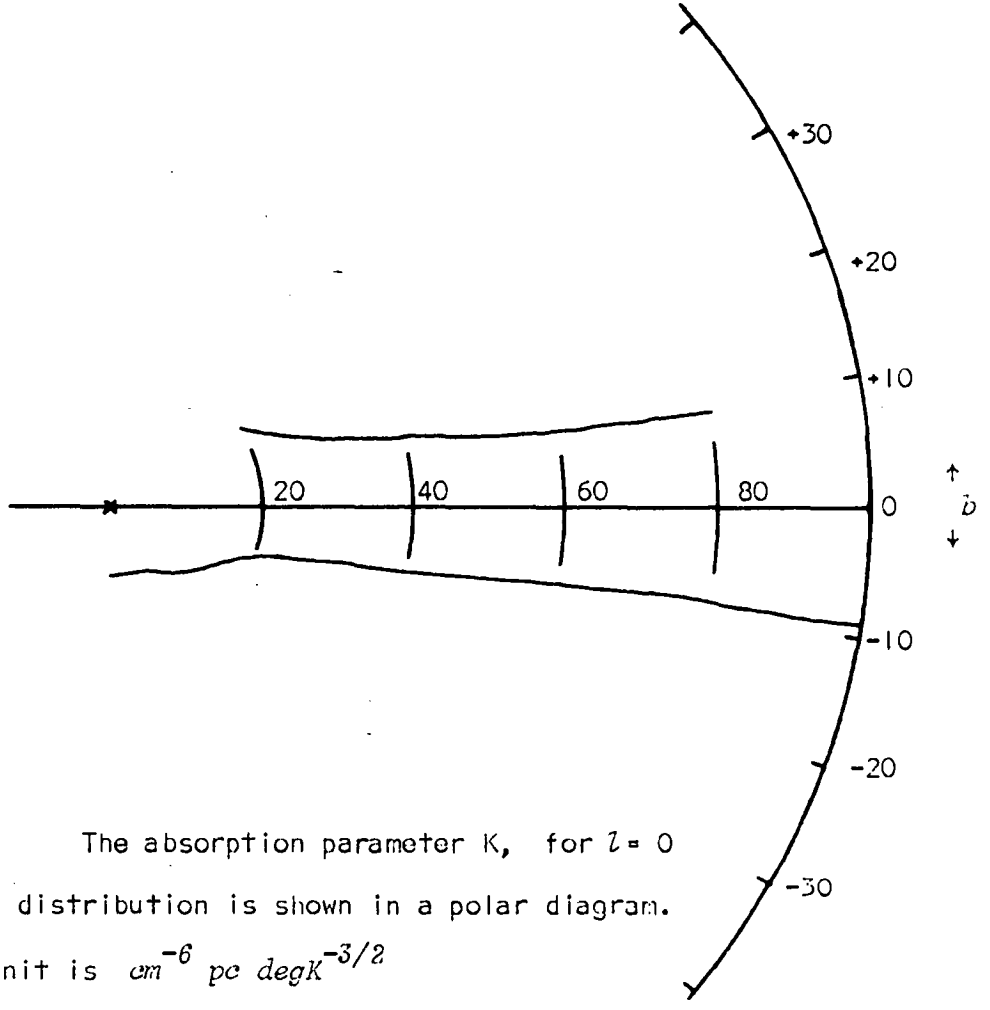

FIGURE 16 The absorption parameter K, for $l = 0$

The latitude distribution is shown in a polar diagram.

The radial unit is $cm^{-6}\ pc\ deg K^{-3/2}$

arm structure seems appropriate, with the absorber concentrated mainly in the arms. The angular size of the Sagittarius arm indicated by the disk emission ($\sim 20^{\circ}$) agrees with this figure.

The interpretation of the absorption is complicated because the parameter K is a function of three quantities, the free electron density, the electron kinetic temperature and the path length. If we assume that the width of the disk region is 500 pc, and that the other quantities are constant along the line of sight, we obtain for the direction of the galactic pole

$$n_e^2 = 4_{10}{-8}\ T_e^{3/2}$$

for n_e in *el cm*$^{-3}$ and T_e in *degK*. Then T_e=8000 degK gives n_e=0.17 cm^{-3}, while T_e=50 degK gives n_e=0.0038 cm^{-3}. The former example uses an electron temperature typical of an HII region, although the smooth distribution of the absorption is far from the localised distributions of HII regions which are found in the vicinity of a hot exciting star. The latter example uses the temperature of neutral hydrogen which does exist in a general distribution, with a density such that this free electron content would imply a relative ionization of $4_{10}{-4}$.

The nature of the electrons responsible for the

absorption of low frequency radio waves cannot be determined with certainty at present, and further discussion of this question is left to the next chapter.

CONCLUSION

The data has been analysed in terms of a model which is as complex as permits a satisfactory solution. Further observations at different frequencies and with higher resolutions would permit the inclusion of the spectral indices as parameters. Nevertheless the results are in general accord with current ideas on galactic structure and cosmic ray electron fluxes. The evidence in favour of the existence of a galactic halo seems the strongest yet presented.

The agreement with the analysis of Chapter 6 is remarkable in view of the differences in approach of the two methods. The conclusion that the earth is embedded in a region of quasi-uniform absorption seems inescapable. The low frequency spectrum for every line of sight in the region of the surveys shows a turn-over that is characteristic of absorption by free-free electron processes, and there is no known emission mechanism that can exhibit such a slope. Even

if the model is changed to include an extra-disk emissivity exhibiting the extreme synchrotron cutoff at the low frequency end, the absorption quantity K will be reduced by at most a factor of 0.7, and the general conclusions will remain as above.

REFERENCES FOR CHAPTER 7

Ariskin,V.I. 1966 *Soviet Astronomy - AJ 9* 722.

Baldwin,J.E. 1955 *Mon. Not. Roy. Astr. Soc. 115* 690.

Baxter,A.J., Wilson,B.G. and Green,D.W. 1969 *Astrophys. J. 155* L145.

Boldt,E.A., Desai,U.D. and Holt,S.S. 1968 *Preprint: Goddard Space Flight Center.*

Boldt,E.A. and Serlemitsos,P.J. 1968 *Preprint: Goddard Space Flight Center.*

Boldt,E.A., Desai,U.D., Holt,S.S. and Serlemitsos,P.J. 1969 Presented at *I.A.U. Symposium No.37: Non-solar Gamma and X-Ray Astronomy* (Rome).

Drake,F.D. 1959 *Astron. J. 64* 329.

Felten,J.E. and Morrison,P. 1966 *Astrophys. J. 146* 686.

Fletcher,R. and Powell,M.D. 1965 *Computer Journal 7* 308.

Gorenstein,P., Kellogg,E.M. and Gursky,H. 1969 *Astrophys. J. 156* 315.

Green,D., Skirrow,J. and Wilson,B.G. 1968 *Canad. J. Phys. 46* S470.

Hamilton,P.A. 1968 *Symposium on Antenna Research* (Melbourne: Radio Research Board).

Hamilton,P.A. and Francey,R.J. 1969 *Nature: in press.*

Harries,J.R., McCracken,K.G., Francey,R.J. and Fenton,A.G. 1967 *Nature 215* 38.

Henry,R.C., Fritz,G., Meekins,J.F., Friedman,H. and Byram,E.T. 1968 *Astrophys. J. 153* L11.

Hoyle,F. 1965 *Phys. Rev. Letters 15* 131.

Hoyle,F. and Ireland,J.G. 1961 *Mon. Not. Roy. Astr. Soc. 122* 35.

Ireland,J.G. 1961 *Mon. Not. Roy. Astr. Soc. 122* 461.

McCuskey,S.W. 1966 *Trans. I.A.U. Vol. XIIB* 425.

Maraschi,L., Perola,G.C. and Schwarz,S. 1968 *Il Nuovo Cim. LIIIB* 443.

Meyer,P. 1969 *Preprint; Univ. Chicago.* To appear in *Ann. Rev. Astron. Astrophys. vol.7.*

Mills,B.Y. 1959 *Paris Symposium on Radio Astronomy* ed. R.N. Bracewell (Stanford: Stanford Univ. Press) p. 431.

Mills,B.Y. 1964 *Ann. Rev. Astron. Astrophys. 1964* 185.

Nelder,J.A. and Mead,R. 1965 *Computer Journal 7* 149.

Payne,A.D. 1969 *Aust. J. Phys. 22* 59.

Seward,F., Chodil,G., Mark,H., Swift,C. and Toor,A. 1967 *Astrophys. J. 150* 845.

Shain,C.A. 1959 *Paris Symposium on Radio Astronomy* ed. R.N. Bracewell (Stanford: Stanford Univ. Press) p. 328.

Shklovsky,I.S. 1960 *Cosmic Radio Waves* (Harvard Univ. Press).

Webber,W.R. 1968 *Aust J. Phys.* *21* 845.

Westerhout,G. 1958 *Bull. Astr. Inst. Netherlands* *14* 215.

CHAPTER 8

FREE ELECTRONS IN THE INTERSTELLAR MEDIUM

INTRODUCTION

In this final chapter the current ideas on the nature of the interstellar medium are summarised. The information on the free electron content derived in the preceding chapter is examined together with other evidence in an attempt to obtain a consistent picture of the interstellar medium.

The study of the space between the stars is as fundamental to astronomy as the study of the stars themselves. Although the particle density in the interstellar medium is very low the total volume is such that interstellar matter may amount to ten percent of the mass of the galaxy. The problem of star formation is initially a problem on the motion of the interstellar gas, while the elucidation of the spiral structure of the galaxy and its evolution is critically dependent on knowledge of this medium. In view of the importance of this field it is perhaps surprising that it is one of the youngest in astrophysics. The explanation is that

it is also one of the most intricate, both experimentally and theoretically.

The experimental difficulties arise from the nature of the measurements. Emission nebulae and the 21 cm emission from neutral hydrogen yield the only direct information on the interstellar medium. In all other cases we measure the effects of the medium on radiation from distant sources. This leads to the problem of separating the effects due to the medium from those due to the nature of the source, and the observations are limited to the directions in which suitable illuminating sources lie. Further difficulties are encountered because the low density of the medium requires observations of, and hence averaging over, large volumes.

The theoretical difficulties arise in part from the shortage of experimental data and also from the complexity of many of the problems. It is apparent that many of the thermodynamic states encountered are far removed from equilibrium, and the simplifications that apply to equilibrium thermodynamics cannot be made. The difficulties in the gas dynamics are such that at the fourth international conference on this subject in 1961 many of the problems remained as originally posed at the first conference in 1949.

OBSERVATIONAL TECHNIQUES

Optical methods:

The interstellar gas was first observed directly in emission nebulae, which are local concentrations of ionized gas excited by a nearby hot star and radiating in the visible spectrum. The emission nebulae have proved of importance in determining the chemical abundances in the interstellar gas. The high excitation produces numerous emission lines from the constituent atoms and a fairly complete analysis is possible. It appears that the abundances of the elements are similar to those found in stellar atmospheres.

Somewhat less direct is the information afforded by the reflection nebulae. These are regions of nebulosity with continuous spectra, surrounding cooler stars. The light from the reflection nebula exhibits a spectrum that is similar to that of the illuminating star, and it is clearly the scattered light from interstellar dust grains in the vicinity of the star.

The existence of these dust grains is also inferred from the interstellar extinction and reddening of starlight, and from optical polarization observations. The interstellar medium exhibits an extinction (the sum of absorption and

scattering effects) of slightly more than one magnitude per kiloparsec, increasing approximately monotonically with $1/\lambda$. The polarization of starlight is found to be practically constant for a group of stars and is clearly a function of the medium between the stars. Both the interstellar reddening and the polarization effects are conveniently explained by postulating the presence of small particles with radii in the range 10^{-7} to 10^{-5} cm depending on the model assumed. The less direct nature of the information on the interstellar grains is indicated by the range of theories on their size, shape and composition. Nevertheless the consensus is that the general composition of the cooler regions of the interstellar medium is the same as the hotter regions seen in emission. It seems that the physical state of a given region depends not on the type of material present but rather on the temperature of the region, determined by the neighbouring stars.

The remaining optical observations of the interstellar medium consist of the study of absorption lines in the spectra of hot distant stars. These spectra contain narrow absorption lines not related to the stars themselves but superimposed on their spectra by the intervening medium. The presence of sodium, calcium, potassium, titanium

and iron as well as CH and CN have been established, and a number of "diffuse bands" remain unidentified but are clearly interstellar in origin. The study of the gas using these lines is restricted by the low abundance of the absorbing atoms and by the small number of stars with suitable spectra. The unabsorbed spectrum must be free of strong lines of the interstellar atoms, which means that generally only the hot massive stars are suitable. These stars are much rarer than the cooler ones, and are found mainly along the galactic plane. Observations at higher galactic latitudes, which would be less confused and ambiguous, are therefore excluded.

In spite of these difficulties the study of the interstellar absorption lines has led to a general picture of the cloud structure of the interstellar medium that has remained unchanged in outline for twenty years. It was observed that the lines due to a single element were often split into several components with widths small compared to their separations. A model was proposed in which the interstellar gas is concentrated in clouds in relative motion, and this has gained general acceptance. The clouds occupy only about ten percent of the total volume and have densities that are several orders of magnitude greater than the surrounding gas.

Radio methods:

The most direct measurements of the interstellar gas arise of course from the emission at λ = 21 cm from a hyperfine transition in the groundstate of atomic hydrogen. The precise frequency of the emission is 1420.405752 MHz and the natural halfwidth of the line is 5_{10}-16 Hz. The excitation of the atom is by collision and hence the brightness temperature of an *optically thick* cloud is the actual kinetic temperature of the gas. Thus the brightness at 21 cm gives information on density and kinetic temperature, the frequency gives the mean velocity of the emission region, and the Doppler broadening of the line gives another measure of the temperature (assuming no turbulence). The 21 cm line is also seen in absorption and it is likely that the absorption measurements provide information on different regions from those seen in emission (Clark, 1965). The advantage of the hydrogen-line technique is that the properties of the line are known in great quantitative detail. In addition hydrogen is the most abundant element in the gas, and the line is detectable over the whole sky.

Information on the distribution of free electrons in the interstellar medium is provided mainly by radio observations except in the relatively few cases where the ionized gas is

visible as an emission nebula. Once again the information is of an indirect nature. In all the methods the electron density is contained in an integral along the line of sight of the observations, and in each case some other parameter of the medium is involved as well.

The Faraday rotation of the plane of polarization of polarized emission travelling through a magneto-ionic medium is described by a rotation measure

$$RM = \int_0^L n_e(r)\, B_{\parallel}(r)\, dr$$

where $n_e(r)$ is the electron density at r,

$B_{\parallel}(r)$ is the component of the magnetic field at r parallel to the line of sight,

and L is the path length in the medium.

The rotation measures of a large number of extragalactic sources have been determined (e.g. Gardner and Whiteoak, 1963) and these undoubtedly provide information on the interstellar free electron density. Unfortunately this information cannot be extracted without ambiguity. The first problem is to determine the amount of Faraday rotation which takes place in the source itself. There is some correlation of rotation measure with galactic latitude but it is not possible

to tell whether the scatter is due to rotation within the sources or complexity of the galactic magnetic field. The total rotation is the cumulative effect of the medium along the line of sight, and the possibility of field reversals makes the interpretation of the rotation measure difficult.

Before the rotation measures can be used to give the free electron density the magnitude of the magnetic field must be obtained by other means. The intensity of the synchrotron emission which dominates the low radio frequency spectrum is a function of the number of radiating electrons and the component of the magnetic field *normal* to the line of sight. An estimate of the cosmic ray electron flux will yield a measure of this component of the field. Unfortunately, as noted earlier, the present uncertainties are large and the best estimate is within a factor of about 5 of 10 μG. Estimates of the field strength are also possible from the polarization of starlight, assuming that this is produced by the field-alignment of the interstellar grains, but the values range from 10^{-5} to 10^{-7} Gauss. There is one method of measuring the field directly — the observation of Zeeman splitting of the 21 cm hydrogen line. The presence of a magnetic field within a neutral hydrogen cloud will cause the radiation from the cloud to be split into two components circularly polarised in opposite senses, and with a frequency

separation of 2.8 Hz per microgauss. Attempts to observe this effect have recently been successful (Verschuur, 1968) and yielded values of 20±3 μG and 9±3 μG for two clouds in the Perseus arm, and 0.55±0.87 μG for a feature in the Orion arm. Thus the problem of choosing a suitable mean field remains, and at best these measurements can be used with the Faraday rotation observations to set rather wide limits on the electron densities.

The absorption of low frequency radio emissions discussed in the last chapter gave values for the integral

$$\int_0^L \frac{n_e^2(r)}{T_e^{3/2}(r)}\, dr \ .$$

Here again the electron density n_e is combined with another parameter, in this case the kinetic temperature T_e of the electron gas. A number of other measurements contribute information on the temperature of the interstellar gas, notably H-line measurements, and the problems of interpretation are not as extensive as in the case of magnetic field measurements; in particular there is no effect corresponding to that of field reversal. However there mat be problems in relating the *mean squared* electron density to the *mean* density, and in all cases the results are dominated by regions

where the temperature is low.

Finally, the most recent tool for investigating the interstellar gas is the pulsating radio source (or pulsar). The frequency-time structure of pulses from these sources is characteristic of an impulse dispersed by propagation through an ionized medium, and this medium is almost certainly interstellar. The dispersion of pulsar radiation gives a measure of

$$\int_0^L n_e(r)\, dr$$

along the line of sight of length L to the source. The unknown in this expression is the source distance. However pulsars are clearly galactic objects, probably associated with supernova remnants, and we can expect independent distance measurements to be available for a number of sources. Already there are distance measures available for the pulsars in the Crab and Vela-Puppis supernova remnants, and direct measures of the average electron densities are therefore available for these directions. A number of pulsars radiate highly polarized radiation and rotation measures yield values of the mean field strength along the line of sight, while the results of absorption line measurements in the pulsar radiation (e.g. the neutral hydrogen line) currently in progress will

give further information on both the interstellar gas and the pulsar distances. Evidently the discovery of the pulsar has provided the most important tool currently available for the study of the interstellar medium.

THE DISTRIBUTION OF THE INTERSTELLAR MATTER

The basic information on the interstellar gas density has been obtained from the hydrogen line observations. Assuming a uniform gas temperature of about 125 degK the mean density indicated is about 0.8 hydrogen atoms / cm^3 near the galactic plane (Westerhout, 1958), corresponding to about 0.025 $M_\odot/pc^3$. However the recent H-line measurements discussed below contradict this uniform temperature assumption and these figures are likely to undergo substantial revision in the next year or so.

The widths and separations of the interstellar absorption lines suggested that the interstellar medium consists of discrete "clouds" occupying about eight percent of the total volume, with densities several orders of magnitude higher than the surrounding medium. This discrete cloud model is widely accepted as the simplest model that will fit the observations. Spitzer (1968a) gives the parameters of a "standard cloud" based on the properties of the interstellar

TABLE I

PARAMETERS OF A "STANDARD CLOUD"

after Spitzer (1968a)

Radius	7	*pc*
No. of clouds per $(Kpc)^3$	$5_{10}4$	
No. in line of sight per Kpc	8	
Fraction of volume occupied	0.07	
Visual extinction in single cloud	0.2	*mag*
Density of hydrogen	10	cm^{-3}
Density of heavy ions	$5_{10}-3$	cm^{-3}
Mass	400	$M_\odot$

absorption lines deduced by Spitzer (1948) and Strömgren (1948), and these are reproduced in Table I. The variability of cloud size and density is large and the categories listed in Table II (Spitzer, 1968b) were first noted by Bok (1948). In particular the existence of the "large clouds" of Table II are required by the statistics of interstellar colour excesses (Schatzman, 1950; Munch, 1952) and the analysis of 21 cm absorption (Clark *et al*, 1962; Clark, 1965). Clark finds that there are about 1.7 large clouds per kiloparsec along a line of sight within the galactic disk.

Spitzer (1968b) gives a brief summary of the observations suggesting that cloud sizes range from less than a parsec to more than fifty parsecs in radius, with number densities from 5 cm^{-3} to 1000 cm^{-3}. He remarks " .... it is clear that for increasingly detailed comparison with observations any [cloud] model must be made more and more complicated".

Gravitational considerations would lead one to expect a decrease in density of the gas with increasing distance from the galactic plane. 21 cm observations in the direction of the north galactic pole by Dieter (1965) tend to confirm this; individual clouds were observed at a probable distance of 100 parsecs with an average diameter of 10 pc and

TABLE II

CATEGORIES OF INTERSTELLAR CLOUDS

after Spitzer (1968b)

Type	*Mass* $M_\odot$	*Radius* pc	*Density* H/cm^3
Small globule	>0.1	0.03	$>4_{10}4$
Large globule	3	0.25	$1.6_{10}3$
Intermediate cloud	$8_{10}2$	4	100
Large cloud	$1.8_{10}4$	20	20

an average density of 2 atoms/cm^3. Gould (1968) assumes a model for the smeared-out gas density in the solar neighbourhood of the form

$$\langle n_H(z) \rangle \simeq 0.7\, e^{-z^2/h_g^2} \quad cm^{-3} \quad \text{for } z < 110 \text{ pc}$$

$$\simeq 1.35\, e^{-z/h_e} \quad cm^{-3} \quad \text{for } z \geq 110 \text{ pc},$$

where z is the distance from the galactic plane, and the constants h_g and h_e have the values 130 pc and 80 pc respectively.

The grains responsible for the optical polarization and extinction have a total density of about 1.4_{10}-26 gm cm^{-3}, that is about one percent of the hydrogen density. This figure is based on the "dirty ice" grain model of van de Hulst (1949). A similar density is obtained for the model of Hoyle and Wickramasinghe (1962) consisting of a graphite core and an ice mantle, while the so-called "Platt particles" (Platt, 1956) would give a density nearer 10^{-28} gm cm^{-3}. It is unfortunate that the data on the interstellar grains are such that almost any theoretical curve can be fitted to them. Apart from the dynamical considerations which depend on the mass of the grains, some indication of their size and chemical composition would assist the discussion of the heating and cooling of the interstellar gas, the free electron content due

to photoionization, and the formation of molecules for which process the grains may act as a catalyst.

A possible major constituent of the interstellar gas is molecular hydrogen. Unfortunately at present this is completely unobservable, being inactive in both the radio region and the optical wavelength range admitted by the atmosphere. The motions and spatial distribution of stars away from the galactic plane imply an overall density of about 0.15 $M_\odot/pc^3$ within the galactic disk (Oort, 1960) but the smeared-out density of known stars is only about 0.075 $M_\odot/pc^3$, which suggests an interstellar gas density of the same magnitude — that is about 3 H atoms cm^{-3}. The possibility of a relatively large density of invisible molecular hydrogen cannot therefore be dismissed. Gould, Gold and Salpeter (1963) have examined the problem of determining the density from existing data, and they conclude that the ratio of molecular to atomic hydrogen lies in the range 0.1 to 10. The experimental prospects of settling this uncertainty are bright, as molecular hydrogen exhibits absorption bands in both the infra-red and the ultra-violet, and satisfactory observations from above the atmosphere will undoubtedly prove decisive.

Finally, in addition to the gas clouds a medium of lower density must exist between the clouds. The evidence for the presence of this medium is the clear separation of the

components of an interstellar absorption line, indicating the discrete and independent nature of the clouds. A typical cloud is not sufficiently massive to be stable under self-gravitation and should disperse in about 10^7 years, and Spitzer (1954) has proposed that the clouds and the intercloud medium are in hydrostatic equilibrium with the kinetic temperature of the tenuous medium sufficiently high for a pressure balance to obtain. This model has gained general acceptance over an alternative explanation by Kahn (1955b) in which the clouds are being continually reformed by collision with one another; an average cloud experiences a collision every 10^7 years in this model, and the "pressure" of the collisions provides the necessary stabilizing factor.

The above evidence for the existence of the intercloud medium is indirect. Until recently the only direct observations of the medium were believed to be those of Dunham (1941), discussed by Strömgren (1948), of very weak absorption lines in the spectra of α *Virginis* and η *Ursae Majoris*. These lines are so faint that apparently the lines of sight do not pass through a cloud at all. Strömgren's analysis yielded a probable density of 0.1 H atoms cm^{-3}. However the H-line absorption work of Clark and Radhakrishnan discussed below suggest that much of the 21 cm emission originates in the

intercloud medium while the absorption is produced by the cool clouds. Nevertheless the remarks of Field and Saslaw (1965) are appropriate: " .... the supposed hydrostatic equilibrium of individual clouds is open to grave doubt, as no one has explained satisfactorily why there should be a low-density high-temperature region uniformly pervading the intercloud regions and preventing the clouds from expanding."

THE TEMPERATURE OF THE INTERSTELLAR GAS

The observations of the interstellar gas show that it is predominantly hydrogen, and that this hydrogen exists in an ionized form in the vicinity of some hot stars and in neutral clouds elsewhere. There is a hot low-density intercloud medium, and the presence of hydrogen in molecular form is possible in (currently) indeterminate quantities. The degree of ionization of the clouds and the intercloud medium is not directly observable. All that one can do is to note that the observations of Faraday rotation, synchrotron emission, the dispersion of pulsar signals, and the absorption of low frequency radio waves all require the presence of free electrons in regions other than the visible emission nebulae. In the absence of any direct measure of the ionization levels it is appropriate to examine the temperatures that are

observed or deduced, and the means by which ionization can take place.

It is important to note that the temperature measurements are only directly related to the degree of ionization in the HII regions. In other cases the temperatures discussed are either the neutral hydrogen *spin* temperature or the gas *kinetic* temperature. Provided that a Maxwellian velocity distribution obtains in the gas the spin temperature will equal the kinetic temperature, and although the evidence seems to indicate that this is the case the possibility of non-Maxwellian distributions should not be ignored (Spitzer, 1968a). The kinetic temperature is defined in terms of the mean speed of the gas particles, and it should not be confused with a thermodynamic temperature describing fully the state of the gas. Whereas the evaluation of the Saha ionization equation for hydrogen gas at interstellar densities implies full ionization for thermodynamic temperatures above about 6000 degK (Strömgren, 1939) it is quite reasonable for the gas to remain neutral at kinetic temperatures of 10,000 degK.

HII regions:

The extent of the ionization in the vicinity of stars was first examined by Strömgren (1939) who showed that a star

embedded in a region of neutral gas with uniform density will form an ionized sphere about itself. This *Stromgren sphere* will be characterized by a sharp transition between the ionized gas and the neutral medium, and the radius will be a function of the gas density and the luminosity of the star. For example in a medium of density 1 H atom cm^{-3} the radius of the HII region about an O7 star would be about 90 pc and the transition from 90% to 10% ionization would occur in a shell about 2 pc thick. Values of the Stromgren radii for different stellar types are reproduced in Table III from the original paper (Strömgren, 1939). These calculations have been revised slightly by Pottasch (1960) and the general predictions of the theory are now consistent with observations of ionized hydrogen in the vicinity of O and B stars.

It should be noted from the Table that only the O and B stars have Stromgren spheres with significant radii. Stars of the same spectral class as the sun, for example, have radii of about 10^{-4} pc. The low occurrence of O and B stars rules out the possibility that the free electrons required by the low frequency absorption measurements for galactic latitudes greater than a few degrees exist in these HII regions. O and B stars are found mainly close to the galactic plane, and a search of southern sky catalogues suggests that

TABLE III

RADII OF STROMGREN SPHERES

IN A MEDIUM WITH n_H = 1 H cm^{-3}

after Strömgren (1939)

Spectral Type	*Temperature*	M_{vis}	*Radius of ionized sphere (pc)*
O5	79000	-4.2	140
O6	63000	-4.1	110
O7	50000	-4.0	87
O8	40000	-3.9	66
O9	32000	-3.6	46
B0	25000	-3.1	26
B1	23000	-2.5	17
B2	20000	-1.8	11
B3	18600	-1.2	7.2
B4	17000	-1.0	5.2
B5	15500	-0.8	3.7
A0	10700	+0.9	0.5

virtually all lines of sight for $b < -40^{\circ}$ are free of HII regions.

The temperature of an HII region is determined in a number of ways. The intensity ratios of emission lines provide values for the temperature on the assumption of thermodynamic equilibrium, since the relative populations of two energy levels E_1 and E_2 are given by

$$\frac{n_2}{n_1} = \frac{g_2}{g_1} e^{-(E_2-E_1)/kT}$$

where n_1 and n_2 are the populations of the two states and g_1 and g_2 are the statistical weights. The comparison of emission lines of different elements also requires some assumption about the relative abundances. The temperatures obtained are in the range 6000 degK to 10,000 degK (Burbidge, Gould and Pottasch, 1963).

Radio measurements of hydrogen recombination lines, "α-transitions" between levels whose quantum numbers differ by 1, also give values for the temperature. The interpretation of these measurements is complicated, but the temperatures given by Mezger and Hoglund (1967) of 4000 degK to 10,000 degK with a mean of 5800 degK are in agreement with the optical work.

Information on the temperature of HII regions is also contained in the observations of the continuum emission at high

radio frequencies, such as at 1390 MHz (Westerhout, 1958; Hill, 1968), but the difficulty in separating the thermal emission from the non-thermal (synchrotron) emission makes this method less reliable than those described above.

The absorption of low-frequency radio waves can, in principle, be used to obtain values for the temperatures. This involves the comparison of surveys at high and low frequencies, and it is usually necessary to make some assumptions about the dimensions and disposition of the absorber. C. Field (1967) has compared the survey by Williams *et al* (1966) at 38 MHz with surveys at higher frequencies and he obtained a mean value of 6900 degK for a number of HII regions.

HI regions:

The only measurements of the temperature of the cloud and intercloud media are those obtained from the 21 cm H-line emission and absorption. The theory of these processes together with the observations to 1967 are reviewed by Kerr (1968). The spin temperature of the neutral hydrogen is related to the brightness temperature of the emission measurements and the optical depth of the absorption measurements. As discussed above, this temperature is probably the kinetic temperature of the gas. The kinetic temperature can also be

obtained from the widths of the line seen in emission or absorption provided that the thermal motions can be separated from the large scale movements and turbulence of the gas.

Emission measurements led to the value of 125 degK being widely accepted as the gas temperature, assumed uniform throughout the galaxy. This value comes from Schmidt (1957) who assumed that the maximum brightness temperature in the galactic plane was in directions of high optical depth, and could therefore be taken as the spin temperature. It has been pointed out by Kahn (1955a) that this temperature is effectively the harmonic mean $[\langle 1/T \rangle]^{-1}$ where the average is taken over the line of sight, and that the interpretation of this temperature in the absence of uniformity is difficult. In view of the more recent results discussed below the remarks of Kerr (1968) are noteworthy: " .... *all results to date* on the distribution of hydrogen in the Galaxy depend on the uniform temperature assumption because there is no easy way to handle a varying temperature when there are so many other uncertainties in the problem" (the italics have been added). Brightness temperatures as low as 60 degK have been observed in small regions (Radhakrishnan, 1960) and interpreted as due to self absorption in a cool cloud, so the problem of a varying temperature distribution must be faced.

The early absorption measurements (Hagen and McClain, 1954; Hagen, Lilley and McClain, 1955) yielded narrow well-defined profiles evidently produced by clouds with temperatures well below 100 degK. The apparent conflict with the emission measurements was explained in terms of different spatial resolution; the emission spectrum was supposed to be the sum total of many clouds while the absorption effects were due to the relatively few clouds in front of the source. This explanation has become steadily less tenable as the quantity and quality of the absorption data have improved (Clark *et al*, 1962; Schuter and Verschuur, 1964; Clark, 1965). The greatest difficulty is found in interpreting the so-called "zero-velocity line" in the direction of the galactic centre. Clark (1965) points out that the path length to the centre is so great that both the absorption and emission lines should consist of many superposed profiles. However the width of the absorption feature ($\sim$90 KHz) is only about one third of the emission feature. He proposes an alternative model in which the absorption occurs in cool dense clouds ($T \simeq 60$ degK, $n_H \simeq 10\ cm^{-3}$) embedded in a hot medium ($T \gtrsim 1000$ degK) of lower density such that a pressure balance obtains. The temperature of the hot medium is such that it would not be visible in absorption measurements. His observations indicate that the

layer of cool clouds is very flat; for sources with $|b| < 19^{\circ}$ all but one showed absorption with optical depth $\tau \gtrsim 0.5$, while no sources at $|b| > 20^{\circ}$ showed any absorption.

Further observations to test this "raisin pudding" model have been undertaken by Radhakrishnan and a preliminary report is available (Radhakrishnan and Murray, 1969). He has made observations in the directions of 35 extragalactic sources at intermediate or high galactic latitudes, so that in all cases relatively local gas was observed. Comparison of profiles with the telescope on source and a beamwidth off source show the same hydrogen in absorption and emission. In no case was the absorption profile an exact scaled image of the emission profile, as it should be if a uniform temperature of 125 degK was appropriate, and in every case there was some hydrogen seen in emission which was not seen in absorption. The observations confirm that the interstellar hydrogen is indeed in the form of a "raisin pudding" with the parameters of the intercloud medium being $n_H \simeq 0.5$ atoms cm^{-3}, $T \gtrsim 1000$ degK. The product $n_H T$ is then $\gtrsim 500$, which is adequate to provide total pressure balance with cool clouds, whose parameters are $n_H \simeq 10$ atoms cm^{-3}, $T \simeq 50$ degK, as proposed by Clark.

The observation that a substantial fraction of the interstellar gas is at a temperature in excess of 1000 degK

raises the question of how this temperature is maintained. The dilution of starlight is so great that it would only sustain a temperature of less than a degree, and its effects would therefore be insignificant in comparison with the 3 degK black-body radiation field. For some time the only acceptable mechanism for sustaining this high temperature was the dissipation of energy from cloud-cloud collisions. However recently the heating effects of cosmic ray particles have been considered, and it seems that sufficient energy may be available from these particles to give the observed temperatures. Spitzer and Tomasko (1968) review the recent work and provide a comprehensive discussion of the factors involved.

A crucial factor is the ionization rate ζ for hydrogen atoms in the medium. Spitzer and Tomasko take

$$6.8_{10}{}^{-18} \lesssim \zeta \lesssim 1.2_{10}{}^{-15} \qquad (\zeta \text{ in } \sec^{-1})$$

in the solar neighbourhood. The upper limit is obtained by including an estimate of the particle contribution in the 2 MeV region by Type I supernovae, assuming one such supernova in the galaxy every 100 years. The ionization rate is important because the collision cross sections for free electrons are much greater than for neutral atoms, and hence the heating effect of cosmic rays is a strong function of the electron density. Spitzer and Tomasko consider the possibility of deviations from

equipartition between the electrons and the neutral atoms but conclude that they are negligible. Their conclusions on temperature and ionization level are summarised in Table IV, which gives the relative ionization and temperature as a function of neutral hydrogen density for the extreme values of ionization rate ζ. It is clear that the upper limit of ζ leads to good agreement with observations for the cool dense clouds but gives rather low values for the more tenuous medium. They remark that " .... the temperature to be expected in an intercloud medium with a density of 0.1 H atoms cm^{-3} or less should be studied further, since the present theory begins to break down for this condition."

The calculations of Spitzer and Tomasko have been extended by Field *et al* (1969) to include the interaction of secondary electrons with atoms, ions and thermal electrons. They take a value of ζ of 7.5_{10}-16 sec^{-1}, somewhat less than the upper limit of Spitzer and Tomasko. Figure I shows their calculated temperatures as a function of the density of nuclei. According to Field (1965) the gas phase at T ≈ 5000 degK is thermally unstable with a lifetime of about 10^6 years. The stable phase at 10,000 degK is therefore identified with the intercloud medium; it would have a density of about 0.11 cm^{-3} of which 15% is ionized, giving an electron density of 0.016 cm^{-3}.

TABLE IV

TEMPERATURE AND RELATIVE IONIZATION

IN THE INTERSTELLAR MEDIUM

according to the model of Spitzer and Tomasko (1968)

	Ionization Rate $\zeta = 6.8_{10}-18\ sec^{-1}$		Ionization Rate $\zeta = 1.17_{10}-15\ sec^{-1}$	
n_H cm^{-3}	n_e/n_H $\times 10^3$	T *degK*	n_e/n_H $\times 10^3$	T *degK*
0.01	7.5	38	270	860
0.03	4.2	30	100	250
0.1	2.2	24	42	120
0.3	1.4	20	21	70
1.0	0.8	17	10	45
3.0	0.6	14	5.5	33
10.0	0.5	12	3	27

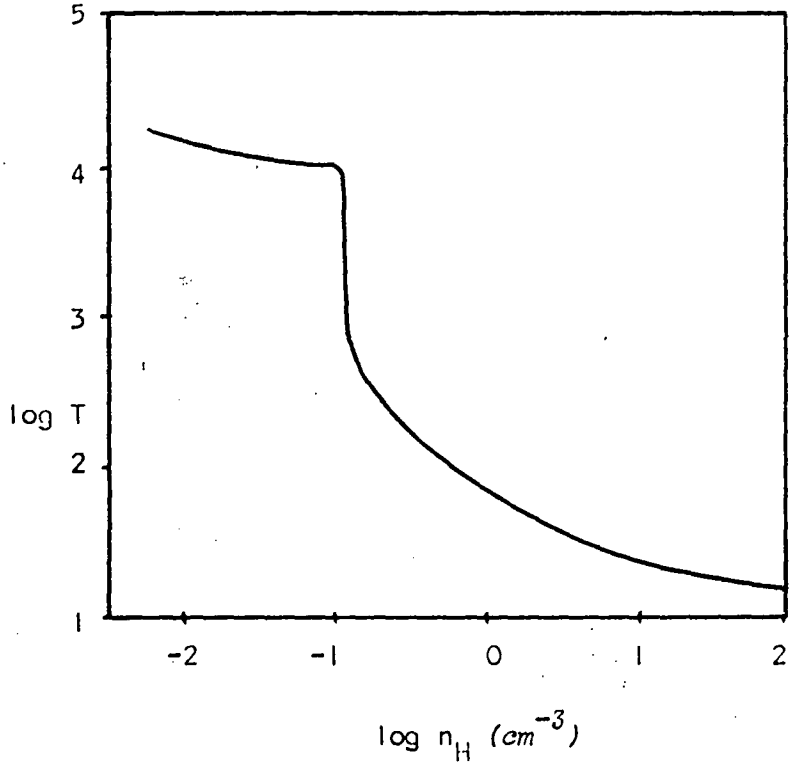

FIGURE 1

Heating of the interstellar gas by cosmic ray particles, as a function of density.

after Field et al (1969)

The clouds would have densities of 10 cm^{-3} and temperatures of about 100 degK, and an electron density of $\sim 3_{10}{}^{-3}$ which is similar to that derived by Spitzer and Tomasko. The observed brightness at 21 cm for this model would be 115 degK, close to the "classical" value of 125 degK.

INTERSTELLAR ELECTRONS

We now turn to the observations of interstellar free electrons. The presence of these electrons is revealed by thermal radio emission, synchrotron emission, Faraday rotation, pulsar dispersion and low frequency absorption. The first two types of observation do not easily yield number densities because of the complex assumptions that must be made about the other parameters of the emission. We will therefore confine this discussion to the remaining processes.

Faraday rotation:

The galactic latitude dependence of the Faraday rotation measures for extragalactic sources has been discussed by Berge and Seielstad (1967), and the summary of their results is reproduced in figure 2. They propose a model consisting of an infinite disk with a constant density of electrons and a magnetic field of constant strength parallel

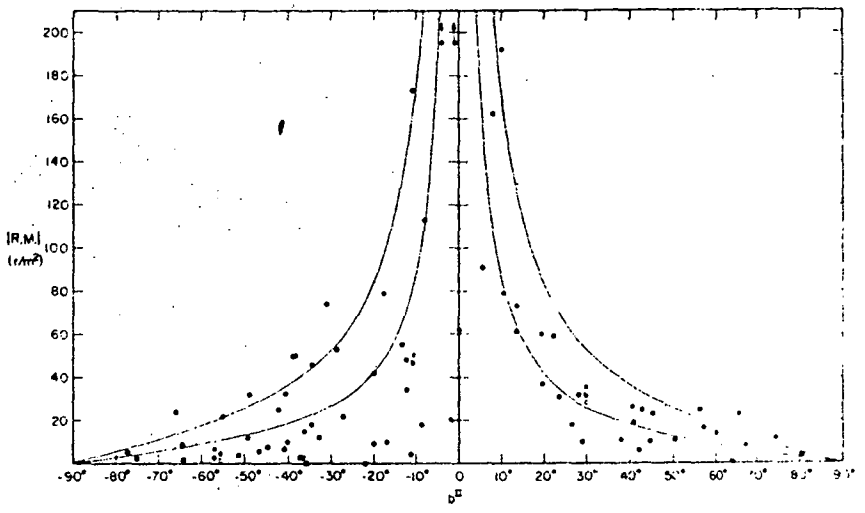

The latitude dependence of the rotation measure absolute magnitudes. The upper curve is $|R.M.| = 30\ |\cot b^{II}|$, and the lower curve is $|R.M.| = 15\ |\cot b^{II}|$.

FIGURE 2

after Berge and Seielstad (1967)

to the plane. The rotation measure for such a model is proportional to $\cot b$ and curves for $30|\cot b|$ and $15|\cot b|$ are given in the figure. The results are more or less consistent with such a model, which leads to a value of

$$\int n_e B_{\parallel} \, dr \simeq 20 \quad cm^{-3} \; \mu G \; pc$$

for the direction of the galactic pole.

Pulsars:

The current state of pulsar astronomy has been comprehensively reviewed by Radhakrishnan (1969). The variation of dispersion measure, that is $\int n_e dr$ in cm^{-3} pc, from his paper is plotted in figure 3. Mills (1969) has proposed a model for the dispersing electrons which are taken to have a density of 0.1 cm^{-3} and to be in a layer of total thickness 200 pc. This predicts that

$$\int n_e \, dr \simeq 10 \, |\mathrm{cosec}\, b|$$

which is illustrated in figure 3. The suitability of this expression is clear; however the scale of the model has been questioned by Radhakrishnan (1969) who considers that " .... the intercloud medium may have a half thickness in excess of 100 pc, and Mills' estimate of 0.1 el cm^{-3} should be considered an upper limit".

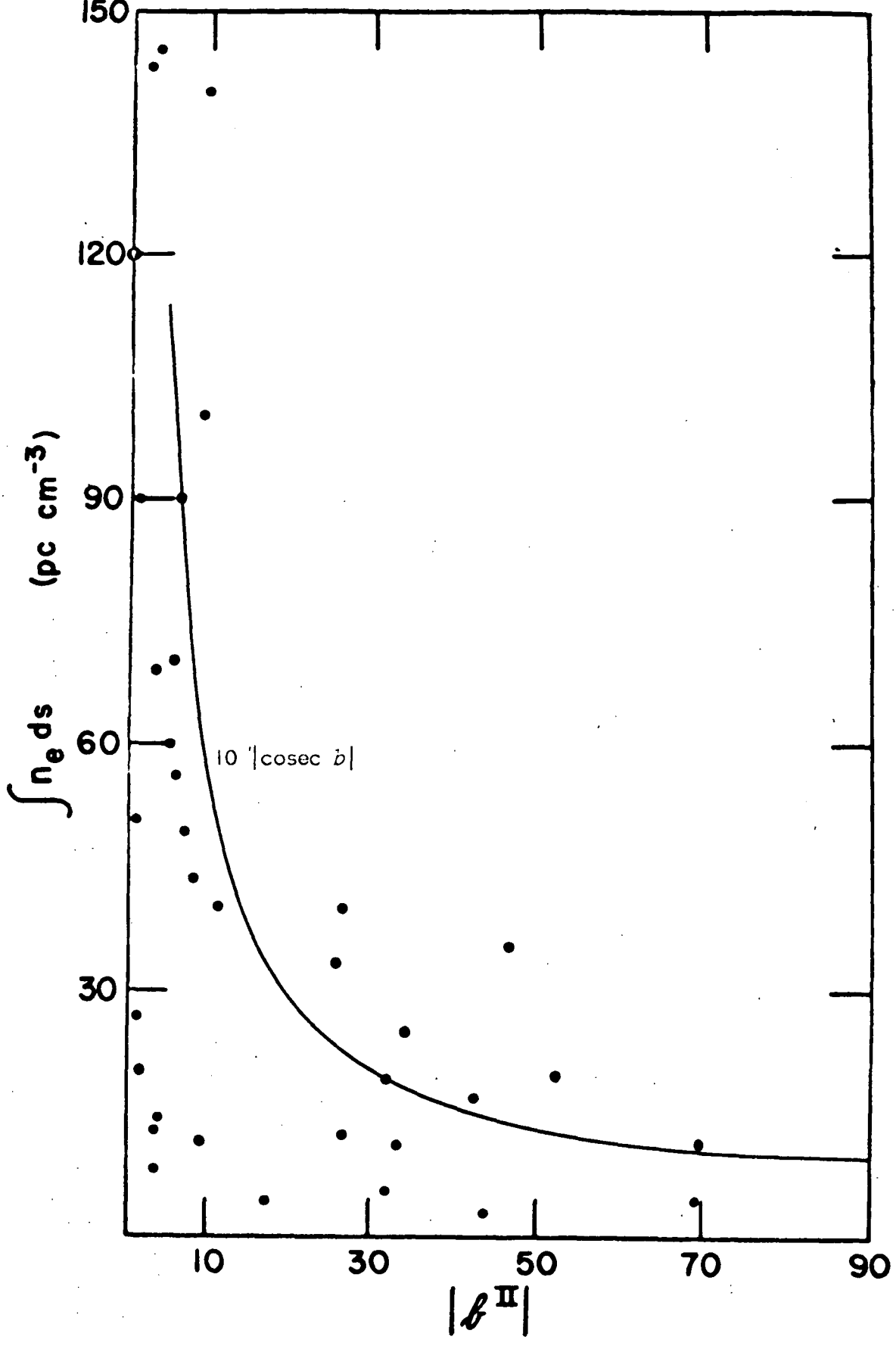

FIGURE 3 Variation of pulsar dispersion with b

Those pulsars emitting highly polarised radiation also provide a measure of the mean line of sight field strength, since the two integrals $\int n_e dr$ and $\int n_e B_{\parallel} dr$ can be measured. To date six pulsars have provided such measurements and the relevant details are given in Table V, after Radhakrishnan (1969).

There are independent distance estimates for two pulsars, namely 2000 pc for NP0532 in the Crab nebula (Trimble, 1968) and 500 pc for PSR0833-45 in Vela (Milne, 1968). These are based on the observed expansion rate of the Crab nebula, and the radio surface brightness of the Vela remnant. The dispersion measures then give $n_e \simeq 0.03$ cm^{-3} for NP0532 and $n_e \simeq 0.14$ cm^{-3} for PSR0833-45. The measurement of H-line absorption in the emission of CP0328 by Gordon *et al* (1969) has yielded a distance measure of $\gtrsim$ 1000 pc, which gives $n_e \lesssim 0.03$ cm^{-3}, in agreement with the Crab pulsar.

Low frequency absorption:

We recall the analyses of the preceding chapters, which indicated a good fit for the law

$$\int \frac{n_e^2}{T_e^{3/2}} dr \propto |\mathrm{cosec}\ b|$$

with the value of the integral at $b = 90^{\circ}$ being 9_{10}-6 $cm^{-6} pc\ deg K^{-3/2}$.

TABLE V

PULSAR MEASUREMENTS OF MAGNETIC FIELDS

after Radhakrishnan (1969)

source	l	b	$\int n_e dr$ $cm^{-3} pc$	field μG
CP0328	145.0	-1.2	26.75	3.5, 2.8
NP0527	183.8	-6.9	49.3	0.9
NP0532	184.5	-5.8	56.88	0.55
PSR0833-45	263.5	-2.8	69	0.8
CP0950	228.9	+43.7	2.98	<0.2
AP2015+28	68.1	-4.0	14.2	2.0

Conclusions:

We note first of all that the Faraday rotation for extragalactic sources and the pulsar dispersion results together imply a mean magnetic field strength of about 2 μG, a figure which is bracketed by the results in Table V for individual pulsars, and which is also acceptable on theoretical grounds (Field *et al*, 1969). The spread of values would seem to agree with the Faraday rotation results (figure 2).

It remains to reconcile the measurements

$$\int n_e dr \simeq 10 \quad cm^{-3} pc \quad \text{[pulsar dispersion]} \qquad (1)$$

and

$$\int \frac{n_e^2}{T_e^{3/2}} dr \simeq 9_{10}{}^{-6} \quad cm^{-6} pc \; degK^{-3/2} \quad \text{[absorption]} \qquad (2).$$

Unfortunately the presence of the temperature factor in (2) provides us with sufficient degrees of freedom for a wide variety of solutions, and no definite statement can be made at this stage on the interstellar electron content. It is possible to take a model such as that of Field *et al* (1969) in which the low frequency absorption is due mainly to weak ionization of the cool clouds while the pulsar dispersion is

the result of a higher degree of ionization in the hot intercloud medium. The path length in cool clouds for b = 90 is likely to be about 4 pc, and an assumed temperature of 50 degK leads to $n_e \simeq 0.028$ cm^{-3} from (2). The relative ionization, $n_e/n_H = 2.8_{10}{}^{-3}$, is within the range of values that could result from cosmic ray heating (Field *et al*, 1969; Spitzer and Tomasko, 1968) although it is close to the upper limit in Table IV. The treatment by Field *et al* predicts an intercloud temperature of 10,000 degK, so that a path length of 200 pc through this medium with $n_e \simeq 0.05$ cm^{-3} would produce little additional absorption, and would give the value required by (1). This 20% ionization of the intercloud gas would also be produced by cosmic rays. The mean line of sight electron density would not greatly exceed that of 0.03 cm^{-3} observed for CP0328 and NP0532. The high value of 0.14 cm^{-3} for PSR0833-45 has already been explained as due to HII regions of the Gum nebula (Manchester *et al*, 1969).

However there are two objections to this model. If the low frequency absorption is essentially confined to clouds the distribution of absorption across the sky would be expected to show greater variation from one line of sight to another than is observed. This would be most obvious in the polar direction where there are on the average about two clouds in a

line of sight. We would also expect to find substantial areas of the sky for which there is little or no absorption, corresponding to the directions in which there are no cool clouds (Radhakrishnan and Murray, 1969). Although the clouds would not necessarily be visible as discrete absorbers with the resolutions used in the low frequency surveys, the absence of appreciable absorption in large areas would still be apparent from the line of sight spectra, which would exhibit the characteristics of the emission spectrum at low frequencies where the clouds are opaque. These arguments led Ellis and Hamilton (1966) to propose that the intercloud medium was responsible for the absorption. Their suggestion that the intercloud gas is fully ionized is no longer acceptable in the light of the recent 21 cm work (Radhakrishnan and Murray, 1969) which suggests the parameters $n_H = 0.5$ cm^{-3} T = 1000 degK for this region, but this data itself provides the second objection to the model of Field *et al* who propose the parameters $n_H = 0.1$ cm^{-3} and T = 10,000 degK.

However the inclusion of a relative ionization of up to 10% in the model of Radhakrishnan and Murray would not affect their results. Taking $n_e = 0.03$ cm^{-3} from the pulsar results, and T = 1000 degK from the HI emission we can obtain (2) if the half width of the intercloud disk is 300 pc. This

number is also more acceptable in the light of recent H-line work (Radhakrishnan: private communication). The required disk thickness is a strong function of the assumed density and temperature; if we increase n_e to 0.04 cm^{-3}, an increase of relative ionization from 6% to 8%, the path length in the medium comes down to 180 pc. We notice also that although this model requires that the absorption in cool clouds be negligible, it is only necessary to reduce the cloud electron density by a factor of about three to satisfy this condition. The corresponding relative ionization of $\sim 10^{-3}$ agrees well with the cosmic ray heating calculations of Spitzer and Tomasko (1968).

We conclude that there are free electrons throughout the interstellar medium with densities in the range 0.01 — 0.04 cm^{-3}, and that the intercloud medium is responsible for the observed effects of Faraday rotation, pulsar dispersion and low frequency absorption, at least for high galactic latitudes. As the line of sight moves down into the galactic plane the relative contribution of the cool clouds would increase, as would that of HII regions. Further low frequency observations at higher resolutions than have hitherto been used will assist the development of this model.

REFERENCES FOR CHAPTER 8

Berge,G.L. and Seielstad,G.A. 1967 *Astrophys. J. 148* 367.

Bok,B.J. 1948 *Centennial Symposia Harvard Obs. Monograph No.7* p. 53

Burbidge,G.R., Gould,R.J. and Pottasch,S.R. 1963 *Astrophys. J. 138* 945.

Clark,B.G. 1965 *Astrophys. J. 142* 1398.

Clark,B.G., Radhakrishnan,V. and Wilson,R.W. 1962 *Astrophys. J. 135* 151.

Dieter,N.H. 1965 *Astron. J. 70* 552.

Dunham,T. 1941 *Publ. Amer. Astr. Soc. 10* 50.

Ellis,G.R.A. and Hamilton,P.A. 1966 *Astrophys. J. 146* 78.

Field,C. 1967 *Mon. Not. Roy. Astr. Soc. 137* 419.

Field,G.B. 1965 *Astrophys. J. 142* 531.

Field,G.B., Goldsmith,D.W. and Habing,H.J. 1969 *Preprint: University of California.*

Field,G.B. and Saslaw,W.C. 1965 *Astrophys. J. 142* 568.

Gardner,F.F. and Whiteoak,J.B. 1966 *Ann. Reviews Astron. Astrophys. 4* 245.

Gordon,C.P., Gordon,K.J. and Shalloway,A.M. 1969 *Nature* *222* 129.

Gould,R.J. 1969 *Aust. J. Phys.* *22* 189.

Gould,R.J., Gold,T. and Salpeter,E.E. 1963 *Astrophys. J.* *138* 408.

Hagen,J.P. and McClain,E.F. 1954 *Astrophys. J.* *120* 368.

Hagen,J.P., Lilley,A.E. and McClain,E.F. 1955 *Astrophys. J.* *122* 365.

Hill,E.R. 1968 *Aust. J. Phys.* *21* 735.

Hoyle,F. and Wickramasinghe,N.C. 1962 *Mon. Not. Roy. Astr. Soc.* *124* 486.

Kahn,F.D. 1955a in *Gas Dynamics of Cosmic Clouds* (New York: Interscience) p. 60.

Kahn,F.D. 1955b *ibid.* p. 115.

Kerr,F.J. 1968 in *Nebulae and Interstellar Matter* ed. B.M. Middlehurst and L.H. Aller (Chicago: Chicago Univ. Press) p. 575.

Manchester,R.N., Murray,J.D. and Radhakrishnan,V. 1969 (in preparation: private communication)

Mezger,P.G. and Höglund,B. 1967 *Astrophys. J.* *147* 490.

Mills,B.Y. 1969 *Proc. Astr. Soc. Aust.* *1* 176.

Milne,D.K. 1968 *Aust. J. Phys.* *21* 201.

Munch,G. 1952 *Astrophys. J. 116* 575.

Oort,J.H. 1960 *Bull. Astr. Inst. Neth. 15* 45.

Platt,J.R. 1956 *Astrophys. J. 123* 486.

Pottasch,S.R. 1960 *Astrophys. J. 132* 269.

Radhakrishnan,V. 1960 *Publ. Astr. Soc. Pacif. 72* 296.

Radhakrishnan,V. 1969 *Preprint: C.S.I.R.O. Radiophysics Division* [*to appear in Proc. Astr. Soc. Aust. 1 (6) Sept. 1969*].

Radhakrishnan,V. and Murray,J.D. 1969 *Proc. Astr. Soc. Aust. 1* 215.

Schatzman,E. 1950 *Ann. d'Astrophys. 13* 367.

Schmidt,M. 1957 *Bull. Astr. Inst. Neth. 13* 247.

Schuter,W.L.H. and Verschuur,G.L. 1964 *Mon. Not. Roy. Astr. Soc. 127* 387.

Spitzer,L. 1948 *Astrophys. J. 108* 276.

Spitzer,L. 1954 *Astrophys. J. 140* 1.

Spitzer,L. 1968a *Diffuse Matter in Space* (New York: Interscience).

Spitzer,L. 1968b in *Nebulae and Interstellar Matter* ed. B.M. Middlehurst and L.H. Aller (Chicago: Chicago Univ. Press) p. 1.

Spitzer,L. and Tomasko,M.G. 1968 *Astrophys. J.* *152* 971.

Strömgren,B. 1939 *Astrophys. J.* *89* 526.

Strömgren,B. 1948 *Astrophys. J.* *108* 242.

Trimble,V. 1968 *Astrophys. J.* *73* 535.

Van de Hulst,H.C. 1949 *Rech. Astron. Obs. Utrecht* *11* part 2.

Westerhout,G. 1958 *Bull. Astr. Inst. Neth.* *14* 215.

Williams,P.J.S., Kenderdine,S. and Baldwin,J.E. 1966 *Mem. Roy. Astr. Soc.* *70* 53.

APPENDIX

COMPUTING TECHNIQUES

The theoretical work discussed in this thesis has involved a considerable amount of computing. Much of this has been of a routine nature and requires no further comment. The first algorithm below belongs in this category, but is included here because of its usefulness and the lack of any published method for evaluating this function. The other algorithms are the outcome of an extensive survey of model fitting via the minimization of some objective function. Although the basic methods are not original the implementations given here have proved very efficient (M.R. Osborne: private communication), and have been accepted for publication on this basis.

The algorithms are given in the form of ALGOL procedures, in *Publication ALGOL*.

```
real procedure XINTK53(x); value x; real x;
comment calculates the function given by Westfold:
```

$$x \int_{x}^{\infty} K_{5/3}(t)\, dt \quad ;$$

```
begin real x2;
      if x≤0.401 then
      begin x2:=x×0.5;  x:=x2↑0.33333333;
            XINTK53:=2.70824×x×(1-13395×x×x+0.75×x2×x2
                  -0.6677×(x2↑3.333333))
      end
      else if x≤1.0 then
            XINTK53:=-1.67372+x×(23.2118+x×(-83.5855
                  +x×(155.68+x×(-160.48+x×(86.515-19.012×x)))))
      else if x≤3.0 then
            XINTK53:=0.738413+x×(0.89747+x×(-1.8946+x×(1.2711
                  +x×(-0.42329+x×(0.06996-0.0045×x)))))
      else if x≤5.0 then
            XINTK53:=1.46497+x×(-1.02937+x×(0.2993
                  +x×(-0.04173+x×0.0023)))
      else  begin x2:=sqrt(x)×exp(-x);   x:=1.0/x;
                  XINTK53:=1.25331×x2×(1.0+x×(0.76389
                        -0.97917×x))
            end
end
```

The **procedure** *simplex* is based on the paper by J.A. Nelder and R. Mead in *The Computer Journal* volume 7 page 149 *et seq*. They described the method as the "simplex method" although the term is unfortunate, in view of the connotations of linear programming. The method is actually a direct search for the minimum of the objective function, with the search strategy being of a "highly opportunist" kind, to quote the authors. In view of the heuristic nature of the process and the absence of any strong theoretical basis it is surprising that this method is the most useful general method that does not require the partial derivatives as well as the function values.

The following algorithm has been accepted for publication in the Algorithm Section of *The Computer Journal*, following certification by the Staff of the Computer Centre, Australian National University.

```
procedure simplex(x,n,index,alpha,beta,gamma,scale,eps,F);
value n,alpha,beta,gamma,scale,eps; integer index,n;
real alpha,beta,gamma,scale,eps; real array x,F;
comment This procedure implements the direct search
method of Nelder and Mead for finding the local minimum
of a function of n variables. The value of the function
at the ith point, with coordinates
        ( x[i,1], x[i,2], .... , x[i,n] ),
is obtained by the call
        f:=function(x,i,n)
where function is a global procedure of the form
        real procedure function(x,i,n) value i,n
        integer i,n real array x.
```

The parameters of simplex are described below.

n The number of variables.

x Up to (n+4) points are tested in each cycle of the search. The coordinates are held in the (n+4) rows of array x[1:n+4,1:n]. On entry to the procedure the coordinates of the initial estimate of the position of the minimum should be in row 1:

(x[1,1], x[1,2], ... , x[1,n]).

On exit from the procedure the positions of the corners of the final simplex will be in the first (n+1) rows, with the position of the minimum given by

(x[index,1], x[index,2], ... , x[index,n]).

index On exit index specifies the row of x containing the coordinates of the located minimum, and the value of the function at this point is delivered in F[index].

alpha, beta, gamma

These parameters control the searching strategy, and correspond to the reflection, contraction, and expansion coefficients of the same names in the source paper. The values recommended for general use by Nelder and Mead are

alpha = 1.0 beta = 0.5 gamma = 2.0 .

scale *This sets the size of the initial simplex, which will be a regular hyper-solid with the length of each edge equal to scale. For rapid convergence scale should be set to twice the expected distance from the initial estimate to the minimum. A poor choice of scale will not prevent convergence but may delay it.*

eps *This is the exit criterion. The process terminates when the standard deviation of the function values at the corners of the simplex is* $\leq$ *eps. This will occur when the simplex contracts into the minimum or if the local region is found to be flat.*

F *This array should have bounds [1:n+1]. It is used during the search, and on exit holds the values of the function at the corners of the final simplex, in the same order that the coordinates are held in x. F[index] will hold the value of the function at the located minimum.;*

```
begin integer np1,np2,np3,np4,i,j,k,ih,newih,ihless1,
      ihplus1,ish,il;
      real fh,fl,fsh,fe,fr,fc,s,p,q,rn,rn1,alpha1,gamma1,
      onelessbeta,newF;
      array c[1:n];
      switch case:=newx,newsh,centroid;
```

```
        np1:=n+1;  np2:=n+2;  np3:=n+3;  np4:=n+4;
        rn:=n;  rn1:=rn+1.0;  onelessbeta:=1.0-beta;
        alpha1:=alpha+1.0;  gamma1:=gamma+1.0;
        eps:=eps×eps;  s:=scale/(rn×1.414214);
        q:=s×(sqrt(rn1)-1.0);  p:=s×rn+q;  il:=0;
        for j:=1 step 1 until n do
        begin s:=x[1,j];  x[j+1,j]:=s+p;  s:=s+q;
              for i:=2 step 1 until j,
              j+2 step 1 until np1 do
              x[i,j]:=s
        end setting up initial simplex;
newx:   for i:=il-1 step -1 until 1,
        il+1 step 1 until np1 do
        F[i]:=function(x,i,n);
        comment evaluate function at corners of simplex;
        fsh:=fl:=F[1];  ish:=il:=1;
        for i:=2 step 1 until np1 do
        begin p:=F[i];
              if p<fl then begin fl:=p;  il:=i  end;
              if p>fsh then begin fsh:=p; ish :=i  end
        end finding highest and lowest corners;
newsh:  ih:=ish;  fh:=fsh;  ish:=il;  fsh:=fl;
        ihless1:=ih-1;  ihplus1:=ih+1;
        for i:=1 step 1 until ihless1,
        ihplus1 step 1 until np1 do
        begin p:=F[i];
              if °p>fsh then begin fsh:=p;  ish:=i  end
        end finding second-highest point;
centroid:
        for j:=1 step 1 until n do
        begin p:=0.0;
              for i:=1 step 1 until ihless1,
              ihplus1 step 1 until np1 do
```

```
        p:=p+x[i,j];
        c[j]:=p:=p/rn;
        x[np2,j]:=alpha1×p-alpha×x[ih,j]
end centroid and reflection;
fr:=function(x,np2,n);
if fr<fl then
begin for j:=1 step 1 until n do
        x[np3,j]:=gamma1×x[np2,j]-gamma×c[j];
        fe:=function(x,np3,n);
        if fe<fr then
        begin newih:=np3;  newF:=fe  end
        else
        begin newih:=np2;  newF:=fr  end;
        goto newil
end;
if fr<fh then
begin newih:=np2;  newF:=fr;
        goto if fr<fsh then k2 else k3
end;
for j:=1 step 1 until n do
x[np4,j]:=beta×x[ih,j]+onelessbeta×c[j];
fc:=function(x,np4,n);
if fc>fh then
begin for j:=1 step 1 until n do
        begin s:=x[il,j];
              for i:=il-1 step -1 until 1,
              il+1 step 1 until np1 do
              x[i,j]:=(x[i,j]+s)×0.5
        end;
        k:=1;  goto test
end;
newih:=np4;  newF:=fc;
```

```
        if fc>fsh then
        begin
k3:     k:=3;  fh:=newF
        end
        else
        begin if fc<fl then
              begin
newil:              il:=ih;  fl:=newF
              end;
k2:           k:=2
        end;
replace:
        for j:=1 step 1 until n do
        x[ih,j]:=x[newih,j];
        F[ih]:=newF;
test:   p:=q:=0.0;
        for i:=1 step 1 until np1 do
        begin s:=F[i];
              p:=p+s;  q:=q+s×s
        end;
        if (q-p×p/rn1)/rn1>eps then goto case[k];
        index:=il
end simplex;
```

It is generally accepted that the most powerful method of function minimization available that requires only first-order partial derivatives of the objective function is that of Davidon as revised by R. Fletcher and M.J.D. Powell and published in *The Computer Journal* volume 7 page 308 *et seq.* However, as in most numerical analysis problems, the results obtained with its use depend critically on the implementation. The Fletcher and Powell process can be subject to numerical instability due to truncation errors in computer floating point arithmetic. The algorithm given below (P.A. Hamilton and J. Boothroyd: to appear in *Communications of the Association for Computing Machinery*) is based on their method, but includes a number of features which have proved of assistance in controlling the stability of the process.

```
real procedure MINIMUM(function,x,g,n,eps,loops,conv);
value n,eps; real function,eps; integer n,loops;
real array x,g; boolean conv;
```

comment *This procedure implements the method of Fletcher and Powell for finding the local minimum of a function of n variables when the first-order partial derivatives of the function are available. function is a real parameter called by name, and the actual parameter should be such that the statement*

f:=function

delivers to f the value of the function at the point

(x[1], x[2], ... , x[n]),

and at the same time sets the contents of **array** *g to the partial derivatives:*

$$g[i] := \frac{\partial\ function}{\partial x[i]} \quad .$$

The parameters of MINIMUM are described below.

function *This formal parameter is replaced by an actual parameter in the call of MINIMUM that supplies the value of the function, and sets the partial derivatives.*

x *This array should have bounds [1:n], and is the vector specifying the current position during the search.*

g *This array should have bounds [1:n], and holds the partial derivatives of the function.*

n *The number of variables.*

eps *An exit criterion.*

loops *On entry, this should specify the permitted number of iterations. On exit it will return the actual number of iterations performed.*

conv *On exit conv will have the value* true *if the process has converged to a minimum.*

At the entry to the procedure the initial estimate of the position of the minimum should be in the vector x. On exit, the position of the located minimum will be returned in x and the procedure name will yield the value of the objective function at the minimum;

```
begin real step,f,fa,fb,ga,gb,gaz,z,w,ita,lambda,
           sg,ghg,sigi,si,oldf;
      integer i,j,ci,cj,iless1,lim,count;
      array s,sigma,gamma[1:n],h[1:(n×(n+1))÷2];

      real procedure dot(a,b); array a,b;
      begin integer i; real s;
            s:=0.0;
            for i:=1 step 1 until n do s:=s+a[i]×b[i];
            dot:=s
      end dot;

      real procedure updot h(b); array b;
      begin integer j; real s;
            s:=0.0;
            for j:=1 step 1 until iless1 do
            s:=s+h[j+ci]×b[j];
            cj:=ci+i;
            for j:=i step 1 until n do
            begin s:=s+h[cj]×b[j];
                  cj:=cj+j
            end;
            updot h:=s
      end updot h;
```

```
        ci:=0;  f:=function;
        for i:=1 step 1 until n do
        begin sigma[i]:=x[i];  gamma[i]:=g[i];
              s[i]:=-g[i];  cj:=ci+i;
              for j:=ci+1 step 1 until cj do h[j]:=0.0;
              h[cj]:=1.0;  ci:=cj
        end;
        conv:=true;  lim:=loops;  eps:=-(n×eps)↑2;
        count:=0;  ga:=dot(g,s);
        for ita:=1.0, step while ga<eps do
        begin step:=0.0;  count:=count+1;
              oldf:=fa:=f;
extrap:       for i:=1 step 1 until n do x[i]:=x[i]+ita×s[i];
              step:=ita+step;  fb:=function;  gb:=dot(g,s);
              if gb<0.0 ∧ fb<fa then
              begin z:=3.0×(fa-fb)/ita+ga+gb;
                    w:=z×z-ga×gb;  lambda:=0.0;
                    if w>0.0 then
                    begin w:=sqrt(w);  gaz:=ga+z;
                          lambda:=if gaz>0.0 then (gaz+w)/(gaz+gb+z)
                                             else ga/(gaz-w)
                    end;
                    ita:=ita×(if lambda>0.0 then2.0×lambda else 4.0);
                    fa:=fb;  ga:=gb;  gotoextrap
              end extrapolation;
interp:       z:=3.0×(fa-fb)/ita+ga+gb;  gaz:=ga+z;
              w:=z×z-ga×gb;
              w:=if w>0.0 then sqrt(w) else 0.0;
              lambda:=ita×(1.0-(if gaz>0.0 then (gaz+w)/(gaz+gb+z)
                                           else ga/(gaz-w)));
              for i:=1 step 1 until n do x[i]:=x[i]-lambda×s[i];
```

```
step:=step-lambda;  f:=function;
if f≠fa ∧ f≠fb ∧ (f>fa ∨ f>fb) then
begin if fa>fb then
      begin for i:=1 step 1 until n do
            x[i] :=x[i]+lambda×s[i];
            f:=function;  step:=step+lambda
      end
      else
      begin gb:=dot(g,s);
            fb:=f;  ita:=ita-lambda;
            goto interp
      end
end interpolation;
if count≥lim ∨ f≥oldf then
begin conv:=false;  goto done  end;
for i:=1 step 1 until n do
begin sigma[i]:=x[i]-sigma[i];
      gamma[i]:=g[i]-gamma[i]
end;
ci:=iless1:=0;
for i:=1 step 1 until n do
begin s[i]:=updot h(gamma);
      iless1:=i;  ci:=ci+i
end;
sg:=dot(sigma,gamma);  ghg:=dot(s,gamma);
ci:=0;
if sg≠0.0 ∧ ghg≠0.0 then
for i:=1 step 1 until n do
begin ci:=cj:=ci+i;
      sigi:=sigma[i]/sg;  si:=s[i]/ghg;
```

```
                for j:=i step 1 until n do
                begin h[cj]:=h[cj]+(sigi×sigma[j]-si×s[j]);
                      cj:=cj+j
                end
            end;
            iless1:=ci:=0;
            for i:=1 step 1 until n do
            begin sigma[i]:=x[i];  gamma[i]:=g[i];
                  s[i]:=updot h(g);
                  iless1:=i;  ci:=ci+i
            end;
            ga:=dot(g,s)
        end;
done:   loops:=count;
        MINIMUM:=f
end MINIMUM
```

All the articles listed in the publications section have been removed for copyright or proprietary reasons.

PUBLICATIONS

The investigations discussed in this thesis have led to the following publications. Where reprints are available, copies have been included in the back of this volume. The papers are listed in chronological order of appearance. Where there have been two or more authors the relative contributions are indicated by the order of the authors.

1. Ellis,G.R.A., Green,R.J. and Hamilton,P.A. 1963
"Observations of Galactic Radiation at 4.7 Mc/s"
Aust. J. Phys. *16* 545 - 551.

2. Ellis,G.R.A. and Hamilton,P.A. 1964
"Absorption of Radio Waves in the Galaxy"
Nature *204* 272 - 273.

3. Ellis,G.R.A. and Hamilton,P.A. 1966
"Cosmic Noise Survey at 4.7 Mc/s"
Astrophys. J. *143* 227 - 235.

4. Ellis,G.R.A. and Hamilton,P.A. 1966
"Ionized Hydrogen in the Plane of the Galaxy"
Astrophys. J. *146* 78 - 87.

5. Hamilton,P.A. 1966
"Ionized Hydrogen in the Plane of the Galaxy"
Symposium on Radio and Optical Studies of the Galaxy
(Canberra: Mt. Stromlo Observatory) 94 - 95.

6. Hamilton,P.A. and Haynes,R.F. 1967
"Source Flux Densities at 153 MHz"
Aust. J. Phys. *20* 697 - 713.

7. Hamilton,P.A. 1968
"An Electronic System for phasing Aerial Arrays"
Proc. I. R. E. E. (Aust.) *29* 56 - 57.

8. Hamilton,P.A. and Haynes,R.F. 1968
"Observations of the Southern Sky at 10.02 MHz"
Aust. J. Phys. *21* 895 - 902.

9. Haynes,R.F. and Hamilton,P.A. 1968
"Observations of 31 Radio Sources between 40 and 130 MHz"
Aust. J. Phys. *21* 87 - 94.

10. Haynes,R.F., Hamilton,P.A. and McCulloch,P.M. 1968
"Observations of 11 Radio Sources near 55 MHz"
Aust. J. Phys. *21* 539 - 542.

11. Komesaroff,M.M., McCulloch,P.M., Hamilton,P.A. and Cooke,D.J. 1968.
"Spectral Fine Structure in Pulsar Radiation"
Nature *220* 358 - 360.

12. Hamilton,P.A. 1968
"The Llanherne Radio Telescope"
Symposium on Aerials Research
(Melbourne: C.S.I.R.O. Radio Research Board).

13. McCulloch,P.M., Hamilton,P.A., Komesaroff,M.M. and Cooke,D.J. 1969
"A Comparison of pulse shapes of Pulsars at different frequencies"
Proc. Astron. Soc. Aust. *1* 225 - 226.

Accepted for Publication:

14. Hamilton,P.A. and Haynes,R.F.
"A Survey of the Southern Sky at 153 MHz"
Australian Journal of Physics

15. Hamilton,P.A. and Boothroyd,J.
"Remark on Algorithm: Function Minimization"
Communications of the Association for Computing Machinery.

16. Hamilton,P.A.
"Algorithm: The Simplex method of Function Minimization"
The Computer Journal.

Submitted for Publication:

17. Hamilton,P.A. and Francey,R.J.
"Synchrotron Emission from the Galaxy and the Diffuse X-Ray Background"
submitted to *Nature.*